



# ANALYSIS OF ENERGY EFFICIENCY OF GAS DRIVEN HEAT PUMPS

## **Dissertation**

zur Erlangung des akademischen Grades

**Doktoringenieur  
(Dr.-Ing.)**

von **M.Sc. Essam Mahrous Elgenady Elgendy**  
geb. am 10. November 1973 in Qaliubya, Ägypten

genehmigt durch die Fakultät für Verfahrens- und Systemtechnik  
der Otto-von-Guericke-Universität Magdeburg

## **Gutachter:**

Prof. Dr.-Ing. Jürgen Schmidt  
Prof. Dr.-Ing. Mohamed Fatouh  
Dr.-Ing. Zhivko Zhekov

**This work is dedicated to...**

my parents, my wife Suzan and my children Mohamed and Nouredin

# ACKNOWLEDGEMENT

I would like to express my profound gratitude and sincere appreciation to Prof. Jürgen Schmidt for his inspiration, indispensable guidance and for teaching me invaluable knowledge throughout the course of my study. With his initial support, this great dream of mine can finally turn to reality, and with his unending guidance throughout the study, I was able to navigate the arduous path down to the very end. I am sure that whatever I have learned while working with him will be very useful in my future endeavors. He has been a great mentor.

I gratefully acknowledge the contributions of my country supervisors. I wish to express my thanks to Prof. Adel Khalil for his valuable guidance and continuous help. I wish to express my deepest gratitude to Prof. Mohamed Fatouh for his continued encouragement, valuable guidance and continuous help during all time of preparation this work.

I am very thankful to my employer Team Consulting for their continued support. I would also like to express my gratitude to Mr. Gunar Boye and Dr. Boye. I will never forget the time when we worked together in the lab and will always value the team spirit.

I am deeply indebted to my country EGYPT for accepting and supporting me to do my Ph.D. in Germany. I would like to express my deep sense of gratitude towards my parents, my wife, and my kids for moral support and encouragement during my study and my whole life.

I cannot leave out my friends, and colleagues who were a great support during the course of my study.

I would like to express my deep gratitude to everyone who helped me shape the ideas explored in this dissertation, either by giving technical advice or encouraging and supporting my work in many other ways. This dissertation would not have come into existence without their hands-on advice and motivation.

Essam Elgendy

Magdeburg, Germany



# Contents

<b>ACKNOWLEDGEMENT</b>	<b>III</b>
<b>CONTENTS</b>	<b>VIII</b>
<b>LIST OF TABLES</b>	<b>IX</b>
<b>LIST OF FIGURES</b>	<b>XIII</b>
<b>NOMENCLATURE</b>	<b>XV</b>
<b>ABSTRACT</b>	<b>XIX</b>
<b>ZUSAMMENFASSUNG</b>	<b>XXI</b>
<b>1 INTRODUCTION</b>	<b>1</b>
<b>2 GAS ENGINE HEAT PUMP (GEHP)</b>	<b>3</b>
2.1 Basic Principles . . . . .	3
2.2 Advantages of GEHP over EHP . . . . .	5
<b>3 LITERATURE REVIEW</b>	<b>7</b>
3.1 Testing Energy Efficiency of the GEHP . . . . .	7
3.2 Economic Aspects of the GEHP . . . . .	9
3.3 Investigations on Performance Improving of the GEHP . . . . .	10
3.3.1 Gas engine drive combined refrigeration systems . . . . .	11
3.3.2 Gas engine drive combined cooling, heating and power system . . . . .	12
3.3.3 Control strategies of the GEHP . . . . .	13
3.3.4 Improving the effectiveness of the GEHP processes . . . . .	14
3.4 Modelling of the GEHP Systems . . . . .	15
3.5 Commercial and Industrial Applications of the GEHP . . . . .	17
3.6 Environmental Effect of the GEHP . . . . .	20
3.7 Investigation of R22 Alternative Refrigerants . . . . .	21
3.8 Conclusions on the Literature Review . . . . .	22

---

<b>4</b>	<b>THEORETICAL ANALYSIS OF A GAS ENGINE HEAT PUMP</b>	<b>25</b>
4.1	Operating Principle of Gas Engine Heat Pump . . . . .	25
4.2	Assumptions . . . . .	25
4.3	Analysis of a Gas Engine Heat Pump . . . . .	26
4.3.1	Adiabatic compression process . . . . .	27
4.3.2	Heat rejection process . . . . .	28
4.3.3	Throttling process . . . . .	29
4.3.4	Heat absorption process . . . . .	29
4.3.5	Gas engine . . . . .	29
4.3.6	Performance characteristics of the GEHP . . . . .	29
4.4	Simulation Results . . . . .	30
4.4.1	Comparison among working fluids . . . . .	30
4.4.2	Effect of evaporation temperature . . . . .	32
4.4.3	Effect of condensation temperature . . . . .	34
4.4.4	Effect of subcooled degrees . . . . .	36
4.4.5	Effect of superheating degree . . . . .	36
4.4.6	Effect of compressor isentropic efficiency . . . . .	39
4.4.7	Effect of engine thermal efficiency . . . . .	39
4.5	Conclusions on Theoretical Analysis of the Gas Engine Heat Pump . . . .	40
<b>5</b>	<b>EXPERIMENTAL TEST RIG AND PROCEDURE</b>	<b>43</b>
5.1	Experimental Test Rig . . . . .	43
5.1.1	Description of the experimental test rig in cooling mode . . . . .	44
5.1.2	Description of the experimental test rig in combined mode . . . . .	46
5.1.3	Description of the experimental test rig in heating mode . . . . .	47
5.2	Data Acquisition . . . . .	49
5.3	Test Rig Commissioning and Experimental Procedure . . . . .	50
5.4	Data Reduction . . . . .	51
5.5	Uncertainty Analysis . . . . .	53
<b>6</b>	<b>EXPERIMENTAL RESULTS AND DISCUSSION</b>	<b>55</b>
6.1	Cooling Mode . . . . .	55
6.1.1	Effect of evaporator water inlet temperature . . . . .	56
6.1.2	Effect of evaporator water volume flow rate . . . . .	58
6.1.3	Effect of ambient air temperature . . . . .	58
6.1.4	Effect of engine speed . . . . .	60
6.2	Combined Cooling and Heating Mode . . . . .	62
6.2.1	Effect of evaporator water inlet temperature . . . . .	63
6.2.2	Effect of evaporator water volume flow rate . . . . .	66
6.2.3	Effect of ambient air temperature . . . . .	67
6.2.4	Effect of engine speed . . . . .	69
6.3	Heating Mode . . . . .	71
6.3.1	Heating mode-I . . . . .	72
6.3.1.1	Effect of condenser water inlet temperature . . . . .	72
6.3.1.2	Effect of condenser water volume flow rate . . . . .	74

6.3.1.3	Effect of ambient air temperature . . . . .	75
6.3.1.4	Effect of engine speed . . . . .	77
6.3.2	Heating mode-II . . . . .	79
6.3.2.1	Effect of condenser water inlet temperature . . . . .	80
6.3.2.2	Effect of ambient air temperature . . . . .	82
6.3.2.3	Effect of engine speed . . . . .	84
6.3.3	Comparison between heating mode-I and mode-II . . . . .	86
6.3.4	Optimum waste heat recovery . . . . .	88
6.4	Conclusions based on Experimental Results . . . . .	90
<b>7</b>	<b>MODELLING AND SIMULATION OF GAS ENGINE DRIVEN HEAT PUMPS</b>	<b>93</b>
7.1	Heat Pump System Model . . . . .	93
7.1.1	Model assumptions . . . . .	94
7.1.2	Scroll compressor . . . . .	95
7.1.2.1	Scroll compressor testing . . . . .	95
7.1.2.2	Scroll compressor modelling . . . . .	98
7.1.2.3	Prediction of refrigerant mass flow rate . . . . .	98
7.1.2.4	Prediction of compressor power . . . . .	101
7.1.2.5	Scroll compressor validation . . . . .	102
7.2	Plate Heat Exchanger . . . . .	105
7.2.1	Single phase flow correlations . . . . .	108
7.2.2	Boiling correlations . . . . .	108
7.2.2.1	Hsieh and Lin correlation . . . . .	110
7.2.2.2	Han, Lee, and Kim correlation . . . . .	110
7.3	Gas Engine . . . . .	111
7.4	Simulation Results and Discussion . . . . .	111
7.5	Conclusions based on Modelling and Simulation Results . . . . .	113
<b>8</b>	<b>SUMMARY AND OUTLOOK</b>	<b>117</b>
8.1	Recommendations for Future Research . . . . .	120
<b>A</b>	<b>SPECIFICATION OF THE SYSTEM MAIN COMPONENTS</b>	<b>121</b>
<b>B</b>	<b>INSTRUMENTS CALIBRATION</b>	<b>123</b>
B.1	Resistance Thermometers (Pt100) Calibration . . . . .	123
B.2	Pressure Switches Calibration . . . . .	124
B.3	Refrigerant Flow Meter Calibration . . . . .	125
B.4	Gas Flow Meter Calibration . . . . .	125
B.5	Engine Coolant Flow Meter Calibration . . . . .	125
B.6	Water Flow Meter Calibration . . . . .	126
<b>C</b>	<b>SPECIFICATIONS OF THE INSTRUMENTATION DEVICES</b>	<b>129</b>
C.1	Data Acquisition Card . . . . .	129
C.2	Pressure Switch . . . . .	129
C.3	Refrigerant Flow Meter . . . . .	129

---

C.4	Gas Flow Meter . . . . .	130
C.5	Engine Coolant Flow Meter . . . . .	130
C.6	Water Flow Meter . . . . .	130
<b>D</b>	<b>UNCERTAINTY ANALYSIS</b>	<b>133</b>
D.1	Water Temperature . . . . .	133
D.2	Refrigerant Temperature . . . . .	133
D.3	Refrigerant Pressure . . . . .	133
D.4	Engine Coolant Temperature . . . . .	134
D.5	Refrigerant Specific Enthalpy . . . . .	134
D.6	Water Specific Enthalpy . . . . .	134
D.7	Refrigerant Mass Flow Rate . . . . .	134
D.8	Refrigerant Heat Loads and Compression Power . . . . .	135
D.9	Gas Volume Flow Rate . . . . .	135
D.10	Gas Engine Heat Energy . . . . .	135
D.11	Water Volume Flow Rate . . . . .	135
D.12	Water Heat Load . . . . .	135
D.13	Engine Coolant Volume Flow Rate . . . . .	136
D.14	Engine Coolant Heat Loads . . . . .	136
D.15	Primary Energy Ratio . . . . .	136
<b>E</b>	<b>FLOW CHART OF THE SIMULATION PROGRAM</b>	<b>137</b>



# List of Tables

5.1	Uncertainty values of the experimental parameters. . . . .	53
6.1	Representative hot water temperatures. . . . .	64
7.1	Single phase heat transfer correlations for plate heat exchangers. . . . .	109
A.1	Specifications of the system main components. . . . .	121
B.1	Specifications of the temperature calibrator. . . . .	123
B.2	Numerical constants of the Pt100 calibration equation. . . . .	124
B.3	Calibration results of the pressure switches. . . . .	125
B.4	Calibration results of the refrigerant flow meter. . . . .	125
C.1	Specifications of the data acquisition card. . . . .	129
C.2	Specifications of the pressure switches. . . . .	130
C.3	Specifications of the refrigerant flow meter. . . . .	130
C.4	Specifications of the diaphragm gas meter. . . . .	130
C.5	Specifications of the diaphragm gas meter. . . . .	131
C.6	Specifications of the water flow meter. . . . .	131



# List of Figures

2.1	Basic definition of a gas engine heat pump. . . . .	4
2.2	Schematic diagram of a simple gas engine heat pump. . . . .	5
2.3	Comparison of energy conversion process between conventional EHP and GEHP . . . . .	6
3.1	Structure of a parallel HPGHP system. . . . .	12
3.2	Schematic view of a gas engine driven solar assisted band conveyor heat pump drying system. . . . .	20
4.1	Simple gas engine driven heat pump. . . . .	26
4.2	Log(p)-h diagram for heat pump circuit. . . . .	27
4.3	Comparison between R134a, R407C and R410A; (A) operating pressures and refrigerant mass flow rate, (B) heat loads and (C) primary energy ratio. . . . .	31
4.4	Effect of evaporation temperature on the performance characteristics of GEHP; (A) operating pressures and refrigerant mass flow rate, (B) heat loads and (C) primary energy ratio. . . . .	33
4.5	Influence of condensation temperature on the performance characteristics of GEHP; (A) operating pressures and refrigerant mass flow rate, (B) heat loads and (C) primary energy ratio. . . . .	35
4.6	Effect of subcooling degrees on the performance characteristics of GEHP; (A) heat loads and (B) primary energy ratio. . . . .	37
4.7	Influence of superheating degrees on the performance characteristics of GEHP; (A) operating pressures and refrigerant mass flow rate, (B) heat loads and (C) primary energy ratio. . . . .	38
4.8	Effect of compressor isentropic efficiency on the performance characteristics of GEHP; (A) heat loads and (B) primary energy ratio. . . . .	40
4.9	Influence of engine thermal efficiency on the performance characteristics of GEHP; (A) heat loads and (B) primary energy ratio. . . . .	41
5.1	Schematic diagram of the experimental test rig in cooling mode with measuring point locations. . . . .	45
5.2	log(p)-h diagram for the primary cycle processes in cooling mode. . . . .	46
5.3	Schematic diagram of the experimental apparatus in heating mode with measuring point locations. . . . .	48
5.4	log(p)-h diagram for the primary cycle processes in heating mode. . . . .	49

---

6.1	Effect of evaporator water inlet temperature on the performance characteristics of the GEHP in cooling mode for different chilled water volume flow rates; (A) operating pressures and refrigerant mass flow rate, (B) heat loads and (C) chilled water temperature and PER. . . . .	57
6.2	Effect of ambient air temperature on the performance characteristics of the GEHP in cooling mode; (A) operating pressures and refrigerant mass flow rate, (B) heat loads and (C) chilled water temperature and PER. . . . .	59
6.3	Effect of engine speed on the performance characteristics of the GEHP in cooling mode; (A) operating pressures and refrigerant mass flow rate, (B) heat loads and (C) chilled water temperature and PER. . . . .	61
6.4	Comparison between experimental and correlated primary energy ratio data in cooling mode. . . . .	63
6.5	Effect of evaporator water inlet temperature on the performance characteristics of the GEHP in combined mode for different water volume flow rates; (A) operating pressures and refrigerant mass flow rate, (B) heat loads and (C) water temperatures and PER. . . . .	65
6.6	Effect of ambient air temperature on the performance characteristics of the GEHP in combined mode; (A) operating pressures and refrigerant mass flow rate, (B) heat loads and (C) water temperatures and PER. . . . .	68
6.7	Effect of engine speed on the performance characteristics of the GEHP in combined mode; (A) operating pressures and refrigerant mass flow rate, (B) heat loads and (C) water temperatures and PER. . . . .	70
6.8	Comparison between experimental and correlated primary energy ratio data in combined mode. . . . .	71
6.9	Effect of condenser water inlet temperature on the performance characteristics of the GEHP in heating mode-I for different water volume flow rates; (A) operating temperatures and refrigerant mass flow rate, (B) heat loads and (C) water temperatures and PER. . . . .	73
6.10	Effect of ambient air temperature on the performance characteristics of the GEHP in heating mode-I; (A) operating temperatures and refrigerant mass flow rate, (B) heat loads and (C) water temperatures and PER. . . . .	76
6.11	Effect of engine speed on the performance characteristics of the GEHP in heating mode-I; (A) operating temperatures and refrigerant mass flow rate, (B) heat loads and (C) water temperatures and PER. . . . .	78
6.12	Comparison between experimental and correlated primary energy ratio data and recovered engine heat in heating mode-II. . . . .	80
6.13	Effect of condenser water inlet temperature on the performance characteristics of the GEHP in heating mode-II; (A) operating temperatures and refrigerant mass flow rate, (B) heat loads and (C) condenser water temperature and PER. . . . .	81
6.14	Effect of ambient air temperature on the performance characteristics of the GEHP in heating mode-II; (A) operating temperatures and refrigerant mass flow rate, (B) heat loads and (C) Condenser water temperature and PER. . . . .	83

---

6.15	Effect of engine speed on the performance characteristics of the GEHP in heating mode-II; (A) operating temperatures and refrigerant mass flow rate, (B) heat loads and (C) condenser water temperature and PER. . . . .	85
6.16	Comparison between experimental and correlated primary energy ratio data in heating mode-II. . . . .	86
6.17	Comparison of the performance characteristics for both mode-I and mode-II; (A) outlet water temperatures, (B) heat loads and (C) PER. . . . .	87
6.18	Effect of heat recovery water inlet temperature on the recovered engine heat for different ambient air temperatures; (A) Heating mode and (B) Combined mode. . . . .	89
7.1	Schematic diagram of the heat pump system. . . . .	94
7.2	Discharged mass flow rate and compressor power versus suction pressure for different discharge pressure and engine speeds. . . . .	96
7.3	Volumetric and isentropic efficiencies versus pressure ratio at 1750 rpm engine speeds. . . . .	97
7.4	Schematic diagram of the compressor internal processes. . . . .	99
7.5	Comparison between predicted and experimented refrigerant mass flow rate and compressor power . . . . .	103
7.6	Comparison between present and previous models. . . . .	104
7.7	Comparison between measured and predicted mass flow rate and compressor power. . . . .	105
7.8	Main dimensions of the plate heat exchanger. . . . .	106
7.9	Evaporator internal stages. . . . .	107
7.10	Comparison between simulated and measured cooling and gas engine energy consumption capacities. . . . .	112
7.11	Comparison between simulated and measured compressor powers and primary energy ratio. . . . .	114
B.1	Calibration of the gas flow meter. . . . .	126
B.2	Calibration of the engine coolant flow meter. . . . .	126
B.3	Calibration of the water flow meter. . . . .	127
E.1	Flow chart of the simulation program. . . . .	138



# NOMENCLATURE

Only commonly used symbols are listed below. The meanings of all other symbols are defined explicitly within the text.

## Latin letter symbols

$A$	$[m^2]$	surface area
$Bo$	$[-]$	boiling number
$COP$	$[-]$	coefficient of performance
$D$	$[m]$	diameter
$e$	$[-]$	error
$G$	$[kg/(s\ m^2)]$	mass flux
$h$	$[kJ/kg]$	specific enthalpy
$k$	$[W/(m\ K)]$	thermal conductivity
$LHV$	$[kJ/m^3]$	lower heating value
$LMTD$	$[K]$	logarithmic mean temperature difference
$\dot{M}$	$[kg/s]$	mass flow rate
$M$	$[kg]$	mass
$N$	$[rpm]$	rotational speed
$Nu$	$[-]$	Nusselt number
$p$	$[kPa]$	pressure
$P$	$[kW]$	power
$PR$	$[-]$	pressure ratio
$Pr$	$[-]$	Prandtl number
$PER$	$[-]$	primary energy ratio
$\dot{q}$	$[kW/m^2]$	heat flux
$\dot{Q}$	$[kW]$	heat flow rate
$Re$	$[-]$	Reynolds number
$s$	$[kJ/(kg\ K)]$	specific entropy
$T$	$[K]$	temperature
$U$	$[W/(m^2\ K)]$	overall heat transfer coefficient
$V$	$[m^3]$	volume
$\dot{V}$	$[m^3/s]$	volume flow rate
$w$	$[kJ/kg]$	specific work
$x$	$[m]$	distance

**Greek letter symbols**

$\alpha$	$[W/(m^2 K)]$	convection heat transfer coefficient
$\beta$	$[degree]$	chevron angle
$\delta$	$[m]$	thickness
$\eta$	$[-]$	efficiency
$\mu$	$[Pa s]$	dynamic viscosity
$\rho$	$[kg/m^3]$	density
$\vartheta$	$[^{\circ}C]$	temperature
$\nu$	$[m^3/kg]$	specific volume
$\xi$	$[-]$	volume ratio

**Subscripts**

<i>act</i>	actual
<i>amb</i>	ambient
<i>av</i>	average
<i>c</i>	carnot
<i>cal</i>	calculated
<i>ch</i>	chilled
<i>corr</i>	correlated
<i>comp</i>	compressor
<i>cont</i>	control valve
<i>cond</i>	condenser
<i>e</i>	exit
<i>eng</i>	engine
<i>evap</i>	evaporator
<i>ex</i>	exhaust
<i>exp</i>	experimental
<i>h</i>	hot
<i>HE</i>	heat engine
<i>HP</i>	heat pump
<i>HR</i>	heat recovery
<i>hyd</i>	hydraulic
<i>i</i>	inlet
<i>l</i>	laminar
<i>m</i>	mechanical
<i>meas</i>	measured
<i>o</i>	outlet
<i>pr</i>	primary
<i>rad</i>	radiator
<i>s</i>	sweept
<i>sat</i>	saturated
<i>sea</i>	seasonal
<i>sec</i>	secondary



<i>sub</i>	subcooled
<i>suc</i>	suction
<i>sup</i>	superheat
<i>t</i>	turbulent
<i>vol</i>	volumetric
<i>w</i>	wall
<i>wat</i>	water

### Abbreviations

EHPs	electric heat pumps
GEHPs	gas engine heat pumps
GWP	global warming potential
HPs	heat pumps
TEWI	total equivalent warming impact
VAHPs	vapor absorption heat pumps
VCHPs	vapor compression heat pumps
VJHPs	vapor jet heat pumps
WP	water pump



# ABSTRACT

Nowadays a sustainable development for more efficient use of energy and protection of environment is of increasing importance. Gas engine heat pump (GEHP) represents one of the most practicable solutions which offers high energy efficiency and is environmentally friendly for heating and cooling applications. The GEHP typically uses the produced work by the engine to drive a vapor compression heat pump. At the same time, the engine waste heat is used for heating purposes. The present work aimed at evaluating the performance characteristics of the GEHP working with R22 alternatives under various operating conditions.

A computer program is written and developed to compare the performance characteristics of the GEHP working with three R22 alternative refrigerants namely; R134A, R407C and R410A. Results indicated that primary energy ratio (*PER*) of R134A and R410A are higher than R407C by 15.5 % and 10.65 %, respectively. It may be noted that R134A is the most suitable refrigerant to replace R22 from energy saving point of view. However, R134A has a lower heating capacity and higher total equivalent warming impact (TEWI) than R410A. Thereby, R410A is the best candidate to replace R22 from energy saving, high heating capacity and environmentally friendly point of views.

A parametric study including internal operating parameters of both gas engine and heat pump using the best alternative (R410A) has been done. The input data for study are evaporation temperature (-3 to 15°C), condensation temperature (30 to 55°C), degree of superheating (0 to 20K), degree of subcooling (0 to 10K), compressor isentropic efficiency (0.6 to 0.8) and engine mechanical efficiency (0.2 to 0.3). Results indicate that primary energy ratio of the GEHP is more influenced by evaporation temperature, condensation temperature, engine speed, mechanical efficiency, isentropic efficiency and subcooling degree in that order. On the other hand, superheating degree has the lowest effect on the *PER* of the GEHP in all modes of operation.

Thus, an experimental GEHP system working with R410A as a primary working fluid has been installed. Water and air were adopted as secondary heat transfer fluids at indoor and outdoor of the heat pump respectively. Test facility is developed and experiments are performed under various external operating parameters. These are water inlet temperature, water volume flow rate, ambient air temperature and engine speed. The performance of the GEHP was characterized by system capacities, outlet water temperatures and primary energy ratio for different operating modes namely cooling,

heating and combined cooling and heating modes. For cooling mode, it is found that the effect of evaporator water inlet temperature is higher than that of evaporator water mass flow rate on the performance characteristics of the GEHP. Maximum primary energy ratio of 1.83 has been obtained. For combined mode, chilled water outlet temperature between 5 and 15°C and average hot water outlet temperature between 38 and 65°C are considered. Maximum primary energy ratio of 2.1 has been obtained.

In heating mode, engine waste heat recovery represents one of the main advantages of a gas engine heat pump (GEHP) as compared to conventional heat pump system. Engine waste heat can be recovered to produce hot water supply (at high ambient air temperature) or to evaporate the refrigerant in the refrigerant circuit (at low air ambient temperature) to enhance the evaporator capacity and avoid frosting problem. The two possibilities have been investigated and the operating parameters such as condenser water inlet temperature, condenser water flow rate, ambient air temperature and engine speed have been studied at both low and high ambient air temperature. At the middle range of ambient air temperature (10 to 15°C), the two possibilities are valid but the performance of the GEHP is different. It has been found that the best mode of the GEHP is achieved when the engine waste heat is transferred to water circuit expect when the ambient air temperature is low.

Based on the above experimental results, combined mode has the highest primary energy ratio and its modelling plays an important role in system controlling and optimizing. Hence, a numerical modelling of the gas engine driven heat pump in cooling mode is performed and system characteristics such as cooling capacity, gas engine energy consumption and primary energy ratio are computed. The modelling of the gas engine heat pump includes modelling of the scroll compressor, the plate evaporator and the gas engine. Discharged refrigerant mass flow rate and compressor power represent the main output parameters of the compressor semi-empirical model. Using the discharged refrigerant mass flow rates along with the available evaporation heat transfer correlations, the system cooling capacity is deduced. Based on the experimental data, a correlation of gas engine energy consumption as function of compressor power, engine speed and ambient air temperature is obtained. The model is validated with the experimental data and it can be used for system controlling and optimizing.

The theoretical and experimental results confirm that the GEHP is a natural choice in applications where there are needs for simultaneous cooling and heating demands as they can improve the overall energy utilization efficiency.

# ZUSAMMENFASSUNG

Eine effizientere Energienutzung und die nachhaltige Entwicklung sind für den Umweltschutz von wachsender Bedeutung. Gasmotorwärmepumpen (GMWP) stellen hierbei eine praktische Lösung dar, die hohe Energieeffizienz und umweltfreundliche Kühl- und Heizanwendungen bietet. Die GMWP nutzt typischerweise die bereitgestellte Arbeit des Motors, um den Verdichter der Wärmepumpe in einem Kaldampfprozess anzutreiben. Gleichzeitig wird die Motorabwärme für Heizzwecke genutzt. Die vorliegende Arbeit richtet sich auf die Bewertung der Leistungscharakteristika der GMWP im Hinblick auf R22 Alternativkältemittel unter verschiedenen Betriebsbedingungen.

Es wurde ein Computerprogramm entwickelt, um die Leistungscharakteristika der GMWP in Betrieb mit drei R22-Alternativkältemitteln (R134A, R407C und R410A) zu vergleichen. Die Ergebnisse zeigten, dass die primärenergiebezogenen Leistungszahlen (*PER*) von R134A und R410A um 15,5 % und 10,65 % höher als die von R407C waren. Dementsprechend ist R134A das am besten geeignete Kältemittel, um R22 in Hinblick auf Energieeinsparung zu ersetzen. Dennoch hat R134A eine geringere Heizleistung und eine schlechtere Klimabilanz als R410A. Dadurch ist R410A das beste Mittel, um R22 im Hinblick auf Energieeinsparung, hohe Heizleistung und Umweltfreundlichkeit zu ersetzen.

In einer Parameterstudie wurden die internen Betriebsparameter von Gasmotor und Wärmepumpe unter Nutzung von R410A untersucht. Die Eingangsdaten der Studie waren die Verdampfungstemperatur (-3 - 15°C), Kondensationstemperatur (30 - 55°C), Grad der Überhitzung (0 - 20K), Grad der Unterkühlung (0 - 10K), der isentrope Verdichterwirkungsgrad (0,6 - 0,8) und der Wirkungsgrad des Motors (0,2 - 0,3). Die Ergebnisse zeigten, dass die primärenergiebezogene Leistungszahl der GMWP vor allem durch Verdampfungstemperatur, Kondensationstemperatur, Motordrehzahl, motorwirkungsgrad, isentropen Verdichterwirkungsgrad und den Unterkühlungsgrad in dieser Reihenfolge beeinflusst wird. Auf der anderen Seite hat der Überhitzungsgrad bei allen Betriebsvarianten den geringsten Einfluss auf die primärenergiebezogenen Leistungszahlen der GMWP.

Für die experimentellen Untersuchungen stand eine GMWP vom Typ AISIN (TGMP 280 C1N) unter Nutzung von R410A als primäres Arbeitsmedium zur Verfügung. Als sekundäre Wärmeübertragungsmedien wurden im Innenraum Wasser und in der äußeren Umgebung Luft verwendet. Mit der Testanlage wurden Experimente unter Variation externer Betriebsparameter, wie Wassereintrittstemperatur, Wasservolumenstrom, Umgebungslufttemperatur und Motordrehzahl, durchgeführt. Die Leistung der GMWP wurde charakterisiert durch Wärmeströme, Wasseraustrittstemperatur und primärenergiebezogene Leistungszahl für verschiedene Betriebsmodi, wie Kühlung,

Heizung und kombinierte Kühlung und Heizung. Für den Kühlmodus ergab sich, dass die Wassereintrittstemperatur im Verdampfer einen höheren Einfluss auf die Leistungscharakteristika der GMWP als die Wasserflussrate im Verdampfer hat. Eine maximale primärenergiebezogene Leistungszahl von 1,83 wurde erreicht. Für den kombinierten Modus wurden eine Kühlwasseraustrittstemperatur zwischen 5 und 15°C und eine Warmwasseraustrittstemperatur zwischen 38 und 65°C betrachtet. Eine maximale primärenergiebezogene Leistungszahl von 2,1 konnte dabei erreicht werden.

Im Heizmodus stellt die Nutzung der Motorabwärme, einen der Hauptvorteile der GMWP im Vergleich zu konventionellen Wärmepumpensystemen dar. Motorabwärme, die bei einem relativ hohen Temperaturniveau zur Verfügung steht, kann gewonnen werden, um Warmwasser bereitzustellen oder um das Kältemittel im Kältemittelkreislauf bei niedrigen Umgebungslufttemperaturen zusätzlich zu verdampfen und so das Verdampfungspotenzial zu verbessern und Vereisungsprobleme am Verdampfer zu vermeiden. Beide Möglichkeiten wurden untersucht und die Betriebsparameter, wie Wassereintrittstemperatur im Kondensator, Wassermassenstrom im Kondensator, Umgebungslufttemperatur und Motordrehzahl wurden bei sowohl niedrigen als auch hohen Umgebungslufttemperaturen analysiert. Bei einer mittleren Umgebungslufttemperatur (10 - 15°C) sind beide Möglichkeiten realisierbar, wobei sich die Leistung der GMWP unterscheidet. Es zeigte sich, dass die GMWP effizienter arbeitete, wenn die Motorwärme bei niedriger Umgebungslufttemperatur zum Wasserkreislauf geleitet wurde.

Basierend auf den obigen experimentellen Ergebnissen weist der kombinierte Modus die höchsten primärenergiebezogenen Leistungszahlen auf und seine Modellierung spielt eine wichtige Rolle in der Steuerung und Optimierung des Systems. Daher wurden eine numerische Modellierung der GMWP im Kühlmodus durchgeführt und Systemcharakteristika, wie Kälteleistung, Gasmotorenergieverbrauch und primärenergiebezogene Leistungszahl, ausgewertet. Die Modellierung der GMWP umfasst die Modellierung des Scroll-Verdichters, des Verdampfers und des Gasmotors. Massenstrom des komprimierten Kältemittels und Verdichterleistung stellen die Hauptausgangsparameter des halbempirischen Verdichtermodells dar. Durch Nutzung des Massenstroms des komprimierten Kältemittels und verfügbare Verdampfungs-Wärmübertragungs-Korrelationen wird die Systemkühlleistung berechnet. Basierend auf den experimentellen Daten wird eine Korrelation des Gasmotorenergieverbrauchs als Funktion von Verdichterleistung, Motordrehzahl und Umgebungslufttemperatur bereit gestellt. Das Modell wird anhand von experimentellen Daten validiert und kann zur Steuerung und Optimierung des Systems genutzt werden.

Die theoretischen und experimentellen Ergebnisse bestätigen, dass die GMWP insbesondere bei gleichzeitigen Kühl- und Heizanwendungen ein hohes Potenzial zur Energieeinsparung besitzt.

# Chapter 1

## INTRODUCTION

Depletion of fossil fuels and environmental pollution are two of main problems in the whole world. Fossil fuels represent the main energy source in the world and its depletion is a risk for energy shortage in the future. In Europe, more than 50 % of the total energy consumption depends on fossil fuels [1]. Cooling and heating processes play an important role in many sectors like residential, commercial, industrial and transportation. The amount of energy used to achieve such loads is a substantial portion of the total energy consumption worldwide [2]. In Germany, heating processes consume around 60 % of the total annual energy which is covered by nearly 80 % of the imported fossil fuels and is responsible for more than 50 % of the total, energy-related carbon dioxide  $CO_2$  emissions [1]. In order to reduce this energy demand and improve energy utilization efficiency, high energy efficient cooling and heating system must be adopted.

Heat pumps (HPs) are a natural choice for cooling and heating applications as they can improve the overall energy utilization efficiency and are environmentally friendly [3, 4, 5, 6]. Based on the working principle, HPs can be classified into two types vapor compression heat pumps (VCHPs) and vapor absorption heat pumps (VAHPs) [7]. According to energy sources, VCHPs can be divided into electric driven heat pumps (EHPs), gas engine driven heat pumps (GEHPs), geothermal energy heat pumps, solar assisted heat pumps, and hybrid power systems heat pumps [8, 9]. In the case of EHPs, fuel is mainly converted to electrical energy at power plants and the waste heat is discharged to the environment, then electrical energy is transmitted to the HPs and is converted to mechanical energy by electrical motor of the HPs. In this process, energy is converted twice and the rate of heat loss is high. However, energy efficiency can become higher if the fuel conversion process is located closer to the required heat load. In this case, heat released in fuel conversion process can be efficiently used. Since GEHPs are harmonious with this concept, they attract the investigators with the high energy efficiency, especially in heating [10, 11, 12]. Moreover, the overall efficiency of GEHP system is significantly improved by 15-25 % when the heat from the engine coolant and exhaust gas is recovered as reported by Nowallowski and Busby [13]. The main applications of GEHPs are space and water heating/cooling purposes [14]. However, they can be integrated to industrial applications [15].

Thus, the objectives of the present work are to:

- evaluate the performance characteristics of air to water R410A heat pump driven by a gas engine in different operating modes namely cooling, heating and combined cooling and heating. In order to achieve this aim, a test facility of the gas engine heat pump is constructed and equipped with the necessary instrumentation. Furthermore, effects of water inlet temperature, water flow rate, ambient air temperature and engine speed on the performance characteristics of the gas engine heat pump are experimentally evaluated.
- develop a simulation program for the main components such as compressor, a heat exchanger and a gas engine to predict the system capacities like cooling/heating capacity and gas engine energy consumption and consequently system primary energy ratio. Moreover, a comparison between simulation results and the experimental data has been done in order to validate the simulation program.
- derive recommendations concerning criteria for the energy efficient operation based on the obtained results of experimental and simulated data.

Chapter (1) gives a brief introduction. Basic principles of a gas engine heat pump are introduced in Chapter (2). Chapter (3) deals with an overview of the literature related to performance characteristics of the gas engine heat pump. Chapter (4) describes the theoretical analysis of the GEHP while Chapter (5) illustrates the experimental test rig including instrumentation, test procedure and data reduction. The results of experimental investigations in cooling, heating and combined cooling and heating modes are discussed in Chapter (6). Modelling of the gas engine heat pump is introduced in Chapter (7), which includes modeling of the main components of the system. Conclusions of theoretical and experimental investigations are given in Chapter (8). Specification of gas engine heat pump components, instruments calibration, specification of the instrumentation devices, uncertainty analysis and flow chart of the simulation program are given in appendices (A), (B), (C), (D), and (E), respectively.



# Chapter 2

## GAS ENGINE HEAT PUMP (GEHP)

### 2.1 Basic Principles

In 1852, the British physicist William Thomson (Lord Kelvin) described for the first time the working principle of pumping heat with a thermodynamic cycle as reported by Rebhan[16]. It has become a common practice now to call a heat pump for any device which extracts heat from a source at low temperature source and gives off this heat at high temperature sink which can be useful. If the purpose of the heat pump is to extract heat from the low temperature source, the device is called a refrigeration system. Therefore, the operating principle of the heat pump is exactly the same as the refrigeration system: the heat is absorbed at low temperature and rejected at high temperature. A heat engine is essentially a heat pump operating in reverse between two temperature levels as shown in Fig. 2.1. A heat engine produces power ( $P$ ) by extracting heat from the high temperature source ( $T_1$ ) and delivering heat ( $\dot{Q}_2$ ) to the intermediate temperature sink ( $T_2$ ), whereas the heat pump delivers heat ( $\dot{Q}_3$ ) at the intermediate temperature sink ( $T_3$ ) by extracting heat ( $\dot{Q}_4$ ) from the low temperature source ( $T_4$ ) and requires a power input ( $P$ ). A gas engine heat pump (GEHP) is combination of the heat engine and the heat pump by using the produced power ( $P$ ) to drive the heat pump. In theory, the maximum coefficient of performance for the gas engine heat pump ( $COP_c$ ) is given by a Carnot cycle operating between the temperatures ( $T_1$ ), ( $T_2$ ), ( $T_3$ ) and ( $T_4$ ); this  $COP_c$  depends on these temperatures as Eq. 2.1:

$$COP_c = \left(\frac{T_1 - T_2}{T_1}\right)\left(\frac{T_3}{T_3 - T_4}\right) \quad (2.1)$$

However, in reality it is not possible to operate the GEHP with a completely reversible cycle (ideal conditions) as a result of technical device operation losses. In fact, real heat pumps have number of deviations as compared to the ideal cycle which led to decrease the system  $COP$ . Condensation and evaporation temperatures need to be higher than the heat sink temperature and lower than the heat source temperature, respectively, to allow heat transfer in limited area heat exchangers. Moreover, pressure drops in the refrigerant lines cause further losses. Fig. 2.2 shows a simple GEHP system. It consists mainly

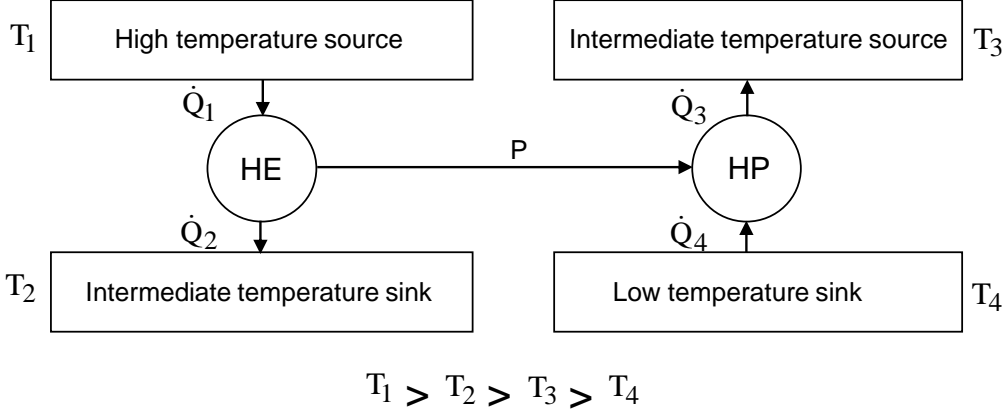


Figure 2.1: Basic definition of a gas engine heat pump.

of two parts: (i) the heat pump, which includes an open compressor, a condenser, an expansion valve and an evaporator, and (ii) the gas engine system. The distinctive part of GEHPs is the gas engine which has a low thermal efficiency (about 30-45%). However the recovered heat from the engine exhaust and engine cooling (approximately 80% [17]) increase the total efficiency of the GEHP system. GEHP efficiency is determined by comparing the amount of energy delivered to the amount of energy consumed. Hence, it is more appropriate to use the primary energy ratio ( $PER$ ), as defined by Holland et al. [18], as the ratio of useful heat delivered to primary energy input.  $PER$  can be related to the coefficient of performance of the heat pump ( $COP_{HP}$ ) and thermal efficiency of the gas engine ( $\eta_{HE}$ ) by the following equation;

$$PER = COP_{HP}\eta_{HE} \quad (2.2)$$

In fact, the gas engine heat pump can be used in several operating modes namely; cooling, heating and combined cooling and heating. Thus, the primary energy ratio of the GEHP system can be evaluated according to the operation mode of the system as follows;

$$PER_{cooling} = \frac{\dot{Q}_{eva}}{\dot{Q}_{gas}} \quad (2.3)$$

$$PER_{heating} = \frac{\dot{Q}_{con} + \dot{Q}_{HR}}{\dot{Q}_{gas}} \quad (2.4)$$

$$PER_{combined} = \frac{\dot{Q}_{eva} + \dot{Q}_{con} + \dot{Q}_{HR}}{\dot{Q}_{gas}} \quad (2.5)$$

where  $\dot{Q}_{eva}$ ,  $\dot{Q}_{con}$ ,  $\dot{Q}_{HR}$  and  $\dot{Q}_{gas}$  represent evaporator, condenser, recovered and gas engine heat flow rates.

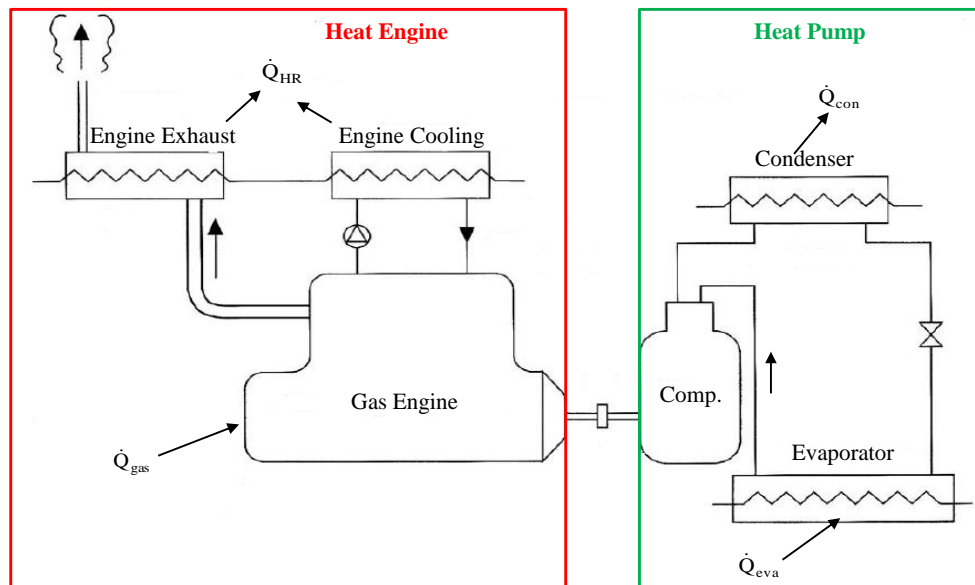


Figure 2.2: Schematic diagram of a simple gas engine heat pump.

## 2.2 Advantages of GEHP over EHP

In many instances, the GEHP is more attractive climate control system [19, 20] and has many advantages as compared with conventional heat pump e.g.:

- **Variable speed operation:** Typically, the GEHP can operate at minimum speed and modulate between a minimum and maximum speed to match the required load. The minimum and maximum speeds are decided by the performance of different engines and compressors. As a result, the part load efficiency of such a system will be high. Its seasonal operational cost and cycling losses will be lower than those of a single speed system with an on-off control system [17].
- **Low fuel utilization:** Lian [21] reported that GEHP system requires approximately third of the energy consumed in a conventional heat pump accompanying with electrical heating to achieve the same heating load (Fig. 2.3)<sup>1</sup>.
- **Cheap energy sources:** GEHPs use cheap energy sources, such as natural gas, propane or liquified petroleum gas (LPG) and biogas instead of electricity, thereby GEHPs become an economic choice [22, 23].
- **Low environmental impact:** As concerns the national interest, the increased use of GEHP allows to differentiate primary sources and, thanks to its high efficiency, to reduce the nation's energy requirements and thus the environmental impact.

<sup>1</sup>This figure is used based on license agreement between the author and Elsevier with license number of 2638830877924.

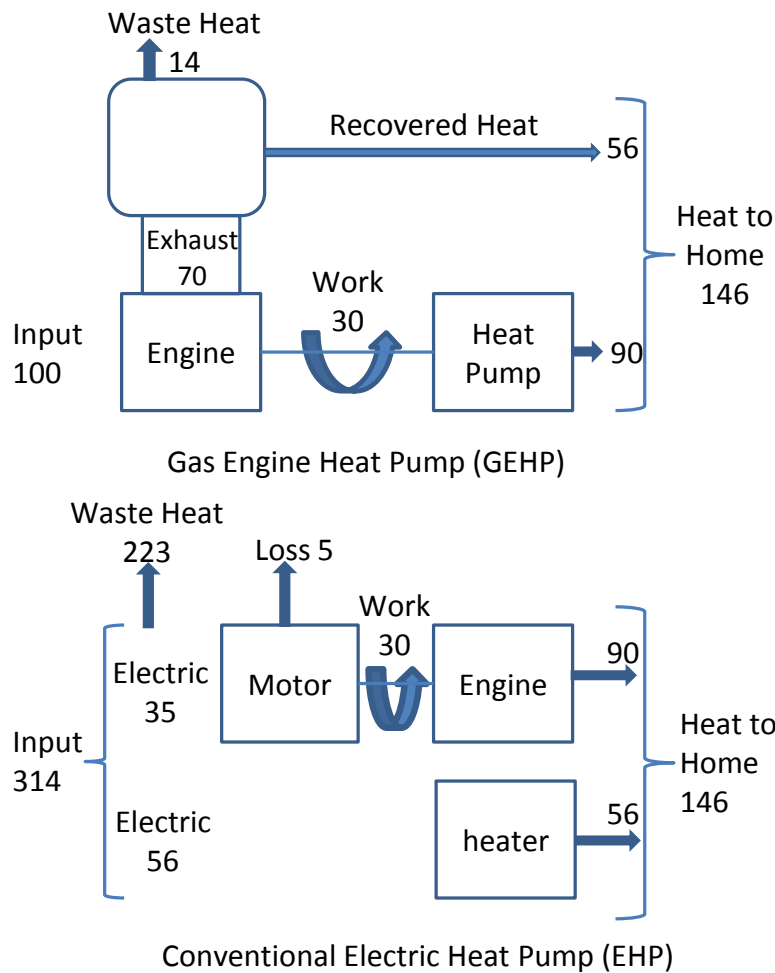


Figure 2.3: Comparison of energy conversion process between conventional EHP and GEHP

- **Reducing electricity demand:** One advantage of the GEHP is reducing the electricity consumption in the cooling and heating seasons by effectively balancing electricity demand, mitigating the electricity peaks and adjusting the energy configuration [22].
- **Central cogeneration plant:** Combined co-generation system coupling with gas engine, heat pump and generator can realize heating, cold and electric supply. For such system, the PER is double that of the separated production system [24].
- **Low ambient air temperature operation:** Frosting is one of the conventional system problems which takes place at low ambient air temperature. This prevent the system from continuing working. However in the gas engine heat pump system, the defrosting process takes place during the system operation using the gas engine exhaust gases. Combined, these features result in efficiency, comfort, and operating cost benefits over conventional heat pump system. Moreover these reasons also rise to the development of unitary GEHP package in Japan, Europe and the USA.

# Chapter 3

## LITERATURE REVIEW

After realizing the importance of environmental pollution and energy recovery, many investigations have been reported on using GEHP as it plays an important role in energy consumption reduction and environment protection. The first investigations on GEHP were performed at late 1970s [25, 26, 26]. On 1 April 1977, the first GEHP was started up in DortmundWellinghofen using open air swimming pool and its performance was evaluated by Bussmann [25]. Fleurschetz [26] proposed a GEHP in an integrated municipal energy supply system and Struck et al. [27] expressed the possibilities and limitations of heating system with GEHP. At the beginning of 1980s, Heiburg and Lohstaeter [28], Menkveld [29] and Morokoshi et al. [30] conducted field tests about the application of GEHPs for home heating and hot water preparation purposes. In 1981 Japanese government began to support investigations about GEHP.

Eustace [31] performed an investigation supported within the framework of the European Commission 2nd Energy R and D Programme in 1984. These showed the affinity of the governments to GEHP. The first merchandized GEHP produced and introduced in market in April 1985 was named as gas-multi. Its first performance tests were done by Ogura et al. [32]. Since then, many products were introduced in the market by Japanese companies. Many investigators focused on the system integral energy efficiency and economic aspects of the units by field tests, improving GEHP by designing, controlling and developing its parts, modeling of GEHP systems, its industrial applications, and testing its environmental effects. In this chapter, some of the areas of the discussion and the corresponding works will be presented and analyzed.

### 3.1 Testing Energy Efficiency of the GEHP

Several investigations have been conducted to predict the performance characteristics of the GEHP experimentally for either space air cooling/heating or water cooling/heating. Regarding to using the GEHP for space air applications, Nowakowski et al. [19] and [33] discussed the development of a high efficiency natural gas engine driven heat pump for residential and light commercial applications. Field test results confirmed that seasonal operating efficiencies with heating  $COP_{sea}$  ranging between 1.0 and 1.5 and cooling

$COP_{sea}$  ranging from 0.8 to 1.1 are obtained. During 1990-91 a large gas distribution company in the southeast US participated in a year-long field test of a 3TR GEHP designed as a packaged, split system for centrally heating ventilation air conditioning (HVAC) systems. This GEHP achieved 4,619hrs of engine operations: 59 % heating and 41 % cooling. Overall coefficients of performance were 1.37 for heating and 1.15 for cooling as presented by Wolfe and Getman [34]. Cornell et al [35] examined house dynamics and energy requirements associated with a variable speed GEHP. Test results showed that the GEHP system maintained excellent comfort conditions during the heating season. Good comfort conditions were maintained during the cooling season except when individual rooms were subjected to high localized solar loading. The system's heating COP ranged from 1.4 (at low speed and 35 to 40°F outdoor air temperatures) to 0.9 at high speed without auxiliary heat and -5°F outdoor air temperature. During cooling operation, system COP ranged from 1.45 (at low speed and 61°F outside air temperature) to 0.64 (at high speed and 100°F outside air temperature).

In the Netherlands, a GEHP, rated at 155kW heating capacity, supplied base-load heating to a city hall. Van Dijk and Lemmens [36] showed that the COP of the system ranged between 1.1 and 1.5, and a yearly gas-saving of 33 % were achieved, compared to the existing non-condensing boilers. A smaller GEHP, rated at 18kW heating and 14kW cooling, was used for air conditioning in a large kitchen. The year round COP for heating was evaluated at 1.16, yielding a gas saving of 23 %. Boye et al. [37] evaluated the performance characteristics of GEHP used for air conditioning. The effect of outside air temperature on primary energy ratio of the GEHP system was studied. When the outside air temperature changed from -2.5°C to 12.5°C, primary energy ratio increased from 0.8 to 1.4 during winter season without engine heat recovery. On the other hand, system primary energy ratio decreased from 1.2 to 0.8 as outside air temperature increased from 20°C to 34°C during summer season. Recently, new field tests of GEHP used in space cooling and heating were introduced by Sohn et al. [38]. Performance data were collected from six 10TR GEHP units installed at six military installations in the southwest of United States. Theoretical analysis showed significantly higher energy efficiency in space heating and cooling by GEHP units compared to a conventional gas furnace for heating and electric direct expansion system for space cooling. Effects of outdoor air temperature and engine speed on system coefficient of performance have been investigated. As outdoor air temperature varied from 65°F to 120°F system coefficient of performance decreased from 1.45 to 1.05 at high engine speed of 2250rpm. On the contrary, system coefficient of performance increased from 1.32 to 1.61 as engine speed changed from 2250rpm to 1900rpm at outdoor temperature of 82°F.

Regarding to use the GEHP in water cooling/heating, Japan's Tokyo Gas installed various units in 15 residential and commercial buildings and evaluated their performance for up to 18 months between 1983 and 1985 [39]. All of the units met cooling and water heating loads during the summer, water heating loads in spring and fall, and space heating loads in the winter. All units used R22 refrigerant. Tokyo Gas monitored gas and electric consumption, operating hours (cycling on/off times, run hours, and defrost time), engine speed, indoor and outdoor temperatures and humidity and refrigerant

temperatures. Based on the field test data, researchers determined both steady-state and seasonal coefficients of performance ( $COP_{sea}$ ) for the units. At the end of tests, researchers determined performance characteristics and pinpointed equipment reliability problems which, in turn, indicated the design modifications needed. Li et al. [40] reported that a cold-hot water gas heat pump unit was designed, and the experimental procedure and main equipments are introduced. The influence of engine speed upon recovery energy, consumption of gas and refrigerant flow is analyzed. Results showed that GEHP has a good part load feature at the load range of 20 % to 100 %. Furthermore, in the case of heating mode, stable cycled water and unchanged temperature of inlet water, the gas consumption, refrigerant flow, recovery heat and energy heating increase with the engine speed, but the coefficient of performance and primary energy ratio decrease as the engine speed increases.

### 3.2 Economic Aspects of the GEHP

Many investigators interested in comparison the GEHP system with other conventional electric heat pump system from economic point of view. Xie et al. [24] compared GEHP to other heating devices, such as an electric driven heat pump, a coal fired boiler, an electric boiler and a gas fired boiler. They reported that GEHP has the highest performances. Its primary energy ratio (PER), exergy efficiency and the energy grade balance efficiency were 1.76, 0.291 and 0.394. An energy calculation model is established for the GEHP based on the experiment of components by Zhang et al. [41]. The model calculates the performance and energy consumption under different working conditions in cooling and heating season, and comparison with those of electric heat pump was conducted. The result showed that the GEHP is more energy saving in lower outside temperature while spends equivalent primary energy in higher temperature. Based on the climate and energy price in Shanghai, gas engine driven heat pump can save about 23 % primary energy and 11.3 % running cost.

The economic analysis of using gas engine and electrical heat pumps for various climate regions of Iran, for both residential and commercial buildings and for both cooling and heating modes, was performed applying three energy-economy approaches by Sanaye et al. [42]. In the first approach, the annual cost of energy consumption for two gas engine and electrical systems was compared. It was found that in both residential and commercial sections and for all studied climate regions, the annual operating cost for electrical heat pumps was higher than that for the gas engine heat pumps. In the second approach, equivalent uniform annual cost method was used as the economic analysis. It was found that in residential section and for various climate regions, GEHP is more economical than the electrical heat pump. In commercial section, for all four climate regions, the electrical heat pumps in all capacities were more economical than gas engine heat pumps. In residential section, the gas price assuming the same numerical equivalent uniform annual cost (EUAC) values for both gas and electric heat pumps was obtained and reported. Furthermore in commercial section, the price of electricity assuming the same EUAC values for both heat pumps was computed and listed. Finally in the third

approach, the payback period of selecting a GEHP instead of an electrical heat pump was computed. It was found that the payback period decreases with increasing system capacity. Brenn et al. [43] compared natural gas driven heat pumps and electrically driven heat pumps with conventional systems for building heating purposes. Moreover, the annual efficiencies of these systems have been investigated in terms of primary energy consumption and  $CO_2$  emissions. The comparison was performed for air-to-water and geothermal heat pump systems in two cases of maximum flow temperatures ( $40^\circ C$  and  $60^\circ C$ ). These temperature levels represent typical modern buildings with large heating surfaces and older buildings with high-temperature radiators, respectively. The calculations showed that natural GEHPs achieve about the same efficiency and  $CO_2$  emissions as electrically driven heat pumps powered with electricity from the most modern natural gas-fired combined cycle power plants. The efficiency of such systems is about twice that of conventional boiler technologies. Furthermore, Xu and Yang [44] studied energy saving when GEHP is used instead of conventional electric heat pump in air conditioning system. Moreover, effects of outdoor air operating condition like dry bulb temperature and relative humidity have been taken into considerations. In summer, the maximum saving primary energy percentage for GEHP is 60.5%. With the outdoor air dry-bulb temperature and the relative humidity rises, the energy saving percentage rises. In winter, the maximum saving primary energy percentage for GEHP is 70%.

The energy saving percentage in the frost area is higher than in other areas. Annual energy savings were anticipated at Exeter's new Plaza leisure complex by Maddox [45]. The system consists of a combined chiller/heat pump recovery unit, a gas engine driven combined heat and power unit and a separate heat pump to recover heat from waste water. Results revealed that the system is reckoned to provide a two-year payback on a minimum utilization of eight months per year. Similar results have been concluded by Lian et al. [21]. They introduced the conception of combination of the GEHP and water-loop heat pump system (WLHPS) in order to reduce the energy consumption of air conditioning system. Moreover, a comparison with a conventional air-conditioning system (CACS) and conventional WLHPS (EHP-WLHPS) in terms of technical characteristics and payback period have been made. It is found that the payback period of GEHP-WLHPS is about 2 years when compared with CACS and 2.6 years with EHP-WLHPS on the average.

### 3.3 Investigations on Performance Improving of the GEHP

Various investigations on improving performance of the GEHP systems have also been made. Improving the performance of the GEHP can take place by one of the following:

- Using the gas engine to drive combined refrigeration systems.
- Using the gas engine to drive combined cooling, heating and power system.
- Improving the control strategy of the GEHP.
- Improving the effectiveness of the GEHP heat transfer processes.



### 3.3.1 Gas engine drive combined refrigeration systems

Many researchers interested in using gas engine to drive combined refrigeration system by using the engine mechanical power to drive a vapor compression heat pump (VCHP) and the engine exhaust heat to operate a vapor absorption heat pump (VAHP) or a vapor jet heat pump (VJHP). The performance of three combined absorption/vapor compression cycles was assessed in a theoretical study with regard to their feasibility to enhance the efficiency and capacity of the GEHP by Howe et al. [46]. Coefficients of performance and the capacity have been calculated for typical heating and cooling applications. Operating parameters and the heat duties were also investigated. It has been revealed that a performance improvement up to 31 % for cooling and 17 % for heating can be accomplished with the desorber-absorber heat exchange (DAHX) cycle, and, respectively, 21 % and 11 % for the simple absorption cycle (SC). The total heat duty increases up to 32 % for the DAHX cycle and 23 % for the SC compared with conventional engine-driven systems. The study also indicated that the increase in heat transfer area is smaller than the increase in heat duty due to more favorable heat transfer coefficients. Initial economic considerations indicated that the change in first cost is small because the increased heat exchange surface requirement is offset by smaller compressor and internal combustion engine (ICE) size. The rotary heat pump is "environmentally friendly", as it uses water as the refrigerant and a gas engine to drive the system.

Riffat et al. [47] analyzed a rotary absorption-compression heat pump using  $H_2O/LiBr$  and  $H_2O/NaOH - KOH - CsOH$  as working fluids. Performance calculations have highlighted the sensitivity of the system to solution temperature and concentration, and of the two refrigerant/absorbent combinations considered, the characteristics of the  $H_2O/LiBr$  pair are most suited for cooling applications. A thermal analysis was used to compare a double-effect system against a single-effect system using  $H_2O/LiBr$ . Each of the systems was analyzed using similar temperatures and concentrations. The calculated values of PER for the double-effect system were found to be 3.35 and 2.5, compared with 1.56 and 1.6 for the single-effect system. However, the capital cost of the double-effect system would be far greater than that of the single-effect, due to the complexity of the design.

Yang et al. [48] discussed the optimization of two sorts of combined absorption/compression refrigeration cycles driven by an engine in cooling mode. Combined absorption/compression refrigeration cycles use ammonia and water as the working fluid. The objective function is the primary energy ratio while the constraint is the total heat-exchange area per unit of cooling capacity ( $F_{tot}$ ). The mathematical model has been developed using the optimization toolbox of MATLAB. The obtained trade-off curve in this study is a useful tool for making the trade-off decision between the operating cost and the capital cost. It can be concluded from the trade-off curve that a too high request for the PER is not reasonable because the slope of the increase in PER decreases with increasing ( $F_{tot}$ ). Moreover, the PER of the combined cycles is always better than the conventional compression cycle at the same ( $F_{tot}$ ) since they make use of both the work and the heat output of the engine. Furthermore, the compressor size and the engine

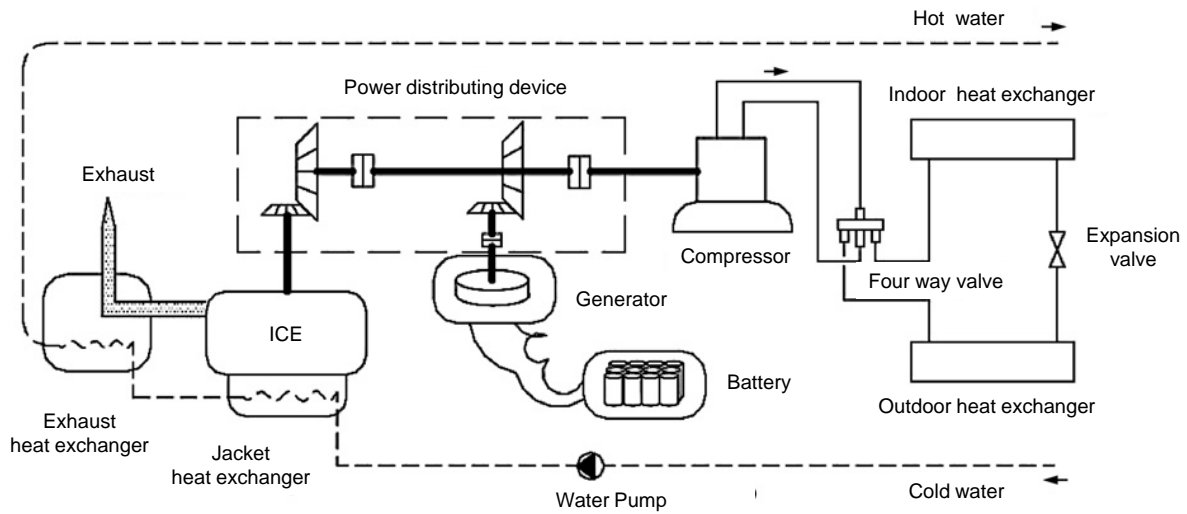


Figure 3.1: Structure of a parallel HPGHP system.

size of the combined cycles are also reduced due to the increased PER. A combined vapor compression-absorption-ejector refrigeration system was theoretically evaluated by Göktun [49]. This integration maximizes the performance of the conventional ejector and absorption cycles and provides high performance for refrigeration. The analysis showed that the combined cycle has a significant increase in system performance over conventional systems. Coefficient of performance of the combined system is higher than its subsystems by about 14%.

### 3.3.2 Gas engine drive combined cooling, heating and power system

GEHP system can be used in combined cooling, heating and power modes [50]. Ying-Lin et al. [51]. designed a hybrid-power gas engine-driven heat pump (HPGEHP) system (Fig. 3.1)<sup>1</sup>. The HPGEHP system mainly comprises three parts such as the power system, the refrigerant system and the water cycle system. The power system includes the ICE, a power distributing device, a generator, battery packs as well as a power control module, etc. The refrigerant system consists of a compressor, an indoor heat exchanger, an outdoor heat exchanger, an expansive valve and a four-way valve, etc. The jacket heat exchanger and the exhaust heat exchanger are important parts of the water cycle system which reclaims the waste heat from the exhaust and jacket in the ICE. Simulation results of the power system showed that for a conventional GEHP system the maximum and minimum thermal efficiencies of the power system are 33% and 22%, respectively; compared with the conventional GEHP system, the power system in the novel HPGEHP system has superior performance with the maximum and minimum thermal efficiencies of 37% and 27%, respectively. An isolated energy-supplying system

<sup>1</sup>This figure is used based on license agreement between the author and Elsevier with license number of 2646390628396.

of the GEHP is discussed by Li et al. [52]. The system has been investigated in several operating modes A(heating, power and cooling), mode B(heating and power), and mode C(heating and cooling). The simulation results show that when the part-load rate of the gas engine is between 70 % to 80 %, the thermal efficiency of the power system is higher, and the maximum can be more than 0.4. Furthermore, among the three different operating modes, the thermal efficiency of the power system is the highest in operating mode C, less in operating mode A, and the least in operating mode B. Notably, in the operating mode C, compared with the conventional GEHP system, the average increase of the thermal efficiency of power system can be about 3.5 %.

Yagyu et al. [53] and [54] designed and tested the performance of a gas engine driven Stirling heat pump using both engine shaft power and engine exhaust heat source. The heat pump is mainly driven by engine shaft power and is partially assisted by thermal power from the engine exhaust heat. By proportioning two energy sources to match heat balance of the driving engine, this heat-assisted Stirling heat pump can be supplied with the maximum share of the original energy fueling the engine and can be operated at the most efficient point. This prototype uses helium gas as a working gas and is constructed as two sets of three-cylinder machines, each a combination of two Stirling sub-systems (one a power producer and one a heat pump). They estimated the total COP as 1.9 and stated that if the HP system could be pressurized up to 5MPa, COP would be improved to 2.42. Moreover developing of the system will provide a CFC-free thermal utilization system technology that satisfies both wide heat demands and various fuel systems.

### 3.3.3 Control strategies of the GEHP

The performance of the GEHP systems could be increased by improving control strategies and systems. During the system operation, the speed of the engine needs to be adjusted under some condition, e.g., a distribution of the thermal load. When the thermal load increases, the engine speed should be increased to match the load, but when the thermal load decreases, the speed should decrease to save energy. Yang et al. [55] developed a new (proportional integral derivative) (PID) fuzzy controlling method to obtain the mechanism of system operation. Moreover, the control scheme in the heating condition of the GEHP was simulated. The dynamic simulation results show that the new controlling method is suitable for the GEHP system. Furthermore, it has the ideal characters of dynamics and stability. The laws of working conditions of the GEHP can be showed perfectly by using this controlling method.

Li et al. [17] described another kind of control strategy for the GEHP, called cascade fuzzy control. The cascade control strategy is effective for systems that have large time constants and disturbances, and a fuzzy control strategy is fit for a system that lacks an accurate model. This cascade fuzzy control structure brings together the best merits of fuzzy control and cascade control structures. In the cascade control system, the secondary controller can overcome the disturbance in the second loop. So, the main disturbance, whose frequency and amplitude are both large, should be included in this

loop. For the GEHP system, the engine speed changes rapidly following a variation in operating condition. So, the engine is disturbed easily in a GEHP system. When the speed of the engine rises, the supply water temperature will rise after a lag time. At that time, the controller would not adjust the throttle if the first control loop did not exist because the temperature has not yet changed. So, the engine speed should be the control input to the secondary loop. If that loop existed, the throttle would be adjusted to keep the speed of the engine unchanged or changed very little. The temperature change of the supply water would be very small. Furthermore, the first controller can aim to overcome this error. The whole effect should be better than one loop if these disturbances had been included in the second loop. The cascade fuzzy control system can be used in process control problems when the temperature, flow and pressure must be controlled within components that have widely varying time constants. Moreover, the performance of the cascade fuzzy control is compared to the cascade PID control strategy, and it is shown by example that the cascade fuzzy control gives a better performance.

An intelligent control simulation is presented to research the dynamic characteristics of the system in the heating operation by Zhao et al. [56]. The GEHP system simulation model consists of eight models for its components including a natural gas engine, a compressor, a condenser, an expansion valve, an evaporator, a cylinder jacket heat exchanger, an exhaust gas heat exchanger and an auxiliary heater. The intelligent control model is composed of the prediction controller model and the combined controller model. The prediction controller based on neural network can be used for predicting the building load at the next moment. The combined controller consists of a PID controller, a fuzzy controller and a Smith controller. The simulation results show that its dynamic and steady characteristics are satisfactory. Furthermore, the intelligent controller can eliminate the disadvantages of long time delay, large inertia and nonlinearity of the heating system and achieve good steady state accuracy and dynamic characteristics. Moreover, it has the feasibility to use in the heating system to realize energy saving and comfort.

### 3.3.4 Improving the effectiveness of the GEHP processes

Improving the effectiveness of the GEHP processes represents one the most methods which researcher was interest in to enhance the performance of the GEHP. Increasing of heat exchangers effectiveness and controlling the system operation especially at the abnormal conditions have been used to achieve such goals. Ott et al. [57] outfitted the GEHP with a graphite foam radiator, demonstrated its thermal efficiency and compared it with a conventional radiator. A sequence of tests was performed with the graphite foam radiator operating in series with the standard aluminum radiator. Laboratory experiments have demonstrated that standard radiator alone, removed 16,555W of heat and had a calculated overall heat transfer coefficient of  $32 \text{ W}/(m^2\text{K})$  for surface area of  $25.4m^2$ . Graphite foam radiator alone, dissipated 14,820W of heat and the overall heat transfer coefficient calculated using  $1.68m^2$  surface area was  $182 \text{ W}/(m^2\text{K})$ . This value is 5.7times greater than the standard radiators overall heat transfer coefficient, establishing the graphite foam as a more efficient radiator at removing heat from the

coolant and transferring it to the surrounding air. Moreover, graphite foam radiator will be smaller in size, lesser weight, requires lesser cooling air, and be quicker at removing heat than a conventional aluminum radiator. A liquid overfeed (LOF) recuperative cycle concept can simplify the hardware design of the GEHP, resulting in reduced cost and improved performance. The overfeed means much more liquid is fed to evaporator than the liquid actually vaporizes. Excess liquid is called overfeed, which returns to low pressure side accumulator or low pressure receiver. By over feeding the evaporator, the inner surface is kept thoroughly wetted and thus achieves optimum heat transfer. Chen et al. [58] investigated the effect of LOF concept on performance of GEHP. Laboratory tests show that LOF improves the energy efficiency of a vapor compression unit by 10%. Also, LOF reduces compressor pressure ratio, thereby improving equipment reliability. Regarding to improve the performance of the GEHP by controlling the system operation, Li and Zhang [59] introduced a new defrosting method by waste heat on the GEHP. From the two aspects of systematic operating reliability and energy balance, the results show that the fluctuation of heat water temperature in the heat-preserved water tank is between 16°C to 25°C, also the heat water temperature in the water tank can be kept over 55°C during the systematic defrosting, so the heat-recycling defrosting method is feasible. Furthermore comparing with reverse defrosting and sensible heat defrosting, the consumed energy for defrosting is the lowest, and the heat supplying and the average performance coefficient is the highest. Hence the waste heat defrosting is an effective and energy-saving defrosting method.

Xu and Yang [44] performed a mathematical model to study the effect of gathering the exhaust heat of the gas engine to prevent the outdoor heat exchanger from frosting. The results show that the outdoor temperature and humidity have less influence on the performance and the energy usage ratio is higher for the no-frosting GEHP than the conventional GEHP; the maximum coefficient of performance for the system is 5.00, while the maximum primary energy ratio is 1.97. It is proved that the exhaust heat can heat the room directly and raise the evaporation temperature to prevent the heat exchanger from frosting to improve the performance of the system. Xu and Yang [60] developed a mathematical model of an improved GEHP by using the waste heat from the gas engine to control the humidity of the room. The model confirm that GEHP, which can control the room humidity, can be used in more areas than the common GEHP. Moreover, results from the analysis show that the GEHP can save more energy than the electrical heat pump. The maximum energy saving for the GEHP is over 63% in summer and over 75% in winter. The maximum PER for the system is over 1.9.

### 3.4 Modelling of the GEHP Systems

Another important area was modelling of the GEHP systems. An early modeling study about the GEHP systems was done by MacArthur and Gerald [61]. They presented a dynamic model of vapor compression heat pump, including a mathematical treatment of the condenser and the evaporator. Lumped-parameter models were developed for the expansion device, the gas engine and the compressor. The spatial variations of

temperature, enthalpy, mass flow rate and density are predicted at each point in time for the two heat exchangers. The engine model consists of five major components: the throttle body sub model to simulate the intake system; engine steady state performance maps developed from a detailed model of the engine; the engine heat transfer sub model for heat flow from the cylinder to the coolant and the ambient; engine structure temperature corrections to the steady state performance maps; and the ignition-off representation of the engine. The three node heat transfer model simulates heat flow between the inner structure of the engine and the coolant, to the outer structure and the environment. The results of the heat pump model for the compressor has been compared with laboratory data at several ambient conditions and compressor speeds. Good agreement between model and laboratory results was demonstrated in the cooling mode for an ambient temperature of 101.5°F and compressor speed of 978rpm as well as for an ambient temperature of 75°F and compressor speed of 1512rpm [61].

D'accadia et al. [62] introduced a finite-time approach to investigate the performance of the GEHP in heating mode. The irreversibilities have been assumed only due to heat transfer under finite temperature differences in order to get optimum performance of the GEHP. The results show that the optimum conditions, based on maximum overall heat flow rate, influenced by several variables occur in operation conditions different from those of prime mover optimization. Moreover, the optimum conditions of such a system are achieved in a range of prime mover Carnot temperature ratios in which the COP is, by far, lower than that of fully reversible equipment (Carnot limit). The provided results by the model with internal heat leaks, are compared to the performances of the actual GEHP. The evaluated COP is very close to that available from the GEHP manufacturers and field test results (1% of the average values). A further comparison has been performed between the model and the GEHP mathematical model. In this case, the COP is also very similar (-3%). Furthermore, the exergetic efficiencies and the irreversibility distributions are in good agreement.

Yang et al. [63] improved a dynamic model taking into consideration the exhaust gas. A computer program was also developed for the model. The results indicate that the exhaust gas flux in the gas heat exchanger fluctuates periodically because of the discontinuous discharge from the cylinders. The feature of non-steady flow is obvious. A comparison of the experimental results indicates that the mathematical model presented could simulate the thermodynamic performance of the system satisfactorily and could be used to guide the design of the exhaust heat recovery system for the GEHP. Zhang et al. [64] established another simulation tool, which contained a theoretical heat recovery model. In this study, the heating performance of the gas engine driven air-to water heat pump was analyzed using a steady state model. The thermodynamic model of a natural gas engine is identified by the experimental data and the compressor model is created by several empirical equations. The heat exchanger models are developed by using heat balances. The system model is validated by comparing the experimental and simulation data, which show good agreement. Following this model, Shin et al. [65] introduced a dynamics modeling of the GEHP in cooling mode. The dynamics modeling of the GEHP was based on conservation laws of mass and energy. The modelling results

revealed that the behavior of simulated temperatures, pressures and COP was found to be close to those of real system. Furthermore, the simulation results were found to be realistic enough to apply for control algorithm design. The model can be applied to build a virtual real-time GEHP system so that it interfaces with a real controller in purpose of prototyping control algorithm. A recently thermal modeling of the GEHP system was developed by Sanaye and Chahartaghi [66]. The model including both the heat pump and engine systems was performed and the system operating parameters such as operating pressures, coefficient of performance and fuel consumption of the GEHP were computed. The simulation results confirm that by increasing the cooling/heating capacity, the compressor pressure ratio, and the compressor specific work, increase up to about the nominal cooling or heating capacities. As a result a higher COP value for the GEHP system was obtained in this case. On the other hand with further increase in cooling/heating capacity, the pressure ratio may increase which provides a decrease in COP of cooling/heating system due to increase in compressor work. The comparison of results from modeling and measured data for the compressor suction and discharge pressures, gas engine fuel consumption, and COP of the GEHP system showed the average values of difference percent points for suction and discharge pressures, fuel consumption and COP of the GEHP system showed 3.4%, 4%, 6.7% and 7.2% in cooling mode and 3.7%, 5.4%, 8.1% and 7.8% in heating mode respectively.

Deng et al. [67] analyzed performance of a household GEHP at varied environment temperature using empirical equations of the system parts. By coupling the equations, the relationships of primary energy ratio and effective gas consumption rate (EGCR) with environment temperature were obtained. The result shows that the system had its optimum performance at 33-35°C in summer and 0-5°C in winter. When the environment temperature diverged from the appropriate temperature, the EGCR of the system would increase and the PER of the system would decrease.

### 3.5 Commercial and Industrial Applications of the GEHP

There are many studies have been found in the open literature interested with commercial and industrial applications of the GEHP. The development and possible uses of the GEHP from the technical and economic aspects for residential space heating was investigated in East Germany by Achim and Manfred [68]. In 1981, an experimental set up of the GEHP was constructed and tested by Joerg [69] for one and two family houses demands. The system has been used in low heating power using air-water-heat pump driven by gas engine. The gas engine used for the first time to drive the heat pump has an output of about 7 kW at 1600 rpm. Results show that the GEHP performance depends on the external air and hot water temperature. Following this study, Newbert [70] showed that the energy consumption could be reduced by 40% with a coupled GEHP for heating a malt house and for drying of malt. Tassou [71] presented a simple methodology which enables the sizing and performance analysis of the GEHP in sewage effluent heat recovery applications. Using typical winter effluent temperatures from sewage treatment plants

in the south of England it is proved that the GEHP systems could provide substantial savings in sewage effluent heat recovery applications when compared to natural gas boilers. The recovered heat can be either used to satisfy the heating needs of the plant or exported to neighboring agricultural or industrial complexes. Maidment et al. [72] investigated the practical and economic viability of a combined cooling and heating system driven by a gas engine in a supermarket. The system consists of a direct-drive screw compressor, which is powered by a throttle controlled gas engine. The waste heat from the engine is used to provide hot water for space heating and for general usage within the catering and toilet facilities in the supermarket. They calculate the energy consumed by the conventional system and that used by a number of alternative combined heating and cooling system configurations. The results revealed that, the commercial and environmental viability of this scheme maybe significantly improved with optimization and economies of scale. Also, further improvements may be achieved if a use for the waste heat, rejected during the summer period is found. One solution to this that has been considered in cold storage facilities is to use the waste heat to power an absorption chiller, which provides cold glycol for use with the chilled food load.

Lazzarin and Noro [22] evaluated the performance of "S. Nicola" HVAC plant in Vicenza set up by a GEHP during three years of operation. The HVAC plant is set up by: (a) Heating and cooling plant (natural gas internal combustion - engine heat pump/chiller and condensing boilers); (b) Ventilation and air conditioning plant to control relative humidity and for the necessary air changing inside the building); (c) Air extraction plant. The nominal cooling power of the plant is 275 kW, while in heating mode the output power is 380 kW. Heat recovery is taken from the lubricating oil, engine cooling water and partly from the exhaust. The nominal power thus recovered is 109 kW in heating mode and 127 kW in cooling mode, to produce hot water at about 70°C. Two hydraulic circuits are provided. The primary one supplies chilled water in summer (7/12°C) and warm water in winter (45/40°C) produced by the heat pump and the secondary one hot water at 70°C given by the heat recovery. The analysis of the plant demonstrated that, from the economic point of view, such an alternative is definitely disadvantageous; sensitivity analysis shows that no selling price of the useful kWh will be competitive with actual plant performances. On the contrary, current plant layout is among the most modern and efficient heating technologies with an overall energy efficiency often better than the co-generation in district heating as stated by Lazzarin and Noro [73].

A gas engine driven prototype system combined cold and heat, whose waste heat was recovered for heating or hot water supply, was set up and tested by Sun et al. [74] and sun [75]. Energetic efficiency evaluation of the combined system of cold and heat is also presented, where primary energy rate and comparative primary energy saving are used. The system gas consumption from natural was about 321 kW at full load. The nominal cooling capacity of prototype was 450.6 kW (Input and output temperature of chilled water are 12°C and 7°C, respectively). The recovered heat quantity from engine jacket cooling and exhaust gas was about 143 kW. The experimental results showed that the primary energy rate of the combined system was about 1.90. Moreover, from the thermodynamic point of view, owing to recover and utilize engine waste heat,



the gas engine driven combined cooling and heating system described has high energy utilization efficiency. Primary energy rate for the combined system of cold and heat, for conventional separate system of cold and heat, and comparative saving of primary energy demand are expressed and calculated. The results revealed that the prototype system save more than 35% of primary energy compared to the conventional separate systems of required energy flows. This indicates a large potential for energy saving in the combined system of cold and heat.

An integrated refrigeration system (IRS) with a gas engine, a vapor-compression chiller and an absorption chiller is set up and tested by Sun [76]. IRS mainly includes three parts; gas engine, vapor compression chiller and LiBr absorption chiller. The power (shaft work), which is used to operate the compression refrigeration cycle in an IRS, is provided by the gas engine. The waste heat from the gas engine is utilized to operate the absorption refrigeration system. The experimental results showed that the refrigerating capacity of the IRS prototype reached  $596.2\text{kW}$  at air conditioning rated conditions in China when the speed of gas engine was  $1800\text{ rpm}$  and  $323.3\text{ kW}$  natural gas was consumed. Moreover PER of prototype reached 1.84 at the rated conditions. The refrigerating capacity of prototype reduced and energy utilization ratio of the prototype increased with the decrease of the gas engine speed. In order to ensure the prototype to operate at high efficiency, it is better to regulate the load of IRS by regulating the speed of the gas engine. Furthermore, the refrigerating capacity and PER of the prototype increased with the increase of the outlet temperature of chilled water or the decrease of the inlet temperature of cooling water.

Mahderekal et al. [77] investigated an innovative 10 TR natural gas engine-driven heat pump for commercial application. The unit was tested at various Air Conditioning and Refrigeration Institute (ARI) heating and cooling conditions in a psychometric chamber at Oak Ridge National Laboratory. The gas COP at  $47^\circ\text{F}$  rating condition exceeded the goal of 1.6 at both high and intermediate engine speeds. The gas COP in cooling mode also exceeded the goal of 1.2 at  $95^\circ\text{F}$  rating condition.

A research project on the GEHP has been recently implemented by Hepbasli and et al. [78]. In this regard, they designed a gas engine driven solar assisted band conveyor heat pump drying system, as shown in Fig. 3.2<sup>2</sup> and applied this system to food drying. The system consists of mainly four sections, namely: (i) a GEHP unit with heating capacity of  $18\text{kW}$ , (ii) a heat pump unit with scroll modified for compression with enhanced vapour injection, (iii) an air solar collector and (iiii) a band conveyor dryer. The project aimed at comparing the new drying system applied for tunnel drying of parsley, broccoli and plums with conventional drying systems (i.e., tray dryer and fluidized bed dryer) based on energy and exergy efficiencies, product quality and economics. The project will help in becoming widespread industrial applications of the GEHP systems in drying processes, especially in food industry.

---

<sup>2</sup>This figure is used based on license agreement between the author and Elsevier with license number of 2642480683987.

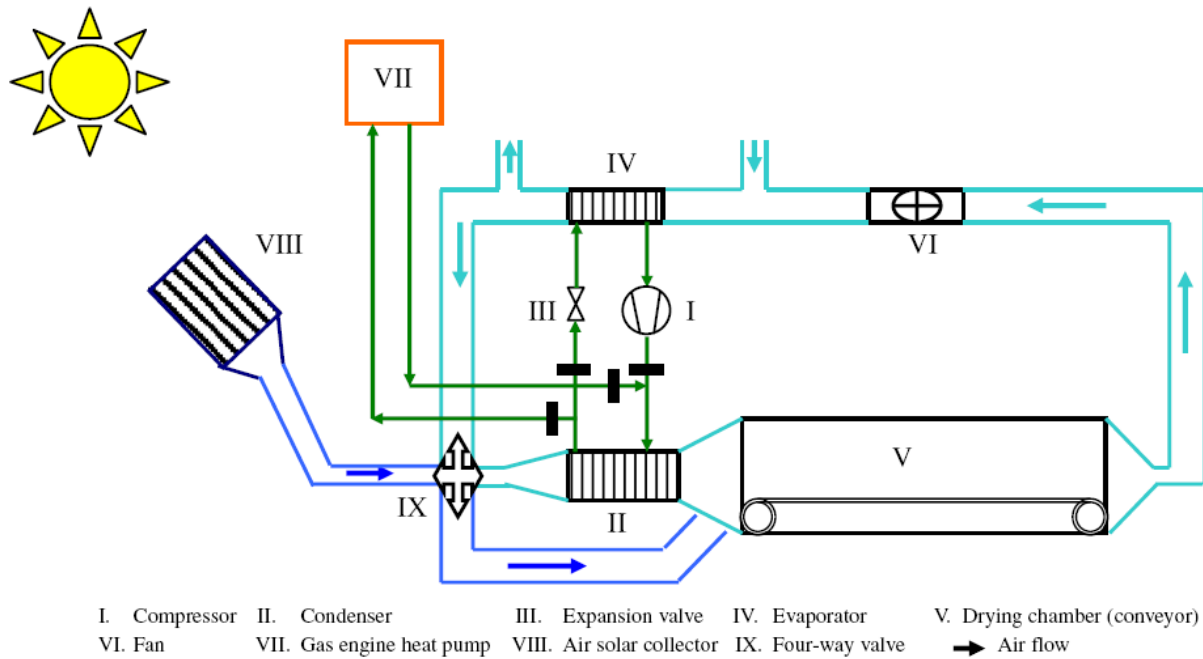


Figure 3.2: Schematic view of a gas engine driven solar assisted band conveyor heat pump drying system.

### 3.6 Environmental Effect of the GEHP

The most important feature of the GEHP systems is the lower harmful effect to the environment. Creamer and Saunders [79] evaluated the exhaust train of a 3.73 kW natural gas engine. The engine was developed for use in the GEHP and is designed for operation at lean air/fuel ratios. The converter tested had a metallic substrate with a cell density of 31cells/cm<sup>2</sup>. Converter tests measured emission performance as a function of the key engine variables: speed, load, spark advance and air/fuel ratio. CO conversion averaged well above 90% whereas hydrocarbon conversion varied between 68.6% and 89.8% over a range of 8 speed and load combinations selected to cover the normal operating range of the engine. Energy efficiency and source air pollutant emission factors of gas heaters, gas engine heat pumps, and electric heat pumps for domestic heating have been evaluated and compared by Ganji [80]. The analysis shows that with the present state of technology, GEHP have the highest energy efficiency followed by electric heat pumps and then gas heaters. Electric heat pumps produce more than twice as much NO<sub>x</sub>, and comparable CO<sub>2</sub> and CO per unit of useful heating energy compared to natural gas heaters. CO production per unit of useful heating energy from gas engine heat pumps without any emission control is substantially higher than electric heat pumps and natural gas heaters. NO<sub>x</sub> production per unit of useful heating energy from natural gas engine heat pumps (using lean burn technology) without any emission control is about the same as effective NO<sub>x</sub> production from electric heat pumps. GEHP produce about one-half CO<sub>2</sub> compared to electric heat pumps.

### 3.7 Investigation of R22 Alternative Refrigerants

Due to the impending ban of refrigerant R22 production, there is a pressing need for studies on the performance characteristics of alternative refrigerants in air-conditioning and heat pump systems. Therefore a survey of the previous investigations on R22 replacement refrigerants in these systems is a very important part of this present study. Radermacher and Jung [81] conducted a simulation study of potential R22 replacements in residential equipment. The coefficient of performance and the seasonal performance factor were calculated for binary and ternary substitutes for R22. They found that for a ternary mixture of R32/R152A/R124 with a concentration of 20 wt %/20 wt %/60 wt %, the COP was 13.7 % larger and the compressor volumetric capacity was 23 % smaller than the respective values for R22. This study found that in general, based on thermodynamic properties only, refrigerant mixtures have the potential to replace R22 without a loss in efficiency. Efficiency gains are possible when counter flow heat exchangers are used and additional efficiency gains are possible when capacity modification is employed.

Some selected refrigerants have been assessed for their suitability as alternatives to R22 for air conditioners by Devotta et al.[82]. Only those refrigerants with zero ozone depletion potential are considered. Among the refrigerants studied (R134A, R290, R407C, R410A, and three blends of R32, R134A and R125), R134A offers the highest COP, but its capacity is the lowest and requires much larger compressors. The characteristics of R290 are very close to those of R22, and compressors require very little modification. For retrofitting, R407C is probably the best candidate. Kondepudi [83] performed experimental "drop-in" (unchanged system, same heat exchangers) testing of R32/R-134A and R32/R152A blends in a two-ton split-system air conditioner. Five different refrigerant blends of R32 with R134A and R152A were tested as "drop-in" refrigerants against a set of R22 baseline tests for comparison. No hardware changes were made except for the use of a hand-operated expansion device, which allowed for a "drop-in" comparison of the refrigerant blends. Hence, other than the use of a different lubricant and a hand-operated expansion valve, no form of optimization was performed for the refrigerant blends. Parameters measured included capacity, efficiency, and seasonal efficiency. The steady state energy efficiency ratio and seasonal efficiency energy efficiency ratio of all the R32/R134A and R32/R152A blends tested were within 2 % of those for a system using R22. The 40 wt %/60 wt % blend of R32/R134A performed the best in a non-optimized system.

Domanski and Didion [84] evaluated the performance of nine R22 alternatives. The study was conducted using a semi-theoretical model of a residential heat pump with a pure cross-flow representation of heat transfer in the evaporator and condenser. The models did not include transport properties since they carried the implicit assumption that transport properties (and the overall heat transfer coefficients) are the same for the fluids studied. Simulations were conducted for "drop-in" performance, for performance in a modified system to assess the fluids' potentials, and for performance in a modified system equipped with a liquid line/suction-line heat exchanger. The simulation results obtained from the "drop-in" evaluation predicted the performance of

candidate replacement refrigerants tested in a system designed for the original refrigerant, with a possible modification of the expansion device. The "drop-in" model evaluations revealed significant differences in performance for high-pressure fluids with respect to R22 and indicated possible safety problems if those fluids were used in unmodified R22 equipment. The simulation results obtained from the constant heat-exchanger-loading evaluation corresponded to a test in a system modified specifically for each refrigerant to obtain the same heat flux through the evaporator and condenser at the design rating point. This simulation constraint ensures that the evaporator pressures are not affected by the different volumetric capacities of the refrigerants studied. The results for the modified system performance showed that capacity differences were larger for modified systems than for the "drop-in" evaluation. However, none of the candidate replacement refrigerants exceeded the COP of R22 at any of the test conditions.

Bivens et al.[85] compared experimental performance tests with ternary and binary mixtures in a split system residential heat pump as well as a window air-conditioner. This study investigated refrigerants R407C, a ternary zeotropic mixture of 23 wt % R32, 25 wt % R125 and 52 wt % R-134A, and R410B, a near azeotropic binary mixture composed of 45 wt % R32 and 55 wt % R125 as working fluids. The heat pump used for the evaluations was designed to operate with R22 and was equipped with a fin-and-tube evaporator with 4 refrigerant flow parallel circuits, and a condenser with five circuits and one sub-cooling circuit. It was found that R407C provided essentially the same cooling capacity as compared with R22 with no equipment modification. R410B provided a close match in cooling capacity using modified compressor and expansion devices. The energy efficiency ratio for R407C versus R22 during cooling ranged from 0.95 to 0.97. The energy efficiency ratio for R410B versus R22 during cooling ranged from 1.01 to 1.04. In summation, in the search for a replacement for refrigerant R22 many refrigerants have been studied. Many of those studied are refrigerant mixtures. The refrigerant mixtures studied by the sources cited in this literature survey are summarized below:

- A. Refrigerant R410A - R32/50 %, R125/50 % (weight percent)
- B. Refrigerant R407B R32/45 %, R125/55 % (weight percent)
- C. Refrigerant R407C R32/23 %, R125/25 %, R134A/52 % (weight percent)

Hence, refrigerant R410A has emerged as the primary candidate to replace R22 in many industrial and residential applications.

### 3.8 Conclusions on the Literature Review

The literature survey revealed that although many investigations were carried out on gas engine heat pump working with R22 alternatives, a little work was conducted on the GEHP running with R410A to evaluate its performance at various operating conditions. Moreover, although secondary heat transfer fluid mass flow rate has a considerable influence on the performance characteristics of the GEHP, previous investigators did not explore its effect even for gas engine heat pump using R410A. However, there is a lack of information on the performance characteristics of the GEHP working with R410 for cooling, heating and combined cooling and heating modes applications. Furthermore,

a thermal modelling of the GEHP including both the heat pump and engine systems is essential. Therefore, the present work aimed at evaluating the performance characteristics of the GEHP for various operating modes namely; cooling mode, heating mode and combined cooling and heating mode. A GEHP fabricated by AISIN Company was installed and equipped with necessary instrumentation. R410A was used as a primary working fluid and water and air was adopted as the secondary heat transfer fluid at both the indoor and outdoor units respectively. Influences of indoor unit water inlet temperature, indoor unit water flow rate, ambient air temperature and engine speed on the performance characteristics of the GEHP were experimentally investigated. Moreover, a thermal modeling of the GEHP was performed and the system operating parameters such as cooling capacity, gas engine heat consumption and primary energy ratio were computed.



# Chapter 4

## THEORETICAL ANALYSIS OF A GAS ENGINE HEAT PUMP

In this chapter, a theoretical analysis of a gas engine heat pump as well as a parametric study have been introduced. Firstly, a comparison of R22 alternatives based on energy analysis is done in order to select the best alternative. Secondly, a full parametric study including both heat pump and gas engine main operating parameters for the best alternative refrigerant have been presented. The effect of evaporation and condensation temperatures, subcooling and superheating degrees, compressor isentropic and engine thermal efficiencies have been discussed.

### 4.1 Operating Principle of Gas Engine Heat Pump

Figure 4.1 shows a schematic diagram of a simple gas engine heat pump. It consists of three main parts namely; a gas engine, a heat pump, and a heat recovery system. The heat pump is a vapour compression heat pump which includes a compressor, a condenser, an expansion valve and an evaporator. The heat recovery system consists of two heat exchangers. The main function of the heat recovery system is to recover both engine cooling heat and exhaust gas heat. The gas engine heat pump can be used in several operating mode namely; cooling, heating and combined cooling and heating mode. In all modes of operation, the gas engine heat consumption ( $\dot{Q}_{gas}$ ) represents the source of the system operation. In cooling mode, the evaporator cooling capacity ( $\dot{Q}_{evap}$ ) is the main target while in combined cooling and heating mode both recovered engine heat ( $\dot{Q}_{HR}$ ) and evaporator cooling capacity are the system goals. Both condenser heating capacity ( $\dot{Q}_{cond}$ ) and recovered engine heat ( $\dot{Q}_{HR}$ ) are the system output in heating mode.

### 4.2 Assumptions

Several assumptions have been made to analysis the gas engine heat pump circuit. They are;

- (a) steady state operation of the system,
- (b) pressure changes only through the compressor and expansion device,

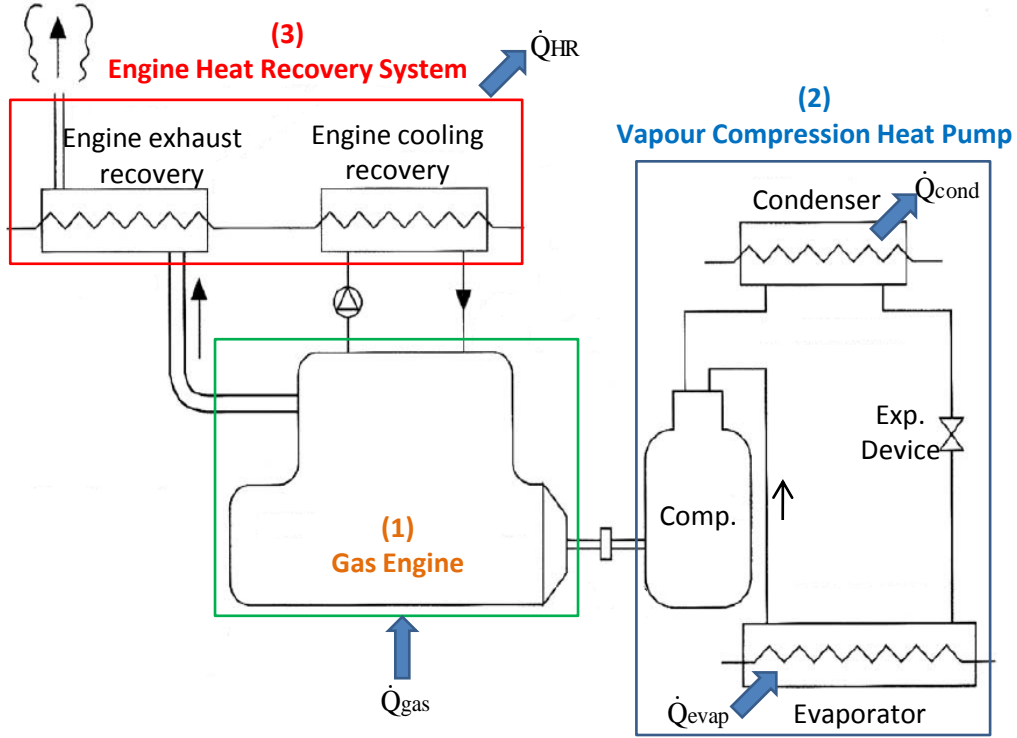


Figure 4.1: Simple gas engine driven heat pump.

- (c) heat losses or heat gain from or to the system are ignored,
- (d) constant source and sink reservoir temperatures,
- (e) constant engine speed of 1750 rpm,
- (f) compressor swept volume ( $V_s$ ) is  $104 \text{ cm}^3/\text{rev}$

### 4.3 Analysis of a Gas Engine Heat Pump

Analysis of the gas engine heat pump includes both vapor compression heat pump and gas engine. Log(p)-h of the heat pump circuit is shown in Fig. 4.2. The various thermodynamic processes involved in the heat pump cycle are;

- (a) adiabatic compression process (1 to 2),
- (b) heat rejection process (2 to 3),
- (c) throttling process (3 to 4),
- (d) heat absorption process (4 to 1).

The cycle operates between the condenser pressure ( $p_{cond}$ ) and the evaporator pressure ( $p_{evap}$ ). The condenser and evaporator pressures are determined according to the condensation and evaporation temperatures, respectively, i.e.

$$p_{cond} = p(\vartheta_{cond}) \quad (4.1)$$

and

$$p_{evap} = p(\vartheta_{evap}) \quad (4.2)$$



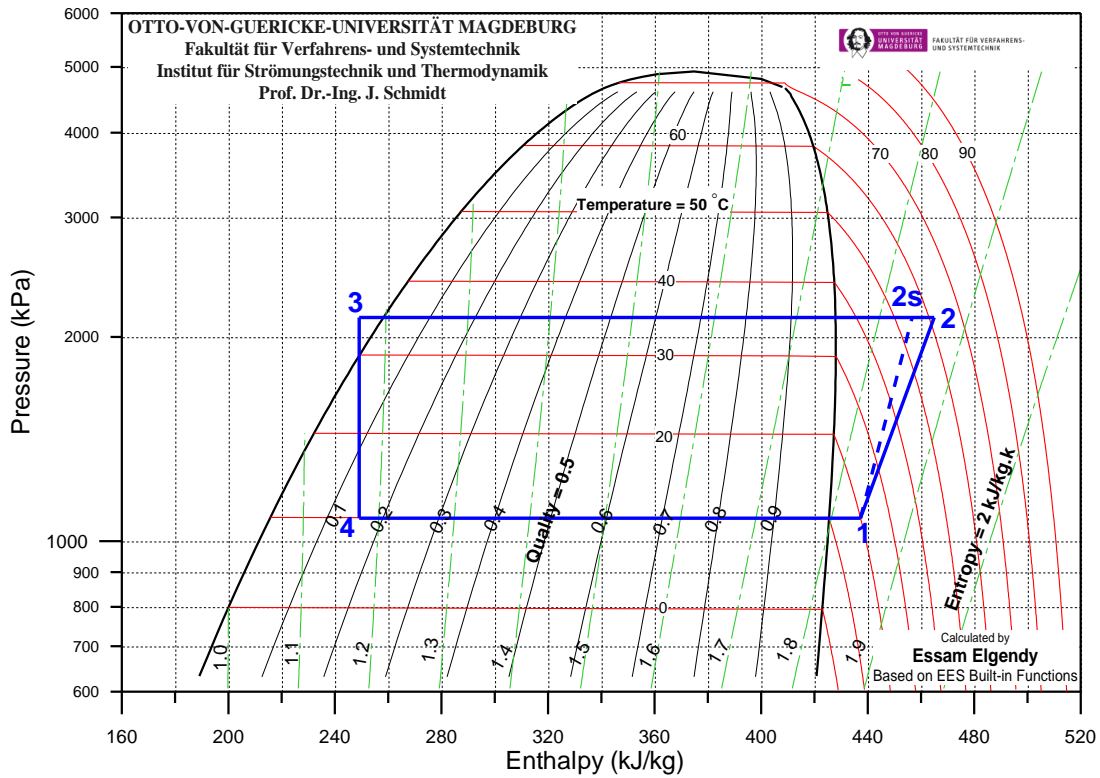


Figure 4.2: Log(p)-h diagram for heat pump circuit.

Since no pressure losses, the following equation may be written.

$$p_3 = p_2 = p_{cond} = p(\vartheta_{cond}) \quad (4.3)$$

and

$$p_4 = p_1 = p_{evap} = p(\vartheta_{evap}) \quad (4.4)$$

The condensation temperature is determined by the temperature of the heat sink whereas the evaporation temperature is determined by the available temperature of the heat source and heat transfer temperature difference.

### 4.3.1 Adiabatic compression process

During this process the vapor refrigerant at low-pressure ( $p_1$ ) and low temperature ( $\vartheta_1$ ) is compressed adiabatically to high-pressure ( $p_2$ ) and temperature ( $\vartheta_2$ ) along the line 1 to 2 on the p-h diagram. Isentropic compressor efficiency ( $\eta_{is,comp}$ ) can be written in the following form;

$$\eta_{is,comp} = \frac{h_{2,is} - h_1}{h_2 - h_1} \quad (4.5)$$

Where  $h_1$  is the specific enthalpy of the superheated vapor refrigerant at the compressor inlet whereas  $h_2$  and  $h_{2,is}$  are the superheated vapor enthalpies at the compressor exit for actual (adiabatic) and ideal (isentropic) compression processes, i.e.

$$h_1 = h(p_{evap}, \vartheta_1) \quad (4.6)$$

$$h_{2,is} = h(p_{cond}, \vartheta_{2,is}) \quad (4.7)$$

$$\vartheta_{2,is} = \vartheta(s_{2,is}, p_{cond}) \quad (4.8)$$

where

$$s_{2,is} = s_{1,is} \quad (4.9)$$

$s_1$  is the specific entropy of the superheated vapor refrigerant at the evaporator pressure ( $p_{evap}$ ) and suction temperature ( $\vartheta_1$ ), i.e

$$s_1 = s(p_{evap}, \vartheta_1) \quad (4.10)$$

Actual specific enthalpy of the superheated vapor refrigerant at the compressor exit ( $h_2$ ) can be calculated using Eq.4.5 as the following;

$$h_2 = h_1 + \frac{h_{2s} - h_1}{\eta_{is,comp}} \quad (4.11)$$

The power required to drive the compressor ( $P_{comp}$ ) is given by

$$P_{comp} = \dot{M}_{ref}(h_2 - h_1) \quad (4.12)$$

where  $\dot{M}_{ref}$  is refrigerant mass flow rate and can be estimated using the following equation;

$$\dot{M}_{ref} = \eta_{vol} V_s N_{comp} \rho_1 \quad (4.13)$$

where  $\eta_{vol}$ ,  $V_s$  and  $N_{comp}$  are the volumetric efficiency, the swept volume and the rotational speed of the compressor, respectively while  $\rho_1$  is the vapor refrigerant density at the compressor suction. Volumetric efficiency of the compressor is calculated as a function of the pressure ratio ( $PR$ ) according to the derived following experimental equation;

$$\eta_{vol} = 0.993618 - 0.05285PR \quad (4.14)$$

where  $PR$  defined as the ratio between condenser pressure to evaporator pressure;

$$PR = \frac{p_{cond}}{p_{evap}} \quad (4.15)$$

### 4.3.2 Heat rejection process

During this process, the high pressure high temperature vapor refrigerant from the compressor is firstly desuperheated and then completely condensed at constant pressure ( $p_{cond}$ ), and finally subcooled as shown by the horizontal line 2-3 on the p-h diagram Fig. 4.2. Thus, the superheated vapor refrigerant is changed into subcooled liquid refrigerant. The refrigerant gives its sensible and latent heats to the cooling medium. The condenser heat load is estimated as;

$$\dot{Q}_{cond} = \dot{M}_{ref}(h_2 - h_3) \quad (4.16)$$

### 4.3.3 Throttling process

The subcooled liquid refrigerant at the condenser pressure ( $p_{cond}$ ) is expanded through the expansion device to low pressure ( $p_{evap}$ ) as shown by the vertical line 3 to 4 on the p-h diagram (Fig. 4.2), i.e

$$h_4 = h_3 \quad (4.17)$$

### 4.3.4 Heat absorption process

During this process, the mixture refrigerant absorbs its latent heat of vaporization from the load, thereby the mixture refrigerant is evaporated and changed into superheated vapor refrigerant at constant pressure ( $p_{evap}$ ) as shown by the horizontal line (4 to 1) on the p-h diagram (Fig. 4.2). The evaporator heat load ( $\dot{Q}_{evap}$ ) can be written given as;

$$\dot{Q}_{evap} = \dot{M}_{ref}(h_1 - h_4) \quad (4.18)$$

### 4.3.5 Gas engine

Gas engine heat consumption can be calculated as a function of compressor power as;

$$\dot{Q}_{gas} = \frac{P_{comp}}{\eta_{th}} \quad (4.19)$$

where  $\eta_{th}$  represents engine thermal efficiency. Recovered engine heat ( $\dot{Q}_{HR}$ ) can be estimated as 75 % of the total heat released [86], i.e

$$\dot{Q}_{HR} = 0.75(\dot{Q}_{gas} - P_{comp}) \quad (4.20)$$

### 4.3.6 Performance characteristics of the GEHP

Performance of the GEHP is calculated as a ratio between the useful heat to the gas engine heat consumption. The primary energy ratio term has been used to describe the GEHP performance as the following;

for cooling mode,

$$PER_{cooling} = \frac{\dot{Q}_{evap}}{\dot{Q}_{gas}} \quad (4.21)$$

for heating mode,

$$PER_{heating} = \frac{\dot{Q}_{cond} + \dot{Q}_{HR}}{\dot{Q}_{gas}} = \frac{\dot{Q}_{tot,heating}}{\dot{Q}_{gas}} \quad (4.22)$$

for combined heating and cooling mode,

$$PER_{combined} = \frac{\dot{Q}_{evap} + \dot{Q}_{HR}}{\dot{Q}_{gas}} = \frac{\dot{Q}_{tot,combined}}{\dot{Q}_{gas}} \quad (4.23)$$

## 4.4 Simulation Results

A computer program based on equations (Eq.4.1) to (Eq.4.23) is developed using EES software [87]. The aim of this program is to comparatively assess the performance of the GEHP working with R134A along with R407C and R410A as alternatives to R22. The input data for simulation are internal operating parameters such as, evaporation temperature, condensation temperature, degrees of superheating, degrees of subcooling and refrigerant type. The program calculates heat loads and primary energy ratio for different operating modes. Then, the effect of operating conditions such as evaporation temperature, condensation temperature, degrees of subcooling, degrees of superheating, isentropic and thermal efficiencies for the best alternative have been discussed.

### 4.4.1 Comparison among working fluids

Figure 4.3 shows a comparison between three of R22 alternative working fluids used for a GEHP in heating mode at constant operating conditions. The working fluids are R134A, R407C and R410A. Condensation temperature ( $40^{\circ}\text{C}$ ), engine speed (1750rpm), subcooling degrees ( $5K$ ), superheating degrees ( $10K$ ) as well as isentropic (70 %) and thermal efficiencies (25 %) are held constant. Evaporation temperature was varied in range of  $-5^{\circ}\text{C}$  to  $15^{\circ}\text{C}$  which represents the heating mode operating range. Comparison of the refrigerant pressures and refrigerant mass flow rates is presented in Fig. 4.3A while comparison of heat loads is introduced in Fig. 4.3B. Primary energy ratio of the GEHP using the selected working fluids is shown in Fig. 4.3C.

Obviously, R410A has the highest operating pressure followed by R407C and R134A. It is well known that the slope of the line representing the relation between  $\ln(p)$  and  $1/\vartheta$  of a refrigerant is a function of its boiling point. The higher boiling point, the steeper the slope of the line. Thus, according to the boiling point, R410A have the highest slope followed by R407C and R134A respectively. According to Eq.4.13 and for constant swept volume ( $104\text{ cm}^3/\text{rev}$ ), engine speed (1750rpm) and volumetric efficiency (0.85), refrigerant mass flow rate depends mainly on the refrigerant density. By other words, the higher operating pressure refrigerant is the higher density and consequently higher mass flow rate. Thus, R410A is the highest operating mass flow rate followed by R407C and R134A. As evaporation temperature changed from  $-5^{\circ}\text{C}$  to  $15^{\circ}\text{C}$  refrigerant mass flow rate increases by 100.05 % and 30.8 % for R410A and R407C relative to R134A. The system heat loads can be estimated using both enthalpy difference and refrigerant mass flow rate Eqs.4.12, 4.16, 4.18 and 4.19. In fact, the high flowing refrigerant mass flow rate leads to high system capacity. Thus, both total heating load ( $\dot{Q}_{tot,heating}$ ) and gas engine heat consumption ( $\dot{Q}_{gas}$ ) are increase as the refrigerant mass flow rate gets larger. Clearly from Fig. 4.3B, R410A has the largest heating capacity and gas engine heat consumption followed by R407C and R134A respectively. As compared to R134A, the rate of increase in total heating load and gas engine heat consumption are 131 % and 142 % for R410A and 49 % and 72 % for R407A. Comparison of the system primary energy ratio of the GEHP using R410A, R407C and R134A is illustrated in Fig. 4.3C. PER is calculated as a ratio between the total useful heating load to the

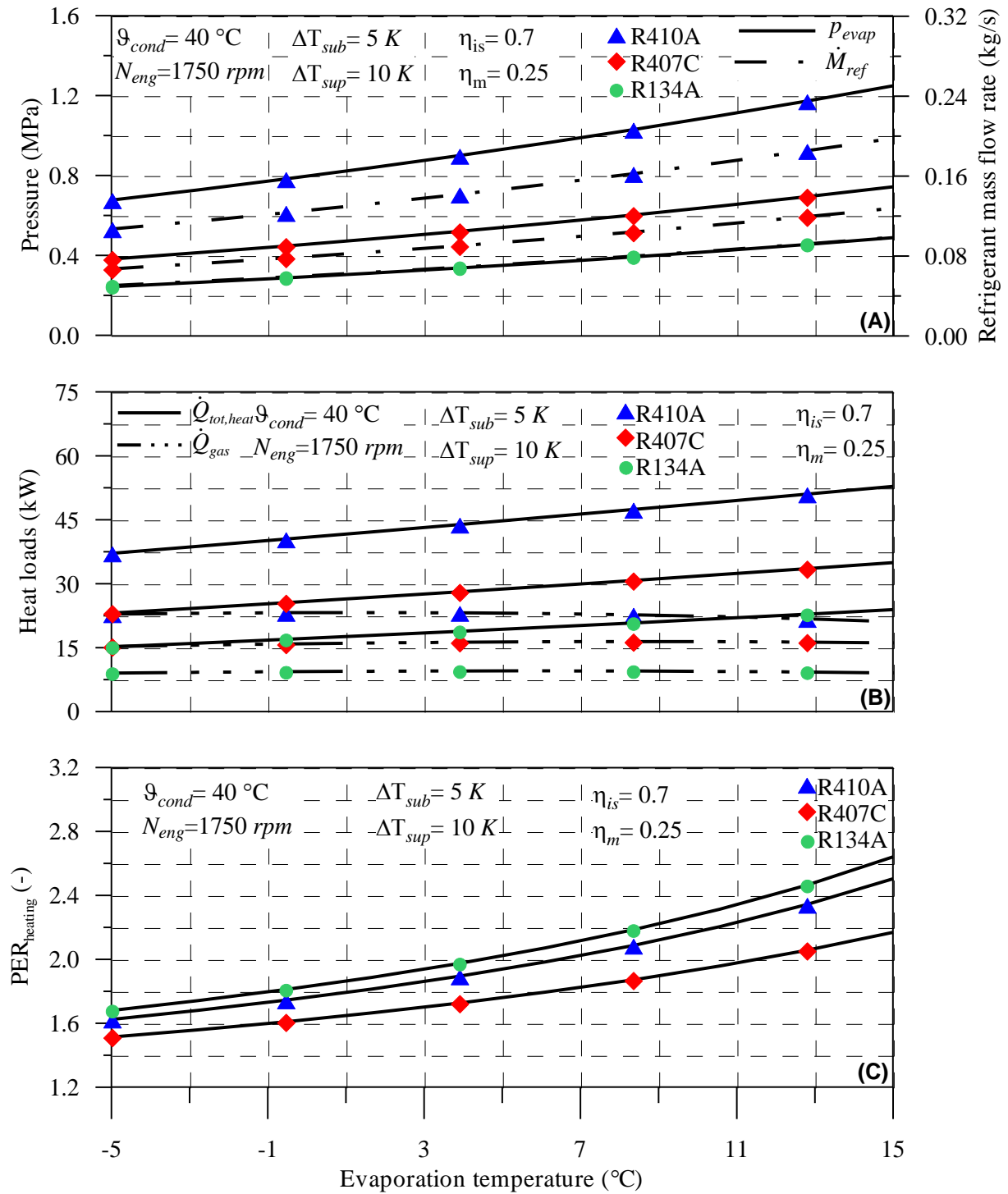


Figure 4.3: Comparison between R134a, R407C and R410A; (A) operating pressures and refrigerant mass flow rate, (B) heat loads and (C) primary energy ratio.

gas engine heat consumption. Obviously, R134A is the highest system primary energy ratio followed by R410A and R407C respectively. PER of R134A and R410A are higher than R407C by 15.5% and 10.65% respectively. This can be attributed to the high rate of increase in total heating capacity as compared to gas engine heat consumption.

Another environmental issue that is addressed in the evaluation of various refrigerants is their impact on global warming. In the ASHRAE Handbook [88], each refrigerant is assigned a global warming potential (GWP) as they are considered greenhouse gases. The GWP is a measure of the direct effect of the refrigerant on global warming by its release into atmosphere, and as such, does not describe the contribution of greenhouse gases such as carbon dioxide produced by the production of energy required to operate equipment that cycles the refrigerant. To account for the total warming effect (the direct and indirect effects), the total equivalent warming impact (TEWI) index is used. The direct warming effect associated with a piece of equipment comes from leakage of the refrigerant into the atmosphere, and typically contributes less to the TEWI than does the indirect effect, making the indirect effect the more critical aspect when considering warming potential. Because the indirect effect is related to energy consumption, the most efficient refrigerant will contribute the least to the TEWI. When R410A, R407C and R134A are compared in this way, R410A contributes the least to the TEWI because it is the most efficient and demands the least use of carbon producing fossil fuels in the creation of energy. Thus, R410A has been used in the frame of this work. A more details parametric study for the performance characteristics of the GEHP using R410A is introduced in the following sections. The parametric study includes effect of evaporation and condensation temperatures, subcooling and superheating degree, isentropic and thermal efficiencies.

#### 4.4.2 Effect of evaporation temperature

Fig. 4.4 shows influence of evaporation temperature on the performance characteristics of the GEHP using R410A. The evaporator temperature was changed from  $-5^{\circ}\text{C}$  to  $15^{\circ}\text{C}$  to simulate the real temperature in both summer and winter seasons. Variations of operating pressures as well as refrigerant mass flow rate versus evaporation temperature is illustrated in Fig. 4.4A. Clearly, evaporator pressure increases as the evaporation temperature increases. On the other hand, for constant condensation temperature ( $40^{\circ}\text{C}$ ) the condenser pressure kept constant. According to Eqs.4.15 and 4.14, pressure ratio goes lower and volumetric efficiency gets higher as the evaporator pressure increases. It should be noted that, as the evaporator pressure increases the vapor density at the compressor increases. For constant engine speed and as a result of increasing in both vapor density and volumetric efficiency, refrigerant mass flow rate increases by 104.8% as the evaporation temperature varied from  $-5^{\circ}\text{C}$  to  $15^{\circ}\text{C}$ . Influence of evaporation temperature on the system heat loads including evaporator cooling capacity, condenser heating capacity, compressor power, gas engine heat consumption and recovered engine heat is shown in Fig. 4.4B. Both evaporator and condenser capacities are directly proportional to evaporation temperature. It can be noted, as evaporation temperature increases the cooling effect (enthalpy difference through the evaporator) increases by 4% while both the enthalpy

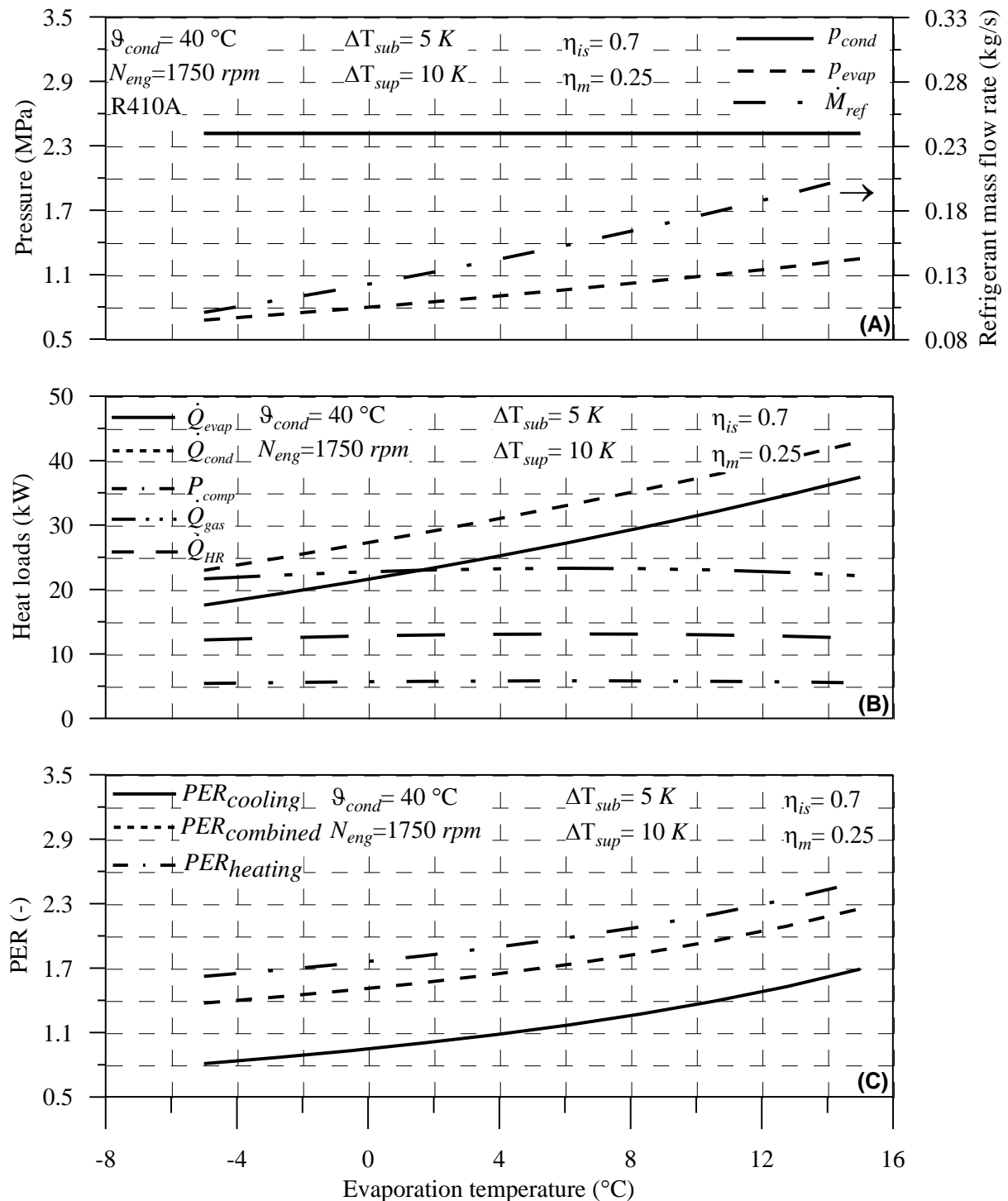


Figure 4.4: Effect of evaporation temperature on the performance characteristics of GEHP; (A) operating pressures and refrigerant mass flow rate, (B) heat loads and (C) primary energy ratio.

difference through the condenser and the compressor specific work are decrease by 8.7 % and 50.1 % respectively. The high rate of increase in refrigerant mass flow rate (104.8 %) and cooling effect (4 %) leads to increasing in evaporator cooling capacity by 113 %. On the other hand, the high rate of increase in refrigerant mass flow rate overcomes the low rate of decrease in condenser enthalpy difference (8.7 %) so the condenser heating capacity gets higher by 86.9 %. Regarding to compressor power, gas engine heat consumption and recovered engine heat, the evaporation temperature has no significant effect on them ( $\pm 1$  %). According to Eqs.4.19 and 4.20 and for assumed constant engine thermal efficiency for the gas engine, both gas engine heat consumption and recovered engine heat depend mainly on the compressor power. The rate of decrease in compressor work (50.1 %) overwhelms the rate of increase in refrigerant mass flow rate (104.8 %) so the compressor power slightly changes ( $\pm 1$  %) as the evaporation temperature varied from  $-5^{\circ}\text{C}$  to  $15^{\circ}\text{C}$ . The effect of evaporation temperature on the primary energy ratio of the GEHP in cooling, heating and combined modes is shown in Fig. 4.4C. The high rate of increase in cooling (113 %) and heating (86.9 %) capacities lead to increase in PER of the system. It can be noted that as the evaporation temperature changed from  $-5^{\circ}\text{C}$  to  $15^{\circ}\text{C}$ , PER of the GEHP in cooling, heating and combined modes increase by 108.5 %, 53 % and 62.4 % respectively.

#### 4.4.3 Effect of condensation temperature

The effect of condensation temperature on the performance characteristics of the GEHP is illustrated in Fig. 4.5. Condensation temperature range ( $30^{\circ}\text{C}$  to  $55^{\circ}\text{C}$ ) was selected to cover both climatic conditions in summer and heating requirements in winter. Dependency of operating pressures as well as refrigerant mass flow rate upon condensation temperature is illustrated in Fig. 4.5A. Obviously, condenser pressure increase as the condensation temperature increases. On the other hand, for constant evaporation temperature of  $5^{\circ}\text{C}$  the evaporator pressure remained constant. According to Eqs.4.15 and 4.14, pressure ratio gets higher and volumetric efficiency goes lower as the condenser pressure increases. It can be noted that, for constant engine speed, suction temperature and pressure refrigerant mass flow rate changed according to the compressor volumetric efficiency. Hence, as the condensation temperature varied from  $30^{\circ}\text{C}$  to  $55^{\circ}\text{C}$  refrigerant mass flow rate decreased by 9.9 %.

Influence of condensation temperature on the system heat loads such as evaporator cooling capacity, condenser heating capacity, compressor power, gas engine heat consumption and recovered engine heat is shown in Fig. 4.5B. Both evaporator and condenser heat capacities are inversely proportional while compressor power is directly proportional to condensation temperature. It can be noted, as condensation temperature increases enthalpy difference through both evaporator and condenser decrease by 24.1 % and 9.7 % respectively while compressor specific work is increases by 88.6 %. Hence, evaporator and condenser capacities decrease by 31.7 % and 18.6 % while compressor power increases by 69.9 % as the condensation temperature increases from  $30^{\circ}\text{C}$  to  $55^{\circ}\text{C}$ . As mentioned before both gas engine heat consumption and recovered engine heat are functions of compressor power, so both of them takes the same behavior of the



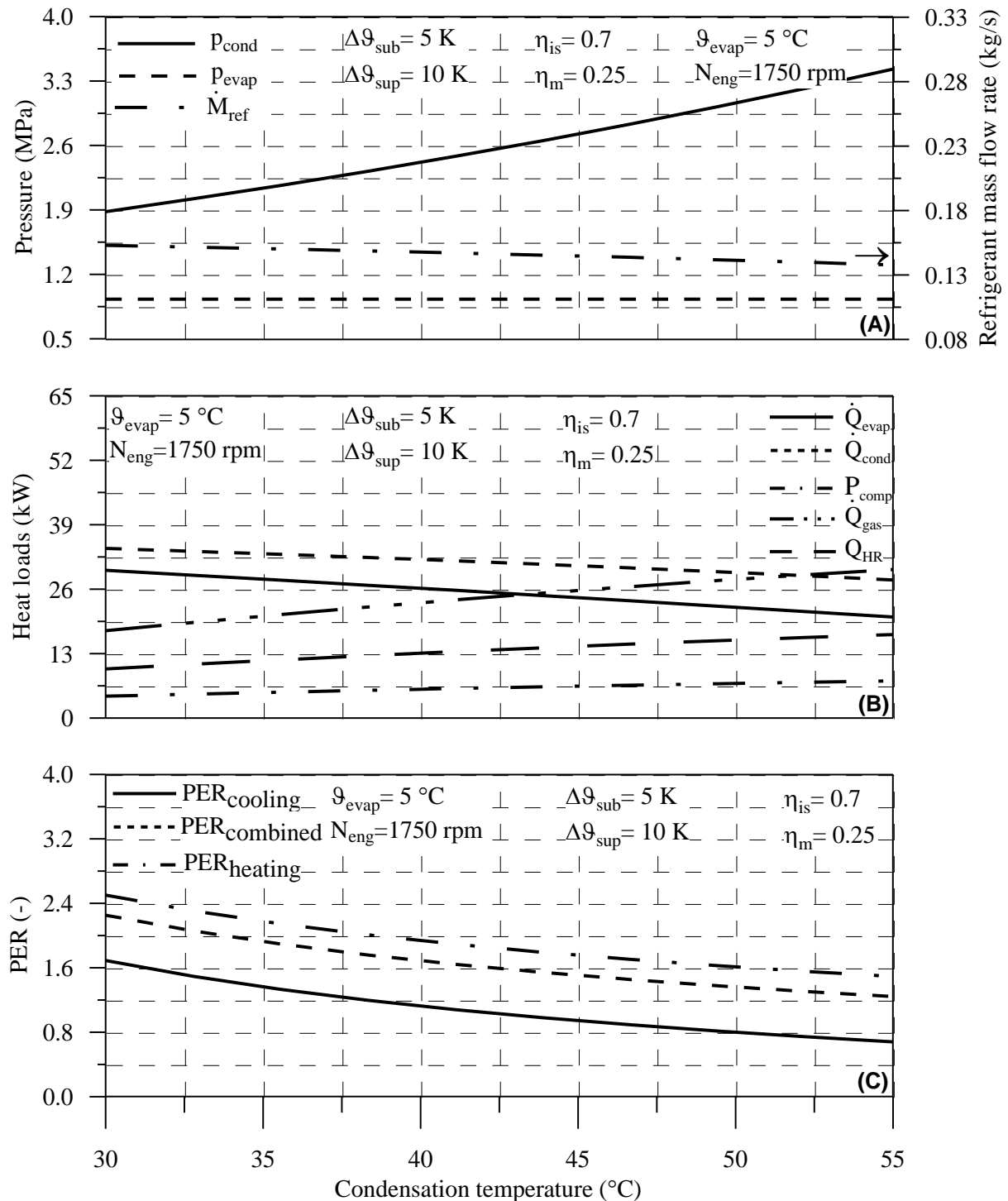


Figure 4.5: Influence of condensation temperature on the performance characteristics of GEHP; (A) operating pressures and refrigerant mass flow rate, (B) heat loads and (C) primary energy ratio.

compressor power. By other words, as condensation temperature increases from 30°C to 55°C both gas engine heat consumption and recovered engine heat increases by 69.9%. Dependency of the primary energy ratio of the GEHP on the condensation temperature in cooling, heating and combined modes is shown in Fig. 4.5C. In fact, the high rate of decrease in system cooling and heating capacities as well as the high rate of increase in gas engine heat consumption leads the PER of the GEHP to decrease. It should be noted that as condensation temperature varies from 30°C to 55°C PER of the GEHP in cooling, heating and combined modes decrease by 59.7%, 44.1% and 39.8% respectively.

#### 4.4.4 Effect of subcooled degrees

Figure 4.6 shows influence of subcooled degrees on the performance characteristics of the GEHP. The subcooled degrees were changed from 0 K to 10 K to cover the actual case in the refrigerant circuit. In fact, for constant evaporation and condensation temperatures both evaporator, condenser pressure and consequently pressure ratio kept constant. Moreover, the constant engine speed leads to constant refrigerant volume flow rate. Hence, the discharged refrigerant mass flow rate remains constant. Dependency of evaporator and condenser capacities upon subcooled degrees are illustrated in Fig. 4.6A. Both evaporator and condenser heat capacities are directly proportional to subcooled degrees. It can be noted, as subcooled degrees increase by 10K enthalpy difference through both evaporator and condenser increase by 10.6% and 8.5% respectively. Hence, evaporator and condenser capacities increase by 10.6% and 8.5% as the subcooled degrees increase by 10K. It should be noted also that the subcooled degrees have no effect on the compressor specific work and consequently the compressor power, gas engine heat consumption and recovered engine heat. The effect of subcooled degrees on the primary energy ratio of the GEHP in cooling, heating and combined modes is shown in Fig. 4.6B. The rate of increase in cooling (10.6%) and heating (8.5%) capacities lead to increase in PER of the system. Obviously, as the subcooled degrees increased by 10K, PER of the GEHP in cooling, heating and combined modes increase by 10.5%, 6.7% and 5.8% respectively.

#### 4.4.5 Effect of superheating degree

The effect of superheating degrees on the performance characteristics of the GEHP is illustrated in Fig. 4.7. The superheating degrees were changed from 0 K to 20 K to cover the real case in the refrigerant circuit. In fact, for constant evaporation and condensation temperatures both evaporator, condenser pressure and consequently pressure ratio kept constant. On the other hand, the suction temperature increases as the superheating degree gets higher. Hence, the refrigerant suction density decreases and consequently refrigerant mass flow rate goes lower. It can be noted that, as the superheating increases by 20K the refrigerant mass flow rate decreases by about 12.4% as shown in Fig. 4.7A. Influence of superheating degrees on the system heat loads such as evaporator cooling capacity, condenser heating capacity, compressor power, gas engine heat consumption and recovered engine heat is shown in Fig. 4.7B. Both evaporator and condenser heat capacities slightly decrease while compressor power slightly increases as the superheating degree increases. It can be noted, as superheating degrees increase by 20K enthalpy

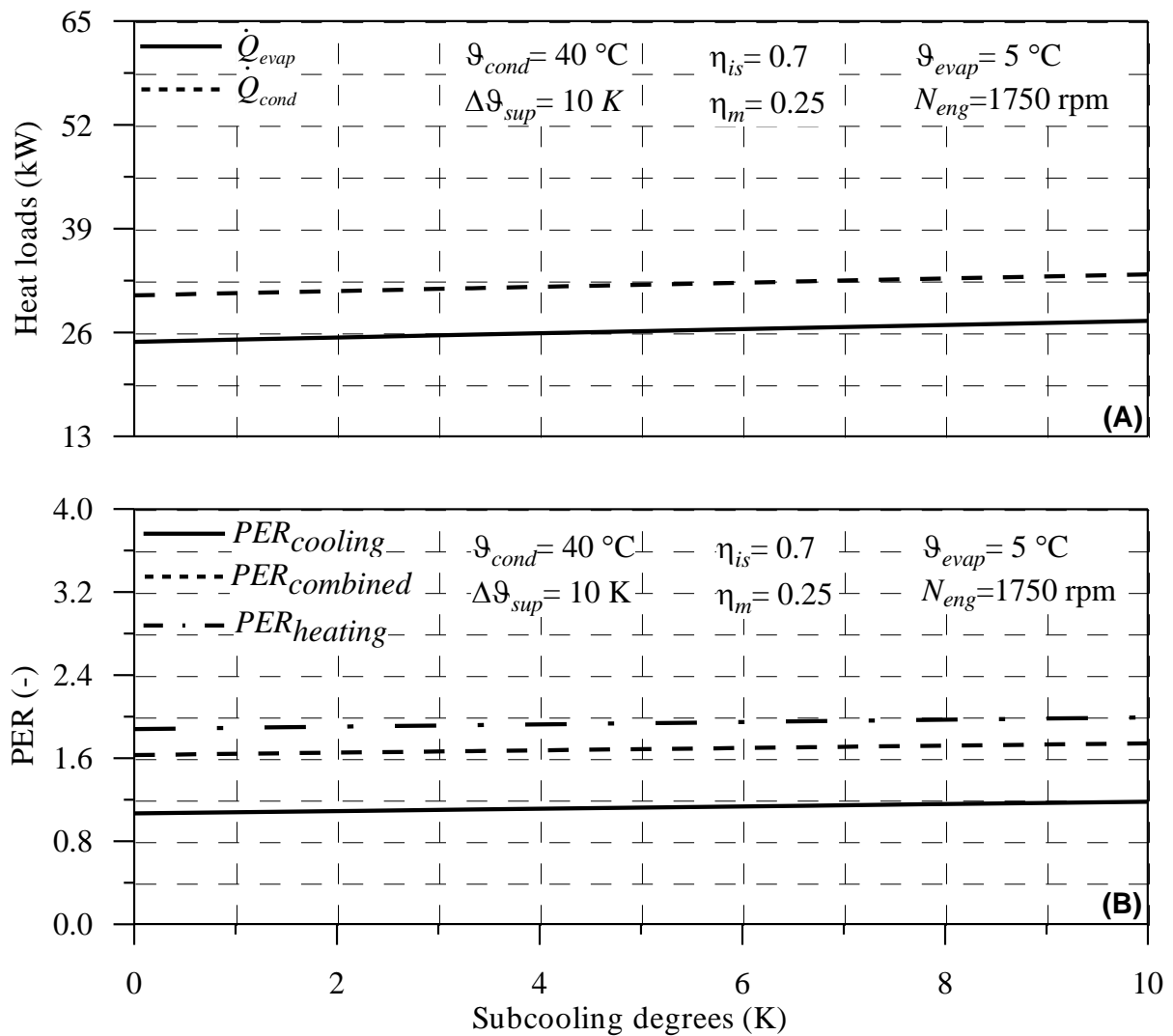


Figure 4.6: Effect of subcooling degrees on the performance characteristics of GEHP; (A) heat loads and (B) primary energy ratio.

difference through both evaporator and condenser as well as compressor specific work increase by 13.33%, 13.54% and 14.68% respectively. Hence, the rate of increase in enthalpy differences overwhelm the rate of decrease in refrigerant mass flow rate and consequently slightly decrease or increase in evaporator capacity, condenser capacity and compressor power. By other words, evaporator and condenser capacities decreases by about 0.68% and 0.46% respectively while compressor power increases by 0.52% as the superheating degrees changed from 0K to 20K. Both gas engine heat consumption and recovered engine heat are calculated as functions of compressor power, Eqs. 4.19 and 4.20. So both of them takes the same behavior like compressor power especially when the thermal efficiency is kept constant. Gas engine heat consumption and recovered engine heat increases by about 0.52% as the superheating degree increases by 20K. Dependency of the primary energy ratio of the GEHP on the superheating degrees in cooling, heating

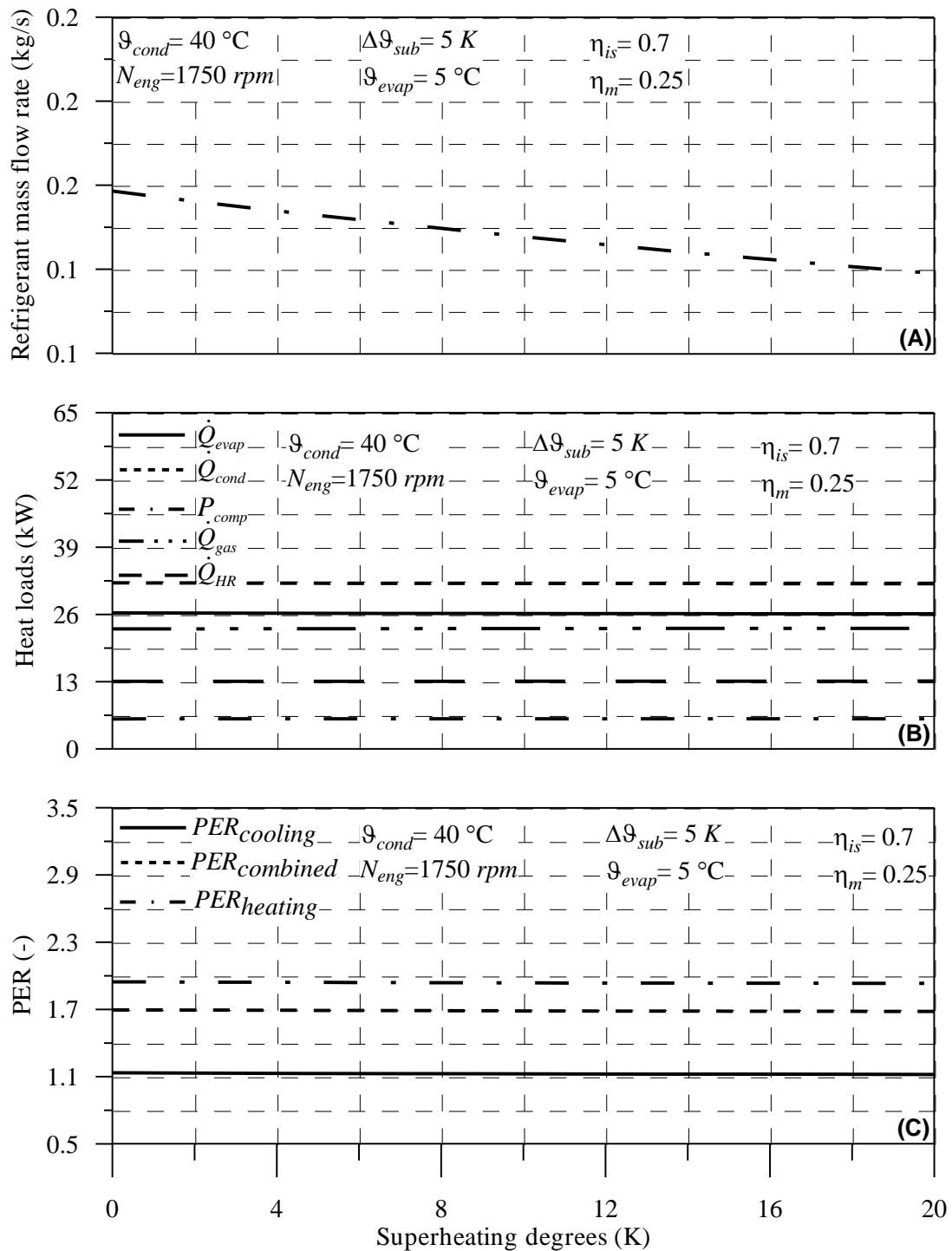


Figure 4.7: Influence of superheating degrees on the performance characteristics of GEHP; (A) operating pressures and refrigerant mass flow rate, (B) heat loads and (C) primary energy ratio.

and combined modes are shown in Fig. 4.7C. In fact, the high rate of decrease in system cooling and heating capacities as well as the high rate of increase in gas engine heat consumption leads the PER of the GEHP to decrease. Clearly, PER of the GEHP in cooling, heating and combined modes decrease by 1.2 %, 0.8 % and 0.7 % respectively as the superheating degree increases by 20 K.

#### 4.4.6 Effect of compressor isentropic efficiency

Figure 4.8 shows influence of compressor isentropic efficiency on the performance characteristics of the GEHP. The isentropic efficiency was changed from 0.6 to 0.8 to cover the actual case in the refrigerant compressor. In fact, for constant evaporation and condensation temperatures both evaporator and condenser pressures and consequently pressure ratio kept constant. Moreover, the constant engine speed leads to constant refrigerant volume flow rate. Hence, the discharged refrigerant mass flow rate remains constant. Moreover, the evaporator capacity kept constant because the isentropic efficiency has no effect of both refrigerant mass flow rate and cooling effect. Dependency of the condenser capacity, compressor power, gas engine heat consumption and recovered engine heat is shown in Fig. 4.8A. Both condenser capacity and compressor power are inversely proportional to isentropic efficiency. It can be noted, as isentropic efficiency increases enthalpy difference through condenser and compressor specific work decrease by 5.1 % and 25 % respectively. Hence, Both condenser capacity and compressor power decrease by 5.1 % and 25 % as the isentropic efficacy increases from 0.6 to 0.8. As mentioned before for constant thermal efficiency both gas engine consumption heat and recovered engine heat take the same behavior of compressor power. Hence, as the isentropic efficiency changes from 0.6 to 0.8 both gas engine consumption heat and recovered engine heat decrease by 25 %. The effect of isentropic efficiency on the primary energy ratio of the GEHP in cooling, heating and combined modes is shown in Fig. 4.8B. Obviously, PER of the GEHP increases in all modes as the isentropic efficiency gets higher due to the high rate of decreasing in gas engine heat consumption. PER of the GEHP in cooling, heating and combined modes increase by 33.3 %, 20.5 % and 17.7 % respectively as the isentropic efficiency varies from 0.6 to 0.8.

#### 4.4.7 Effect of engine thermal efficiency

The effect of engine thermal efficiency on the performance characteristics of the GEHP is shown in Fig. 4.9. The thermal efficiency was varied from 0.2 to 0.3 to simulate the real case in the gas engine. In fact, for constant evaporation and condensation temperatures both evaporator and condenser pressures and consequently pressure ratio kept constant. Moreover, the constant engine speed leads to constant refrigerant volume flow rate. Hence, the discharged refrigerant mass flow rate remains unchanged. Moreover, evaporator capacity, condenser capacity as well as compressor power are kept constant because the thermal efficiency has no effect on the performance of the vapor compression refrigeration system. Dependency of the gas engine heat consumption and recovered engine heat upon engine thermal efficiency are shown in Fig. 4.9A. Both gas engine heat consumption and recovered engine heat are directly proportional to thermal efficiency. It can be noted, as

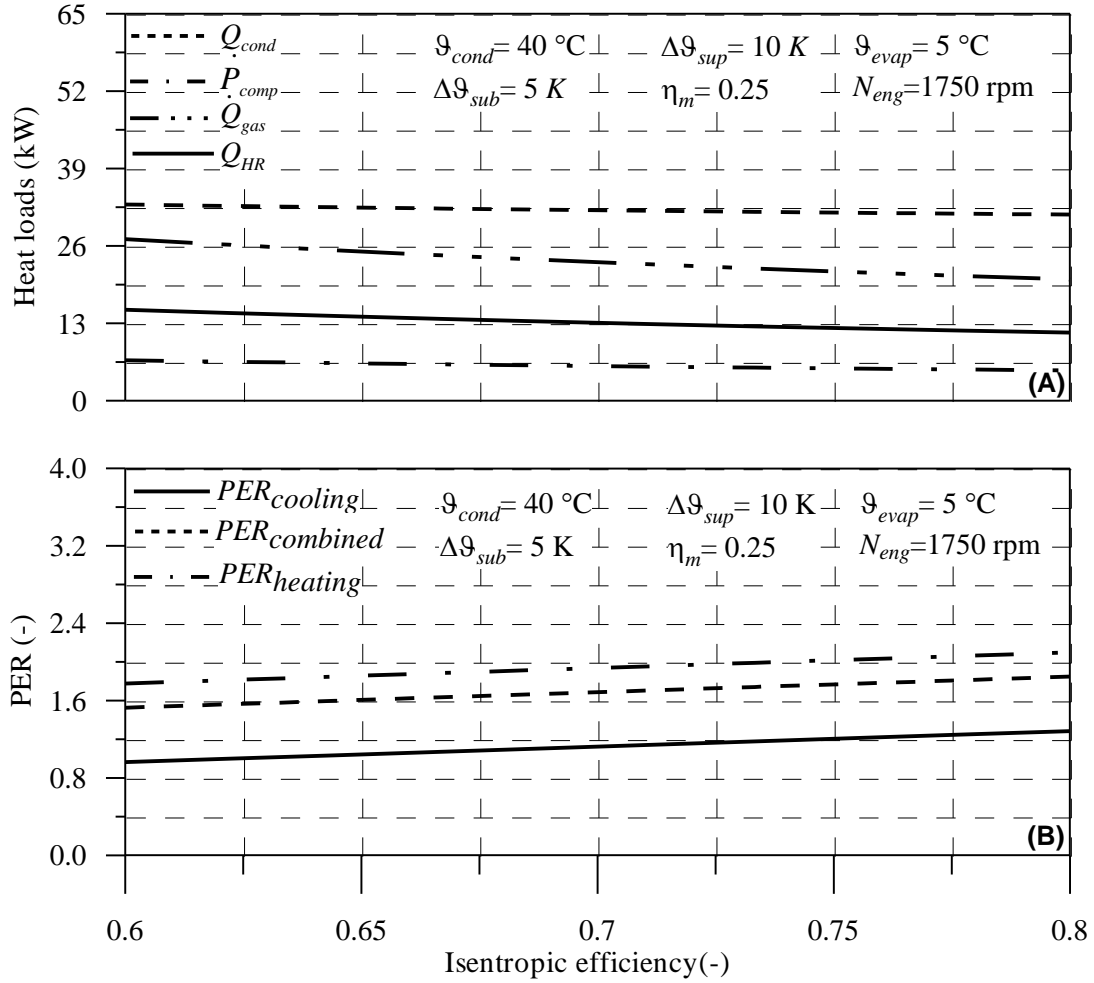


Figure 4.8: Effect of compressor isentropic efficiency on the performance characteristics of GEHP; (A) heat loads and (B) primary energy ratio.

thermal efficiency increases from 0.2 to 0.3 gas engine heat consumption and recovered engine heat decrease by 33.3% and 44.4%. The influence of thermal efficiency on the primary energy ratio of the GEHP in cooling, heating and combined modes is shown in Fig. 4.9B. Obviously, PER of the GEHP increases in all modes as the thermal efficiency gets higher due to the high rate of decreasing in gas engine heat consumption. PER of the GEHP in cooling, heating and combined modes increase by 50%, 24% and 27% respectively as the thermal efficiency varied from 0.2 to 0.6.

## 4.5 Conclusions on Theoretical Analysis of the Gas Engine Heat Pump

According to the energy analysis of the gas engine heat pump in cooling, heating and combined modes of operation, the following conclusions can be drawn:

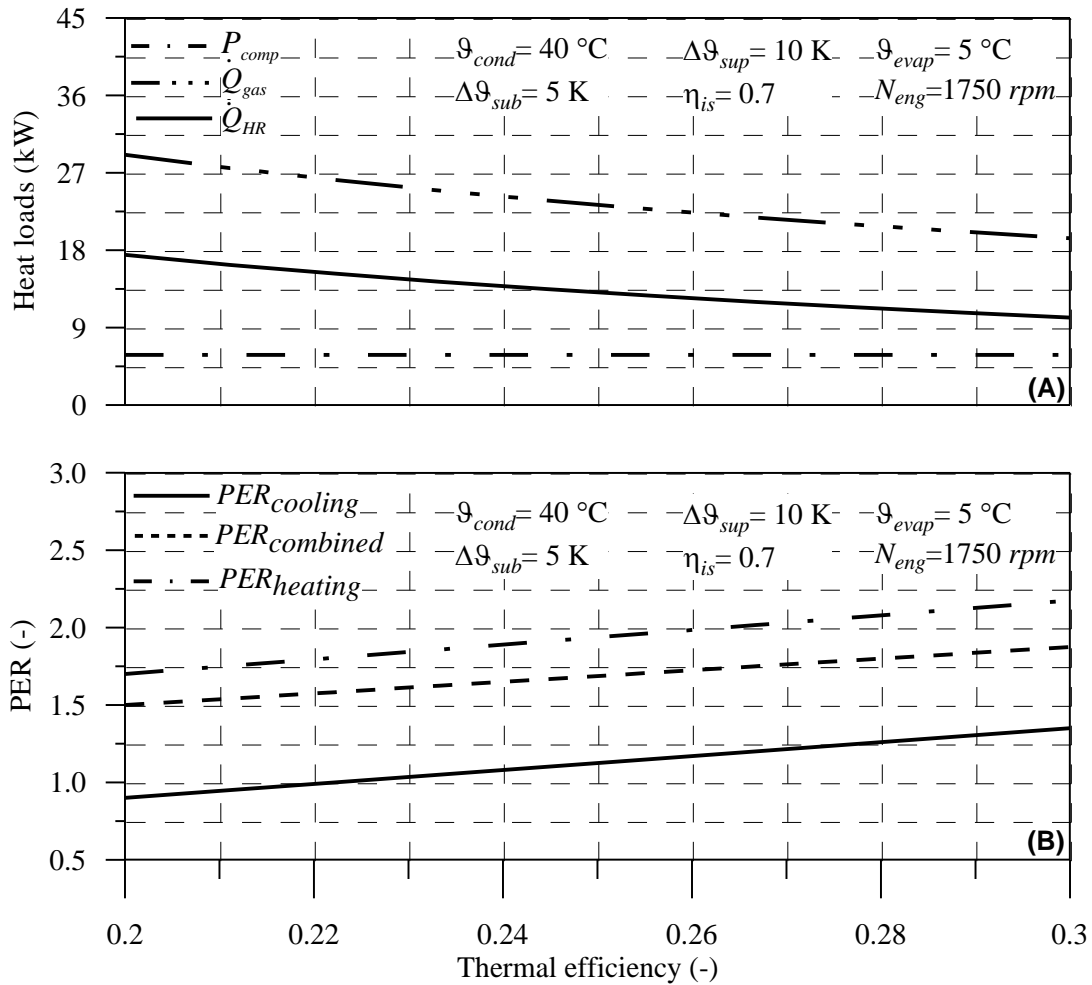


Figure 4.9: Influence of engine thermal efficiency on the performance characteristics of GEHP; (A) heat loads and (B) primary energy ratio.

- R410A is the best choice as alternative refrigerant for R22 due to its environmental protection and high energy efficiency utilization.
- Primary energy ratio of the GEHP is more influenced by evaporation temperature, condensation temperature, thermal efficiency, isentropic efficiency and subcooling degree in that order.
- As the evaporation temperature changed from  $-5$  to  $15\text{ }^{\circ}\text{C}$ , PER of the GEHP in cooling, heating and combined modes increase by 108.5%, 53% and 62.4% respectively.
- Both gas engine heat consumption and recovered engine heat increases by 69.9% as condensation temperature changed from  $30$  to  $55\text{ }^{\circ}\text{C}$ .
- As the subcooled degree increased by  $10\text{ K}$  PER of the GEHP in cooling, heating and combined modes increase by 10.5%, 6.7% and 5.8% respectively.

- Superheating degree has the lowest effect on the PER of the GEHP in all modes of operation.
- Both evaporator and condenser heat capacities slightly decrease (0.68 and 0.46 %) while compressor power slightly increases (0.52 %) as superheating degree increases by 20K.
- PER of the GEHP in cooling, heating and combined modes increase by 33.3 %, 20.5 % and 17.7 % respectively when the isentropic efficiency varies from 0.6 to 0.8.
- As thermal efficiency increases from 0.2 to 0.3 gas engine heat consumption and recovered engine heat decrease by 33.3 % and 44.4 % respectively.

According to the above conclusions, an experimental plant is designed and constructed to investigate the performance of the GEHP using R410A for cooling and heating applications.



# Chapter 5

## EXPERIMENTAL TEST RIG AND PROCEDURE

Literature survey revealed that the GEHP represents a natural choice in solving both energy and environment problems. Moreover, R410A represents a good replacement for R22 in both cooling and heating applications. Therefore, an experimental test rig fabricated by AISIN was installed and equipped with the necessary instrumentation to evaluate the performance characteristics of an air to water heat pump driven by gas engine. The objectives of the experimental work on the gas engine heat pump system are to:

- predict the effect of different external operating parameters such as water inlet temperature and water flow rate, engine speed and ambient air temperature on the performance of the gas engine heat pump
- compare the performance characteristics of the gas engine heat pump under various operating modes namely; cooling, heating and combined cooling and heating

In this chapter, experimental test rig is described. Also, test procedures and operating conditions for cooling and heating operating modes as well as data reduction techniques are explained.

### 5.1 Experimental Test Rig

Figure 5.1 shows a schematic diagram of the experimental test rig in cooling mode, which includes an outdoor unit, an indoor unit, measuring instruments and operational and safety control devices. The outdoor unit is a GEHP (TGMP 280 C1N) produced by AISIN company in Japan and has nominal cooling and heating capacities of 28 and 34 *kW*, respectively. While the indoor unit contains water tanks, chilled and hot water pumps and a plate heat exchanger. The plate heat exchanger is used as an evaporator in the cooling mode or a condenser in the heating mode. The recovered heat from the engine block and exhaust gas is used for enhancing the heating capacity of the GEHP in two ways;

- (i) to evaporate the refrigerant using the sub heat exchanger at the suction line of the compressor (in heating mode),
- (ii) to heat the water in the tank.

This test rig has three circuits; namely primary working fluid circuit, engine coolant circuit and secondary working fluid circuit. R410A is used as a primary working fluid while both water and air are used as secondary heat transfer fluids at the heat source (evaporator) and the heat sink (condenser). In engine coolant circuit, both ethylene-water mixture (65 % by volume) and propylene-water mixture (45 % by volume) are used as cooling mediums. The primary working fluid circuit is a vapor compression heat pump (VCHP). It comprises an expansion device, an evaporator, two open scroll compressors and a condenser followed by a receiver, a filter-drier and a sight glass. The expansion device is an electronic expansion valve whereas compressors are similar and have total swept volume of  $104 \text{ cm}^3/\text{rev}$  according to AISIN catalog data. Only one compressor has been used at lower system capacity while during all the presented experiments the two compressors have been used. The evaporator type is brazed plate heat exchanger with heat transfer area of  $4.6 \text{ m}^2$ . Two pressure-stats, one on the suction side and the other on the discharged side, are used to protect the compressor from under and over operating pressures. If the pressure exceeds its limits, the compressor would be automatically disconnected. In order to reduce the heat transfer to and from the surroundings, the primary fluid circuit is thermally insulated. The specifications of the system main components such as engine, compressor and indoor unit heat exchanger given in the Appendix (A).

### 5.1.1 Description of the experimental test rig in cooling mode

In cooling mode, the output mechanical power from the engine is used to drive the compressor of the vapor compression refrigeration system. Both water tanks are cooled using the cooling capacity of the evaporator.

#### -Primary working fluid circuit

As the refrigerant flows through the evaporator, it absorbs heat. As a result, superheated refrigerant vapor leaves the evaporator and then goes to the compressor. The compressor increases the pressure of the refrigerant and delivers superheated vapor (state point 2) to the condenser (state point 5) through an oil separator and a reversing valve. The condensation heat of refrigerant vapor released to the outside air flowing through the condenser. Thus, R410A vapor gets condensed (state point 8) and collected into the receiver, which prevent uncondensed vapor from passing through the heat pump cycle. Then, it flows through sub-cooler after passes through a filter-drier, which absorbs the water vapor that may enter the cycle. The liquid refrigerant in the sub-cooler is sub-cooled (state point 9) by transfer its heat to the throttled refrigerant flowing through valve ( $V_3$ ). Mass flow rate of the sub-cooled refrigerant is measured before passing through electronic expansion valves ( $V_4$ ) and ( $V_5$ ) using flow meter ( $F_1$ ).

Now the sub-cooled refrigerant flows into the indoor unit where it is evaporated (state point 15) using the water coming out from the tank. Superheated refrigerant coming out from both sub-cooler (state point 11) and indoor unit (state point 6)

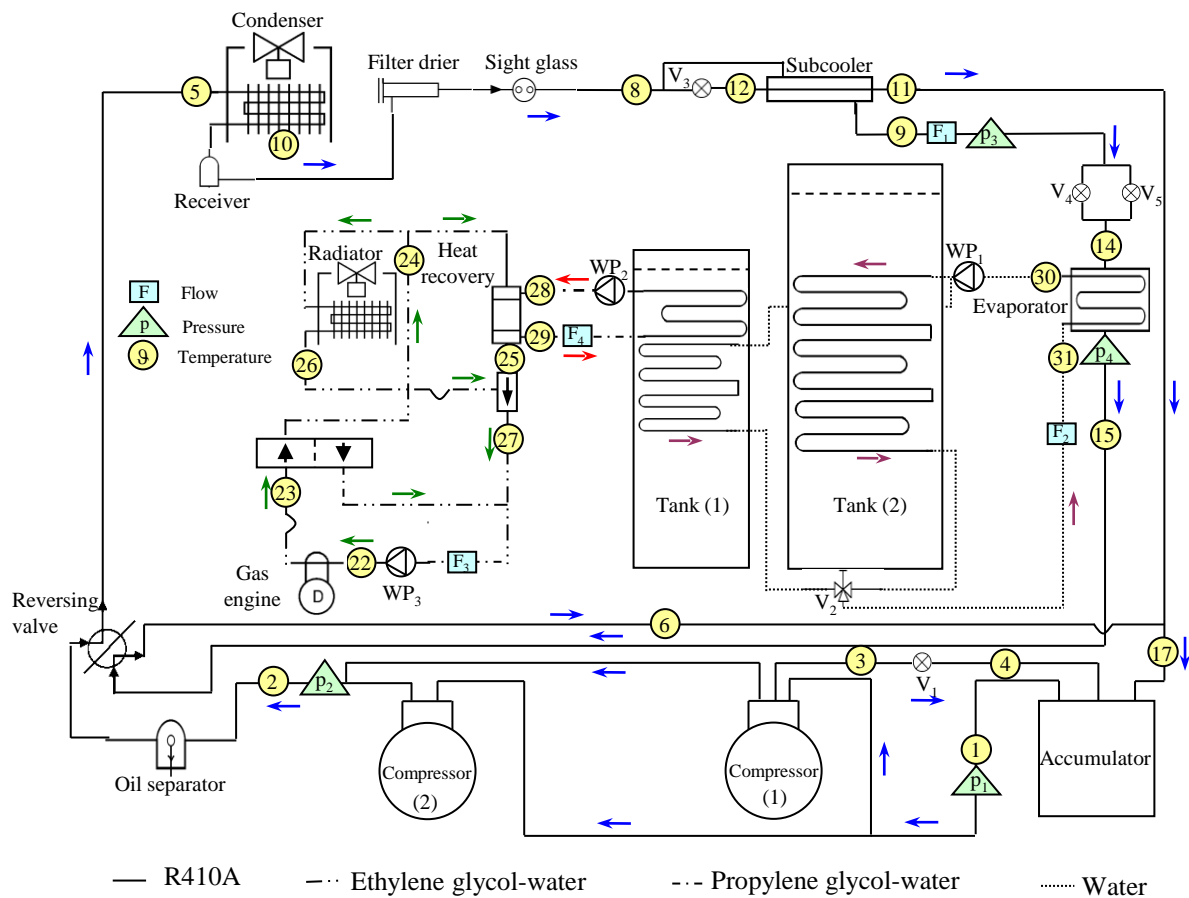


Figure 5.1: Schematic diagram of the experimental test rig in cooling mode with measuring point locations.

are mixed (state point 17) before entering the accumulator and then returning back to the compressors (state point 1). Fig. 5.2 shows primary cycle processes on p-h diagram.

### -Engine coolant circuit

Engine coolant circuit includes the gas engine, a coolant tank, coolant pump, valves and coolant pipeline. Coolant discharged from the coolant pump (state point 22) is heated by the heat released from the engine block and exhaust gas (state point 23). The heated coolant returns to the coolant pump by making a shortcut via a thermostat valve when coolant temperature is low (lower than  $53^{\circ}\text{C}$ ) at engine start-up. When coolant temperature is high (higher than  $53^{\circ}\text{C}$ ) coolant flows into heat recovery heat exchanger and radiator (state point 24) to dissipate heat. The coolant exit from both heat recover heat exchanger (state point 25) and radiator (state point 26) is mixed (state point 27) and its volume flow rate is measured using ultrasonic flow meter ( $F_3$ ) before returning back to the coolant pump. Heat gained in heat recovery heat exchanger is supplied to the water in the tank (1) using propylene-water mixture as a working medium (state points 28 and 29).

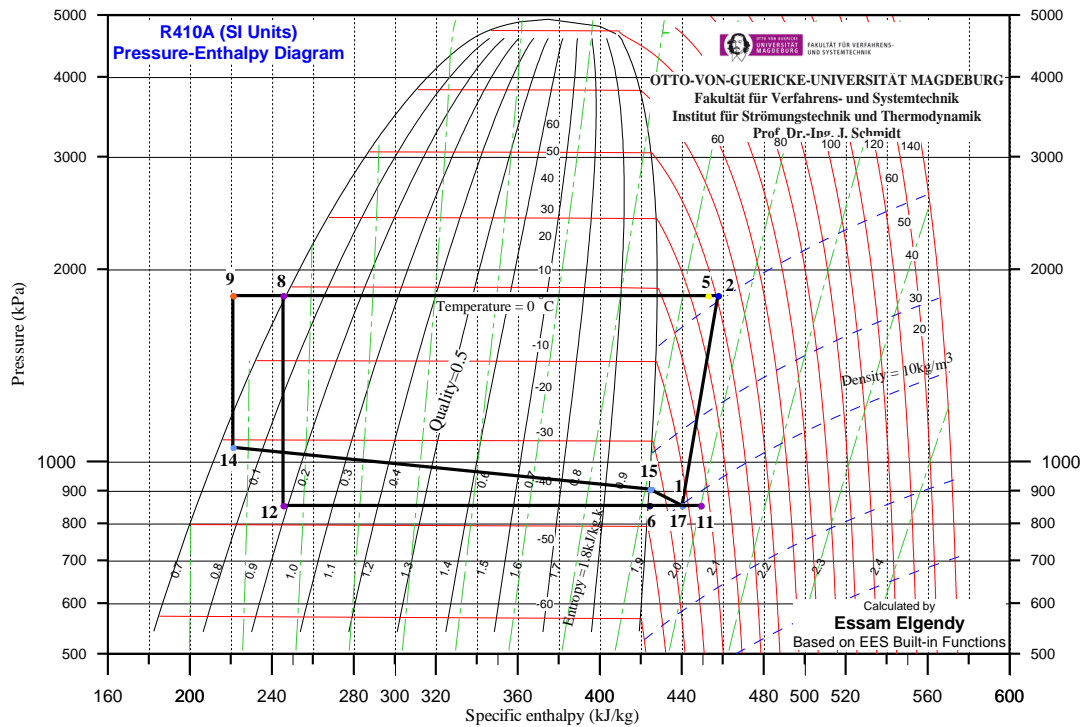


Figure 5.2:  $\log(p)$ - $h$  diagram for the primary cycle processes in cooling mode.

### -Secondary fluid circuit

The experimental test rig has two secondary heat transfer fluid circuits; namely chilled water circuit and outdoor air circuit. The chilled water circuit contains a chilled water tank of  $1m^3$ , a chilled water pump, an evaporator and control valves. The water pump (single phase, variable speed) is used to suck and pump the chilled water through the evaporator and chilled water pipeline. The chilled water flow rate is adjusted via pump speed. The chilled water circuit is thermally insulated to minimize heat gain. The outdoor air circuit consists of an air filter, a fan and a condenser. The chilled water coming out from indoor unit (state point 30) is pumped to storage tank (1) using a variable speed water pump ( $WP_1$ ). In the case of engine heat recovery, storage tank (2) is used for hot water while storage tank (1) is used as heat source for the evaporator. The volume flow rates of both chilled and hot waters are measured using ultrasonic flow meters ( $F_2$ ) and ( $F_4$ ) respectively. Temperature of air inlet to outdoor unit (state point 10) is measured using PT100 sensors to study the effect of ambient air temperature on the performance characteristics of the GEHP.

### 5.1.2 Description of the experimental test rig in combined mode

The working principle of the experimental test rig in the combined cooling and heating mode is the same like in the cooling mode. The cooling capacity supplied from the evaporator while the heat demands satisfied by the engine heat recovery. Hence, tank (1) has been used to store the received chilled water from the evaporator while tank (2) is used to store the hot water transferred from the engine heat recovery.

### 5.1.3 Description of the experimental test rig in heating mode

In the heating mode, the output mechanical power from the engine is used to drive the compressor of the vapor compression heat pump system. The heat demands supplied from both the condenser of the VCHP and the engine heat recovery. Consequently, hot water temperature levels are different because it comes from different sources. A higher hot water temperature levels is obtained from the engine heat recovery. On the other hand, a lower heating capacity can supplied from the engine heat recovery. Figure 5.3 shows a schematic diagram of the experimental test rig in the heating mode while Fig. 5.4 shows primary cycle processes on p-h diagram. According to engine heat recovered from the engine block and exhaust gas utilization the system can be worked into two modes:

Mode-I : in which the recovered engine heat is transferred to the water in order to reach higher hot water supply (using the heat recovery heat exchanger).

Mode-II: in which the recovered engine heat is transferred to the refrigerant to evaporate it especially at low ambient air temperature (using the sub heat exchanger).

#### -Primary working fluid circuit

As the refrigerant flows through the compressor (state point 1), the compressor raises the pressure of the refrigerant and delivers superheated vapor (state point 2) to the condenser (indoor unit) (state point 5) through an oil separator and a reversing valve. The condensation heat of refrigerant vapor released to the water flowing through the condenser. Thus, R410A vapor gets condensed (state point 6) and its mass flow rate is measured using flow-meter ( $F_1$ ) before flows to sub-cooler. The liquid refrigerant in the sub-cooler is sub-cooled (state point 8) by transfer its heat to the throttled refrigerant flowing through valve ( $V_3$ ). In case of mode-I, valve ( $V_5$ ) is closed so the sub-cooled refrigerant converted to mixture phase by passing through electronic expansion valves ( $V_4$ ). As the refrigerant mixture flows through evaporator, it is evaporated by the heat transferred from the ambient air. In case of mode-II, valve ( $V_5$ ) is opened and the refrigerant is throttled using expansion devices ( $V_5$ ) and ( $V_4$ ). Hence, the refrigerant is evaporated using the heat transferred from ambient air and the recovered heat from the engine. Superheated refrigerant coming out from sub-cooler (state point 10), sub heat exchanger (state point 12) and outdoor unit (state point 13) are mixed (state point 15) before entering the accumulator and then returning back to the compressors (state point 1).

#### -Engine coolant circuit

Engine coolant circuit includes the gas engine, a coolant tank, coolant pump, valves and coolant pipeline. Coolant discharged from the coolant pump (state point 20) is heated by the heat released from the engine block and exhaust gas (state point 21). The heated coolant returns to the coolant pump by making a shortcut via a thermostat valve when coolant temperature is low (lower than  $53^\circ\text{C}$ ) at engine start-up. When coolant temperature is high (higher than  $53^\circ\text{C}$ ) coolant flows into sub heat exchanger (Mode-II) while it flows through all of sub, radiator and heat recovery heat exchangers when coolant temperature is very high (higher than  $67^\circ\text{C}$ ). The coolant exit from both heat recover heat exchanger (state point 25) and radiator (state point 26) is mixed (state point 27) and

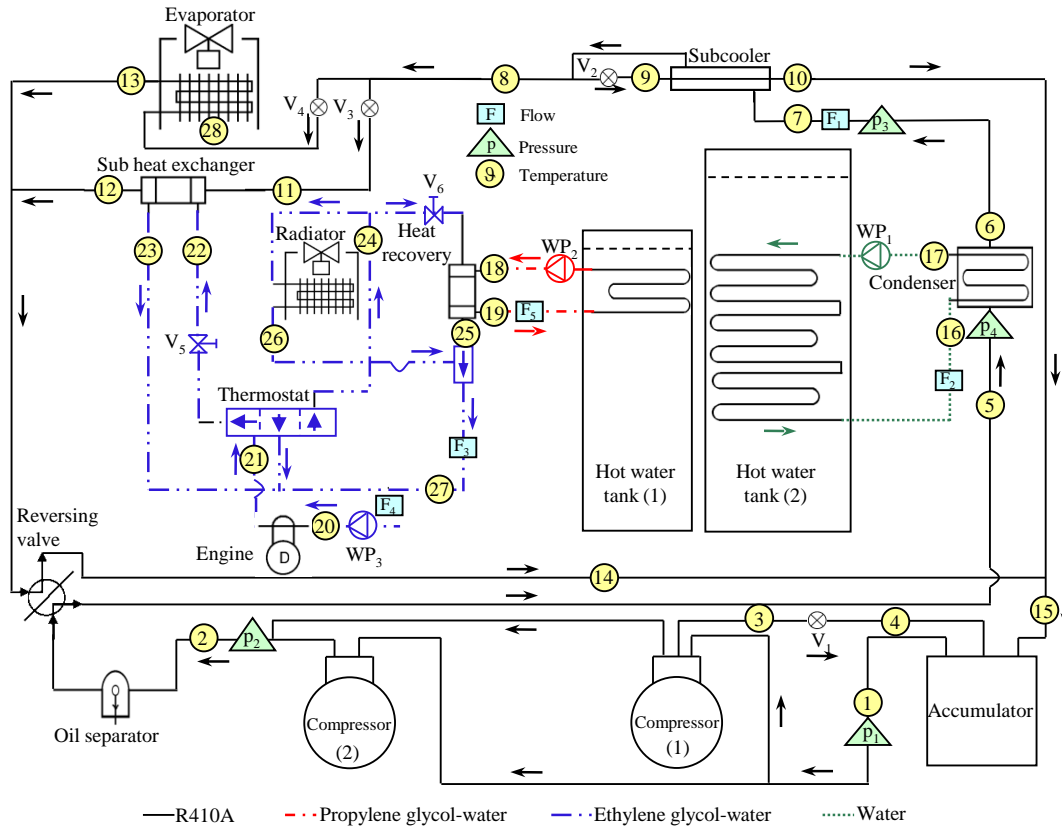


Figure 5.3: Schematic diagram of the experimental apparatus in heating mode with measuring point locations.

its volume flow rate is measured using ultrasonic flow meter ( $F_3$ ) before returning back to the coolant pump. Heat gained in heat recovery heat exchanger is supplied to the water in the tank (1) using propylene-water mixture as a working medium (state points 18 and 19).

### -Secondary fluid circuit

The experimental test rig has two secondary heat transfer fluid circuits; namely hot water circuit and outdoor air circuit. The hot water circuit contains a hot water tank of  $1m^3$  capacity, a hot water pump, a condenser and control valves. The water pump (single phase, variable speed) is used to suck and pump the hot water through the condenser and hot water pipeline. The hot water flow rate is adjusted via pump speed. The hot water circuit is thermally insulated to minimize heat loss. The outdoor air circuit consists of an air filter, a fan and an evaporator. The hot water coming out from indoor unit (state point 17) is pumped to storage tank (1) using a variable speed water pump ( $WP_1$ ). Storage tank (1) is used for hot water coming from engine heat recovery (Mode-I) while storage tank (2) is used for the hot water coming out from condenser. The volume flow rates of hot waters are measured using ultrasonic flow meters ( $F_2$ ) and ( $F_5$ ) respectively.

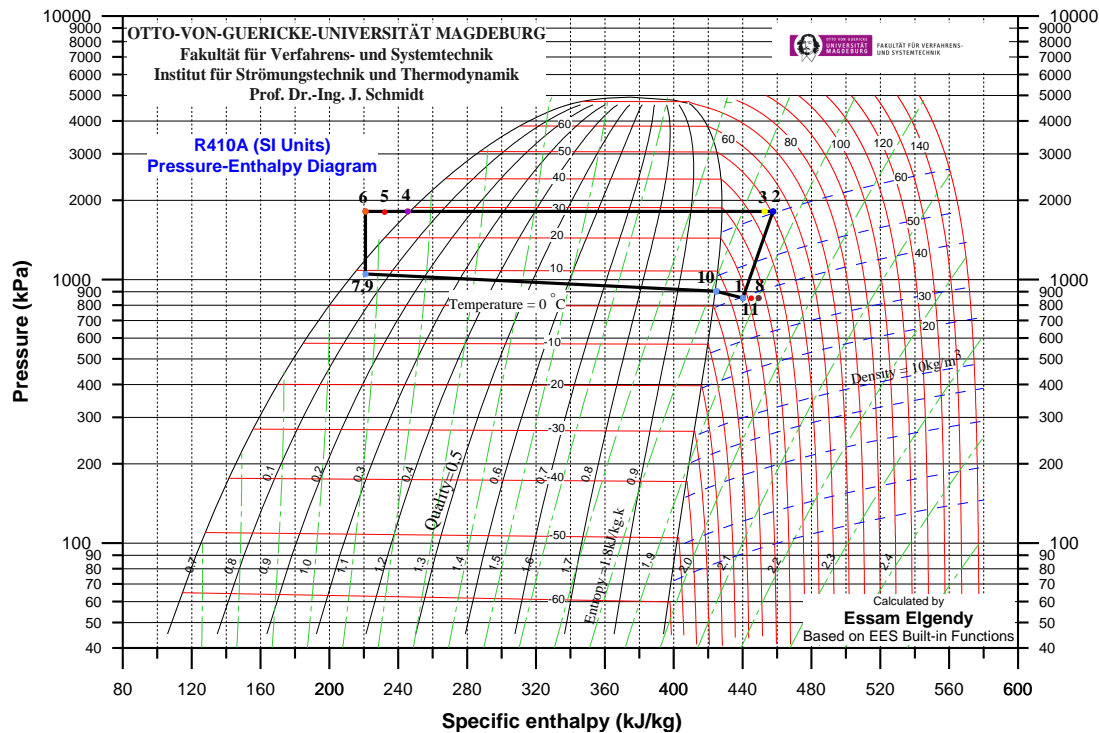


Figure 5.4: log(p)-h diagram for the primary cycle processes in heating mode.

## 5.2 Data Acquisition

Operating parameters to be measured during the course of experimental runs are:

- temperature at various locations in primary, secondary and engine coolant circuits,
- flow rate through primary, secondary and engine coolant circuit,
- pressure at four locations in the primary working fluid circuit,
- gas engine fuel consumption.

Temperature, pressure and flow rate locations are shown in Fig. 5.3. Pre-calibrated PT100 sensors are used to measure operating temperatures. Calibration of the sensors are given in Appendix (B). Digital pressure gauges (Ceraphant PTC31) are used to indicate the pressure at the four locations in the primary working fluid circuit. Refrigerant mass flow rate is measured using KROHNE Optimass 7000-T10 while engine coolants and water volume flow rates are measured using Ultego II flow sensors. Gas engine fuel consumption is measured using diaphragm gas meter (BK-G4) produced by Elster GmbH Germany. All the measuring instruments have been installed and connected to 64 channels in the data acquisition cards (Field Point FP-1000) manufactured by National Instruments Germany GmbH company. All the measured data are recorded using DIAdem software [89]. The specifications of the instrumentation devices are given in Appendix (C). The system control is established using PRIVA software which provides several possibilities

for the mode and consequently system operation. The valves setting, engine speed, low and high pressure as well as the system alarms are recorded and controlled using Aisin software which is accompanying the outdoor unit package.

### 5.3 Test Rig Commissioning and Experimental Procedure

The test rig commissioning includes checkup and testing of the individual components and the whole test rig after completing the installation. Then, dealing with the technical problems arising at the start up and operation of the test rig is carried out. Various leakage tests have been undertaken for the refrigerant circuit using the soap bubbles, halide lamp and the electronic leakage detector. After successful sealing of the test rig, the heat pump circuit has been evacuated using a vacuum pump. Thus, avoiding the presence of moisture or non-condensable gases in the heat pump circuit. Then, charging a small amount of R410A vapor to break the vacuum then re-evacuating the system. The vacuum is held for 24 hours, after that the correct right amount of R410A is charged to the circuit. The pressure levels in the circuit and the sight glass determine the correct charge of R410A. The system is allowed to run till steady state of the operating conditions is reached. The temperature in both chilled and hot water tanks were maintained with 0.1°C of the target temperature and water was pumped into the indoor unit and the engine heat recovery heat exchangers. The experimental procedure has been done as the following;

- Turn on the main power supply, indoor unit controller and computer which is data acquisition cards are installed in.
- Select the required operating mode (cooling/heating) using the touch screen of the indoor unit controller.
- Run Aisin software and select time step recording (every second/minute) and give name for the data file.
- Run Diadem software and start the recording program.
- Run Tc-Select software and select the operating mode, working fluid as well as run both indoor heat exchanger and heat recovery pumps.
- Wait till the engine speed reach 1200 rpm and check that the compressors are engaged with the engine using Aisin presented data.
- Select the required engine speed, electronic valve steps ( $V_3, V_5$  and  $V_6$ ). These setting are repeated every 10 minutes manually.
- When the required conditions are reached for the proposed mode, stop the recording process for both Aisin and Diadem. For cooling mode always the experiment ends when the water temperature reaches 5°C while for heating mode the experiment ends at condenser pressure of 3 MPa.



- Combine Aisin and Diadem data files and prepare the raw data file to the analysis program using a developed macro in XL software.
- Calculate output results with the help of a devolved program using EES software.
- Make filtration of the data using a developed macro in XL software (i.e delete the data points which are not match with the logic such as vapor points at the condenser outlet or at the flow meter measuring point as well as the liquid points the evaporator exit).

## 5.4 Data Reduction

The raw data of temperature, pressure and flow rate of R410A, ethylene glycol-water mixture, propylene glycol-water mixture and water are used to estimate the performance characteristics of the heat pump and its components. Using the measured data of operating pressures and temperatures of R410A, the inlet and outlet specific enthalpy values of each component are estimated with the help of a computer program using EES software [87]. Then, energy and mass balances are carried out for the main components of the gas engine heat pump to compute their loads in addition to system overall performance. The refrigerant indoor unit capacity ( $\dot{Q}_{indoor}$ ) can be written based on either primary working fluid (Eq.5.1) or secondary working fluid (Eq.5.2) as follows;

$$\dot{Q}_{indoor} = \dot{M}_{ref,pr} |h_{15} - h_9|, \quad (5.1)$$

$$\dot{Q}_{indoor} = \dot{V}_{wat} \rho_{wat} |h_{30} - h_{31}|. \quad (5.2)$$

Applying energy balance around sub-cooler, secondary refrigerant mass flow rate ( $\dot{M}_{ref,s}$ ) flowing through sub-cooler can be calculated as follows;

$$\dot{M}_{ref,s} = \frac{\dot{Q}_{sub}}{(h_{11} - h_8)}, \quad (5.3)$$

where

$$\dot{Q}_{sub} = \dot{M}_{ref,pr} (h_8 - h_9). \quad (5.4)$$

( $\dot{M}_{ref,pr}$ ) is the primary refrigerant mass flow rate which is measured using flow meter  $F_1$ . Applying mass and energy balance equations at the mixing point between 6,11 and 17 yields to the following equation;

$$\dot{M}_{sub,hex} = \frac{\dot{M}_{ref,s}(h_{17} - h_6) - \dot{M}_{ref,s}(h_{17} - h_{11})}{(h_6 - h_{17})}. \quad (5.5)$$

Then, sub heat exchanger load ( $\dot{Q}_{sub,hex}$ ) can be calculated using Eq.5.6 as follows;

$$\dot{Q}_{sub,hex} = \dot{M}_{sub,hex} (h_7 - h_8). \quad (5.6)$$

Total heat released from the engine ( $\dot{Q}_{eng,tot}$ ) can be estimated using the following formula;

$$\dot{Q}_{eng,tot} = \dot{Q}_{rad} + \dot{Q}_{HR} + \dot{Q}_{sub,hex}, \quad (5.7)$$

where the radiator ( $\dot{Q}_{rad}$ ) and the heat recovery ( $\dot{Q}_{HR}$ ) loads can be calculated using Eq.5.8 and Eq.5.9 respectively as;

$$\dot{Q}_{rad} = \dot{V}_{ethy,rad} \rho_{ethy} (h_{24} - h_{26}), \quad (5.8)$$

$$\dot{Q}_{HR} = \dot{V}_{ethy,HR} \rho_{ethy} (h_{24} - h_{25}). \quad (5.9)$$

Ultrasonic flow meter  $F_3$  is used to measure the coolant volume flow rate flowing to both the radiator and the heat recovery heat exchanger. While for each heat exchanger it can be calculated using the mass and energy balances equations as the following;

$$\dot{V}_{ethy,rad} = \dot{V}_{ethy,rad,HR} \frac{\vartheta_{25} - \vartheta_{27}}{\vartheta_{25} - \vartheta_{26}}, \quad (5.10)$$

$$\dot{V}_{ethy,HR} = \dot{V}_{ethy,rad,HR} - \dot{V}_{ethy,rad}. \quad (5.11)$$

In order to estimate the compressor power, both refrigerant mass flow rate discharged from compressor to outdoor unit ( $\dot{M}_{comp,dis}$ ) and to accumulator ( $\dot{M}_{cont}$ ) should be calculated. So, applying mass and energy balances on the accumulator yields to the following equation;

$$\dot{M}_{cont} = \dot{M}_{comp,dis} \frac{h_{17} - h_1}{h_1 - h_4}. \quad (5.12)$$

Then compressor power ( $P_{comp}$ ) is described as;

$$P_{comp} = \dot{M}_{comp,dis} (h_2 - h_1) + \dot{M}_{cont} (h_3 - h_1). \quad (5.13)$$

The performance of the GEHP is estimated by means of three main parameters primary energy rate (PER), gas engine energy consumption ( $\dot{Q}_{gas}$ ) and cooling/heating capacity ( $\dot{Q}_{indoor}$ ) [90]. PER can be expressed as the following;

- for cooling mode,

$$PER_{cooling} = \frac{\dot{Q}_{evap}}{\dot{Q}_{gas}}, \quad (5.14)$$

- for combined cooling and heating mode,

$$PER_{combiend} = \frac{\dot{Q}_{evap} + \dot{Q}_{HR}}{\dot{Q}_{gas}}, \quad (5.15)$$

- for heating mode,

$$PER_{heating} = \frac{\dot{Q}_{cond} + \dot{Q}_{HR}}{\dot{Q}_{gas}}, \quad (5.16)$$

where;

$$\dot{Q}_{gas} = \dot{V}_{gas} LHV, \quad (5.17)$$

where LHV represent gas lower heating value and  $\dot{V}_{gas}$  is the measured gas volume flow rate.

## 5.5 Uncertainty Analysis

The experimental error analysis indicates the implication of error of the measured parameters on the uncertainty of the results. Detailed analysis of the various experimental parameters is carried out using the differential method described by Moffat [91] and Kline and McClintok [92] and Holman [93]. Detailed analysis of the experimental error are given in Appendix (D). Table 5.1 summarizes the experimental error in the various parameters.

Table 5.1: Uncertainty values of the experimental parameters.

<i>Parameter</i>	<i>Uncertainty %</i>
<i>Refrigerant mass flow rate</i>	1.26
<i>Gas volume flow rate</i>	2.08
<i>Refrigerant pressure</i>	1.92
<i>Refrigerant temperature</i>	3.43
<i>Water temperature</i>	1.76
<i>Engine coolant temperature</i>	0.60
<i>Water volume flow rate</i>	3.05
<i>Engine coolant volume flow rate</i>	2.25
<i>Water specific enthalpy</i>	1.76
<i>Refrigerant specific enthalpy</i>	3.93
<i>Indoor unit capacity (Water side)</i>	3.52
<i>Indoor unit capacity (Refrigerant side)</i>	4.12
<i>Gas engine heat energy</i>	2.08
<i>Compressor power</i>	4.12
<i>Gas engine heat recovery</i>	2.32
<i>Primary energy ratio</i>	3.52



# Chapter 6

## EXPERIMENTAL RESULTS AND DISCUSSION

All experimental runs of air to water gas engine heat pump were conducted using R410A as primary working fluids for water cooling and heating applications. In this chapter some of these experiments are presented. Experimental results presented in three modes; cooling, heating and combined cooling and heating.

In the cooling mode, the gas engine has been used to drive a vapor compression refrigeration system without engine heat recovery. However, the engine heat recovery has been used in the combined mode in addition to the vapor compression refrigeration system. In the heating mode, the gas engine has been used to drive a vapor compression heat pump and the engine heat recovery has been used either to enhance the heating performance of the heat pump system or to heat the supplied water. For each mode, the effects of water inlet temperature, water volume flow rate, engine speed and ambient air temperature have been discussed.

### 6.1 Cooling Mode

Stiemle [94] reported that water temperature between 6 and 12°C is recommended for summer air-conditioning chiller units. Hence, evaporator water flow rate was selected to obtain water temperature at the evaporator outlet within the above recommended range. Moreover the system performance was studied at two engine speeds (1300 and 1750 $rpm$ ). All the experiments were carried out at ambient air temperature ranged from 19.7 to 35°C without using engine heat recovery. The effects of important parameters such as evaporator water inlet temperature, evaporator water flow rate, ambient air temperature, and engine speed will be discussed.

Figure 6.1 illustrates the effect of evaporator water inlet temperature and its flow rate on the performance of the GEHP while the effects of ambient air temperature and engine speed on the performance of the GEHP are presented in Figs. 6.2 and 6.3 respectively.

### 6.1.1 Effect of evaporator water inlet temperature

Influence of evaporator water inlet temperature, when other external operating parameters are maintained constant, on the performance characteristics of the GEHP system can be predicted from Fig. 6.1. Keeping the evaporator water flow rate at about  $2.38\text{m}^3/\text{h}$ , evaporator water inlet temperature was varied from 13 to  $24^\circ\text{C}$  to cover wide ranges of climatic conditions for air conditioning. Moreover, both engine speed and ambient air temperature were held constant at  $1750\text{rpm}$  and  $23.4^\circ\text{C}$  respectively. Variations of the measured condensing and evaporating pressures and refrigerant mass flow rate with the evaporator water inlet temperature are illustrated in Fig. 6.1A. It is seen that the rate of increasing in evaporating pressure (26 %) is higher than that of the condensing pressures (2.6 %), thereby the pressure ratio ( $p_{cond}/p_{evap}$ ) decreases as the evaporator water inlet temperature increases. Refrigerant mass flow rate increases with evaporator water inlet temperature. The increase in the refrigerant mass flow rate is mainly due to increase in both vapor density at compressor inlet and the volumetric efficiency. Figure 6.1A reveals this trend of the refrigerant mass flow rate. This figure confirms that the refrigerant mass flow rate is increased by 27.2 % over the entire considered range of the evaporator water inlet temperatures.

System cooling capacity as well as gas engine energy consumption as a function of evaporator water inlet temperature are plotted in Fig. 6.1B. System cooling capacity increases (29.2 %) while gas engine energy consumption slightly decreases (3.8 %) as evaporator water inlet temperature increases. It may be noted that when the evaporator water inlet temperature varied from about 13 to  $24^\circ\text{C}$ , the cooling effect ( $h_{15} - h_{14}$ ) is reduced by 18 %. Thus, the increase in refrigerant mass flow rate (27.2 %), which overwhelms the reduction in specific enthalpy change, yields higher system cooling capacity (Eq.5.2). On the contrary, the gas engine energy consumption is decreased by 3.8 % as evaporator water inlet temperature varies among the entire range.

Figure 6.1C presents variations of primary energy ratio (PER) and chilled water temperature with evaporator water inlet temperature. As the system cooling capacity increases, temperature difference through them increases for constant water mass flow rate, thereby higher chilled water temperatures were obtained at higher evaporator water inlet temperature as shown in Fig. 6.1C. Furthermore, chilled water temperature between 5 and  $15^\circ\text{C}$  were obtained. It should be noted that temperature levels of 5 to  $15^\circ\text{C}$  may be adequate for cooling food processing machines which need cooling water temperature that can not achieve with cooling tower (because the required cooling temperature is lower than the wet bulb temperature at the considered location). Variation of the PER of the GEHP with evaporator water inlet temperature is presented also in Fig. 6.1C. Primary energy ratio of the GEHP increases (27.8 %) with changing of evaporator water inlet temperature from 13 to  $24^\circ\text{C}$ . The high rate of increasing in the cooling capacity (29.2 %) and the low rate of decreasing in the gas engine energy consumption (4 %) are responsible for the high rate of increasing in PER (27.8 %) as shown in Fig. 6.1C. Therefore, evaporator water inlet temperature has a significant effect on the performance characteristics of the GEHP[95].

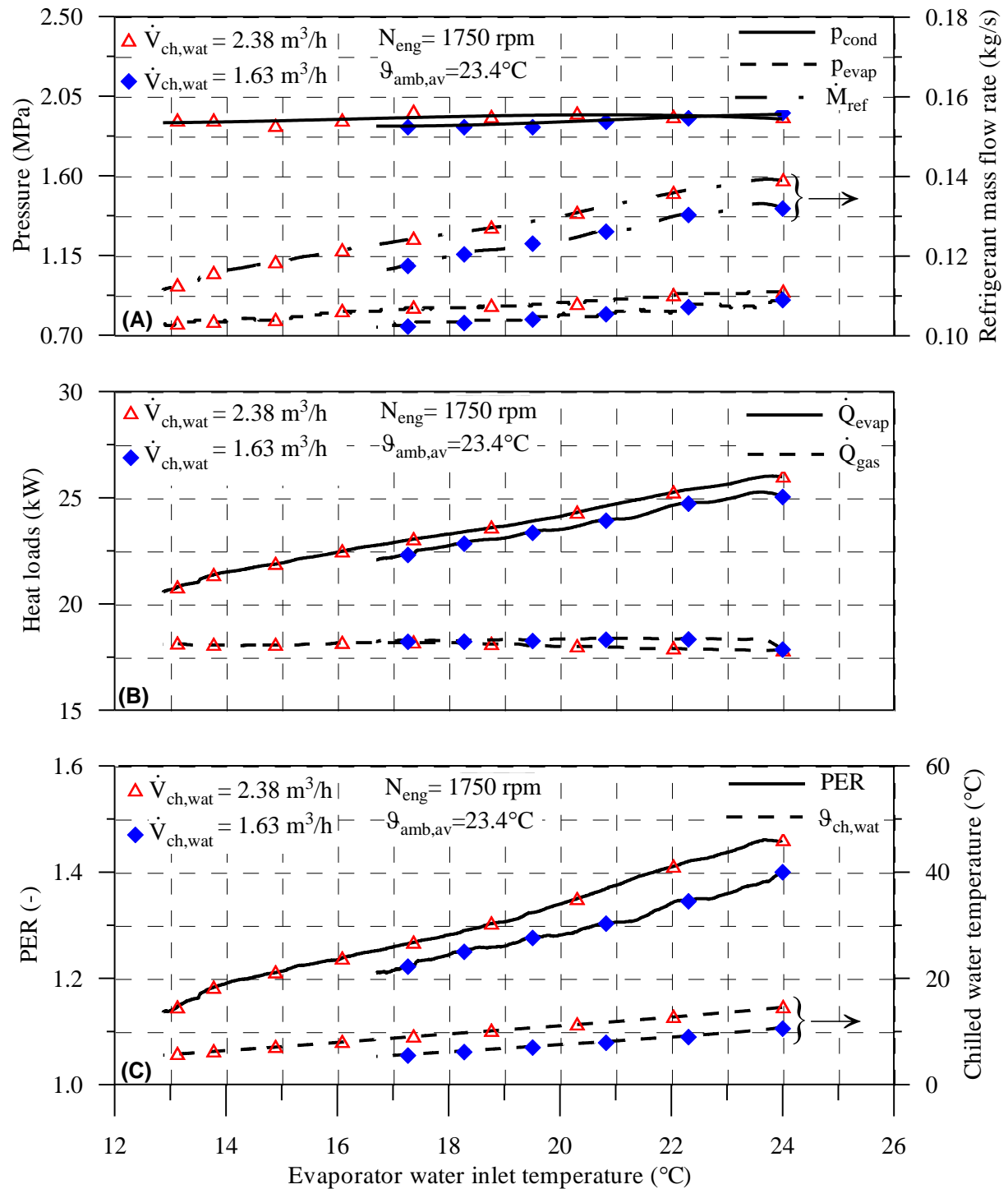


Figure 6.1: Effect of evaporator water inlet temperature on the performance characteristics of the GEHP in cooling mode for different chilled water volume flow rates; (A) operating pressures and refrigerant mass flow rate, (B) heat loads and (C) chilled water temperature and PER.

### 6.1.2 Effect of evaporator water volume flow rate

The effect of evaporator water flow rate on the performance characteristics of air to water gas engine heat pump in cooling mode is shown in Fig. 6.1. The chilled water flow rate is adjusted using chilled water pump speed controller. Minimum and maximum pump speed gives a lower and higher water flow rate of  $1.63\text{m}^3/\text{h}$  and  $2.38\text{m}^3/\text{h}$  respectively. Figure 6.1A shows the variations of the evaporating and condensing pressures and refrigerant mass flow rate with the evaporator water flow rate. Clearly, the pressure ratio decreases with the evaporator flow rate increase. This behavior can be explained by the fact that higher flow rates, result in slightly higher condenser pressure (3.2%) and higher evaporator pressure (9.1%), thereby the pressure ratio is reduced. The refrigerant mass flow rate increases (6%) with the evaporator water flow rate as illustrated in Fig. 6.1A. This is due to the increase in both volumetric efficiency and vapor density at the compressor inlet. The volumetric efficiency increases as result of decrease in pressure ratio while, the increase in density is mainly due to the increase in the evaporator pressure with evaporator water flow rate.

Figure 6.1B presents effect of evaporator water flow rate on both cooling capacity and gas engine energy consumption. It can be noted that, cooling capacity increases (3.1%) while gas engine energy consumption decreases (2%) as the evaporator water flow rate changes from  $1.63$  to  $2.38\text{m}^3/\text{h}$ . Slightly change in the pressure ratio (Fig. 6.1A.) leads to decrease in the cooling effect by 2.1% which can not overwhelms the high rate of increase in the refrigerant mass flow rate. So, cooling capacity increases with a value of 3.1% as a result of increasing the evaporator flow rate from  $1.63$  to  $2.38\text{m}^3/\text{h}$ .

Figure 6.1C demonstrates variation of primary energy ratio as well as chilled water temperature for different evaporator water flow rate. As the evaporator flow rate increases from  $1.63$  to  $2.38\text{m}^3/\text{h}$ , the primary energy ratio (PER) also increases by 5%. However, this increasing is mainly due to the rate of increasing in the cooling capacity and the rate of decreasing in the gas engine energy consumption. Obviously, the chilled water temperature at exit of the evaporator increase with evaporator water mass flow rate (Fig. 6.1C.) which it attributed mainly to the increase in the cooling capacity. An average chilled water temperature of about  $10^\circ\text{C}$  which is suitable for factory cooling (chiller water systems).

### 6.1.3 Effect of ambient air temperature

Variation of the performance characteristics of the GEHP related to different ambient air temperatures of  $19.7^\circ\text{C}$  and  $35^\circ\text{C}$  is shown in Fig. 6.2. Both engine speed and evaporator water flow rate remain constant at  $1300\text{rpm}$  and  $2.46\text{m}^3/\text{h}$  respectively. Measured values of the condensing and evaporating pressures and the refrigerant mass flow rate as a function of the evaporator water inlet temperature for different ambient temperatures are presented in Fig. 6.2A. It is clear that as the ambient air temperature increases both condensing pressure and evaporating pressure increases but with different rates. As ambient air temperature changes from  $19.7$  to  $35^\circ\text{C}$ , the condensing pressure increases by



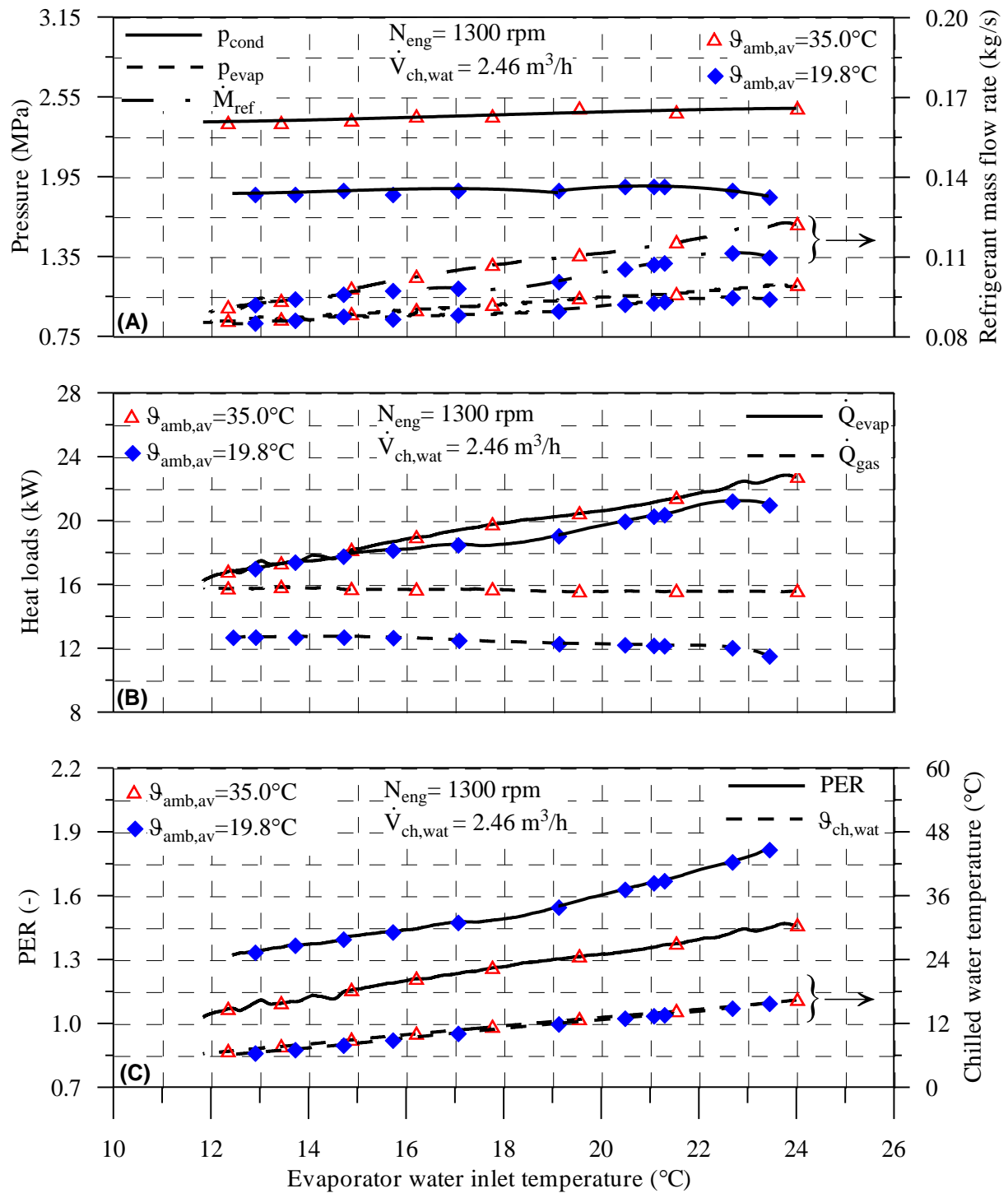


Figure 6.2: Effect of ambient air temperature on the performance characteristics of the GEHP in cooling mode; (A) operating pressures and refrigerant mass flow rate, (B) heat loads and (C) chilled water temperature and PER.

29.7% while the evaporating pressure increases by 5%. Both effects led to increase the pressure ratio and consequently decrease the volumetric efficiency. On the other hand, refrigerant vapor density at the compressor inlet increases as a result of the evaporating pressure increases. Obviously, the refrigerant mass flow rate increases (7%) when the ambient air temperature increases. This is can attributed mainly to increase in vapor density at compressor inlet. This fact is illustrated in Fig. 6.2A.

Variation of both cooling capacity and gas engine energy consumption for different ambient air temperatures is illustrated in Fig. 6.2B. It was noted that the cooling effect ( $h_{15} - h_{14}$ ) varied from 194 to 184kJ/kg (-5%) as the ambient air temperature changes from 19.7°C to 35°C. The combined effect of both refrigerant mass flow (7%) and cooling effect (-5%) led to slightly increase in the system cooling capacity (2%) as an average value over the entire range of the evaporator water inlet temperature. Increasing of the ambient air temperature has a remarkable effect on the gas engine energy consumption. Obviously, the gas engine energy consumption increase by 24% as the ambient air temperature varies from 19.7 to 35°C and this can be attributed to the decrease in gas engine efficiency.

Figure 6.2C shows the effect of the ambient air temperature on the primary energy ratio as well as the chilled water temperature. Since the rate of increasing in the gas engine energy consumption is higher than that in the cooling capacity, PER decreases by 24%. Average PER of the GEHP changed from 1.225 to 1.575 as the ambient air temperature varied from 35 to 19.7°C. The chilled water temperature slightly increased with ambient air temperature (Fig. 6.2C.) which it attributed mainly to the increase in the cooling capacity. The obtained chilled water temperature (5.5 to 17°C) covers the recommended ranges of summer air-conditioning chiller units reported by Stiemle [94].

#### 6.1.4 Effect of engine speed

Variation of the performance characteristics of the GEHP against the evaporator water inlet temperature for different engine speeds (1300 and 1750rpm) are illustrated in Fig. 6.3. Both the water volume flow rate and the ambient air temperature were held constant at  $2.67m^3/h$  and 24.5°C respectively. Figure 6.3A explains variation of the measured condensing and evaporating pressures as well as the refrigerant mass flow rate for different engine speeds. It can be noted that, as the engine speed increased from 1300 to 1750rpm the evaporating pressure decreases (10.3%) while the condensing pressure slightly remains constant. So, pressure ratio tends to increase and consequently the compressor volumetric efficiency decreases. On the other hand, increasing of the engine speed from 1300 to 1750rpm (30.7%) led to increase discharged refrigerant volume flow rate. The rate of increase in the refrigerant mass flow rate due to engine speed is more pronounced than the rate of decreasing resulting from volumetric efficiency decreasing. Hence, the refrigerant mass flow rate increases by 24.7%.

Variation of the cooling capacity as well as the gas engine energy consumption for different engine speeds is illustrated in Fig. 6.3B. As a result of decreasing the evaporating pressure, the cooling effect ( $h_{15} - h_{14}$ ) decreases which led the cooling

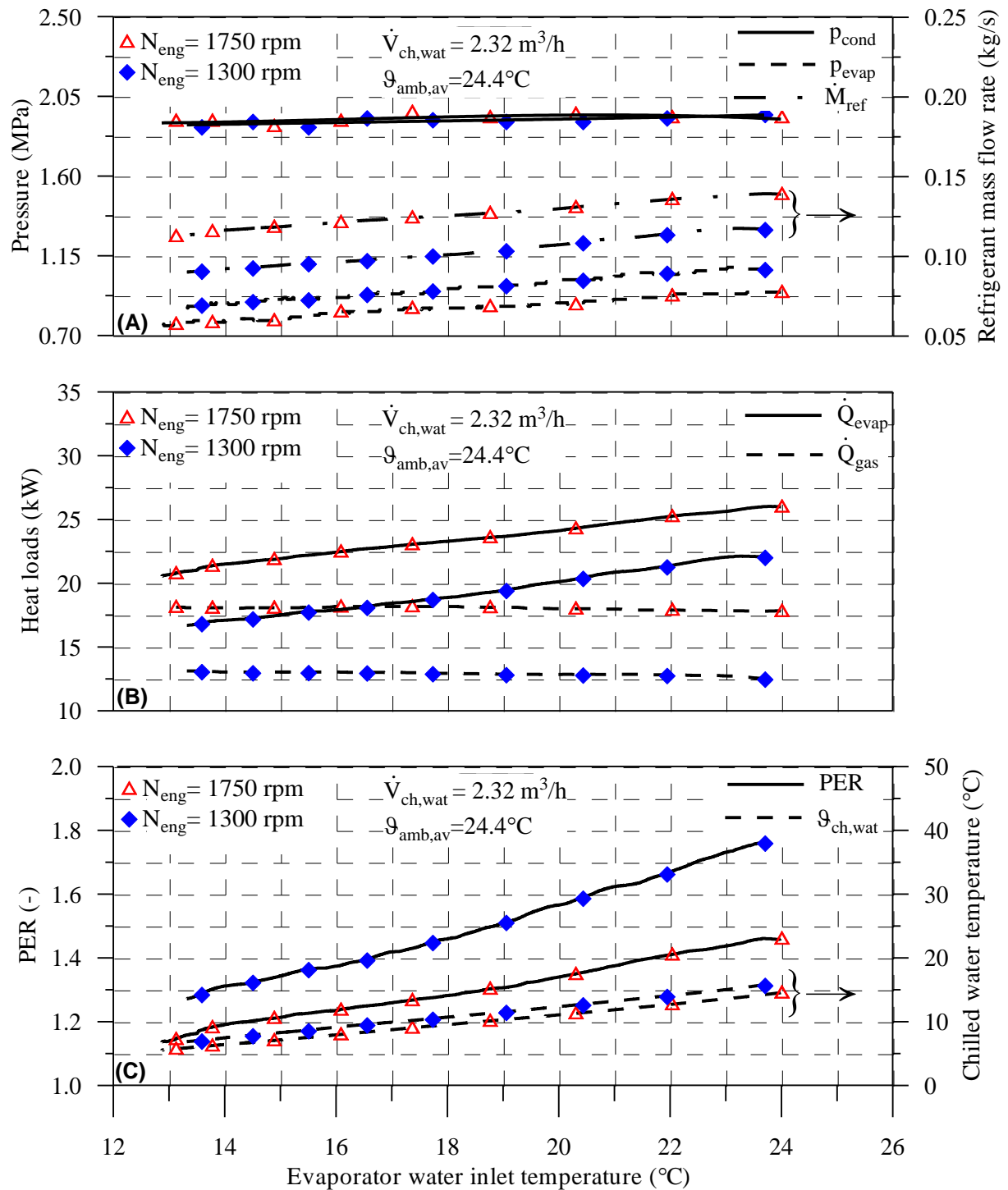


Figure 6.3: Effect of engine speed on the performance characteristics of the GEHP in cooling mode; (A) operating pressures and refrigerant mass flow rate, (B) heat loads and (C) chilled water temperature and PER.

capacity to decrease. On the other hand, refrigerant mass flow rate increases by 20.5 % which enable the system cooling capacity to increase. The high rate of increase in the cooling capacity resulting from refrigerant mass flow rate increasing overwhelms the low rate of decreases resulting from the evaporating pressure decreasing. So, it can notes that the cooling capacity increases by 23.6 % as the engine speed raises from 1300 to 1750rpm. Moreover, the gas engine energy consumption is increased by 38 % as the engine speed increase from 1300 to 1750rpm which can be seen from Fig. 6.3B. This trend can be attributed to the high rate of gas consumption at the higher engine speeds.

The effect of engine speed on both primary energy ratio as well as chilled water temperature is explained in Fig. 6.3C. Since the rate of increasing in the gas engine energy consumption (38 %) is higher than that in the cooling capacity (20.5 %), PER decreases (19 %) as a result of increasing of engine speed. Hence, it should be noted that an optimization of the engine speed is very important because higher engine speed gives higher cooling capacity but with lower PER. Figure 6.3C presents also variation of the chilled water temperature for different engine speeds. It can be noted that, range of the chilled water temperature lie in the recommended range for factory cooling and summer air-conditioning chiller. Primary energy ratio has been correlated as a function of the evaporator water inlet temperature, evaporator water volume flow rate, engine speed and ambient air temperature in the following form

$$PER_{cooling,corr} = 0.02917\vartheta_{ch,wat} - 0.0545\dot{V}_{ch,wat} - 0.0005N_{eng} - 0.0147\vartheta_{amb} + 2.1098, \quad (6.1)$$

where  $\vartheta_{ch,wat}$  is the evaporator water inlet temperature in ( $^{\circ}\text{C}$ ),  $\dot{V}_{ch,wat}$  represents the chilled water volume flow rate in ( $m^3/h$ ),  $N_{eng}$  refers to the engine speed in ( $rpm$ ) and  $\vartheta_{amb}$  is the ambient air temperature in ( $^{\circ}\text{C}$ ). The above equation is valid in the following ranges:  $11.8 \leq \vartheta_{ch,wat} \leq 28.3$ ,  $1.57 \leq \dot{V}_{ch,wat} \leq 3.17$ ,  $1287 \leq N_{eng} \leq 1767$  and  $7 \leq \vartheta_{amb} \leq 35$ . Fig. 6.4 illustrates a comparison between the experimental and correlated primary energy ratio. It should be noted that 92.8 % of all the data points lie within  $\pm 6\%$  error percentage. The resulting data points outside  $\pm 6\%$  error percentage can be attributed to unsteady state during experiments starting up.

## 6.2 Combined Cooling and Heating Mode

In this mode, the GEHP works in cooling mode and the engine waste heat recovery is used in water heating. As mentioned before that water temperature between 6 and  $12^{\circ}\text{C}$  is recommended for summer air-conditioning chillers. Hence, the evaporator water flow rate was selected to obtain water temperature at the evaporator outlet within the above recommended range. Hot water temperatures for different applications are given in Table 6.1 [96]. The system hot water outlet temperature was adjusted between 45 and  $65^{\circ}\text{C}$  to provide heating requirements for several applications like shaving, residential dish washing and laundry. All the experiments were done in cooling mode with engine heat recovery at ambient air temperature between 24.1 and  $33.8^{\circ}\text{C}$ . As a result of this, effect of ambient air temperature was considered. Moreover the system performance was studied at two engine speeds (1200 and 1750rpm). The influences of the evaporator water

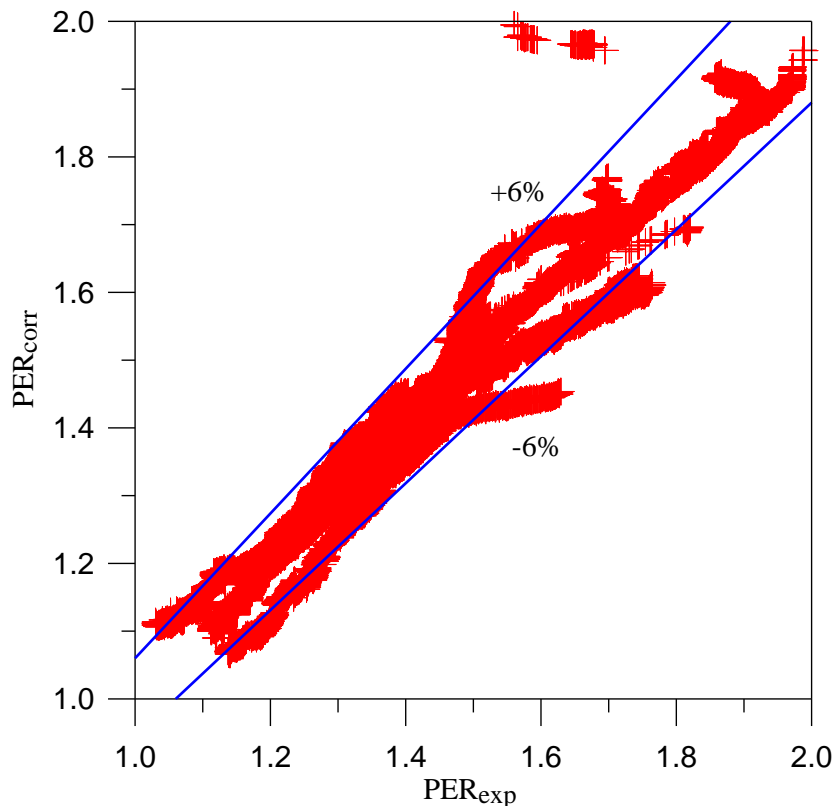


Figure 6.4: Comparison between experimental and correlated primary energy ratio data in cooling mode.

inlet temperature, evaporator water flow rate, ambient air temperature and engine speed on performance characteristics of the gas engine heat pump, using R410A as a working fluid, are discussed in this section. Fig. 6.5 indicates the effect of evaporator water inlet temperature and its volume flow rate on the performance of GEHP while the effect of ambient air temperature and engine speed on the performance of GEHP is presented in Figs. 6.6 and 6.7 respectively.

### 6.2.1 Effect of evaporator water inlet temperature

Dependency of performance characteristics of the GEHP upon the evaporator water inlet temperature for different chilled water flow rates is shown in Fig. 6.5. Keeping the evaporator water flow rate at about  $3.6\text{m}^3/\text{h}$ , the evaporator water inlet temperature was varied from  $12.2$  to  $20^\circ\text{C}$  to cover wide ranges of climatic conditions for air conditioning. Moreover, both engine speed and ambient air temperature were held constant at  $1750\text{rpm}$  and  $23.5^\circ\text{C}$  respectively. Variations of the measured condensing and evaporating pressures and refrigerant mass flow rate with the evaporator water inlet temperature are illustrated in Fig. 6.5A. It is seen that the evaporating pressure change ( $17.9\%$ ) is higher than that of the condensing pressures ( $2.59\%$ ), thereby the pressure ratio ( $p_{cond}/p_{evap}$ ) decreases as the evaporator water inlet temperature increases. Refrigerant mass flow rate increases with evaporator water inlet temperature. The increase in the refrigerant mass flow rate

Table 6.1: Representative hot water temperatures.

<i>Use</i>	<i>Temperature (°C)</i>
<i>Space cooling (chilled water)</i>	5-8
<i>Factory cooling</i>	0-10
<i>Fish farming</i>	20-40
<i>Therapeutic bath</i>	35
<i>Showers</i>	43
<i>Hand washing</i>	40
<i>Shaving</i>	45
<i>Surgical scrubbing</i>	43
<i>Domestic coin-operating laundries</i>	50-60
<i>Residential dish washing and laundry</i>	60
<i>Factory heating and hot water supply</i>	40-80

is mainly due to increase in both vapor density at compressor inlet and the volumetric efficiency. Figure 6.5A reveals this trend of the refrigerant mass flow rate. This figure confirms that the refrigerant mass flow rate is increased by 16.8% over the entire considered range of the evaporator water inlet temperatures. Variations of the cooling capacity, waste heat recovery and gas engine energy consumption with the evaporator water inlet temperature are shown in Fig. 6.5B. It is evident from this figure that all heat loads increase with evaporator water outlet temperature. System cooling capacity increases (17.2%) while gas engine energy consumption slightly decreases (1.7%) as the evaporator water inlet temperature increases. It may be noted that when the evaporator water inlet temperature varied from about 12.2 to 20°C, the cooling effect ( $h_{15} - h_{14}$ ) is reduced by 1.8%. Thus, the increase in refrigerant mass flow rate (16.8%), which overwhelms the reduction in specific enthalpy change, yields higher system cooling capacity (Eq.5.1). It is observed that the cooling water temperature difference through the heat recovery increases when the the chilled water temperature raises. In general, as the evaporator water inlet temperature changes from 12.2 to 20°C., the waste heat recovery increase by 24% while the gas heat consumption decreases by 0.7%.

Measured chilled and hot water outlet temperatures against the evaporator water inlet temperature are presented in Fig. 6.5C, which indicates that chilled water temperature increases while the hot water outlet temperature ( $\vartheta_{h,wat} = 65^\circ\text{C}$ ) decreases when the evaporator water inlet temperature increases. As the system cooling capacity increases, temperature difference through them increases for constant water mass flow rate, thereby higher chilled water temperatures were obtained at higher evaporator water inlet temperature as shown in Fig. 6.5C. Furthermore, chilled water temperature between 6.5 and 12.5°C were obtained. It should be noted temperature levels of 6.5 to 12.5°C may be adequate for cooling food processing machines which need cooling water temperature. On the other hand, the hot water temperature between 55.8 and 63°C are obtained. The obtained hot water can be used in several applications like domestic

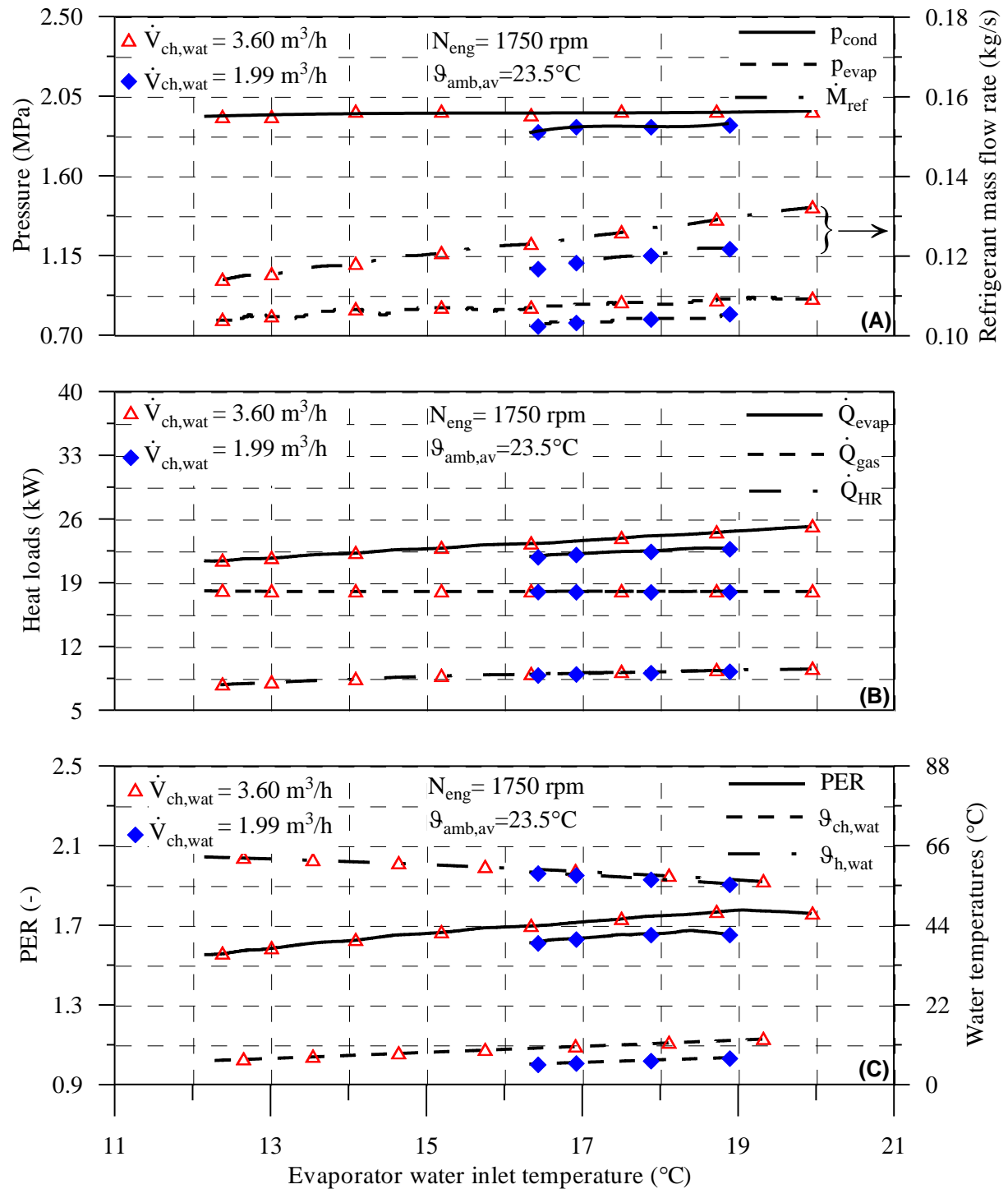


Figure 6.5: Effect of evaporator water inlet temperature on the performance characteristics of the GEHP in combined mode for different water volume flow rates; (A) operating pressures and refrigerant mass flow rate, (B) heat loads and (C) water temperatures and PER.

coin-operating laundries and residential dish washing as presented in Table 6.1. The effect of evaporator water inlet temperature on primary energy rate can be also predicted from Fig. 6.5C. A higher evaporator water inlet temperature yields a higher PER[97]. This trend is mainly due to a large increase in both cooling capacity and heat recovery compared to a small decrease in the gas engine heat consumption as shown in Fig. 6.5B. Clearly, the primary energy ratio of the GEHP increases by 14.8% as the evaporator water inlet temperature varies from 12.2 to 20°C.

### 6.2.2 Effect of evaporator water volume flow rate

Influence of the evaporator water flow rate on the performance characteristics of the gas engine heat pump, when other external operating parameters are maintained constant, can be predicted from Fig. 6.5. Two different chilled water flow rate of 1.99 and 3.6m<sup>3</sup>/h have been considered to study the performance characteristics of the GEHP. Figure 6.5A shows the variations of the evaporating and condensing pressures and refrigerant mass flow rate with the evaporator water flow rate. The pressure ratio decreases with the evaporator flow rate increase. This behavior can be explained by the fact that higher flow rates, result in slightly increase condenser pressure (3.7%) and higher evaporator pressure (11.4%), thereby the pressure ratio is reduced. The refrigerant mass flow rate increases (6.2%) with the evaporator water flow rate as illustrated in Fig. 6.1A. This is due to the increase in both volumetric efficiency and vapor density at the compressor inlet. The volumetric efficiency increases as result of decrease in pressure ratio while, the increase in density is mainly due to the increase in the evaporator pressure with evaporator water flow rate.

System cooling capacity, heat recovery load and gas engine energy consumption versus evaporator water inlet temperature for evaporator water flow rate of 3.6 and 1.99m<sup>3</sup>/h are illustrated in Fig. 6.5B. It can be seen that both engine heat recovery load and gas consumption remain nearly constant while cooling capacity increases when the evaporator water flow rate. The increase in evaporator cooling capacity is mainly due to the increase in the chilled water mass flow rate increases. This figure confirms that the cooling capacity increases by 6.6% as the evaporator volume mass flow increases from 1.99 to 3.6m<sup>3</sup>/h.

Measured outlet water temperatures from both evaporator and heat recovery heat exchanger versus the evaporator water inlet temperature for evaporator water flow rate of 3.6 and 1.99m<sup>3</sup>/h are presented in Fig. 6.5C. It is seen that both chilled and hot water outlet temperatures increase as the evaporator water flow rate increases. An average evaporator outlet water temperature of about 9.5°C and heat recovery outlet water temperature lies between 55 and 62°C are obtained over the considered range of the evaporator inlet water temperature. Hot water temperatures of such levels are adequate for various applications such as domestic laundries, showers and lavatory while chilled water temperature of 9°C is suitable for factory cooling (chiller water systems). Fig. 6.5C. illustrates also primary energy ratio as a function of the evaporator water inlet temperature for chilled water flow rate of 1.99 and 3.6m<sup>3</sup>/h. Clearly, the primary



energy ratio increases with the evaporator water flow rate. This behavior is mainly due to increase in the cooling capacity with the evaporator water flow rate as shown in Fig. 6.5C PER increases by 4.8 % when the evaporator volume flow rate changes from 1.99 to  $3.6\text{m}^3/\text{h}$ .

### 6.2.3 Effect of ambient air temperature

The effect of ambient air temperature on the performance characteristics of the gas engine heat pump related to different ambient air temperatures of 24.1 and 33.8°C is shown in Fig. 6.6. Both engine speed and evaporator water flow rate remain constant at 1750rpm and  $3.38\text{m}^3/\text{h}$  respectively. Measured values of the condensing and evaporating pressures and the refrigerant mass flow rate as a function of the evaporator water inlet temperature for different ambient temperatures are presented in Fig. 6.6A. It is clear that as the ambient air temperature increases both condensing pressure and evaporating pressure increases but with different rates. As the ambient air temperature changes from 24.1 to 33.8°C, the condensing pressure increases by 28 % while the evaporating pressure increases by 4 %. Both effects led to increase the pressure ratio and consequently decrease the volumetric efficiency. On the other hand, the refrigerant vapor density at the compressor inlet increase as a result of the evaporating pressure increase. Obviously, the refrigerant mass flow rate increases (6.6 %) when the ambient air temperature increases. This is attributed mainly to increase in the vapor density at compressor inlet. This fact is illustrated in Fig. 6.6A.

Influence of the ambient air temperature on the cooling capacity, heat recovery load and gas engine energy consumption can be predicted from Fig. 6.6B. It is evident from the figure that the cooling capacity, heat recovery load and gas heat consumption increase with the ambient air temperature. It was noted that the cooling effect ( $h_{15} - h_{14}$ ) decreased by 2 % as the ambient air temperature changes from 19.7 to 35°C. The combined effect of both refrigerant mass flow (6.6 %) and cooling effect (-2 %) led to increase in the system cooling capacity (7.3 %) as an average value over the entire range of evaporator water inlet temperature. Obviously, the gas engine energy consumption increase by 19.4 % as the ambient air temperature varies from 24.1 to 33.8°C and this can be attributed to the decrease in gas engine efficiency. It should be noted, at higher values of evaporator water inlet temperature, heat recovery increases by 15 % while at the lower evaporator water inlet temperature, heat recovery remains constant.

Variations of measured evaporator and heat recovery water outlet temperatures with the evaporator water inlet temperature for two ambient air temperatures (24.1 and 33.8°C) are illustrated in Fig. 6.6C. It can be seen that the evaporator water outlet temperature increases with the ambient air temperature. Clearly, the influence of the ambient air temperature on the evaporator water outlet temperature is minor. Fig. 6.6C presents also the primary energy ratio against the evaporator water inlet temperature for ambient air temperature of 24.1 to 33.8°C. It can be seen that the primary energy ratio at ambient air temperature of 34.8°C is lower than that at ambient air temperature of 24.1°C. This is because of the rate of increase in gas heat consumption is higher than

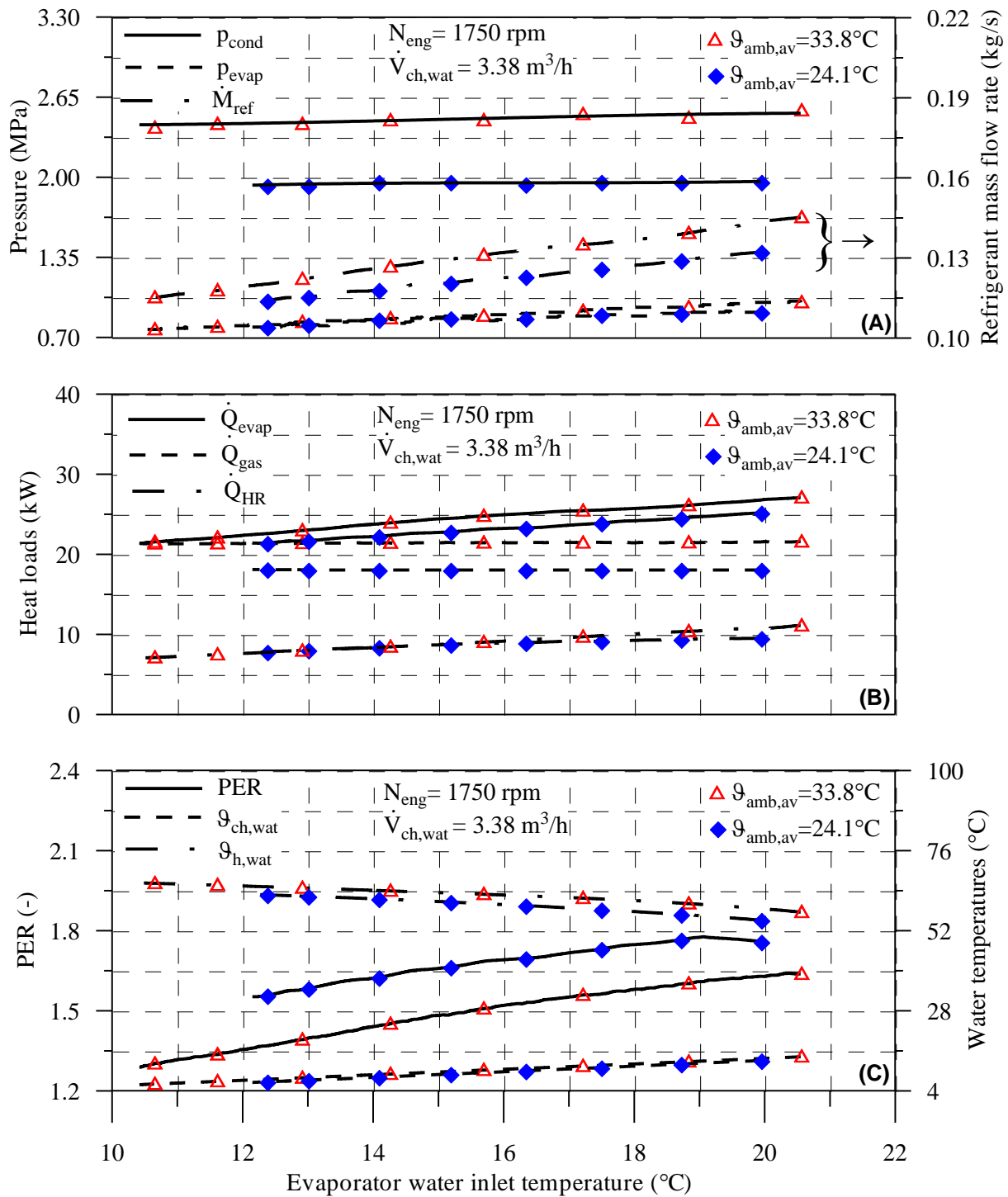


Figure 6.6: Effect of ambient air temperature on the performance characteristics of the GEHP in combined mode; (A) operating pressures and refrigerant mass flow rate, (B) heat loads and (C) water temperatures and PER.

that in both cooling capacity and heat recovery load as shown in Fig. 6.6B. As the ambient air temperature varies from 24.1 to 34.8°C, PER decreases by 12.8% as shown in Fig. 6.6C.

#### 6.2.4 Effect of engine speed

Performance characteristics of the GEHP against evaporator water inlet temperature for different engine speeds (1200 and 1750rpm) are illustrated in Fig. 6.7. Both the water volume flow rate and the ambient air temperature were held constant at 3.38 and 20.6°C respectively. Figure 6.7A explains variation of the measured condensing and evaporating pressures as well as the refrigerant mass flow rate for different engine speeds. It can be noted that, when the engine speed increased from 1200 to 1750rpm the evaporating pressure decreases (13.75%) while the condensing pressure increases by 6.5%. So, the pressure ratio tends to increase and consequently the compressor volumetric efficiency decreases. On the other hand, increasing of the engine speed from 1200 to 1750rpm (45.8%) led to increase discharged refrigerant volume flow rate. The rate of increase in the refrigerant mass flow rate due to engine speed is more pronounced than the rate of decreasing resulting from the volumetric efficiency decreasing. Hence, the refrigerant mass flow rate increases by 29.4%.

Figure 6.7B shows the cooling capacity, heat recovery load and gas heat consumption versus the evaporator water inlet temperature at engine speed of 1200 and 1750rpm. Clearly, higher engine speed yields higher cooling capacity, heat recovery load and gas heat consumption. As a result of increasing the pressure ratio, the cooling effect ( $h_{15} - h_{14}$ ) decreases which lead the cooling capacity to decrease. On the other hand, the refrigerant mass flow rate increases by 29.4% which enable the system cooling capacity to increase. The high rate of increase in the cooling capacity resulting from refrigerant mass flow rate increasing overwhelms the low rate of decreases resulting from pressure ratio increasing. So, it can be noted that the cooling capacity increases by 27% as the engine speed raises from 1200 to 1750rpm. Moreover, both gas engine energy consumption and waste heat recovery are increased by 38% and 56.5% as the engine speed changes from 1200 to 1750rpm which can be seen from Fig. 6.7B. This trend can be attributed to the high rate of gas consumption at the higher engine speeds.

Figure 6.7C illustrates measured chilled and hot water outlet temperatures as well as primary energy ratio as function of the evaporator water inlet temperature for two engine speeds. Clearly, the chilled water outlet temperature decreases while hot water outlet temperature increases when the engine speed increases. Variations of external operating parameters yield an average chilled and hot water outlet temperatures are (6.2 to 15.9°C) and (50 to 65°C) respectively, which are within the recommended range for different applications. Since the rate of increasing in the gas engine energy consumption (56.6%) is higher than that in the cooling capacity (27%) and waste heat recovery (34%), PER decreases (20%) as a result of increasing of engine speed. Hence, it should be noted that an optimization of the engine speed is very important because higher engine speed gives higher cooling capacity but with lower PER. Primary energy ratio has been

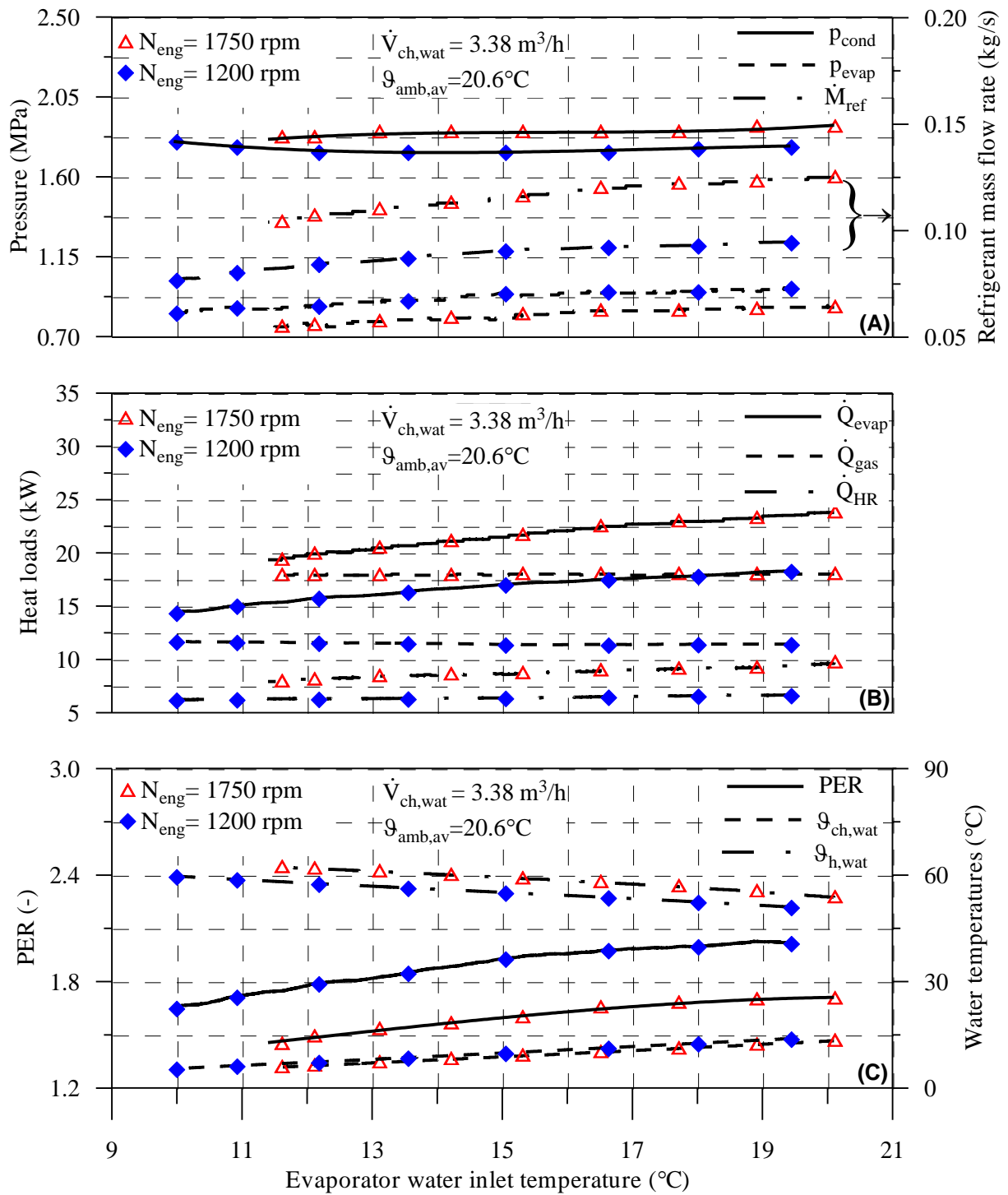


Figure 6.7: Effect of engine speed on the performance characteristics of the GEHP in combined mode; (A) operating pressures and refrigerant mass flow rate, (B) heat loads and (C) water temperatures and PER.

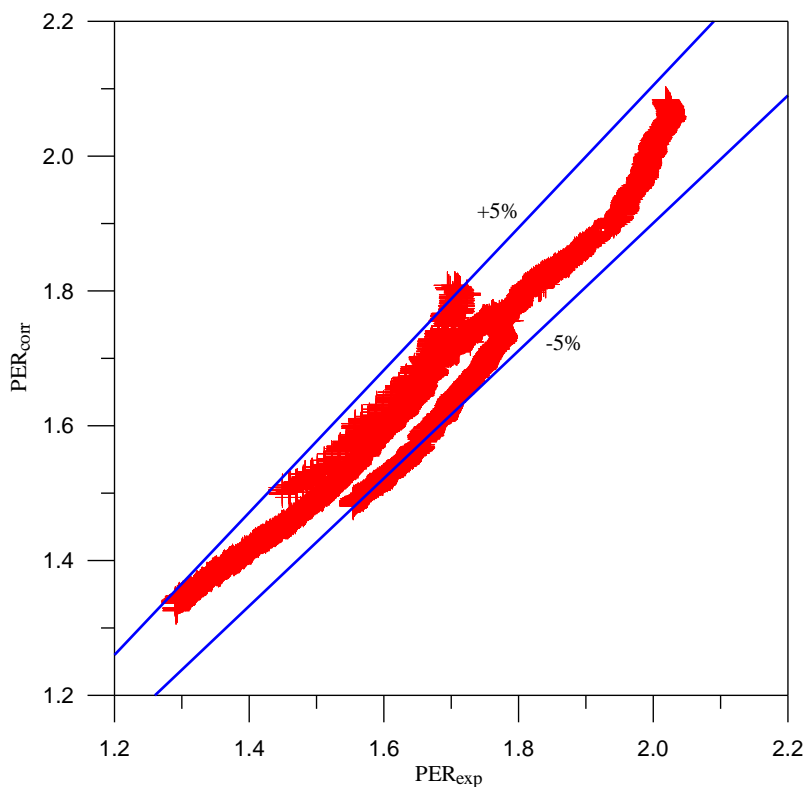


Figure 6.8: Comparison between experimental and correlated primary energy ratio data in combined mode.

correlated as a function of the evaporator water inlet temperature, evaporator water volume flow rate, engine speed and ambient air temperature in the following form;

$$PER_{combined,corr} = 0.03613\vartheta_{ch,wat} - 0.0125\dot{V}_{ch,wat} - 0.0004N_{eng} + 0.0326\vartheta_{amb} + 2.0691 \quad (6.2)$$

Where  $\vartheta_{ch,wat}$  is the evaporator water inlet temperature in ( $^{\circ}\text{C}$ ),  $\dot{V}_{ch,wat}$  represents the chilled water volume flow rate in ( $\text{m}^3/\text{h}$ ),  $N_{eng}$  refers to engine speed in ( $\text{rpm}$ ) and  $\vartheta_{amb}$  is the ambient air temperature in ( $^{\circ}\text{C}$ ). The above equation is valid in the following ranges:  $12.2 \leq \vartheta_{ch,wat} \leq 21$ ,  $1.99 \leq \dot{V}_{ch,wat} \leq 3.6$ ,  $1200 \leq N_{eng} \leq 1750$  and  $24.1 \leq \vartheta_{amb} \leq 33.8$ . Fig. 6.2 illustrates a comparison between experimental and correlated primary energy ratio. It should be noted that 99% of all the data points lie within  $\pm 5\%$  error percentage.

### 6.3 Heating Mode

In this mode, the gas engine has been used to drive a vapor compression heat pump as well as the engine waste heat is recovered to enhance the heating performance of the GEHP system. Recovered engine heat represents one of the main advantages of the gas engine heat pump system as compared with conventional heat pump systems [98]. In order to optimize the utilization of the recovered engine heat, two options of heat recovery utilization have been applied and compared. The first choice is to use the

recovered engine heat to heat the supplied water while the other option is to transfer it to the refrigerant cycle in order to evaporate the refrigerant especially at lower ambient temperatures. According to engine heat recovered from the engine block and exhaust gas utilization the GEHP system can be operated in two modes:

Mode-I : in which the recovered engine heat is transferred to the water in order to reach higher hot water supply (using the heat recovery heat exchanger). Both electronic valves  $V_3$  and  $V_5$  are closed manually to ensure that all the recovered engine heat is transferred to water circuit (see Fig. 5.3).

Mode-II: in which the recovered engine heat is transferred to the refrigerant to evaporate it especially in low ambient air temperatures (using the sub heat exchanger). Electronic valve  $V_6$  is closed manually to ensure that all the recovered engine heat is transferred to water circuit (see Fig. 5.3).

### 6.3.1 Heating mode-I

In this mode-I, the system hot water outlet temperature was adjusted between 35 and 70°C to provide heating requirements for several applications like shaving, residential dish washing and laundry. All the experiments were done at ambient air temperature between 10.7 and 25.8°C. As a result of this, effect of the ambient air temperature was considered. Moreover the system performance was studied at two engine speeds (1300 and 1750rpm). The influences of condenser water inlet temperature, condenser water flow rate, ambient air temperature and engine speed on performance characteristics of the GEHP are discussed in this section. Figure 6.9 indicates the effects of condenser water inlet temperature and its volume flow rate on the performance of GEHP while the effects of ambient air temperature and engine speed on the performance of the GEHP are presented in Figs. 6.10 and 6.11 respectively.

#### 6.3.1.1 Effect of condenser water inlet temperature

Dependency of the performance characteristics of the GEHP upon the condenser water inlet temperature for different condenser water flow rates is shown in Fig. 6.9. Keeping the condenser water flow rate at about  $16.6m^3/h$ , condenser water inlet temperature was varied from 35.8 to 48°C to cover wide ranges of hot water applications [99]. Moreover, both engine speed and ambient air temperature were held constant at 1750rpm and 24°C respectively. Variations of the measured condensing and evaporating temperatures and refrigerant mass flow rate with the condenser water inlet temperature are illustrated in Fig. 6.9A. It is seen that the condensing temperature change (18%) is higher than that of the evaporating temperature (8.1%), thereby the pressure ratio ( $p_{cond}/p_{evap}$ ) increases as the condenser water inlet temperature increases. Refrigerant mass flow rate slightly increases with condenser water inlet temperature. The increase in the refrigerant mass flow rate is mainly due to increase in vapor density at compressor inlet. Figure 6.9A reveals this trend of the refrigerant mass flow rate. This figure confirms that the refrigerant mass flow rate is increased by 2.1% over the entire considered range of the condenser water inlet temperatures.

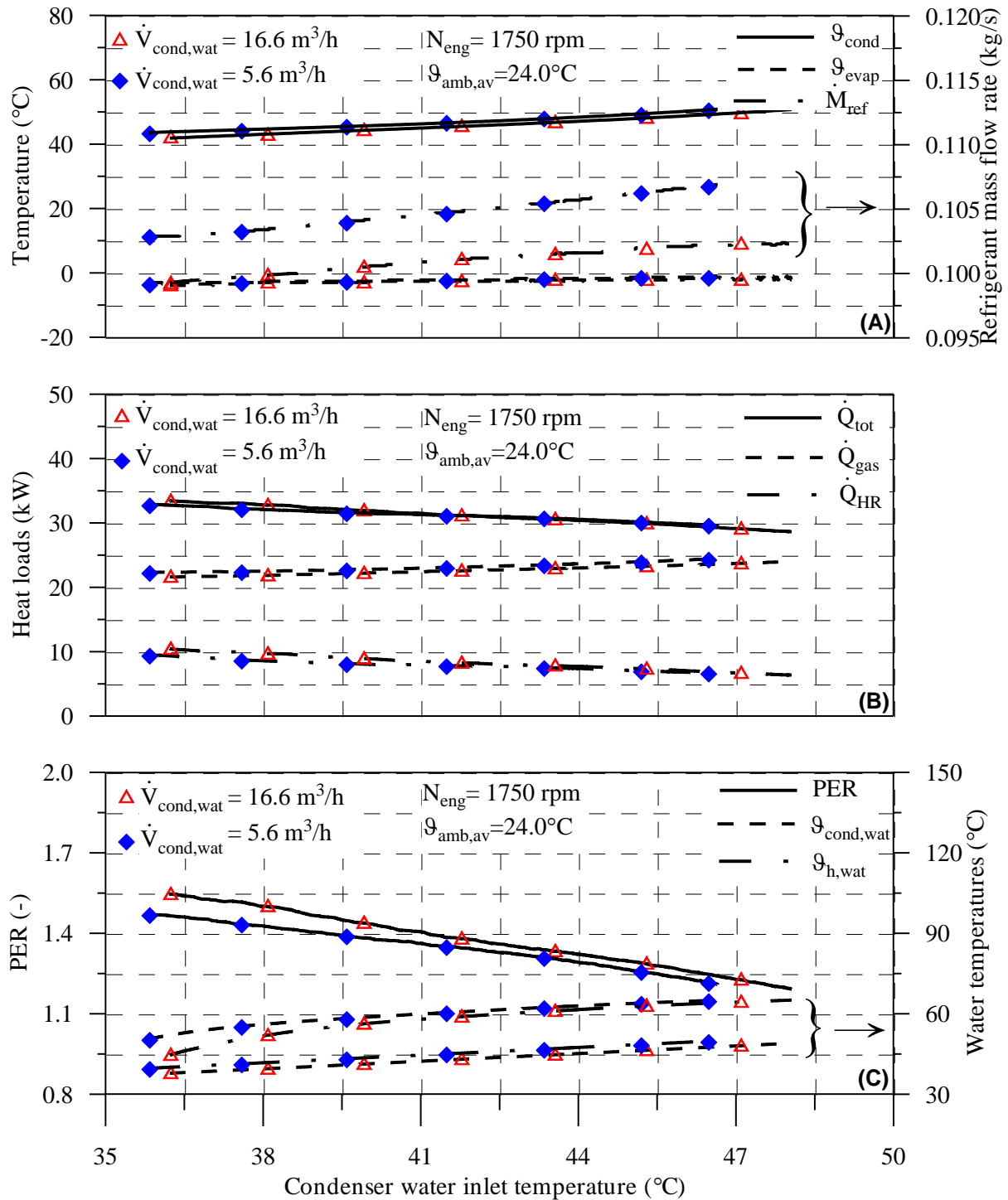


Figure 6.9: Effect of condenser water inlet temperature on the performance characteristics of the GEHP in heating mode-I for different water volume flow rates; (A) operating temperatures and refrigerant mass flow rate, (B) heat loads and (C) water temperatures and PER.

Variations of total heating capacity, waste heat recovery and gas engine energy consumption with condenser water inlet temperature are shown in Fig. 6.9B. It is evident from this figure that total heating capacity and waste heat recovery decrease while gas engine heat consumption increases when condenser water outlet temperature increase. It may be noted that when the condenser water inlet temperature varied from about 35.8 to 48°C, the specific enthalpy change ( $h_{14} - h_{15}$ ) is reduced by 6.8%. Thus, the decrease in the specific enthalpy (6.8%), which overwhelms the increase in refrigerant mass flow rate, yields lower system heating capacity (Eq.5.1). On the other side, it is observed that both of the condenser and heat recovery water temperature differences decreases causing the total heating capacity to decrease. In general, as the condenser water inlet temperature changes from 35.8 to 48°C, both total heating capacity and gas engine heat recovery decrease by 3.5% and 61.5% respectively while gas engine heat consumption increases by 11.6%. This can be attributed to the decrease in temperature difference between the engine coolant and hot water temperatures as the condenser water inlet temperature increases. In which, the engine coolant temperature is nearly constant while the hot water temperature increases so the temperature difference decreases and consequently the engine heat recovery decreases.

Measured condenser and heat recovery water outlet temperatures against the condenser water inlet temperature are presented in Fig. 6.9C, which indicates that the condenser and heat recovery water outlet temperatures increase when condenser water inlet temperature increases. Clearly, hot water outlet temperatures lie within the recommended ranges listed in Table 6.1. The effect of condenser water inlet temperature on the PER can be predicted from Fig. 6.9C. A higher condenser water inlet temperature yields a lower PER. This trend is mainly due to both decrease in total heating capacity and increase in the gas engine heat consumption as shown in Fig. 6.9B. Clearly, primary energy ratio of the GEHP decreases by 29.2% as the condenser water inlet temperature varies from 35.8 to 48°C.

### 6.3.1.2 Effect of condenser water volume flow rate

Influence of the condenser water flow rate on the performance characteristics of the GEHP, when other external operating parameters are maintained constant, can be predicted from Fig. 6.9. Two different condenser water flow rate of 16.6 and 5.6m<sup>3</sup>/h have been considered to study the performance characteristics of the GEHP. Figure 6.9A shows variations of the evaporating and condensing temperatures and the refrigerant mass flow rate for different evaporator water flow rates. Clearly, the pressure ratio increases with the condenser flow rate increase. This behavior can be explained by the fact that higher flow rates, result in slightly decrease in the condensing pressuretemperature (1.4%) and decrease the evaporating temperature (2.1%), thereby the pressure ratio is increased. The refrigerant mass flow rate decreases (3.9%) with the condenser water flow rate as illustrated in Fig. 6.9A. This is due to the decrease in both volumetric efficiency and vapor density at the compressor inlet. The volumetric efficiency decreases as result of increase in pressure ratio while, the decrease in density is mainly due to the decrease in the evaporating temperature with condenser water flow rate.



Total heating capacity, gas engine heat recovery and gas engine energy consumption versus condenser water inlet temperature for condenser water flow rate of 16.6 and  $5.6\text{m}^3/\text{h}$  are illustrated in Fig. 6.9B. It can be seen that both gas engine heat recovery and heating capacity increase while gas engine energy consumption decreases when the condenser water flow rate increases. The increase in total heating capacity is mainly due to the increase in the condenser water mass flow rate. This figure confirms that both the total heating capacity and waste heat recovery increases by 2.1 %, 7 % respectively as the condenser volume mass flow increases from 5.6 to  $16.6\text{m}^3/\text{h}$ . Furthermore, the gas engine energy consumption decreases by 2 % as the condenser flow increases from 5.6 to  $16.6\text{m}^3/\text{h}$ .

Measured outlet water temperatures from both condenser and gas engine heat recovery versus the condenser water inlet temperature for condenser water flow rate of 16.6 and  $5.6\text{m}^3/\text{h}$  are presented in Fig. 6.9C. It is seen that hot water outlet temperatures decrease as the condenser water flow rate increases. Condenser water outlet temperature ranges from 38 to  $48^\circ\text{C}$  and heat recovery water outlet temperature lies between 45 and  $65^\circ\text{C}$  in the considered range of the condenser inlet water temperature. Hot water temperatures of such levels are adequate for various applications such as domestic laundries, showers and lavatory. Figure 6.9C illustrates PER as a function of the condenser water inlet temperature for condenser water flow rate of 5.6 and  $16.6\text{m}^3/\text{h}$ . Clearly, the PER increases with the condenser water flow rate. This behavior is mainly due to decrease in the gas engine heat consumption and the increase in both total heating capacity and waste heat recovery with the condenser water flow rate as shown in Fig. 6.9C. PER increases by 4.9 % as an average value when the condenser water flow rate changes from 5.6 to  $16.6\text{m}^3/\text{h}$ .

### 6.3.1.3 Effect of ambient air temperature

The effect of the ambient air temperature related to different ambient air temperatures of 11.9 and  $22^\circ\text{C}$  on the performance characteristics of the GEHP is shown in Fig. 6.10. Both engine speed and condenser water flow rate remain constant at  $1300\text{rpm}$  and  $20\text{m}^3/\text{h}$  respectively.

Measured values of the condensing and evaporating temperatures and the refrigerant mass flow rate as a function of the condenser water inlet temperature for different ambient temperatures are presented in Fig. 6.10A. It is clear that as the ambient air temperature increases the evaporating temperature increase. As the ambient air temperature changes from 11.9 to  $22^\circ\text{C}$ , the evaporating temperature increases by 8.7 % which led to decrease the pressure ratio and consequently increase the volumetric efficiency. Obviously, the refrigerant mass flow rate increases slightly (4.3 %) when the ambient air temperature increases. This fact is illustrated in Fig. 6.10A.

Influence of the ambient air temperature on the total heating capacity, gas engine heat recovery and gas heat energy consumption can be predicted from Fig. 6.10B. It is evident from the figure that the total heating capacity, gas engine heat recovery and

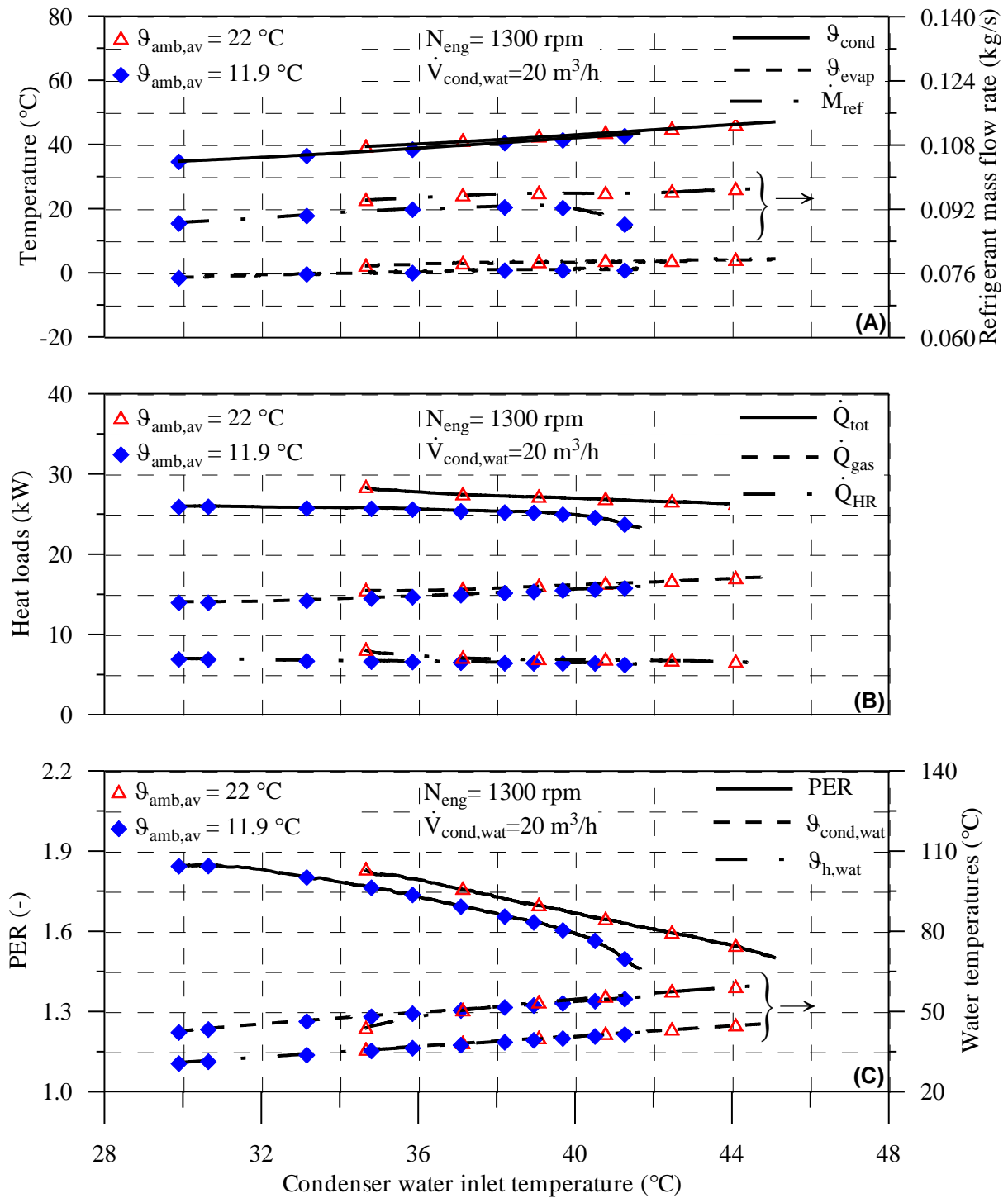


Figure 6.10: Effect of ambient air temperature on the performance characteristics of the GEHP in heating mode-I; (A) operating temperatures and refrigerant mass flow rate, (B) heat loads and (C) water temperatures and PER.

gas engine heat consumption increase as the ambient air temperature increases. As the ambient air temperature increases from 11.9 to 22°C, the total heating capacity, gas engine heat recovery and gas heat consumption increase by 7.3 %, 6.6 % and 3.2 % respectively. The increase in both the total heating capacity and the gas engine heat recovery can be attributed to increase in the condenser water temperature difference. Variations of measured condenser and heat recovery water outlet temperatures with the condenser water inlet temperature for two ambient air temperatures (11.9 and 22°C) are illustrated in Fig. 6.10C. It can be seen that the heat recovery water outlet temperature decreases with the ambient air temperature. Clearly, the influence of the ambient air temperature on the condenser water outlet temperature is minor. Fig. 6.10C presents the system PER against the condenser water inlet temperature for ambient air temperature of 11.9 and 22°C. It can be seen that the PER at ambient air temperature of 22°C is higher than that at ambient air temperature of 11.9°C. This is because of the rate of increase in the total heating capacity is higher than that in gas engine heat consumption as shown in Fig. 6.10B. As the ambient air temperature varies from 11.9 to 22°C, PER increases by 3% as an average value for the considered water condenser outlet temperature.

#### 6.3.1.4 Effect of engine speed

Performance characteristics of the GEHP as a function of the condenser water inlet temperature at two engine speeds of 1300 and 1750rpm are presented in Fig. 6.11. Both the water volume flow rate and the ambient air temperature were held constant at 18.82m<sup>3</sup>/h and 21.7°C respectively.

Figure 6.11A illustrates variation of the measured condensing and evaporating temperatures as well as refrigerant mass flow rate for different engine speeds. It can be noted that, when the engine speed increased from 1300 to 1750rpm the evaporating temperature decreases (21 %) while the condensing temperature increases by 5.7 %. So, the pressure ratio tends to increase and consequently the compressor volumetric efficiency decreases. On the other hand, increasing of the engine speed from 1300 to 1750rpm (34.6 %) led to increase discharged refrigerant volume flow rate increases. The rate of increase in the refrigerant mass flow rate due to the engine speed is more pronounced than the rate of decreasing resulting from the volumetric efficiency decreasing. Hence, the refrigerant mass flow rate increases by 7.3 %.

Figure 6.11B shows the total heating capacity, gas engine heat recovery and gas engine heat consumption versus the condenser water inlet temperature at engine speeds of 1300 and 1750rpm. Clearly, higher engine speed yields higher heating capacity, gas engine heat recovery and gas engine heat consumption. This trend can be attributed to the high rate of gas consumption at the higher engine speeds. It should be noted that as the engine speed increases by 34.6 %, all of total heating capacity, gas engine heat recovery and gas engine heat consumption increase by 15 %, 28 % and 39 % respectively. The high rate of increase in gas engine energy consumption overwhelms the system PER to decrease at the engine high speed as indicated in Fig.6.11C. As the engine speed

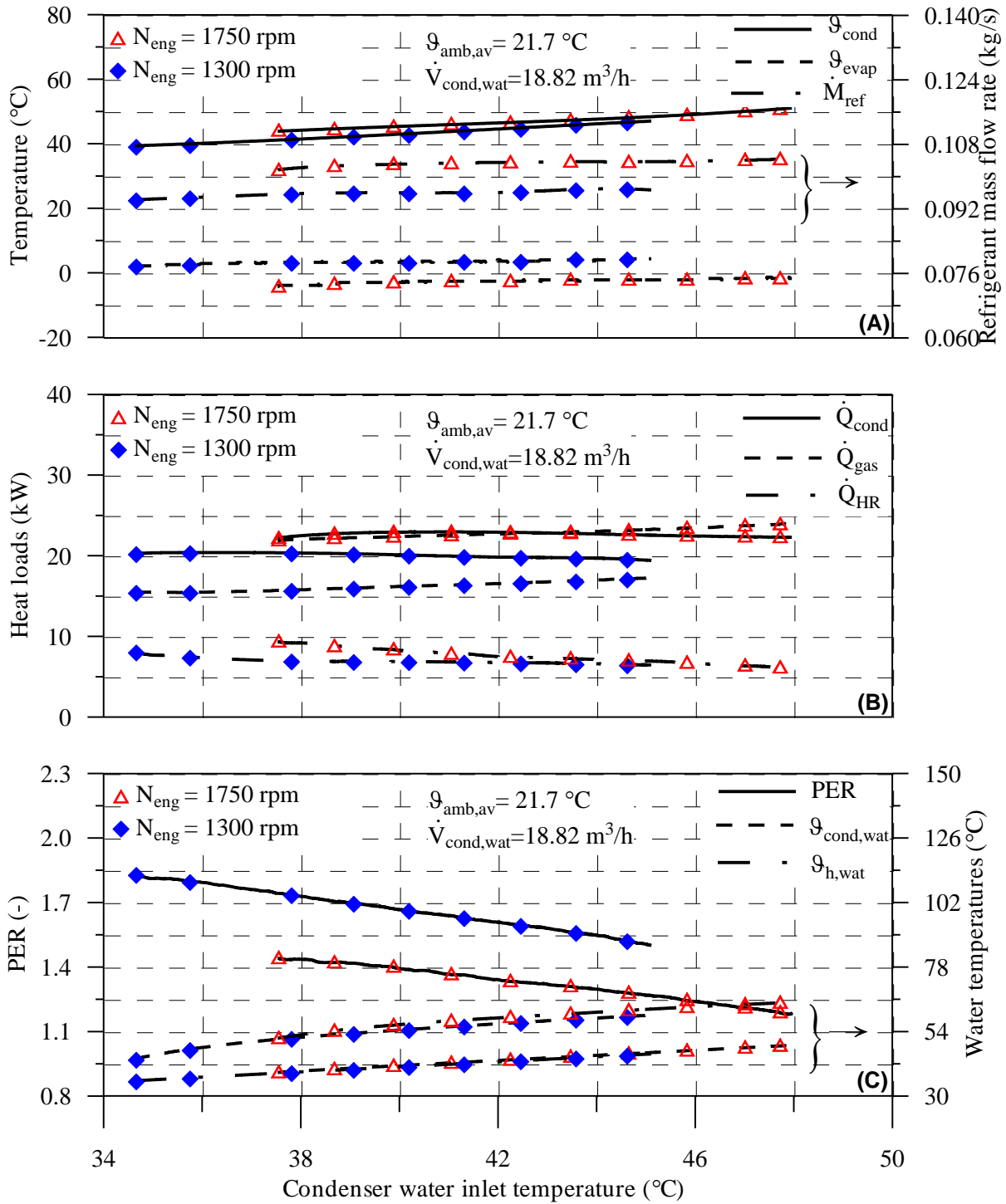


Figure 6.11: Effect of engine speed on the performance characteristics of the GEHP in heating mode-I; (A) operating temperatures and refrigerant mass flow rate, (B) heat loads and (C) water temperatures and PER.

increase from 1300 to 1750 $rpm$ , system PER decreases by 16.7%. Figure 6.11C illustrates also the measured hot water outlet temperatures as a function of the condenser water inlet temperature for two engine speeds. Clearly, the condenser and heat recovery water outlet temperatures increase when the engine speed increases. Variations of external operating parameters yield an average hot water outlet temperature between 35 and 65°C, which is within the recommended range for different applications. Primary energy ratio and recovered engine heat have been correlated as a function of the condenser water inlet temperature, condenser water volume flow rate, engine speed and ambient air temperature in the following forms

$$PER_{heating,corr} = -0.024\vartheta_{cond,wat} - 0.0005\dot{V}_{cond,wat} - 0.0005N_{eng} + 0.004\vartheta_{amb} + 3.25 \quad (6.3)$$

$$\ln(\dot{Q}_{HR,corr}) = -0.0342\vartheta_{cond,wat} - 0.0004\dot{V}_{cond,wat} + 0.0006N_{eng} + 0.0096\vartheta_{amb} + 2.172 \quad (6.4)$$

Where  $\vartheta_{cond,wat}$  is the condenser water inlet temperature in (°C),  $\dot{V}_{ch,wat}$  represents the condenser water volume flow rate in ( $m^3/h$ ),  $N_{eng}$  refers to engine speed in ( $rpm$ ) and  $\vartheta_{amb}$  is the ambient air temperature in (°C). The above equation is valid in the following ranges:  $24.8 \leq \vartheta_{cond,wat} \leq 48.8$ ,  $5.24 \leq \dot{V}_{cond,wat} \leq 16.64$ ,  $1287 \leq N_{eng} \leq 1765$  and  $8 \leq \vartheta_{amb} \leq 26$ .

Figure 6.12 illustrates a comparison between experimental and correlated primary energy ratio and recovered engine heat data. It should be noted that 97.5% of all the data points lie within  $\pm 4\%$  error percentage for primary energy ratio and 75% of all the data points lie within  $\pm 10\%$  error percentage for recovered engine heat energy ratio.

### 6.3.2 Heating mode-II

Low evaporator capacity and frosting are the main problems which take place during the operation of the GEHP at lower ambient air temperature. Actually at lower ambient air temperature, the logarithmic mean temperature difference between the air and the refrigerant gets lower. So, the evaporator heat transfer area should be enlarged to recompense the evaporator capacity. But unfortunately the evaporator heat transfer area is fixed and designed for cooling mode operation. Hence, the engine heat recovery is transferred to the evaporator to enhance the evaporator capacity and to avoid frosting problem and this mode is called mode-II.

The hot water supply temperature was adjusted between 37 and 50°C to provide heating requirements for several applications like therapeutic bath, hand washing and shaving. All the experiments were done at ambient air temperature between -3.3 and 13°C. As a result of this, effect of the ambient air temperature was considered. Moreover the system performance was studied at two engine speeds (1750 and 2200 $rpm$ ). The influences of condenser water inlet temperature, condenser water flow rate, ambient air temperature and engine speed on performance characteristics of the GEHP are discussed in this section. Figure 6.13 indicates the effects of condenser water inlet temperature and its volume flow rate on the performance of GEHP while the effects of ambient air

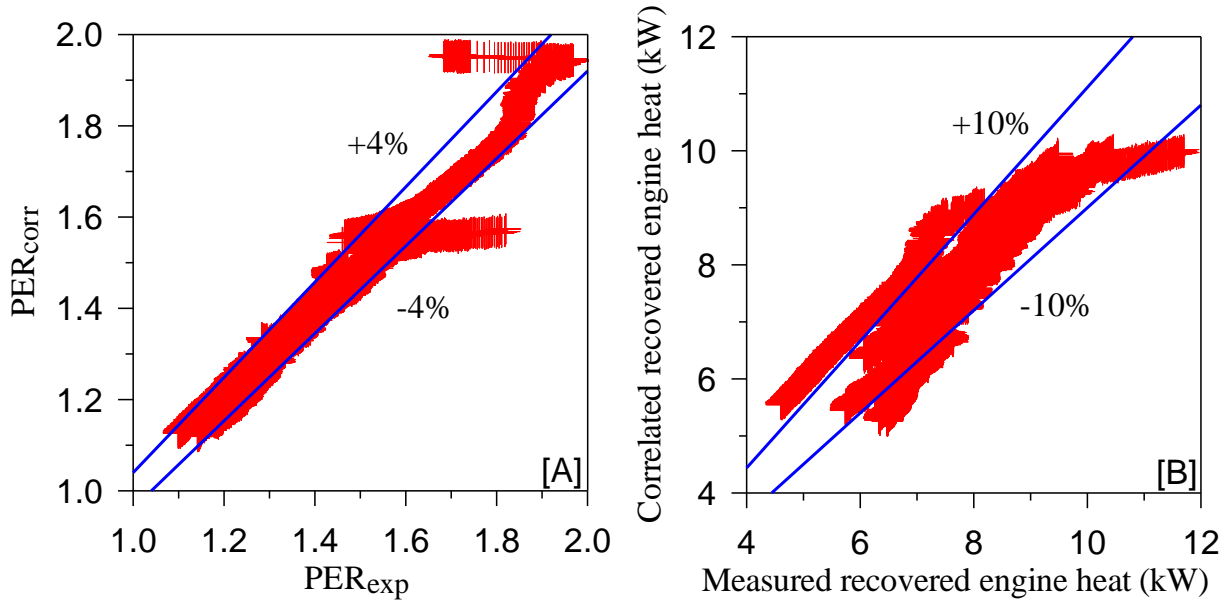


Figure 6.12: Comparison between experimental and correlated primary energy ratio data and recovered engine heat in heating mode-II.

temperature and engine speed on the performance of the GEHP are presented in Figs. 6.14 and 6.15 respectively.

### 6.3.2.1 Effect of condenser water inlet temperature

Effect of condenser water inlet temperature on the performance characteristics of the GEHP is shown in Fig. 6.13. Keeping the condenser water flow rate at about  $14.3\text{m}^3/\text{h}$ , condenser water inlet temperature was varied from 34 to  $48.7^\circ\text{C}$  to cover wide ranges of hot water applications. Moreover, both engine speed and ambient air temperature were held constant at  $1750\text{rpm}$  and  $7^\circ\text{C}$  respectively. Variations of the measured condensing and evaporating temperatures and refrigerant mass flow rate with the condenser water inlet temperature are illustrated in Fig. 6.13A. It is seen that the condensing temperature change (30%) is higher than that of the evaporating temperature (17%), thereby the pressure ratio ( $p_{cond}/p_{evap}$ ) increases as the condenser water inlet temperature increases. Refrigerant mass flow rate slightly increases with condenser water inlet temperature. The increase in the refrigerant mass flow rate is mainly due to increase in vapor density at compressor inlet. Figure 6.13A reveals this trend of the refrigerant mass flow rate. This figure confirms that the refrigerant mass flow rate is decreased by 3% over the entire considered range of the condenser water inlet temperatures.

Variations of condenser heating capacity and gas engine energy consumption with condenser water inlet temperature are shown in Fig. 6.13B. It is evident from this figure that condenser heating capacity decreases while gas engine heat consumption increases with condenser water outlet temperature. It may be noted that when the condenser water inlet temperature varied from about 34 to  $48.7^\circ\text{C}$ , the decrease in both

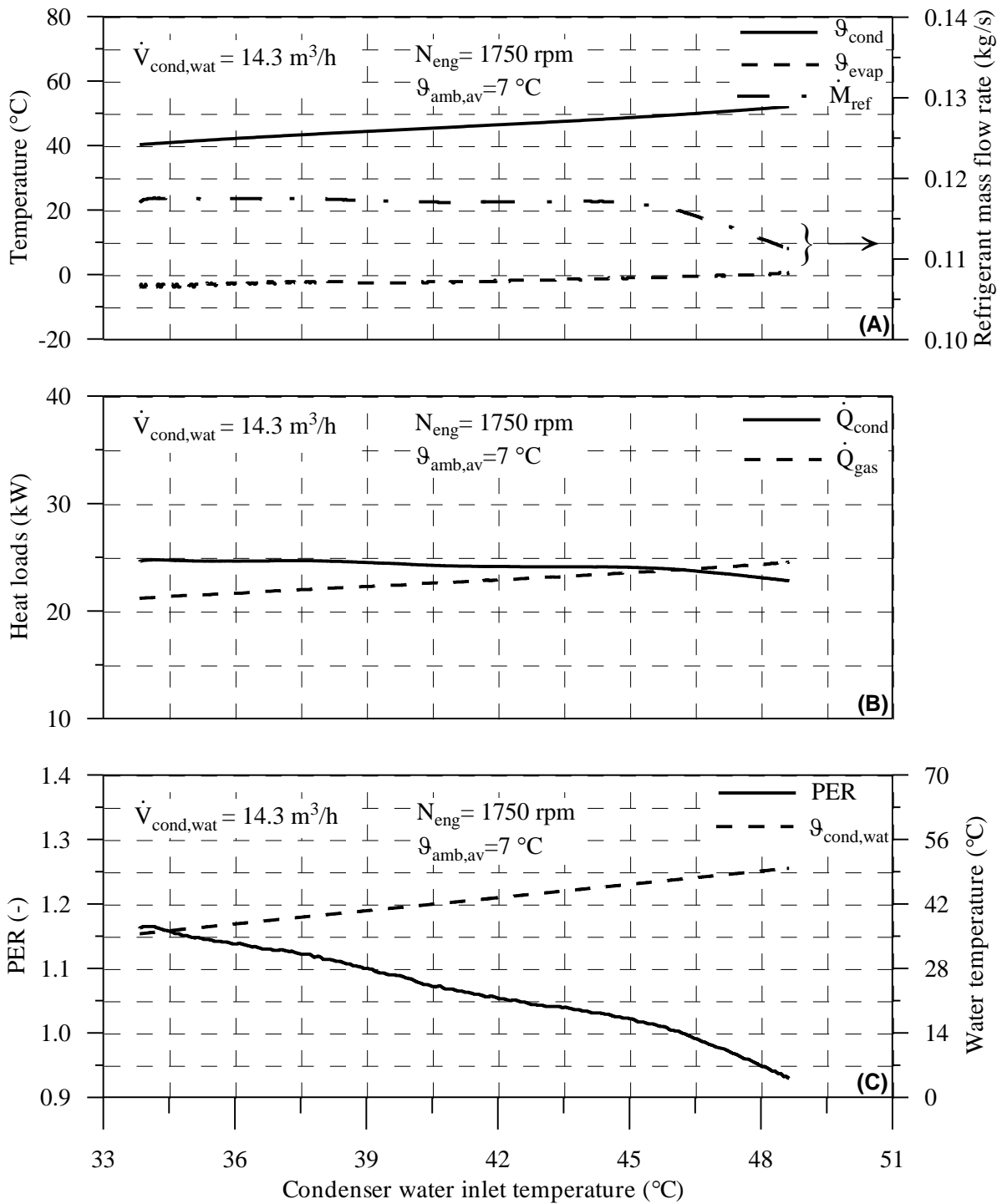


Figure 6.13: Effect of condenser water inlet temperature on the performance characteristics of the GEHP in heating mode-II; (A) operating temperatures and refrigerant mass flow rate, (B) heat loads and (C) condenser water temperature and PER.

refrigerant mass flow rate and condenser specific enthalpy difference yields lower system heating capacity (Eq.5.1). On the other side, it is observed that the condenser water temperature differences decreases causing the condenser heating capacity to decrease. In general, as the condenser water inlet temperature changes from 34 to 48.7°C, the condenser heating capacity decreases by 7% while gas engine heat consumption increases by 15%. Measured condenser water outlet temperatures against the condenser water inlet temperature are presented in Fig.6.13C, which indicates that the condenser and heat recovery water outlet temperatures lie within the recommended ranges listed in Table 6.1. The effect of condenser water inlet temperature on the PER can be predicted from Fig. 6.13C. A higher condenser water inlet temperature yields a lower PER. This trend is mainly due to both decrease in the condenser heating capacity and increase in the gas engine heat consumption as shown in Fig. 6.13B. Clearly, primary energy ratio of the GEHP decreases by 26.25% as the condenser water inlet temperature varies from 34 to 48.7°C. Moreover, PER of the GEHP lie between 0.92 and 1.16 which indicates that the GEHP still better than other heating system such as coal fired and gas fired boilers[24].

### 6.3.2.2 Effect of ambient air temperature

The effect of the ambient air temperature related to different ambient air temperatures of -3.3 and 13°C on the performance characteristics of the GEHP is shown in Fig. 6.14. Actually at lower ambient air temperature, the engine speed is going to increase to higher values. But the engine speed can be fixed at constant value manually using Aisin software. Both engine speed and condenser water flow rate remain constant at 1750rpm and 14.3m<sup>3</sup>/h respectively. Measured values of the condensing and evaporating temperatures and the refrigerant mass flow rate as a function of the condenser water inlet temperature for different ambient temperatures are presented in Fig. 6.14A. It is clear that as the ambient air temperature increases the evaporating temperature increase. As the ambient air temperature changes from -3.3 to 13°C, both the evaporating and condensing temperatures increase by 6.7% and 17% which led to decrease the pressure ratio and consequently increase the volumetric efficiency. Obviously, the refrigerant mass flow rate increases (30%) when the ambient air temperature increases. This fact is illustrated in Fig. 6.14A.

Influence of the ambient air temperature on the condenser heating capacity and gas heat energy consumption can be predicted from Fig. 6.14B. It is evident from the figure that the condenser heating capacity and gas engine heat consumption increase as the ambient air temperature increases. As the ambient air temperature increases from -3.3 to 13°C, the condenser heating capacity and gas heat consumption increase by 30% and 8.3% respectively. The increase in the condenser heating capacity can be attributed to decrease in both the ambient air temperature and engine speed. The engine speed should be increased to enhance the system capacities. Variations of measured condenser water outlet temperatures with the condenser water inlet temperature for two ambient air temperatures (-3.3 and 13°C) are illustrated in Fig. 6.14C. Clearly, the influence of the ambient air temperature on the condenser water outlet temperature is minor.



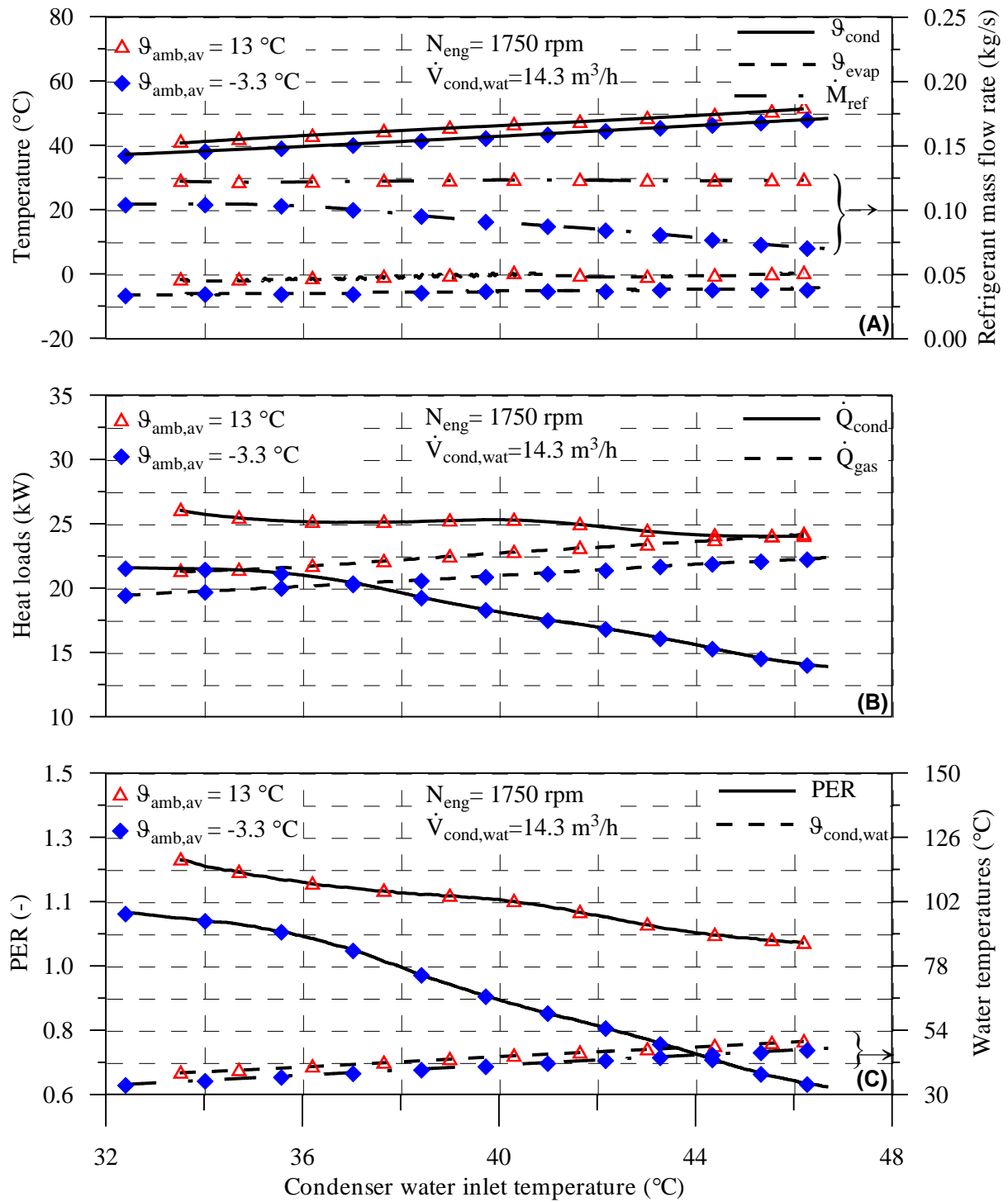


Figure 6.14: Effect of ambient air temperature on the performance characteristics of the GEHP in heating mode-II; (A) operating temperatures and refrigerant mass flow rate, (B) heat loads and (C) Condenser water temperature and PER.

Figure 6.14C presents the system PER against the condenser water inlet temperature for ambient air temperature of  $-3.3$  and  $13^{\circ}\text{C}$ . It should be noted that the PER of the GEHP decrease as the ambient air temperature decrease. Moreover, the PER becomes very low at the higher condenser water inlet temperature. It should be noted at condenser water inlet temperature higher than  $40^{\circ}\text{C}$ , the PER is less than 0.9 and consequently the GEHP is not effective as compared with other heating system such as gas fired boiler.

### 6.3.2.3 Effect of engine speed

Performance characteristics of the GEHP as a function of the condenser water inlet temperature at two engine speeds of 1750 and 2200rpm are presented in Fig. 6.15. Both the water volume flow rate and the ambient air temperature were held constant at  $11.9\text{m}^3/\text{h}$  and  $4^{\circ}\text{C}$ , respectively. Figure 6.15 explains variation of the measured condensing and evaporating temperatures as well as refrigerant mass flow rate for different engine speeds. It can be noted that, when the engine speed increased from 1750 to 2200rpm the evaporating temperature decreases (8.8%) while the condensing temperature increases by 4.4%. So, the pressure ratio tends to increase and consequently the compressor volumetric efficiency decreases. On the other hand, increasing of the engine speed from 1750 to 2200rpm (25.7%) led to increase in discharged refrigerant volume flow rate. The rate of increase in the refrigerant mass flow rate due to the engine speed is more pronounced than the rate of decreasing resulting from the volumetric efficiency decreasing. Hence, the refrigerant mass flow rate increases by 11.1%.

Figure 6.15B shows the condenser heating capacity and gas engine heat consumption versus the condenser water inlet temperature at engine speeds of 1750 and 2200rpm. Clearly, higher engine speed yields higher condenser heating capacity and gas engine heat consumption. This trend can be attributed to the high rate of gas consumption at the higher engine speeds. It should be noted that as the engine speed increases by 25.7%, all of condenser heating capacity and gas engine heat consumption increase by 19.1% and 28.8% respectively.

The high rate of increase in gas engine energy consumption overwhelms the rate of increase in condenser heat load which led PER of the system to decrease at the engine high speed as indicated in Fig. 6.15C. As the engine speed increase from 1750 to 2200rpm, system PER decreases by 10%. Fig. 6.15C illustrates also the measured condenser water outlet temperature as a function of the condenser water inlet temperature for two engine speeds. Clearly, the condenser water outlet temperature increase when the engine speed increases. Variations of external operating parameters yield an average hot water outlet temperature between  $36$  and  $48^{\circ}\text{C}$ , which is within the recommended range for different applications. Primary energy ratio has been correlated as a function of the condenser water inlet temperature, condenser water volume flow rate, engine speed and ambient air temperature in the following form

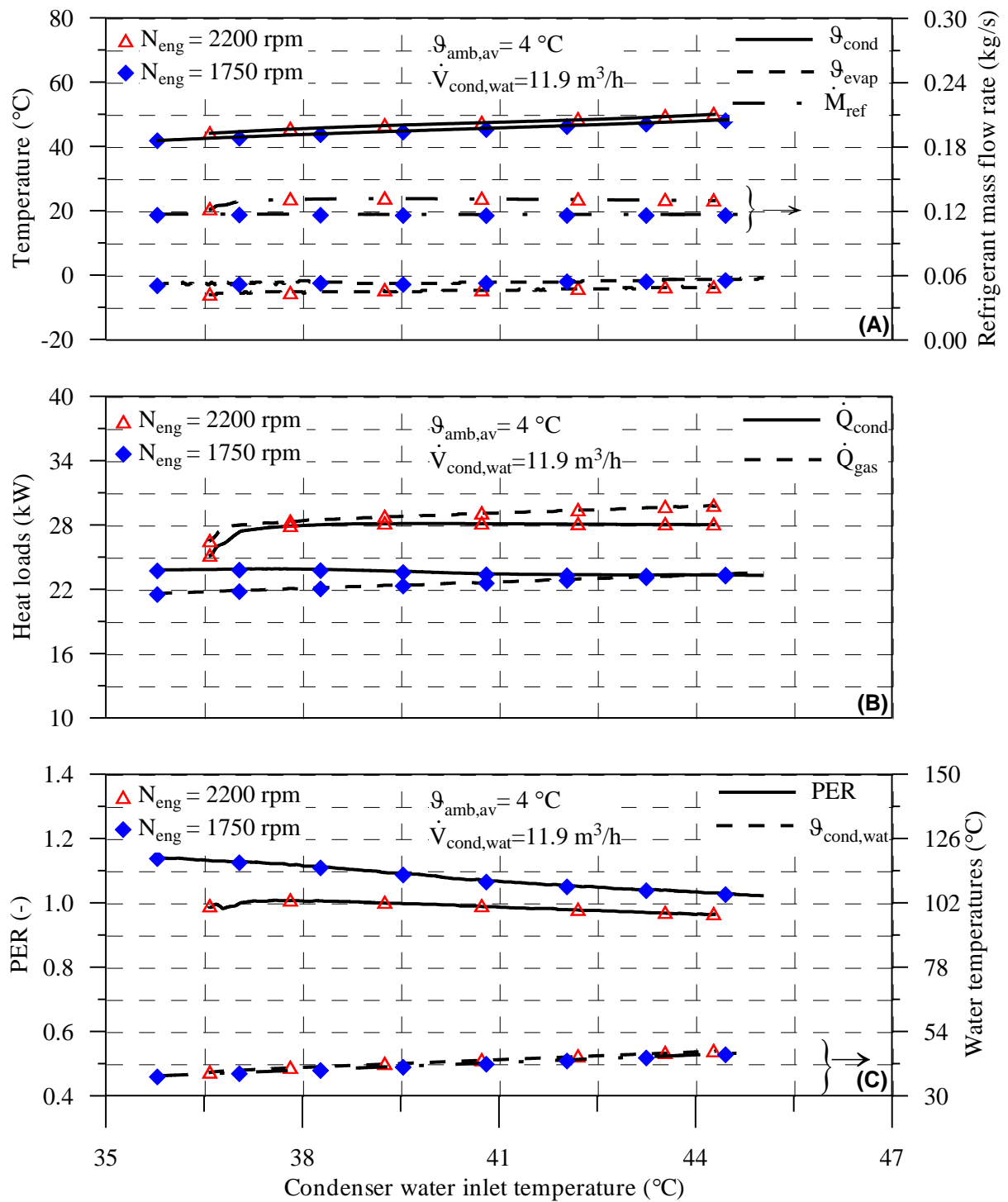


Figure 6.15: Effect of engine speed on the performance characteristics of the GEHP in heating mode-II; (A) operating temperatures and refrigerant mass flow rate, (B) heat loads and (C) condenser water temperature and PER.

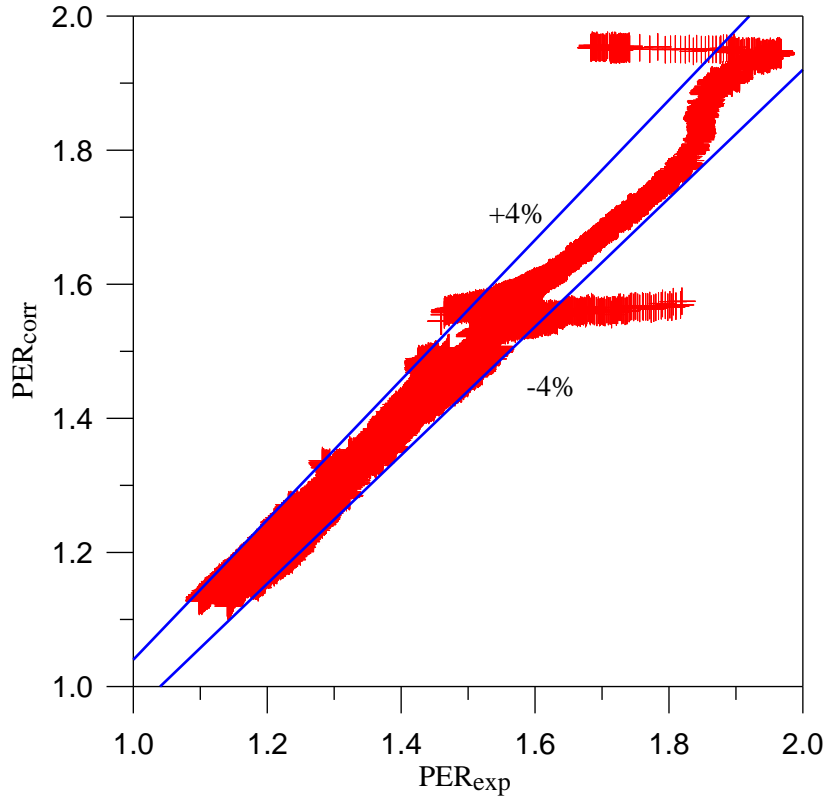


Figure 6.16: Comparison between experimental and correlated primary energy ratio data in heating mode-II.

$$PER_{heating,corr} = -0.0146\vartheta_{cond,wat} - 0.0015\dot{V}_{cond,wat} - 0.00009N_{eng} + 0.0081\vartheta_{amb} + 1.7815 \quad (6.5)$$

Where  $\vartheta_{cond,wat}$  is the condenser water inlet temperature in ( $^{\circ}\text{C}$ ),  $\dot{V}_{ch,wat}$  represents the condenser water volume flow rate in ( $\text{m}^3/\text{h}$ ),  $N_{eng}$  refers to engine speed in ( $\text{rpm}$ ) and  $\vartheta_{amb}$  is the ambient air temperature in ( $^{\circ}\text{C}$ ). The above equation is valid in the following ranges:  $27.8 \leq \vartheta_{cond,wat} \leq 48.6$ ,  $4.8 \leq \dot{V}_{cond,wat} \leq 21$ ,  $1733 \leq N_{eng} \leq 2212$  and  $-3 \leq \vartheta_{amb} \leq 13$ . Fig. 6.5 illustrates a comparison between experimental and correlated primary energy ratio. It should be noted that 89.1% of all the data points lie within  $\pm 4\%$  error percentage. The resulting data points outside  $\pm 4\%$  error percentage can be attributed to unsteady state during experiments starting up. In the following section, a comparison between the prescribed modes I and II has been investigated.

### 6.3.3 Comparison between heating mode-I and mode-II

Fig 6.17 shows comparison of performance characteristics of the GEHP for the prescribed mode-I and mode-II. In mode-I recovered engine heat is transferred to the water supply while in mode-II recovered engine heat is transferred to the refrigerant in dependence to ambient air temperature. The controlling process of the gas engine heat is done

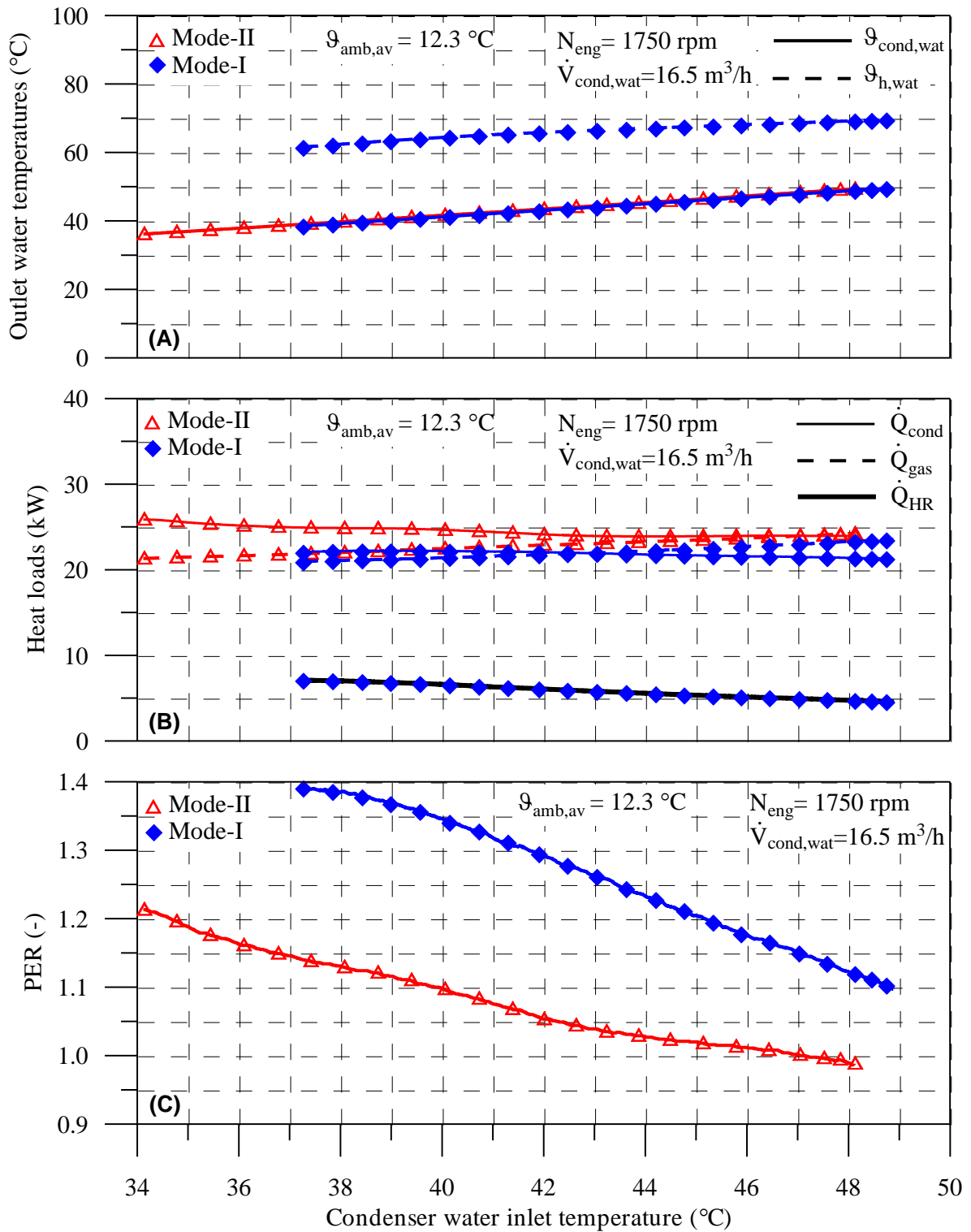


Figure 6.17: Comparison of the performance characteristics for both mode-I and mode-II; (A) outlet water temperatures, (B) heat loads and (C) PER.

manually using the electronic valves. Measured condenser and heat recovery water outlet temperatures against the condenser water inlet temperature are presented in Fig. 6.17.A, which indicates that the condenser and the heat recovery water outlet temperatures increase when condenser water inlet temperature increases. In the two modes, the condenser water outlet temperature lies between 35 and 50°C while for mode-I a higher hot water temperature can be achieved as a result of recovered engine heat transfer. Variations of heat loads with the condenser water inlet temperature are shown in Fig. 6.17.B. It is evident from this figure that condenser heating capacity and gas engine energy consumption are higher when recovered engine heat is transferred to refrigerant. In general, as the condenser water inlet temperature changes from 37.2 to 48°C, both condenser heating capacity and gas engine energy consumption increase by 13% and 12.4% respectively for mode-II. In fact condenser heating capacity for mode-II is larger as a result of transferring the engine heat recovery to the evaporator.

The effect of condenser water inlet temperature on the PER for the two modes can be predicted from Fig. 6.17.C. A higher PER can be reached when the engine recovered heat is transferred to the water. Clearly, primary energy ratio of the GEHP increases by 17.5% as an average value over the entire range of the condenser water inlet temperature from 37.2 to 48°C. This trend is mainly due to decrease in the gas engine heat consumption.

### 6.3.4 Optimum waste heat recovery

Recovered engine heat represents one of the main advantages of the gas engine heat pump system as compared with conventional heat pump systems. The engine heat recovery depends mainly on the operation mode, engine speed, heat recovery water inlet temperature, heat recovery water flow rate as well as the ambient air temperature. As mentioned before the engine heat recovery can be increased by increasing the engine speed or the heat recovery water flow rate. On the other hand, it is important to study the effect of heat recovery water inlet temperature on the recovered engine heat.

Figure 6.18 shows influence of heat recovery water inlet temperature on the recovered engine heat at different ambient air temperatures for both combined and heating modes of operation. Keeping the engine speed at the rated value of 1750rpm, heat recovery water inlet temperature was varied from 37.5 to 62.5°C to cover several applications of water heating. Clearly, the recovered engine heat gets higher at the higher ambient air temperature as a result of the high engine operation temperature and high heat source temperature. On contrary, it gets lower at the higher heat recovery water inlet temperature. For the heating mode, when the ambient air temperature changes from 13 to 25.8°C recovered engine heat increased by 17.5%. However, as the water inlet temperature varied from 42°C to 61.5°C recovered engine heat decreased by 64%. For the combined mode, as the ambient air temperature changes from 18.6 to 34.8°C recovered engine heat increased by 41.2% as an average value over the entire range of the water inlet temperature. Also, it should be noted that recovered engine heat decreased from 11 to 5.4kW as the water inlet temperature varied from 37.5 to 59°C at ambient

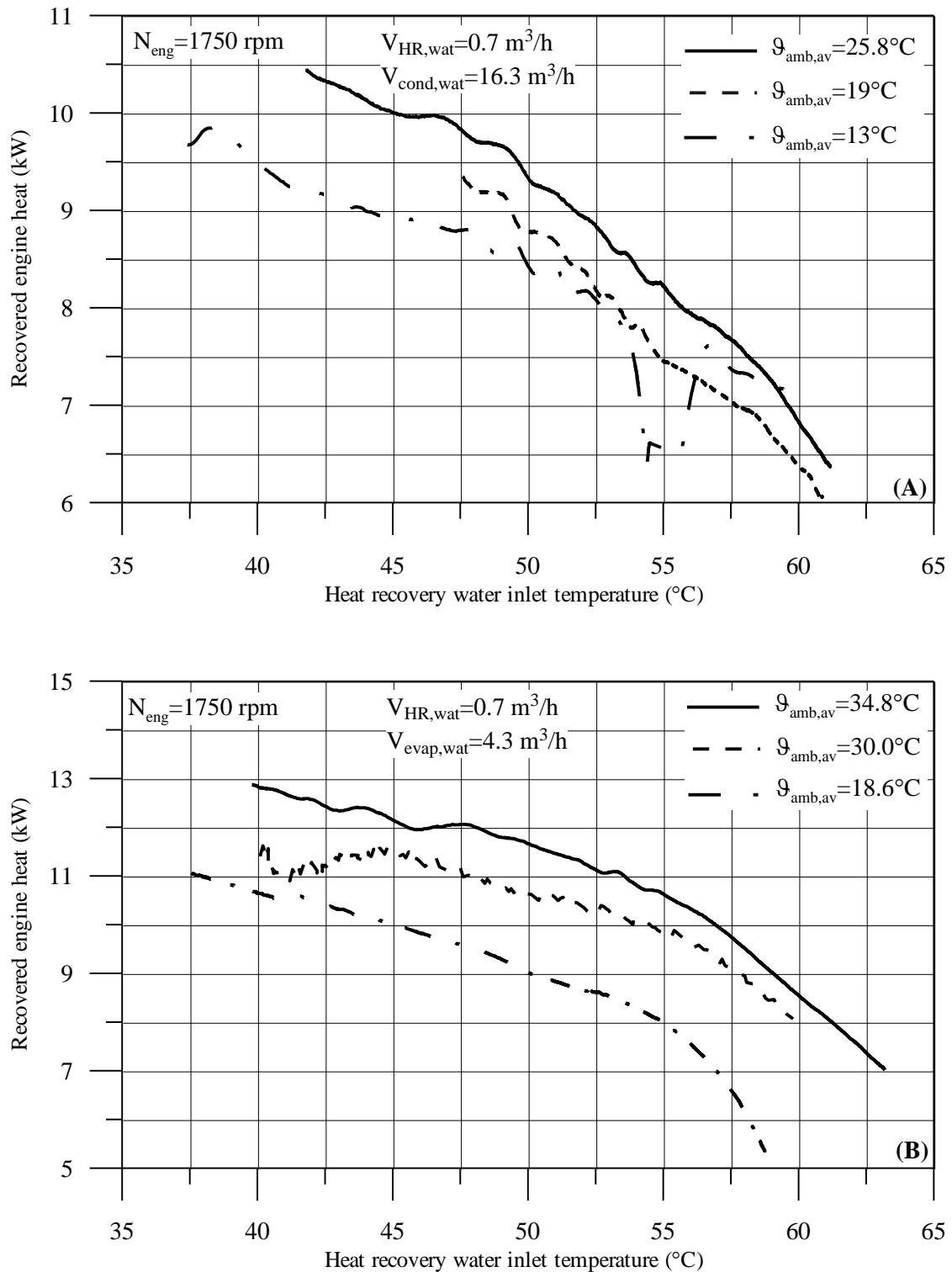


Figure 6.18: Effect of heat recovery water inlet temperature on the recovered engine heat for different ambient air temperatures; (A) Heating mode and (B) Combined mode.

air temperature of 18.6°C in combined mode. The above results confirmed that the recovered water inlet temperature has a significant effect on the recovered engine heat in both combined and heating modes of operation and consequently the system primary energy ratio[100]. Moreover, the quantity of recovered engine heat can be increased by enlarging the heat exchanger surface area or decreasing the water inlet temperature.

## 6.4 Conclusions based on Experimental Results

In this chapter, performance characteristics of the gas engine heat pump, working with R410A as primary refrigerant, have been experimentally determined over a wide range of external operating conditions. The gas engine heat pump has been tested in several operating modes namely; cooling, combined and heating mode. In the cooling mode, the gas engine has been used to drive the compressor of a vapor compression refrigeration system. While for the combined mode, the gas engine waste heat has been recovered for heating demands beside the vapor compression refrigeration cycle. In the heating mode, the gas engine has been used to drive the vapor compression heat pump and the waste engine heat has been recovered. The recovered engine heat can be used either to enhance the heating performance of the heat pump cycle or for water heating. Based on the reported results, the following conclusions can be drawn:

- Best results concerning high energy efficiency have been obtained in combined mode in which PER up to 2.1 has been reached. Moreover, the primary energy ratio can be increased by increasing of evaporator water inlet temperature and by decreasing engine speed.
- Gas engine heat pump can be used to provide both cold (5 to 15°C) and hot water (38 to 65°C) for different applications such as air conditioning, factory cooling and hot water supply. Moreover, the high primary energy ratio of the GEHP makes it more attractive to achieve such demands[101].
- Evaporator water inlet temperature has the highest influence on the system performance followed by engine speed, ambient air temperature and water volume flow rate in that order in all mode of operation.
- Engine speed is inversely proportionally to the system primary energy ratio and directly proportional to the system capacity. Hence, Engine speed should be optimized to get the required capacity with highest primary energy ratio[102].
- Primary energy ratio of the GEHP system in heating mode (especially at low ambient air temperature) is relatively small as compared to both cooling and combined modes. This can be attributed to the low surface area of the evaporator in the outdoor unit of Aisin package. Therefore, the use of recovered engine heat in the refrigerant circuit overcomes the low surface area of the evaporator and avoids frosting problem.



- 
- Recovered engine heat could be higher when the surface area of the heat exchanger increased but at the same time the system initial cost gets higher. Hence, the heat exchanger surface area should be optimized.
  - At ambient air temperature higher than 10°C, higher primary energy ratio could be obtained (17%) when the recovered engine heat is transferred to water circuit.
  - The outlet hot water temperature is ranging from 38 to 65°C when the recovered engine heat is transferred to water while it is limited to 40°C at lower ambient air temperature.
  - Better results for the system in heating mode could be obtained by replacing the outdoor heat exchanger with larger one or changing the secondary fluid from air to water.
  - In combined mode, it is better to use the condenser heat load in heating purposes.
  - The outdoor unit has been designed by Aisin to recover the engine waste heat in cooling mode. Hence, the combined mode is preferable.



# Chapter 7

## MODELLING AND SIMULATION OF GAS ENGINE DRIVEN HEAT PUMPS

Modelling of GEHP systems play an important role in system optimizing and consequently the required loads are provided with highest system energy efficiency. Moreover, system modelling reduces development cost by making it easier to build systems, to reuse previous built components within new systems, to change systems to suit changing requirements such as functional enhancement and platform changes, and to understand systems. Furthermore, system modelling is helpful in adjusting the controlling process.

Modelling of the GEHP systems can be classified as steady and dynamic state simulations. In this chapter a steady state simulation model of the gas engine driven heat pump is performed and system main parameters such as system cooling/heating capacity, gas engine energy consumption and primary energy ratio are computed. The modelling of the gas engine heat pump includes modelling of the heat pump system as well as the gas engine. The main target of heat pump modelling is to obtain the system cooling/heating capacity while the gas engine energy consumption is the goal of the gas engine modelling. Hence, the system primary energy ratio can be evaluated. The gas engine heat pump model is validated by comparing experimental and simulation data. The results can give a better understanding, controlling and improving energy efficiency of the GEHP systems.

### 7.1 Heat Pump System Model

Heat pump system consists of an open scroll compressor, a plate heat exchanger (indoor heat exchanger), an electronic expansion valve and a slit fin heat exchanger (outdoor heat exchanger). Fig. 7.1 shows a schematic diagram of the heat pump system including the measurement points of pressure, temperature and flow rate. In order to evaluate the system cooling/heating capacity, modelling of the scroll compressor and the plate heat exchanger evaporator is carried out. Refrigerant mass flow rate and compressor power

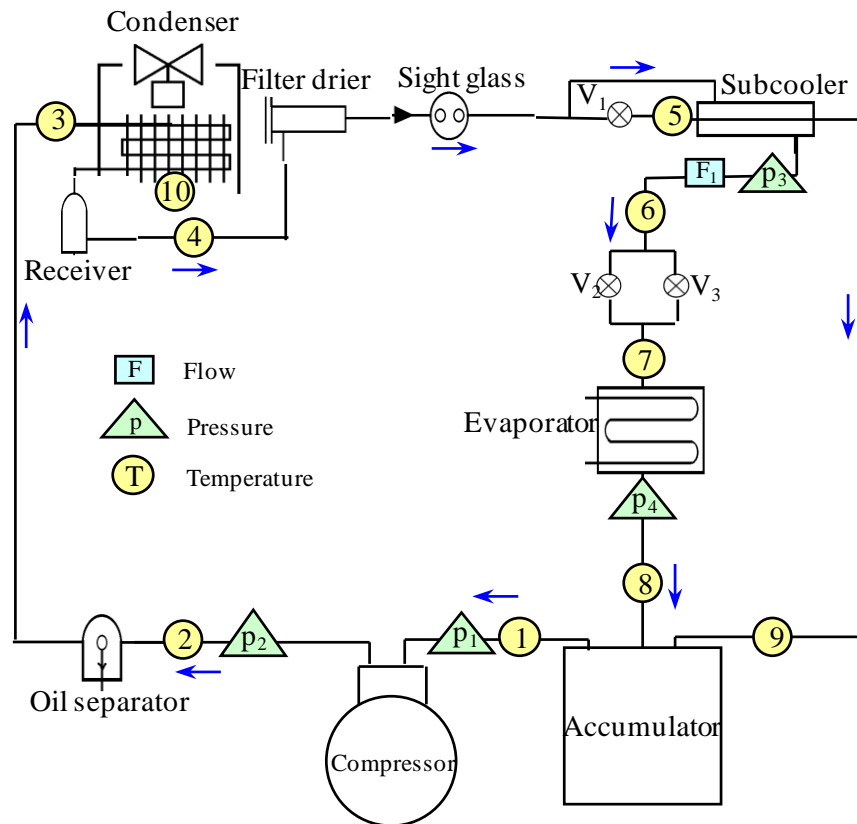


Figure 7.1: Schematic diagram of the heat pump system.

represent the main output results from the compressor model. Using the discharged refrigerant mass flow from the compressor model as an input data to the plate heat exchanger model, the system cooling/heating capacity can be estimated.

### 7.1.1 Model assumptions

For thermal analysis of the vapor compression heat pump (VCHP), a number of assumptions have been made. They are:

- the refrigerant is appropriately charged,
- steady state operation of the system,
- no pressure drop, i.e. pressure changes only through the compressor and expansion device,
- heat losses or heat gain from or to the system are ignored,
- the expansion valve can maintain constant superheating degrees. Therefore, the sub-cooling and superheat degrees are considered constant during the calculations.

### 7.1.2 Scroll compressor

Compressor plays an important role in determining the performance of the heat pump system as it controls the flowing refrigerant mass flow rate. In this section, the experimental performance characteristics of an open variable speed scroll compressor is introduced. Then, a realistic model with variable compressor parameters which can be used to predict mass flow rate and compressor power is presented.

#### 7.1.2.1 Scroll compressor testing

Performance characteristics of the scroll compressor are evaluated by discharged mass flow rate, input power, isentropic and volumetric efficiencies [103]. The considered scroll compressor has a swept volume ( $V_s$ ) of  $104\text{cm}^3/\text{rev}$ . The compressor is characterized with 30 tests which cover a wide range of operating conditions. Suction pressure changes from 690 to 1100kPa and discharge pressure varied from 1490 to 2450kPa which covers the operating pressures of the system in cooling and heating modes of operation. Moreover, the performance of the compressor is testes at different engine speeds of 1300 and 1750rpm. All recorded data are analyzed using the EES program [87] to estimate the compressor performance characteristics. Compressor isentropic efficiency ( $\eta_{is}$ ) and volumetric efficiency ( $\eta_{vol}$ ) can be estimated using the following equations:

$$\eta_{is} = \frac{w_{is}}{w_{act}}, \quad (7.1)$$

$$\eta_{vol} = \frac{\dot{M}_{ref} \nu_{suc}}{N_{comp} V_s}, \quad (7.2)$$

where  $w_{is}$  and  $w_{act}$  denote to isentropic and actual compressor specific works, respectively, while  $\nu_{suc}$  and  $V_s$  represent specific volume at the compressor suction and swept volume, respectively. Effects of suction pressure, discharge pressure and engine speed on the scroll compressor performance characteristics can be predicted from Figs. 7.2 and 7.3.

Variation of the discharged mass flow rate with suction pressure for different discharge pressures and engine speeds is shown in Fig. 7.2, which reveals that the discharged mass flow rate is directly proportional to the suction pressure. This can be attributed to increase in suction density with increasing suction pressure. Clearly, discharged refrigerant mass flow rate at suction pressure of 1025kPa is higher than that at suction pressure of 754.6kPa by about 34% at engine speed of 1750rpm and discharge pressure of 2450kPa. Sensitivity of the discharged refrigerant mass flow rate to suction pressure increases as engine speed increases. Also, effect of both discharge pressure and engine speed on the discharged mass flow rate can be predicted from Fig. 7.2, which confirms that as the discharge pressure decreases from 2450 to 1990kPa, the discharged mass flow rate increases by 3.5%. This indicates that effect of discharge pressure on discharged mass flow rate is insignificant, i.e the discharged mass flow rate is not enormously influenced by compressor discharge pressure. Thus, discharged mass flow rate is more sensitive to suction pressure than discharged pressure. Discharged mass flow rat at engine speed of 1750rpm is higher than that at engine speed of 1300rpm by 37%. This

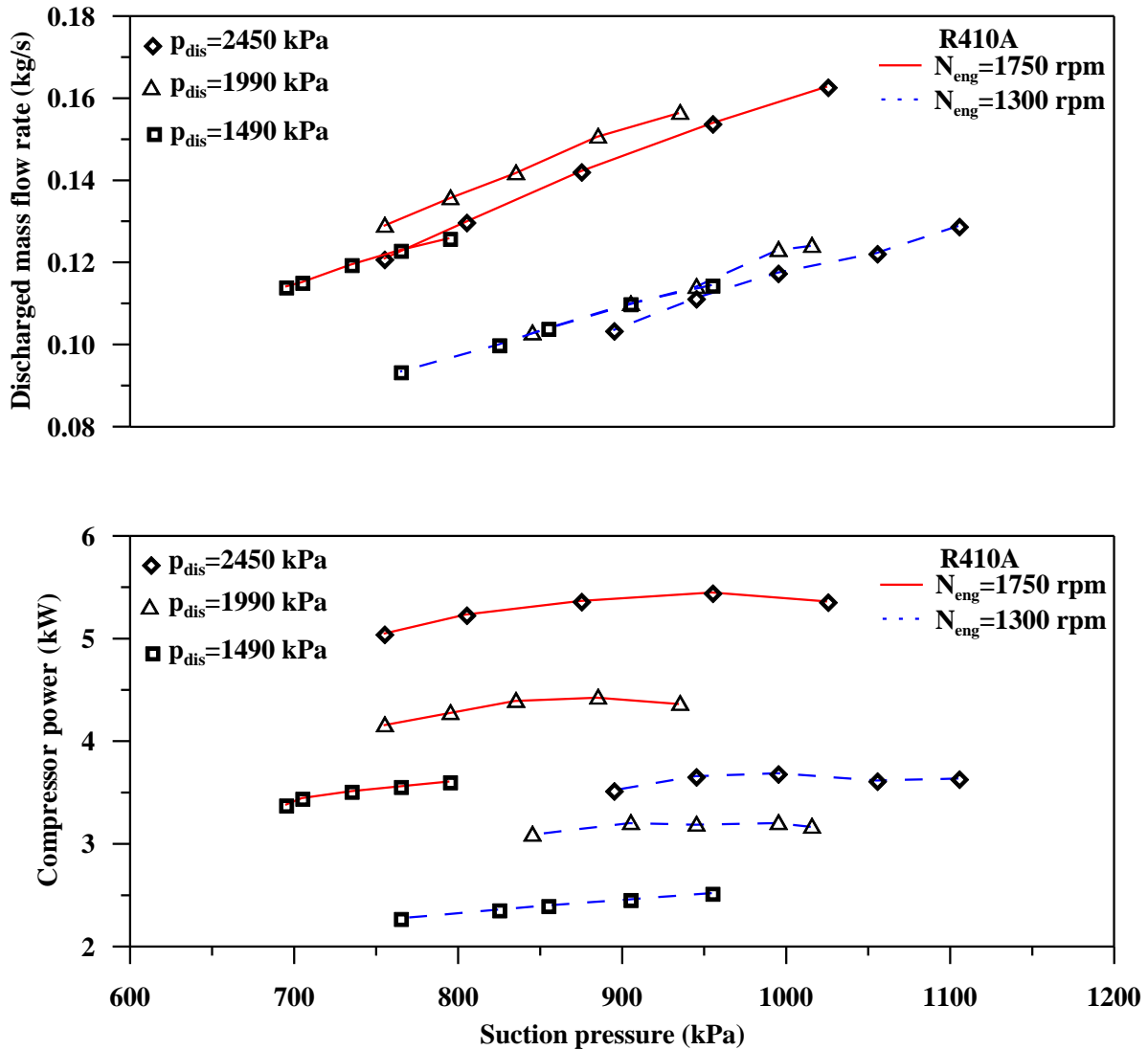


Figure 7.2: Discharged mass flow rate and compressor power versus suction pressure for different discharge pressure and engine speeds.

is because of engine speed has a significant effect on volume flow rate, which causes the discharged mass flow rate to increase. It can be concluded that the discharged mass flow rate is more sensitive to engine speed followed by suction pressure and discharge pressure in that order. Figure 7.2 illustrates scroll compressor power as a function of the suction pressure for different discharge pressures and engine speeds. As mentioned earlier in Fig. 7.2, discharged mass flow rate increases as suction pressure increases. On the other hand, compressor specific work decreases as the suction pressure increases. The high rate of increase in discharged mass flow rate overcomes the rate of decrease in compressor specific work which allows the compressor power to increase. It can be noted that the compressor power increases by 7.1% as the suction pressure increases from 754.6 to 934.6 kPa at engine speed of 1750 rpm and discharge pressure of 1990 kPa.

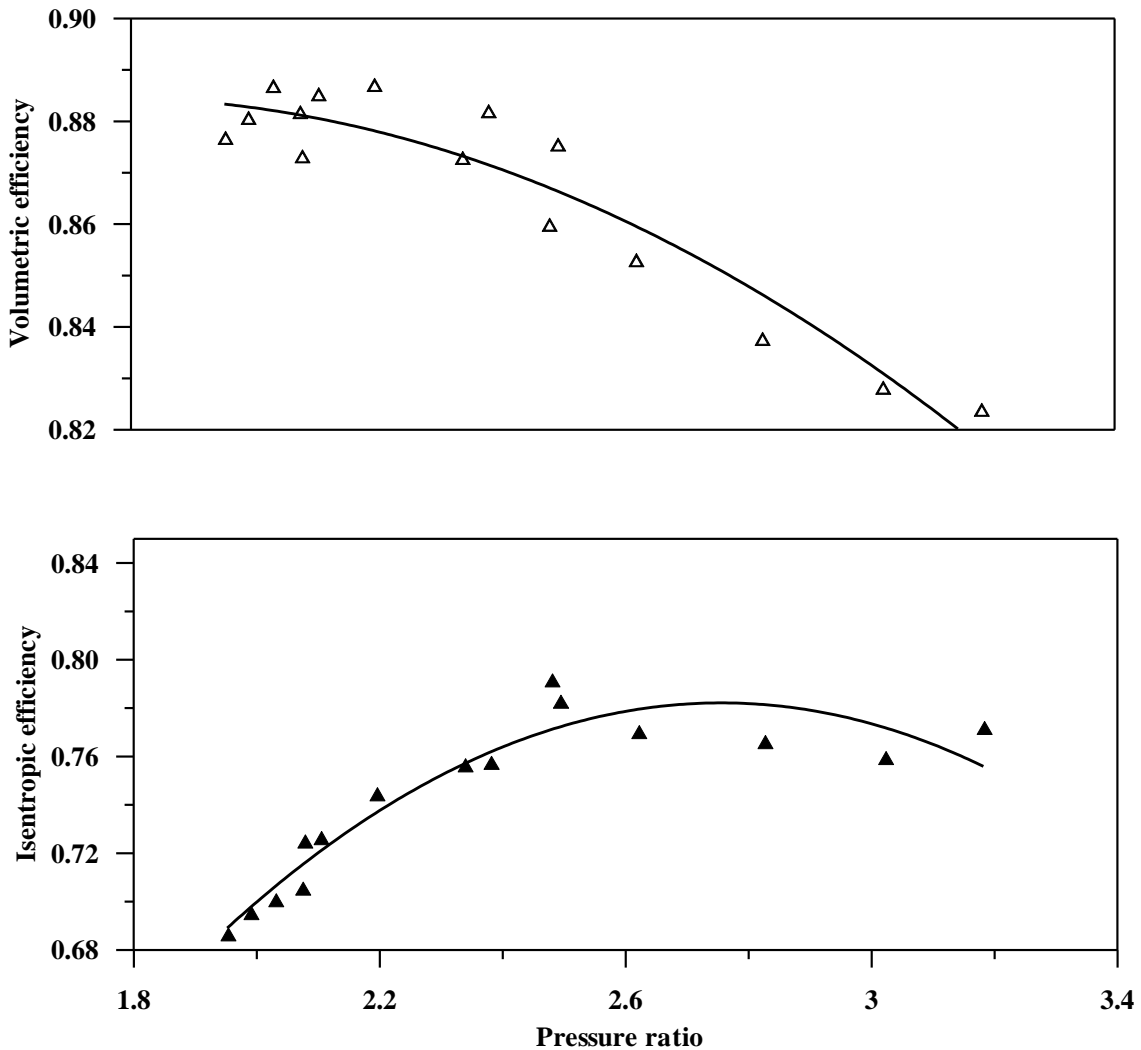


Figure 7.3: Volumetric and isentropic efficiencies versus pressure ratio at 1750 rpm engine speeds.

Clearly, compressor power is enormously influenced by compressor discharge pressure. This is evident by the fact that compressor power at discharge pressure of 2450kPa is higher than that at discharge pressure of 1490kPa by about 42% at engine speed of 1750rpm. This figure demonstrates that the scroll compressor running with speed of 1750rpm needs higher input power by about 46% compared to that one running with speed 1300rpm at suction and discharge pressures of 950 and 2450kPa, respectively. It can be observed that the compressor power is more sensitive to engine speed followed by discharge pressure and suction pressure in that order. Combined effect of both suction and discharge pressure on the compressor efficiencies can be obtained from discharge to suction pressure ratio. Fig. 7.3 explains the effect of pressure ratio on compressor volumetric and isentropic efficiencies, respectively at constant engine speed of 1750rpm. Clearly, volumetric efficiency is inversely proportional (see, Fig. 7.3) while isentropic efficiency is directly proportional (see, Fig. 7.3) to pressure ratio. It can be noted that

volumetric efficiency decreases by 7% while isentropic efficiency increases by 13% when pressure ratio changes from 1.95 to 3.2. The rate of increase in compressor volumetric efficiency at pressure ratio of 1.95 (2.2%) is lower than that at pressure ratio of 2.67 (6.7%). On the contrary, the rate of increase in isentropic efficiency at pressure ratio of 1.95 (9%) is higher than that at pressure ratio of 2.67 (0.6%). It should be noted that, both volumetric and isentropic efficiencies are higher influenced by pressure ratio than engine speed [103].

### 7.1.2.2 Scroll compressor modelling

Semi-empirical models in which thermodynamic assumptions are made are found in the literature. In those models, data are not very difficult to obtain: e.g. refrigerant inlet state, outlet refrigerant pressure and compressor speed [104]. The refrigerant mass flow rate is affected by a suction temperature increase and the compression process is considered isentropic to the "adapted" pressure and isochoric until the discharge pressure. Fig. 7.4a shows a simple diagram of the considered compressor while Fig. 7.4b represents the compressor internal processes on p-h diagram. As indicated in Fig. 7.4b the progression of refrigerant states through the compressor is divided into four processes as follows;

- 1→2 : isobaric heating up in the suction pipe due to a heat transfer with a fictitious wall at temperature ( $\vartheta_w$ ).
- 2→3 : isentropic compression in which the gas is compressed until the volume created by the scrolls matches exhaust volume ( $V_{ex}$ ). It can be stated that the pressure at state point 3 is defined as intermediate pressure ( $p_{int}$ ).
- 3→4 : isochoric compression in the exhaust chamber until the pressure equals the discharge pressure ( $p_{dis}$ ).
- 4→5 : isobaric cooling down in the discharge pipe due to a heat transfer to ambient.

In order to simulate the scroll compressor, a number of assumptions have been made. These are:

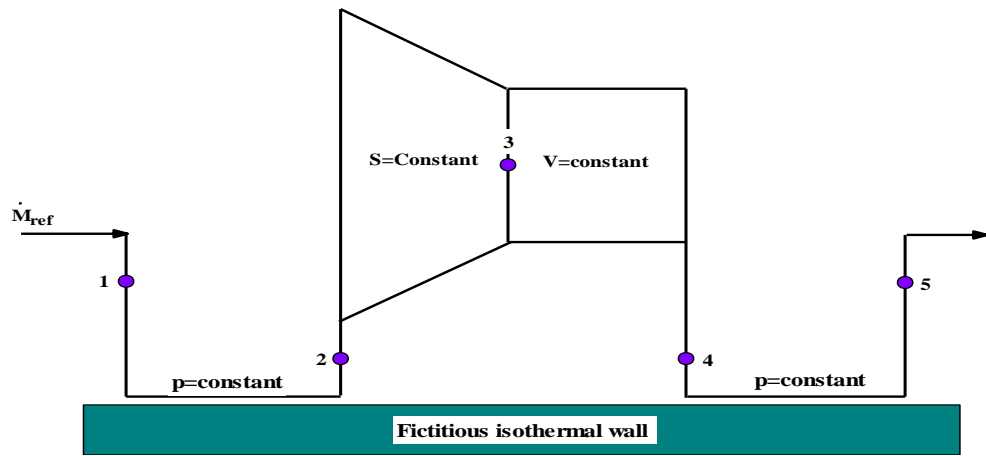
- (a) Steady state flow conditions,
- (b) no pressure drop in both suction and discharge ports,
- (c) swept volume ( $V_s$ ) is given by the manufacturer,
- (d) The fictitious wall temperature ( $\vartheta_w$ ) has no significant influence on the mass flow rate so that its value was constant (100°C)[105].

### 7.1.2.3 Prediction of refrigerant mass flow rate

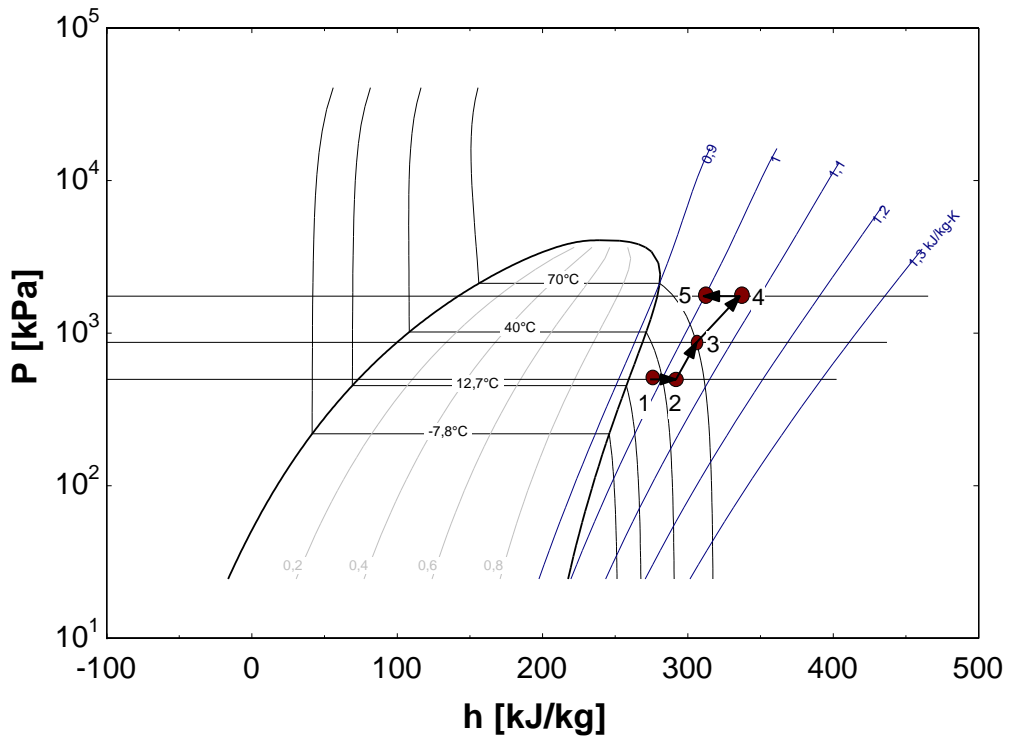
The refrigerant mass flow rate through the compressor ( $\dot{M}_{ref,cal}$ ) is calculated applying the following equation;

$$\dot{M}_{ref,cal} = \rho_2 V_s N_{com}, \quad (7.3)$$





(a)



(b)

Figure 7.4: Schematic diagram of the compressor internal processes.

where  $\rho_2$  is the vapor density at the compressor suction (state point 2),  $V_s$  represents the compressor swept volume and  $N_{comp}$  is the compressor rotation speed. The superheated vapor density at state point 2 can be computed as function of  $p_2$  and  $\vartheta_2$ ;

$$\rho_2 = f(p_2, \vartheta_2). \tag{7.4}$$

Since pressure drops in suction pipe is neglected, one can write;

$$p_2 = p_1 = p_{suc}. \quad (7.5)$$

Where the suction ( $p_{suc}$ ) and discharge ( $p_{dis}$ ) pressures can be calculated from phase change evaporating ( $\vartheta_{evap}$ ) and condensing ( $\vartheta_{cond}$ ) temperatures as the following;

$$p_{suc} = p_{sat}(\vartheta_{evap}). \quad (7.6)$$

$$p_{dis} = p_{sat}(\vartheta_{cond}). \quad (7.7)$$

where  $p_{sat}(\vartheta)$  is the saturation pressure of the refrigerant. Both evaporating  $\vartheta_{evap}$  and condensing  $\vartheta_{cond}$  temperatures are calculated using chilled water ( $\vartheta_{ch, wat}$ ) and ambient air temperatures ( $\vartheta_{amb}$ ) respectively applying the following assumptions;

$$\vartheta_{evap} = \vartheta_{ch, wat} - \Delta\vartheta_1. \quad (7.8)$$

$$\vartheta_{cond} = \vartheta_{amb} + \Delta\vartheta_2. \quad (7.9)$$

in which  $\Delta\vartheta_1$  and  $\Delta\vartheta_2$  are assumed as constant values 6K and 8K respectively. The rate of heat transfer during suction process ( $\dot{Q}_{suc}$ ) can be estimated using the following;

$$\dot{Q}_{suc} = UA_{suc}LMTD_{suc} = \dot{M}_{ref, cal}(h_2 - h_1), \quad (7.10)$$

where  $\dot{M}_{ref, cal}$  is the refrigerant mass flow rate while log-mean temperature difference ( $LMTD_{suc}$ ) is defined by the following equation;

$$LMTD_{suc} = \frac{(\vartheta_w - \vartheta_1) - (\vartheta_w - \vartheta_2)}{\ln \frac{\vartheta_w - \vartheta_1}{\vartheta_w - \vartheta_2}}. \quad (7.11)$$

Actual compressor suction temperature at state point 1 ( $\vartheta_1$ ) is calculated according to the following equation;

$$\vartheta_1 = \vartheta_{evap} - \Delta\vartheta_{sup}. \quad (7.12)$$

where  $\Delta\vartheta_{sup}$  is the superheating degrees at state point (1). Specific enthalpy ( $h_1$ ) of superheated vapor at state point (1) is calculated based on suction pressure ( $p_{suc}$ ) and  $\vartheta_1$ . Assuming an iterative value for product of overall heat transfer coefficient and heat transfer surface area during the isobaric heating process in the suction line ( $UA_{suc} > 0$ ), leads for estimation of exit specific enthalpy of suction process ( $h_2$ ). Now, superheated vapor temperature ( $\vartheta_2$ ) at end of isobaric heating process can be calculated as;

$$\vartheta_2 = f(p_{suc}, h_2), \quad (7.13)$$

As a result the vapor density  $\rho_2$  can be obtained, then substituted into Eq.7.3 to evaluate the refrigerant mass flow rate. It can be stated that the optimum  $UA_{suc}$  can be found by minimization of the discrepancy function  $\mu(\dot{M}_{ref})$ , which depends on the relative errors between measured ( $\dot{M}_{ref, meas}$ ) and calculated ( $\dot{M}_{ref, cal}$ ) refrigerant mass flow rates. This function is defined as follows [103];

$$\mu(\dot{M}_{ref}) = \sqrt{\frac{1}{n} \sum_{i=1}^n \left( \frac{\dot{M}_{ref, meas} - \dot{M}_{ref, cal}}{\dot{M}_{ref, meas}} \right)^2}, \quad (7.14)$$

where n is the number of tests.

#### 7.1.2.4 Prediction of compressor power

Compression process includes both isentropic compression and isochoric compression processes. Refrigerant pressure during the isentropic compression process increases from suction pressure ( $p_{suc}$ ) to the intermediate pressure ( $p_{int}$ ). Isochoric compression process begins from the intermediate pressure ( $p_{int}$ ) until the refrigerant pressure equals the discharge pressure ( $p_{dis}$ ). Thus, the compressor power ( $P_{comp}$ ) can be calculated as follows;

$$P_{comp} = \left( \frac{\dot{M}_{ref}(h_3 - h_2)}{\eta_{ps,is}} \right) + \dot{M}_{ref} \nu_{3,real} (p_{dis} - p_{int}), \quad (7.15)$$

The pseudo-isentropic efficiency ( $\eta_{ps,is}$ ) is expressed by Eq.7.16 as reported by Duprez et. al [105];

$$\eta_{ps,is} = \phi \left( \frac{p_{int}}{p_{suc}} \right) + \gamma, \quad (7.16)$$

where  $\phi$  and  $\gamma$  represent the coefficients of the linear law of the pseudo-isentropic efficiency. The intermediate pressure can be calculated from both specific entropy and specific volume at the end of the isentropic process as follows;

$$p_{int} = p(s_3, \nu_3), \quad (7.17)$$

Specific entropy at the end of isentropic compression process ( $s_3$ ) can be calculated as;

$$s_3 = s_2 = s(p_{suc}, \vartheta_2), \quad (7.18)$$

Specific entropy at the end of isobaric heating up stage ( $s_2$ ) can be calculated as a function of both suction pressure  $p_{suc}$  and  $\vartheta_2$ . The specific volume at state point (3) can be estimated from the following equation;

$$\nu_3 = \frac{V_{ex}}{M_{suc}}, \quad (7.19)$$

where  $M_{suc}$  is calculated using Eq.7.20 as follows;

$$M_{suc} = \rho_2 V_s. \quad (7.20)$$

The exhaust volume ( $V_{ex}$ ) is estimated as;

$$V_{ex} = \frac{V_s}{\xi}. \quad (7.21)$$

The best compressor parameters ( $\phi$ ,  $\gamma$  and  $\xi$ ) can be determined by minimization of the discrepancy function  $\mu(P_{comp})$ , which is given by Eq.7.22 as reported by Cuevas and Lebrun [103]. This function depends on the relative errors between measured compressor power ( $P_{comp,meas}$ ) and calculated compressor power ( $P_{comp,cal}$ ).

$$\mu(P_{comp}) = \sqrt{\frac{1}{n} \sum_{i=1}^n \left( \frac{P_{comp,meas} - P_{comp,cal}}{P_{comp,meas}} \right)^2}. \quad (7.22)$$

All the compressor parameters ( $UA_{suc}$ ,  $\phi$ ,  $\gamma$  and  $\xi$ ) can be obtained after minimization of the functions ( $\mu(\dot{M}_{ref})$ ) and ( $\mu(\dot{M}_{ref})$ ). In previous simulation models [104, 103, 106, 105], these parameters are kept constant to predict the compressor performance under any operating conditions. Thus, the prediction of compressor performance with minimum error cannot be achieved under all operating conditions.

In order to minimize the obtained error for prediction of both refrigerant mass flow rate and compressor power, correlations for the compressor parameters have been done as a function of operating conditions. In the following sections, a validation of the compressor model with available scroll compressor data sheets is presented and a comparison with the previous models has been established before applying the model to the GEHP scroll compressor.

#### 7.1.2.5 Scroll compressor validation

Three compressor were selected from the data sheet of Bitzer company [107] which include different compressor sizes and working with R134A. Compressors swept volumes are 25, 43 and  $61m^3/h$ . Optimum compressor parameters ( $UA_{suc}$ ,  $\phi$ ,  $\gamma$  and  $\xi$ ) are estimated at each operating point based on data sheets of the considered compressors. Then, the optimum compressor parameters are correlated with the relevant parameters which achieve minimum error at all points [108]. Figure 7.5 shows a comparison between the predicted and experimental refrigerant mass flow rate and compressor power of R134A scroll compressors. Experimental data are presented by symbols while predicted results are shown by solid lines. The comparison has been done under different operating conditions of condensing (30, 40 and  $50^\circ C$ ) and evaporating temperatures ( $-4$  to  $12^\circ C$ ). The average error percentage for the three compressors are 0.04 %, 0.08 % and 0.43 % for mass flow rate while for compressor power are 0.05 %, 0.04 % and 0.11 %.

Another validation with previous modelling techniques to compare between constant and variable compressor parameters has been done. Figure 7.6 shows error percentages for obtained mass flow rate and compressor power using the constant and variable compressor parameters. It can be noted that the discrepancy of the predicted mass flow rate lies between 5 % and 10 %, while the discrepancy of the predicted power is about 5 % using constant compressor parameters and they are comparable to those reported by Duprez et al., [105]. In case of variable compressor parameters, 92.4 % of the estimated discharged mass flow rate lies within 0.7 % error percentage while 96.2 % of the predicted compressor power achieves 0.8 % error percentage for variable compressor parameters. The reported results revealed that error percentages using variable compressor parameters are lower than those using constant compressor parameters. Hence, the present model predictions are very close to the experimental data compared to the prediction of the reported models in literature.

The above results revealed that the variable compressor parameters achieve lowest error percentage so it will be used in the current modelling. Therefore, correlations for the compressor parameters are deduced as a function of operating conditions such as

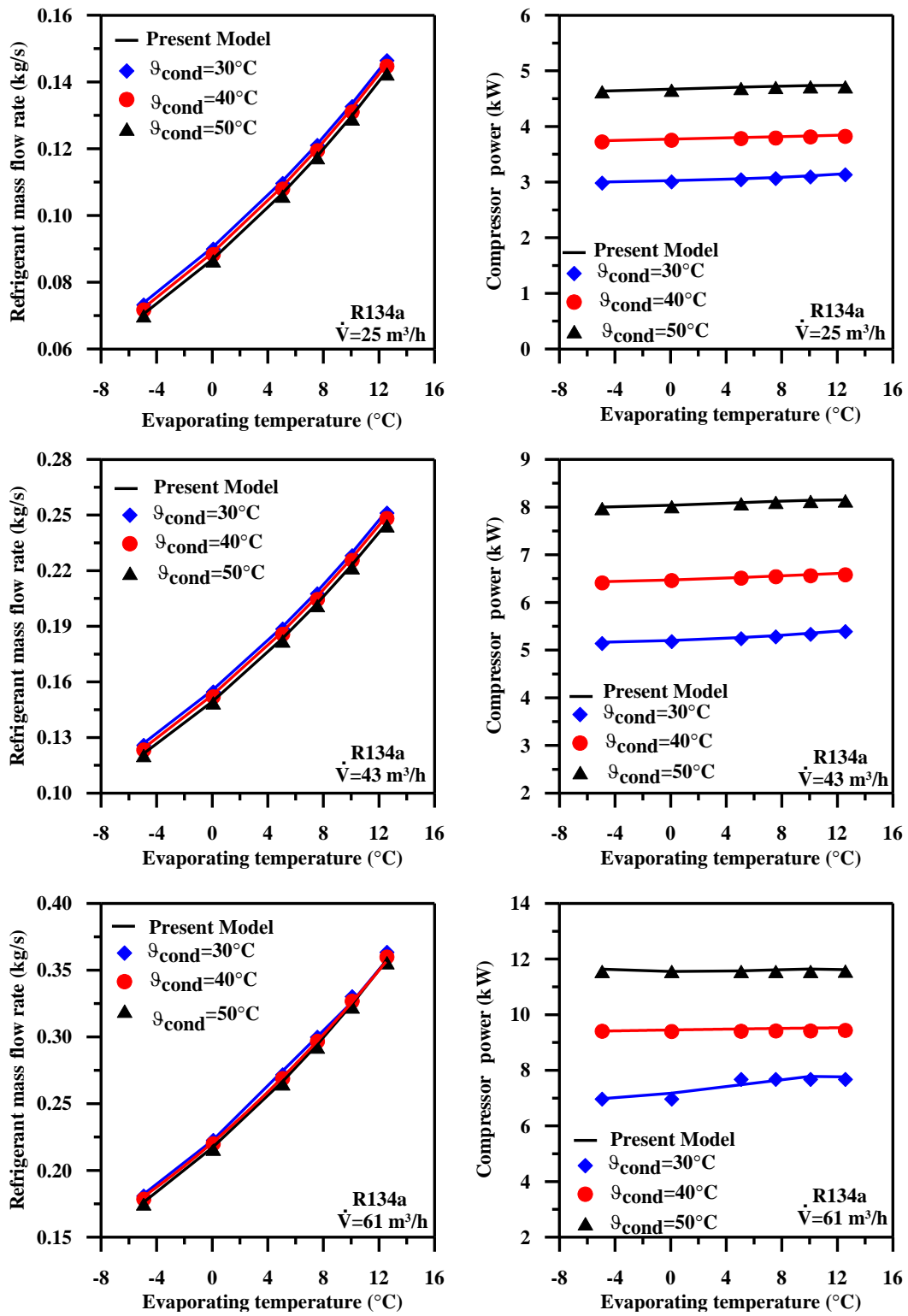


Figure 7.5: Comparison between predicted and experimented refrigerant mass flow rate and compressor power

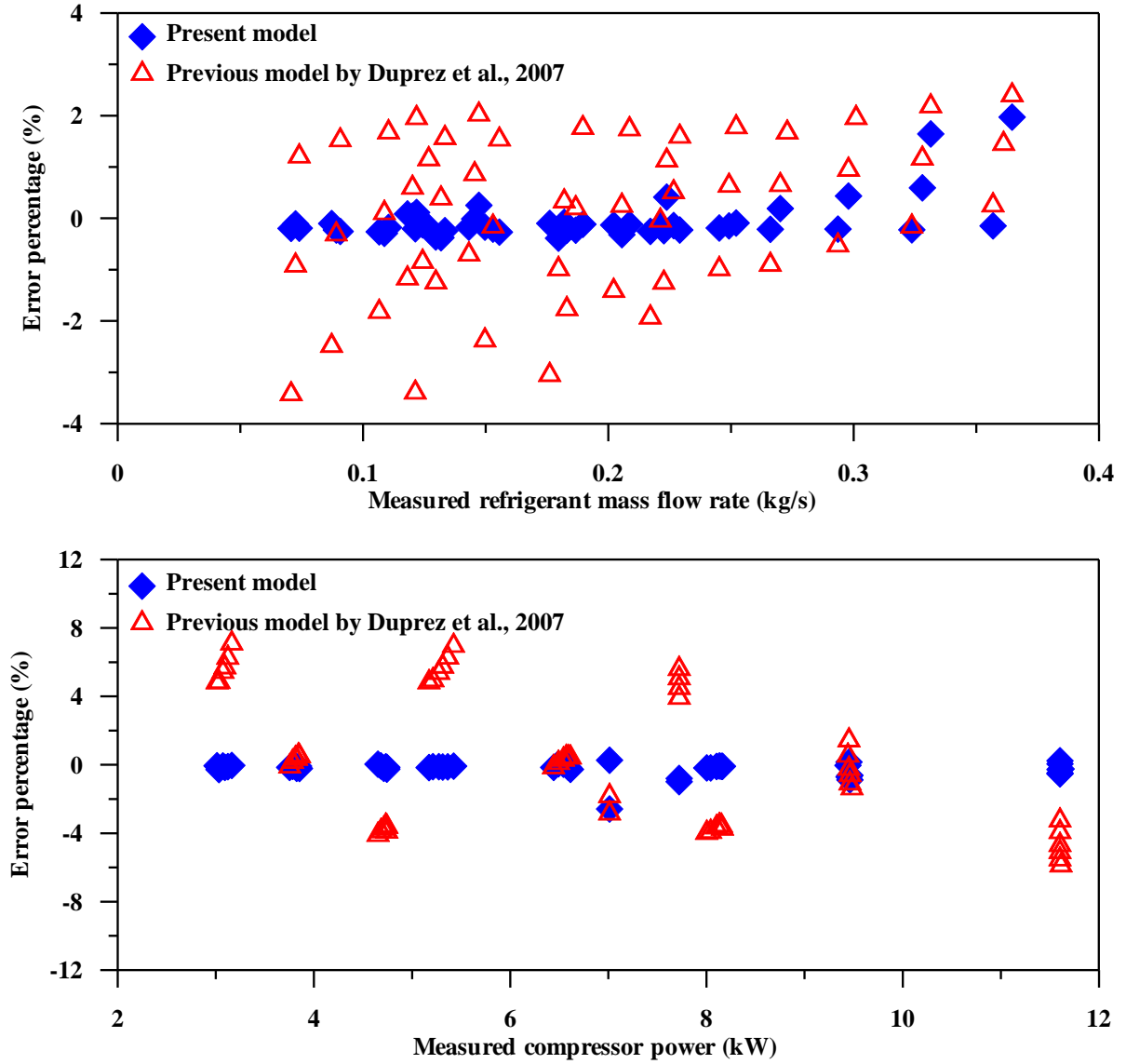


Figure 7.6: Comparison between present and previous models.

suction pressure and temperature, discharge pressure and engine speed. Both  $UA_{suc}$  and  $\phi$  can be calculated as;

$$\ln(UA_{suc}) = 10^{-5} \times (-3.847N_{eng} - 69.59P_{suc} + 67.01P_{dis} + 2508\vartheta_{suc} + 290600), \quad (7.23)$$

$$\ln(\phi) = 10^{-5} \times (-12.07N_{eng} + 32.77P_{suc} - 9.715P_{dis} + 53.56\vartheta_{suc} - 14160), \quad (7.24)$$

It can be noted that other compressor parameters like  $\xi$  and  $\gamma$  are kept 4.322 and 0.02, respectively which gives better results [108]. A computer program is written to solve the above equations using EES software [87]. The model input data are refrigerant type, evaporating temperature ( $\vartheta_{evap}$ ), condensing temperature ( $\vartheta_{cond}$ ) and degrees of superheating ( $\Delta\vartheta_{sup}$ ). Figure 7.7 shows comparison between calculated and measured mass flow rate and compressor power. In fact, all the estimated points are within 2% error percentage for both mass flow rate and compressor power.

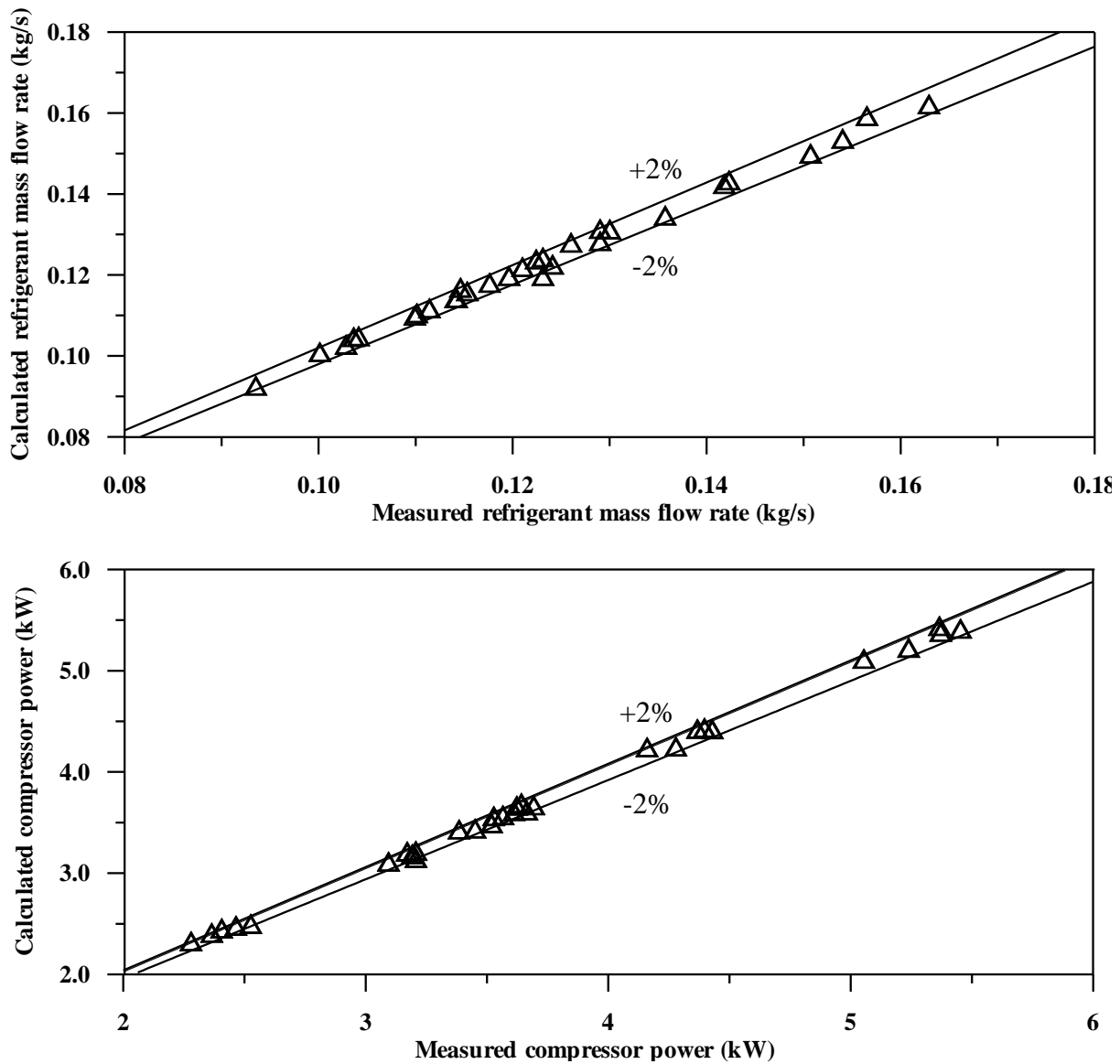


Figure 7.7: Comparison between measured and predicted mass flow rate and compressor power.

## 7.2 Plate Heat Exchanger

The indoor unit heat exchanger type is a brazed plate heat exchanger. It consists of 80 plates, which make 39 refrigerant channels and 40 water channels. Figure 7.8 shows a schematic diagram of the evaporator plate heat exchanger<sup>1</sup>. It works as an evaporator in cooling mode and as a condenser in heating mode. In this work, the evaporator plate heat exchanger will be considered.

For the thermal modelling, a relatively simple model is used. The evaporator is divided

<sup>1</sup>This figure is used based on license agreement between the author and Elsevier with license number of 2658841161448

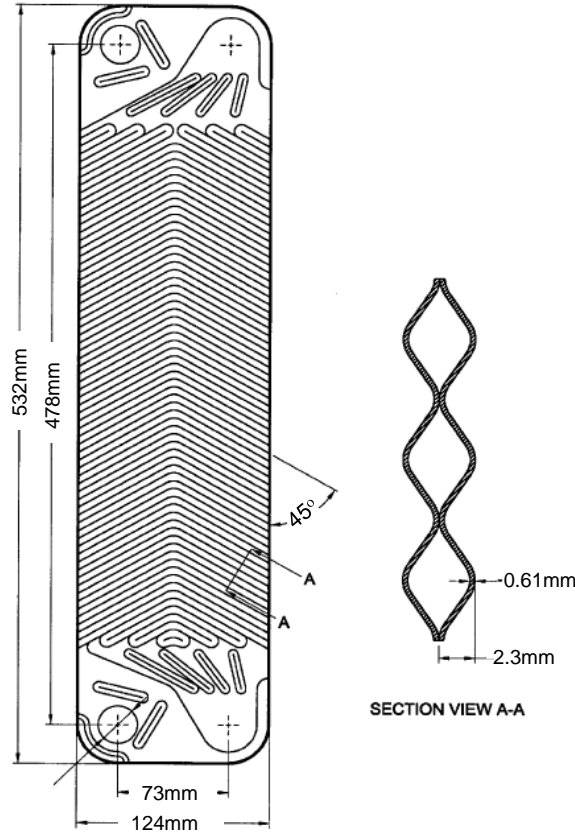


Figure 7.8: Main dimensions of the plate heat exchanger.

into two zones, one for evaporation and the other for superheating (see Fig. 7.9). System cooling capacity represents the summation of heat transferred in the two zones as;

$$\dot{Q}_{evap} = \dot{Q}_{sat} + \dot{Q}_{sup}, \quad (7.25)$$

Superheating heat transfer ( $\dot{Q}_{sup}$ ) can be calculated from the knowledge of discharged refrigerant mass flow rate, suction pressure and constant superheating degrees for the evaporator as the following;

$$\dot{Q}_{sup} = \dot{M}_{ref}(h_{evap,o} - h_{sat,v}) \quad (7.26)$$

Required heat transfer area for superheating zone ( $A_{sup}$ ) can be calculated as follows;

$$A_{sup} = \frac{\dot{Q}_{sup}}{LMTD_{sup}U_{sup}}, \quad (7.27)$$

where the logarithmic mean temperature difference  $LMTD_{sup}$  for the plate heat exchanger can be estimated like as counter flow using the following equation [109];

$$LMTD_{sup} = \frac{(\vartheta_{ch,wat} - \vartheta_{15}) - (\vartheta_b - \vartheta_{sat})}{\ln \frac{\vartheta_{ch,wat} - \vartheta_{15}}{\vartheta_b - \vartheta_{sat}}}, \quad (7.28)$$



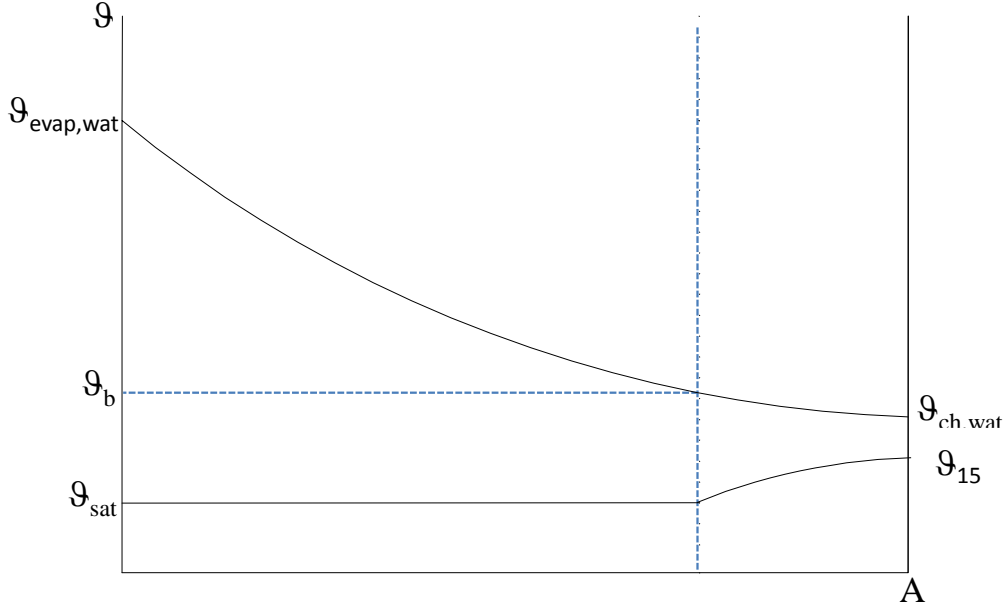


Figure 7.9: Evaporator internal stages.

and overall heat transfer coefficient  $U_{sup}$  during superheating zone can be calculated as;

$$\frac{1}{U_{sup}} = \frac{1}{\alpha_{wat,sup}} + \frac{1}{\alpha_{ref,sup}} + R_{fouling} + \frac{\delta_{plate}}{k_{plate}}, \quad (7.29)$$

$\vartheta_b$  represents the water temperature corresponding to dry saturated vapor refrigerant and can be calculated as;

$$\vartheta_b = \frac{\dot{Q}_{sup}}{\dot{M}_{wat}c_{wat}} + \vartheta_{ch,wat}, \quad (7.30)$$

Values of fouling resistance ( $R_{fouling}$ ), plate thickness ( $\delta_{plate}$ ) and plate thermal conductivity ( $k_{plate}$ ) are  $0.000128 \text{ m}^2\text{kW}^{-1}$ ,  $0.613\text{mm}$ ,  $16.3\text{Wm}^{-1}\text{K}^{-1}$ , respectively [110]. Hence, evaporation heat transfer area ( $A_{evap}$ ) can be calculated as;

$$A_{evap} = A_{sat} + A_{sup}. \quad (7.31)$$

Then evaporation heat transfer rate ( $\dot{Q}_{sat}$ ) can be evaluated with solving the following series of governing equations;

$$\dot{Q}_{sat} = U_{sat}A_{sat}LMTD_{sat}. \quad (7.32)$$

$$LMTD_{sat} = \frac{(\vartheta_{evap,wat} - \vartheta_{sat}) - (\vartheta_b - \vartheta_{sat})}{\ln \frac{\vartheta_{evap,wat} - \vartheta_{sat}}{\vartheta_b - \vartheta_{sat}}}, \quad (7.33)$$

$$\dot{Q}_{sat} = \dot{M}_{wat}c_{wat}(\vartheta_{evap,wat} - \vartheta_b), \quad (7.34)$$

$$\frac{1}{U_{sat}} = \frac{1}{\alpha_{wat,sat}} + \frac{1}{\alpha_{ref,sat}} + R_{fouling} + \frac{\delta_{plate}}{k_{plate}}, \quad (7.35)$$

where  $\vartheta_{evap,wat}$  is the evaporator water inlet temperature. Among the experimental runs, refrigerant mass flow rate changed from 0.09 to 0.14  $kg s^{-1}$  while chilled water mass flow rate varied from 0.6 to 0.75  $kg s^{-1}$ . Regarding to the evaporation zone, the refrigerant saturation temperature lies between -2.5 and 9.5°C and the refrigerant heat flux range is 11 to 12.8  $kW m^{-2}$ . Different correlations for the heat transfer coefficients have been tested to calculate the water, single phase refrigerant and boiling heat transfer coefficients with minimum error in cooling capacity estimations. These correlations will be introduced in the following sections.

### 7.2.1 Single phase flow correlations

Heat transfer coefficient in plate heat exchangers has been investigated for several years, and the amount of work that has been carried out is quite extensive. A general theory or correlation covering all geometrical parameters and combinations of plate heat exchangers does not exist. The large amount of possible combinations which results from the variation of the geometric parameters of the plate heat exchangers makes such a theory almost impossible. Each investigation should be regarded as a special case whose results are only applicable for the specific geometry and combinations tested. Unfortunately, this investigation cannot present all geometry parameters in detail. There are more than 30 practical correlations starting with Troupe et al. [111] in 1960, and continuing up to one of the latest correlations published by Longo and Gasparella (2007), [112]. Table 7.1 illustrates some of these correlations.

### 7.2.2 Boiling correlations

Boiling inside tubes is dominated by two phenomena: convective boiling and nucleate boiling. Although many boiling correlations have been developed for the characterization of heat transfer and pressure drop in plate heat exchanger, there is no clear agreement which effect is dominant. It seems to have been accepted that at high heat fluxes or low qualities, nucleate boiling has a larger influence than convective boiling [113], [114] and [115]. Moreover, some correlations also regard the influence of geometric parameters as in the case of single-phase. They prove that variables such as the chevron angle, the pitch, and the hydraulic diameter should not be forgotten in the correlations [114] and [109]. Other papers [116] have contributed to a better understanding of the boiling heat transfer coefficient for four different refrigerants; R134A [117], [118], [119] and [112], R22 [109], and [120] Ammonia [114], [118] and [121] and R410A [122] and [109]. In the frame of this thesis, only R410A flow boiling correlations have been introduced.

Table 7.1: Single phase heat transfer correlations for plate heat exchangers.

<i>Investigator</i>	<i>Correlation</i>	<i>Comments</i>
<i>Kumar (1984), [123]</i>	$Nu = C_1 Re^m Pr^{0.33} (\mu/\mu_w)^{0.17}$	$\beta = 60^\circ$ , $\phi = 1.17$ $Re < 20$ , $C_1 = 0.562$ , $m = 0.326$ $20 < Re < 400$ , $C_1 = 0.306$ , $m = 0.529$ $Re > 400$ , $C_1 = 0.108$ , $m = 0.703$
<i>Heavner et al. (1993), [124]</i>	$Nu = 0.118 \phi^{0.28} Re^{0.72} Pr^{0.5} (\mu/\mu_w)^{0.17}$	$0^\circ \leq \beta \leq 67^\circ$ , $\phi = 1.17$ $400 < Re < 10000$ , $3.3 < Pr < 5.9$
<i>Wanniarachchi et al. (1995), [125]</i>	$Nu = (Nu_t^3 + Nu_t^3)^{0.333} Pr^{1/3} (\mu/\mu_w)^{0.17}$ $Nu_t = 3.65 m^{0.445} Re^{0.339}$ $Nu_t = 12.6 m^{1.142} Re^{0.646 + 0.0011 m}$ $m = 90 - (\beta)(180/\pi)$	$1 < Re < 10000$ , $20^\circ \leq \beta \leq 62^\circ$
<i>Longo and Gasparella (2007), [112]</i>	$Nu = 0.277 Re^{0.766} Pr^{0.333}$	$\beta = 65^\circ$ $200 < Re < 1200$ , $5 < Pr < 10$
<i>Haberschill et al. (2002), [126]</i>	$Nu = 0.328 Re^{0.732} Pr^{0.333}$	
<i>Kim (1999), [127]</i>	$Nu = 0.295 Re^{0.64} Pr^{0.32} (\frac{\pi}{2} - \beta)^{0.09}$	
<i>Marrriott (1979), [128]</i>	$Nu = 0.374 Re^{0.668} Pr^{0.33} (\mu/\mu_w)^{0.17}$	
<i>VDI-Wärmeatlas (1997), [129]</i>	$Nu = 0.0136 Re^{0.4} Pr^{0.344}$	$Re > 400$
<i>Yan and Lin (1999), [117]</i>	$Nu = 0.2121 Re^{0.78} Pr^{0.33} (\mu/\mu_w)^{0.14}$	
<i>Taluk et al. (1995), [130]</i>	$Nu = 0.25 Re^{0.7} Pr^{0.4} (\mu/\mu_w)$	
<i>Buonopane and Troupe (1969), [131]</i>	$Nu = 0.4322 Re^{0.62} Pr^{0.4}$	

### 7.2.2.1 Hsieh and Lin correlation

The correlation proposed by Hsieh et. al [122] is based on the experimental data obtained for R410A . The experiments were performed for several mass flow rates, heat fluxes, and system pressures in a heat exchanger characterized by a chevron angle of  $\pi/3$ ;

$$\alpha_{ref,sat} = \alpha_{ref,l} 88 Bo^{0.5}, \quad (7.36)$$

where the all-liquid non-boiling heat transfer coefficient,  $\alpha_{ref,l}$ , is determined from an empirical correlation proposed for R410A;

$$\alpha_{ref,l} = 0.2092 \frac{k_l}{D_h} Re^{0.78} Pr^{0.33} (\mu/\mu_w)^{0.14}, \quad (7.37)$$

Where boiling number ( $Bo$ ) can be calculated as;

$$Bo = \frac{\dot{q}}{G h_{fg}}, \quad (7.38)$$

in which  $q$  is the heat flux,  $G$  is the mass flux and  $h_{fg}$  represents the latent heat of vaporization.

### 7.2.2.2 Han, Lee, and Kim correlation

Han et al. [109] developed a correlation based on experiments with refrigerants R22 and R410A. They varied the mass flow rate of refrigerant, the evaporating temperature, the vapor quality, and the heat flux. Several chevron angles and pitches were also studied. In this case, the Nusselt number is given by;

$$Nu = Ge_1 Re_{eq}^{Ge_2} Bo_{eq}^{0.3} Pr^{0.4}, \quad (7.39)$$

where the coefficients  $Ge_1$  and  $Ge_2$  are functions of the heat exchanger geometry, unlike the Hsieh and Lin correlation presented above;

$$Ge_1 = 2.81 \left(\frac{p_{co}}{D_h}\right)^{-0.041} \left(\frac{\pi}{2} - \beta\right)^{-2.83}, \quad (7.40)$$

$$Ge_2 = 0.746 \left(\frac{p_{co}}{D_h}\right)^{-0.082} \left(\frac{\pi}{2} - \beta\right)^{0.61}, \quad (7.41)$$

In this correlation,  $Re_{eq}$  and  $Bo_{eq}$  are respectively the equivalent Reynolds and boiling numbers, in which an equivalent mass flux is used in their definitions and are defined as;

$$Bo_{eq} = \frac{q}{G_{eq} h_{fg}}, \quad (7.42)$$

$$Re_{eq} = \frac{G_{eq} D_h}{\mu_l}, \quad (7.43)$$

$$G_{eq} = G \left(1 - x + x \left(\frac{\rho_l}{\rho_v}\right)\right) \frac{G_{eq} D_h}{\mu_l}. \quad (7.44)$$

The previous correlations have been tested to calculate the cooling capacity with minimum resulting error as compared to the experiments. Wanniarachchi et al., [125] and Kim [127] have been used to calculate water heat transfer coefficient at low and high flow rate respectively. Furthermore, it has been found that Wanniarachchi et al., [125] and Hsieh and Lin [122] correlations are the best correlations to estimate refrigerant single phase and evaporation heat transfer coefficients and hence the system cooling capacity with minimum resulting error [132].

### 7.3 Gas Engine

Thermal modelling of the gas engine can be achieved by either mathematical modelling or experimental correlations. Since the heat transfer in internal combustion engines is transient and three dimensional with moving boundaries process in every cycle, modelling the heat transfer process by the mathematical way is rather a complex process [133]. On the other hand, identifying the model from experimental data is a relatively simple way to acquire the thermodynamic characteristics of the gas engine. The engine performance is mainly function of load, speed and ambient air temperature. In the GEHP system modelling, the concerning parameter is the gas engine energy consumption. In order to get the relationship between the gas engine energy consumption in a wide range of loads, speeds and ambient air temperatures, experiments on the gas engine have been conducted in a wide range of compressor power (2-5kW), speeds (1200-1750rpm) and ambient air temperatures (19-36°C). A correlation is deduced to get the gas engine energy consumption based on the measured data for the gas engine at different operating conditions as the following;

$$\dot{Q}_{gas} = 1.407P_{comp} + 0.005N_{eng} + 0.0821\vartheta_{amb}, \quad (7.45)$$

where  $P_{comp}$  is the compressor power in kW,  $N_{eng}$  is the engine speed in rpm and  $\vartheta_{amb}$  is the ambient air temperature in °C. Coefficient of multiple determinations ( $R^2$ ) of this correlation is 0.96.

All the above equations are used to estimate the GEHP main parameters such as cooling capacity, gas engine energy consumption and primary energy ratio. Appendix E explains the flow chart of the simulation program.

### 7.4 Simulation Results and Discussion

According to cooling mode operation, two situations are considered in the solution of the GEHP system: (1) for given engine speed, the cooling capacity and the performance of the system can be calculated. (2) for given cooling load, the engine speed can be estimated and the corresponding performance is obtained. The model is validated with the prescribed system. The temperature of the chilled water and water flow rate are measured. Hence, the cooling capacity of the system can be calculated. In addition, the natural gas volume flow rate is measured by diaphragm gas meter, which has been used to calculate the

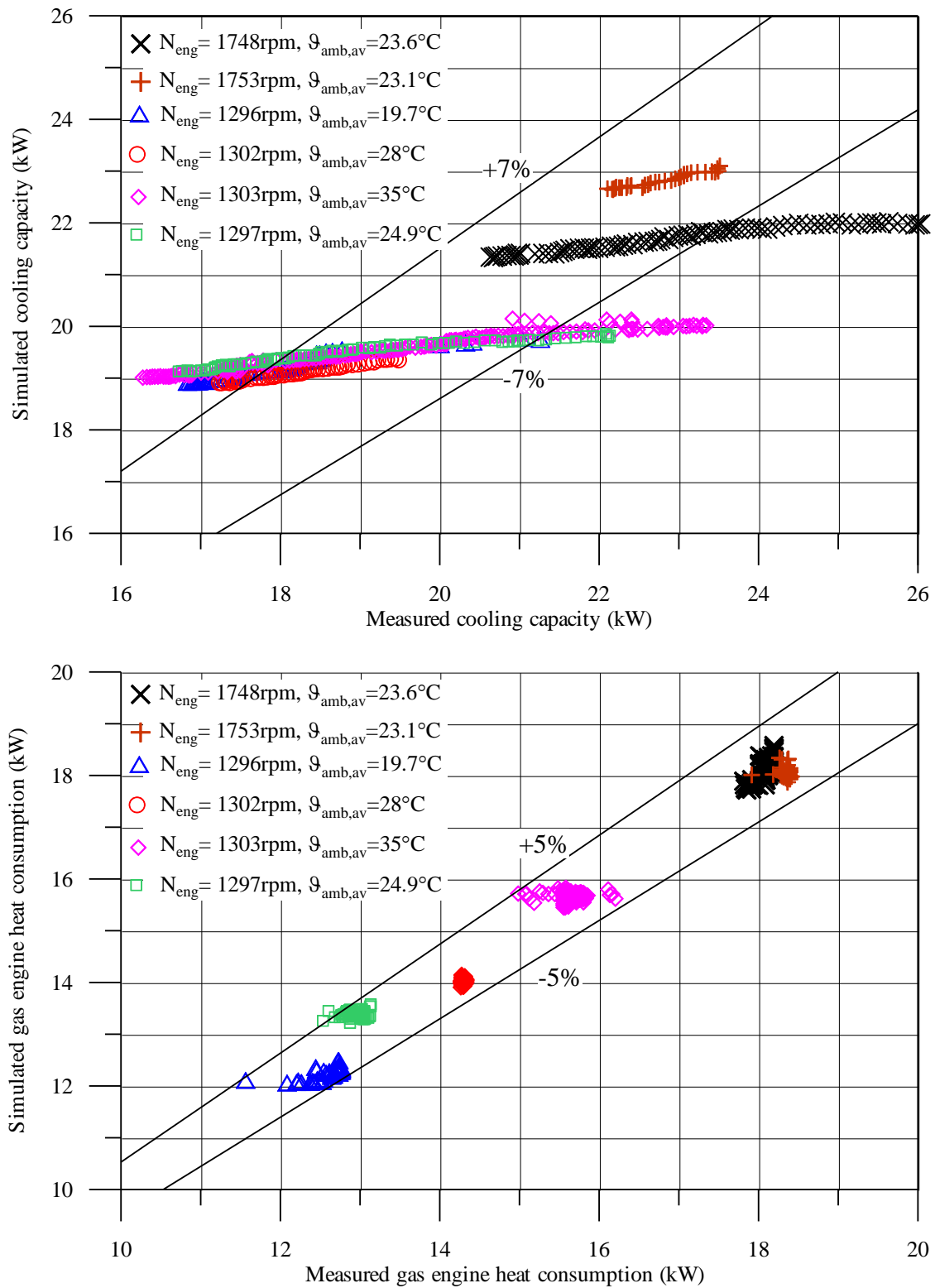


Figure 7.10: Comparison between simulated and measured cooling and gas engine energy consumption capacities.

gas engine energy consumption. Engine speed changed from 1300rpm to 1750rpm and ambient temperature varied from 19.7°C to 35°C. Figures 7.10 and 7.11 show comparison between measured and simulated results. The model error percentage to simulate cooling capacity is 7% while it is 5% to predict the gas engine energy consumption or compressor power. This may be attributed to the accuracy of the heat transfer correlations in plate heat exchanger model. A better heat transfer correlations could be obtained by testing the heat exchanger using water as hot and cold fluids. Then, estimate the single phase correlations with relatively high accuracy. On the other hand, the obtained error in modelling system primary energy ratio is relatively small (about 6%) which enable us to evaluate the system energy efficiency under different working conditions. Moreover, the present model can be used for better understanding, controlling, optimizing the GEHP system by evaluating its energy efficiency at various operating conditions.

## 7.5 Conclusions based on Modelling and Simulation Results

In this chapter, a semi-empirical model is developed to simulate the performance of the GEHP system. The performance of the GEHP system is characterized by the system cooling capacity, gas engine energy consumption and primary energy ratio. The model focuses on simulation of scroll compressor and plate evaporator to get system cooling capacity and on the gas engine to obtain the gas engine energy consumption and then estimate the system primary energy ratio. The obtained refrigerant mass flow rate from the compressor model is used with the aid of heat transfer correlations to calculate the system cooling capacity. On the other hand, a correlation of the gas engine energy consumption is obtained as a function of engine load, speed and ambient air temperature based on actual measurements for the prescribed system. Based on the reported results, the following conclusions are drawn:

- Scroll compressor modelling plays an important role in determining the performance of GEHP because it determines the discharged refrigerant mass flow rate and consequently cooling capacity as well as the compressor power which is used to estimate the gas engine energy consumption.
- The testing results of the scroll compressor conclude that the discharged mass flow rate is more sensitive to engine speed followed by suction pressure and discharge pressure in that order. However, the compressor power is more sensitive to engine speed followed by discharge pressure and suction pressure in that order. Furthermore, both volumetric and isentropic efficiencies are higher influenced by pressure ratio than engine speed.
- A minimum resulting error for prediction of both refrigerant mass flow rate and compressor power have been obtained when correlations for the compressor modelling parameters as a function of operating conditions have been used.
- Validation of the compressor model showed that the present model predicts data that are very close to the available experimental data in literature. Moreover, comparing

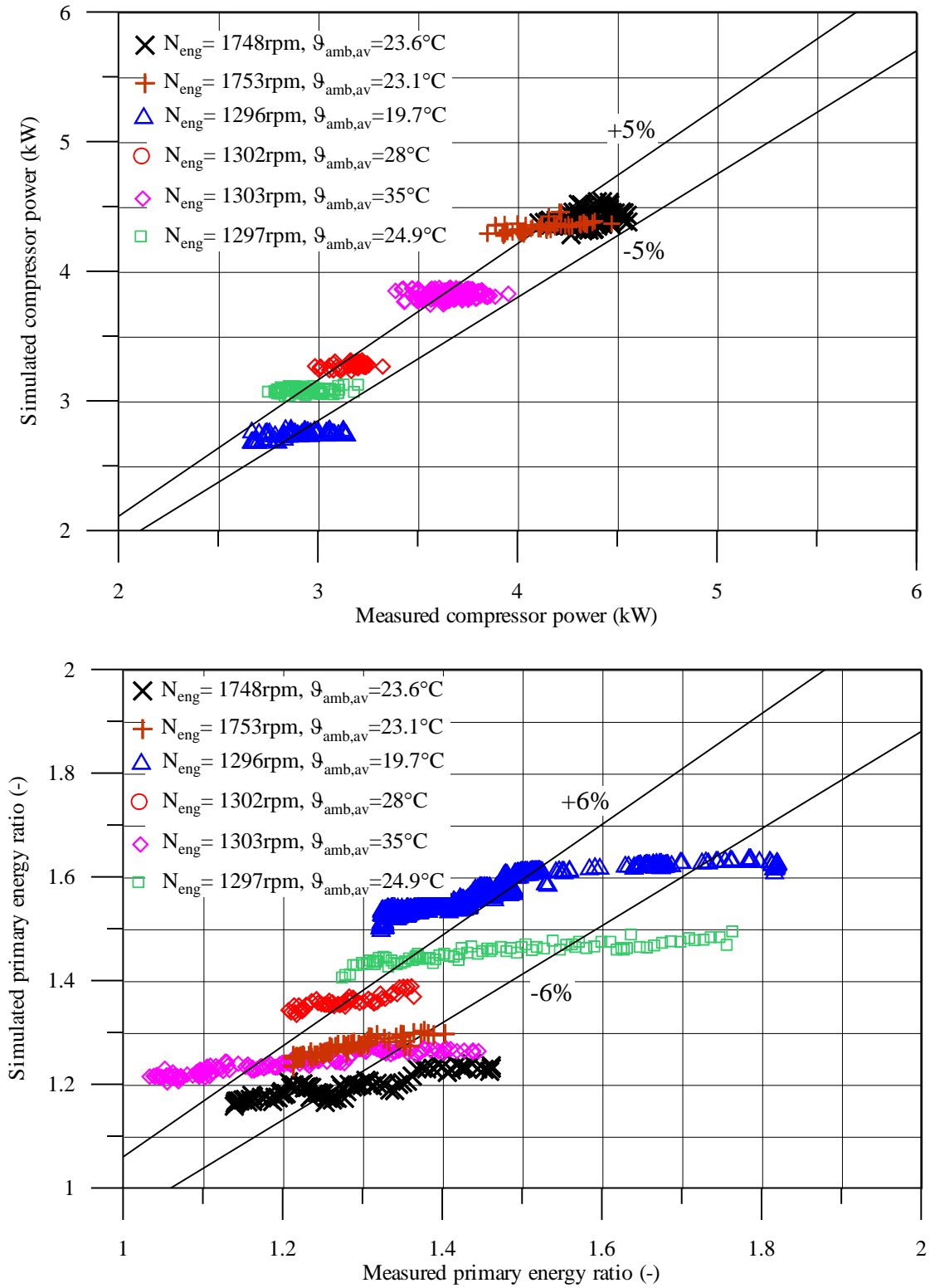


Figure 7.11: Comparison between simulated and measured compressor powers and primary energy ratio.



the present model with previous models confirms that error percentages using the present model (less than 4%) are lower than those using the previous model (5% to 10%). Furthermore, the model error percentage to predict both mass flow rate and compressor power is within 2% as comparing with experimental data.

- Regarding to the plate heat exchanger, several heat transfer correlations have been tested to calculate the cooling capacity with minimum resulting error. It has been found that Wanniarachchi et al. [125], and Hsieh et. al [122] correlations are the best correlations to estimate the refrigerant single phase and evaporation heat transfer coefficients.
- The model accuracy to predict system cooling capacity, gas engine energy consumption and primary energy ratio is about 7%, 5%, 6% respectively. Therefore, the present model can be used for a better understanding, controlling, optimizing the GEHP system by evaluating its energy efficiency at various operating conditions.



# Chapter 8

## SUMMARY AND OUTLOOK

The objective of the present work is to estimate the performance characteristics of the gas engine heat pump (GEHP) working with R410A under various operating conditions. It consists of experimental and theoretical investigations. The experimental work aimed at evaluating the performance of the GEHP for different operating modes namely cooling, combined cooling and heating and heating mode. The engine heat recovery utilization is essential in order to enhance the system primary energy ratio. Hence, there are two sub heating mode based on the engine heat recovery utilization. The first mode when this heat is transferred to the water side in order to get higher water temperature levels and higher system primary energy ratio. The second sub heating mode occur when the engine heat recovery is transferred to the refrigerant to evaporate it especially at the lower ambient air temperature. The operating parameters for the prescribed modes are water flow rate, water inlet temperature, engine speed and ambient air temperature. Based on the reported experimental results, the following conclusion may be drawn:

### - Cooling mode

- For the considered chilled water temperature range between 5 and 15°C, primary energy ratio of the GEHP up to 1.8 has been obtained which confirms the high energy efficiency of the system in different cooling applications such as air conditioning and factory cooling.
- The performance characteristics of the GEHP is enormously influenced by evaporator water inlet temperature than its volume flow rate. Primary energy ratio of the GEHP increases (27.8 %) with changing of evaporator water inlet temperature from 13°C to 24°C.
- Cooling capacity increases (3.1 %) while gas engine energy consumption decreases (2 %) as the evaporator water flow rate changes from  $1.63m^3/h$  to  $2.38m^3/h$ . However, PER of the GEHP changed from 1.23 to 1.57 as the ambient air temperature varied from 35°C to 19.7°C.
- As the engine speed changed from 1300 to 1750rpm, the rate of increasing in the gas engine energy consumption (38 %) is higher than that in the cooling capacity (20.5 %) and hence PER decreases (19 %).

### - Combined cooling and heating mode

- Best results concerning high energy efficiency have been obtained in combined mode in which PER up to 2.1 has been reached. Moreover, the primary energy ratio can be increased by increasing of water inlet temperature or decreasing engine speed.
- Chilled water temperature ranges between 6.5 and 12.5°C and hot water temperature lies between 55.8 and 63°C are obtained. The obtained chilled and hot water can be used in air conditioning, industry and domestic applications.
- Evaporator water inlet temperature has the highest influence on the system performance followed by engine speed, ambient air temperature and water volume flow rate in that order. Primary energy ratio of the GEHP increases by 14.8 % as the evaporator water inlet temperature varies from 12.2°C to 20°C.
- Engine heat recovery load and gas consumption remain nearly constant while cooling capacity increases (6.6 %) when the evaporator water flow rate increases from 1.99m<sup>3</sup>/h to 3.6m<sup>3</sup>/h.
- Gas engine energy consumption increase by 19.4 % as the ambient air temperature varies from 24.1°C to 33.8°C. However, PER decreases (20 %) as a result of increasing of engine speed from 1200 to 1750rpm.
- It should be noted that recovered engine heat decreased from 11kW to 5.4kW as the heat recovery water inlet temperature varied from 37.5°C to 59°C.

### - Heating mode

- Primary energy ratio of the GEHP system in heating mode (especially at low ambient air temperature) is relatively small as compared to both cooling and combined modes. This can be attributed to the low surface area of the evaporator in the outdoor unit of Aisin package. Therefore, the use of recovered engine heat in the refrigerant circuit overcomes the low surface area of the evaporator and avoids frosting problem.
- The outlet hot water temperature is ranging from 38 to 65°C when the recovered engine heat is transferred to water while it is limited to 40°C at lower ambient air temperature.
- As the ambient air temperature increases from 10.7°C to 25.8°C, the total heating capacity, gas engine heat recovery and gas heat consumption increase and by 3.6 %, 31.3 % and 4.7 % respectively.
- As the recovered engine heat is transferred to water circuit, primary energy ratio of the GEHP decreases by 29.2 % as the condenser water inlet temperature varies from 35.8°C to 48°C. However, total heating capacity and waste heat recovery increases by 2.1 %, 7 % respectively as the condenser volume mass flow increases from 5.62m<sup>3</sup>/h to 16.64m<sup>3</sup>/h. Moreover, when the engine speed changed from 1300rpm to 1750rpm, system PER decreases by 16.7 %.

- Better results for the system in heating mode could be obtained by replacing the outdoor heat exchanger with larger one or changing the secondary fluid from air to water.
- High energy efficiency can be obtained by decreasing condenser water inlet temperature and engine speed.

#### **- Theoretical work**

In the theoretical part, firstly a parametric study of the GEHP using R410A (as it is the best choice as alternative refrigerant for R22 due to its environmental protection and high energy efficiency utilization) has been made. Then, a simulation model for the GEHP system in best operating mode (cooling mode) has been developed. Modelling of the GEHP includes modelling of the heat pump system as well as the gas engine. The main target of heat pump modelling is to obtain the system cooling capacity while the gas engine energy consumption is the goal of the gas engine modelling. Modelling of the heat pump includes modelling of both scroll compressor and plate heat exchanger.

#### **- Scroll compressor modelling**

- The experimental performance characteristics of an open variable speed scroll compressor is investigated firstly and then a realistic model with variable compressor parameters which can be used to predict mass flow rate and compressor power is presented.
- The discharged mass flow rate is more sensitive to engine speed followed by suction pressure and discharge pressure in that order. On the other hand, it can be observed that the compressor power is enormously influenced by engine speed followed by discharge pressure and suction pressure in that order. Furthermore, both volumetric and isentropic efficiencies are enormously influenced by pressure ratio than engine speed.
- A minimum resulting error for prediction of both refrigerant mass flow rate and compressor power have been obtained when correlations for the compressor modelling parameters as a function of operating conditions have been used.
- Validation results of the compressor model showed that the present model predicts data that are very close to the available experimental data in literature. Moreover, comparing the present model with previous models confirms that error percentages using the present model (less than 4%) are lower than those using the previous model (5% to 10%). Furthermore, the model error percentage to predict both mass flow rate and compressor power are within 2% as comparing with experimental data.

#### **- Plate heat exchanger**

- Regarding to the plate heat exchanger, several heat transfer correlations have been tested to calculate the cooling capacity with minimum resulting error. Kim [127]

and Wanniarachchi et al. [125] have been used for water heat transfer coefficients calculations at high and low flow rates, respectively. Furthermore, it has been found that Wanniarachchi et al. [125] correlation and Hsieh et al. [122] correlation are the best correlations to estimate refrigerant single phase and evaporation heat transfer coefficients and hence the system cooling capacity with minimum resulting error.

#### - Simulation results of the GEHP

- According to the gas engine heat pump simulation model, the model accuracy to predict system cooling capacity, gas engine energy consumption and primary energy ratio is about 7 %, 5 %, 6 % respectively.
- The present model can be used to better understanding, controlling, optimizing the GEHP system by evaluating its energy efficiency at various operating conditions.

## 8.1 Recommendations for Future Research

In this study, it has been shown a significant savings in primary energy by utilizing GEHP. However, there are several areas where further investigation required in improving the overall performance of the system. Some of the areas needing further study are:

- Investigation of the water to water GEHP as its performance is higher than the air to water GEHP which is introduced in the frame of this work.
- For higher energy efficiency of the system in both combined and cooling modes, the released heat from the condenser should be recovered.
- Using the desuperheating heat in the condenser and recovered engine heat for heating at high temperature level.
- Better results for the system in heating mode could be obtained by replacing both the outdoor and engine heat recovery heat exchangers with larger ones to enhance the system performance.
- Investigation of multi stage vapor compression heat pumps to increase the coefficient of performance of the heat pump and consequently the primary energy ratio of the GEHP.
- Using the novel injection techniques instead of the conventional expansion device to reduce the throttling and pumping losses of vapor compression system.
- Measuring the engine shaft power which is important for better calculations of compressor power and engine mechanical efficiency and consequently improves the system modelling.

# Appendix A

## SPECIFICATION OF THE SYSTEM MAIN COMPONENTS

The experimental apparatus uses a GEHP (TGMP 280 C1N) produced by AISIN Company in Japan as outdoor unit. The nominal cooling capacity is  $28kW$ , while in heating mode the capacity is  $34kW$ . Specifications of the system main components such as the gas engine, the compressor and the indoor unit heat exchanger are explained in Table A.1.

Table A.1: Specifications of the system main components.

<i>Component</i>	<i>Main specifications</i>	<i>Value</i>
<i>Gas engine</i>	Type Displacement Rated output Revolution range	Water-cooled straight 4-cycle OHV 0.952 L 7.5 kW Cooling 1000 to 1600 rpm Heating 1000 to 2800 rpm
<i>Compressor</i>	Type Displacement Refrigerant Power transmission system Revolution range	Scroll $52 \text{ cm}^3/\text{rev}$ R410A 1 Poly V-belt Cooling 1700 to 2720 rpm Heating 1700 to 4760 rpm
<i>Indoor unit heat exchanger</i>	Type Model Number of plates Total surface area Chevron angle	Brazed plate heat exchanger GEA WTT GmbH - AE5 80 $4.62 \text{ m}^2$ $45^\circ$
<i>Heat recovery heat exchanger</i>	Type Model Number of plates Working fluids	Brazed plate heat exchanger BXC-244-PEBX-12 13 Ehtylen water mixture/R410A





# Appendix B

## INSTRUMENTS CALIBRATION

### B.1 Resistance Thermometers (Pt100) Calibration

The resistance thermometers calibration is carried out using precision temperature calibrator TP28850 manufactured by SIKA company. This temperature calibrator is designed to demonstrate a number of commonly used methods of temperature measurement, and provide the means for calibration and accuracy comparisons of different methods. This precision temperature calibrator is operated by an electronically controlled heating block made of brass and allowing being thermostat up to 600°C. The heating block has a bore serving as location hole for the specimen. An adapter sleeve can be inserted in that bore. The sleeve serves as an adapter between specimen (temperature switch, thermostat, thermocouple, thermometer, resistance thermometers) and heating block bore. The heating block is insulated against the housing. The main specifications of the temperature calibrator are given in Table B.1.

Table B.1: Specifications of the temperature calibrator.

<i>Parameter</i>	<i>Range</i>
<i>Heating block temperature balancing</i>	0-850°C in 1/10 K resolution
<i>Heating block control accuracy</i>	+/- 0.5K
<i>Heating block control stability</i>	+/- 0.5K
<i>Measuring element within heating block control</i>	PID-controller / Pt100
<i>Heating block control stability</i>	+/- 0.5K
<i>Temperature sensor inputs</i>	Thermocouple type K, S, E, J, T and Pt100
<i>Resolution and measuring inaccuracy</i>	-200 up to +200°C: +/- 0.1 % v.E. +/- 0.1°C

The calibration results are tabulated and the curve of each thermometers resulting in a single equation describing the correction of all thermometers as the following;

$$\vartheta_{n,act} = A_n \vartheta_n - B_n \quad (\text{B.1})$$

Where,  $\vartheta_{n,act}$  is the calibrator temperature and  $\vartheta_n$  represents the thermometer reading. Table B.2 gives numerical constants of above equation for all Pt100 measuring points.

Table B.2: Numerical constants of the Pt100 calibration equation.

<i>Measuring point</i>	$A_n$	$B_n$
1	0.9580	0.0000
2	0.9702	0.0000
3	0.9945	0.0639
4	1.0136	0.5323
5	0.9926	0.2327
6	0.9904	0.2660
7	0.9947	0.0639
8	0.9945	0.2171
9	0.9708	0.0000
10	0.9918	0.2286
11	0.9872	0.2693
12	1.0045	0.5633
13	1.0031	1.5187
14	1.0144	0.7565
15	0.9923	0.2204
16	1.0307	0.2204
17	0.9886	0.2715
18	0.9923	0.2204
19	0.9923	0.2204
20	1.0273	0.2362
21	1.0307	0.2811
22	1.0482	1.4766
23	1.0213	0.4536
24	1.0057	0.3491
25	0.9957	0.4128
26	1.0034	0.4630
27	1.0163	0.1496
28	1.0185	1.0342
29	1.0042	0.4532
30	1.0102	0.4748
31	1.0151	0.9762

## B.2 Pressure Switches Calibration

The Ceraphant-PTC31 pressure switches are calibrated by Endress+Hauser Company. The calibrated process was done according to fix point method. Table B.3 illustrates the results of the calibration for the pressure switches.

Table B.3: Calibration results of the pressure switches.

<i>Pressure switch</i>	<i>Measuring point</i>	<i>Reference pressure</i>	<i>Device output</i>	<i>Deviation %</i>
<i>Before compressor</i>	1	0.4400	0.4108	-0.03
	2	24.450	24.450	0.00
	3	48.796	48.812	0.02
	4	72.723	72.708	-0.02
	5	97.421	97.423	0.00
<i>After compressor</i>	1	0.0015	0.0021	0.01
	2	2.5628	2.5633	0.01
	3	5.0394	5.0409	0.02
	4	7.5376	7.5384	-0.01
	5	10.033	10.036	0.03

### B.3 Refrigerant Flow Meter Calibration

The refrigerant flow meter (Optimass 7000-T10) works according to Coriolis principle and is calibrated by KROHNE Company. Table B.4 illustrates the results of the calibration for the refrigerant flow meter.

Table B.4: Calibration results of the refrigerant flow meter.

<i>Measuring point</i>	<i>Measured mass flow rate</i>	<i>Actual mass flow rate</i>	<i>Error %</i>
<i>1</i>	15.1635	15.1770	-0.089
<i>2</i>	17.6145	17.6221	-0.043
<i>3</i>	21.0300	21.0315	-.0070

### B.4 Gas Flow Meter Calibration

The diaphragm gas flow meter (BK-G4) is calibrated by elster instromet Company. Fig. B.1 illustrates the results of the calibration for the gas flow meter. The error percentage ranges from -8 % to 5 % based on ambient air temperature. All the experiential runs have been made in ambient air temperature ranges from 20°C to 25°C so the error percentage range lies between 1 % and 3 %.

### B.5 Engine Coolant Flow Meter Calibration

The turbine meter engine coolant flow meter (KHKU-100 Arnite) is calibrated by Digmaesa Company. Fig. B.5 illustrates the results of the calibration for the engine coolant flow

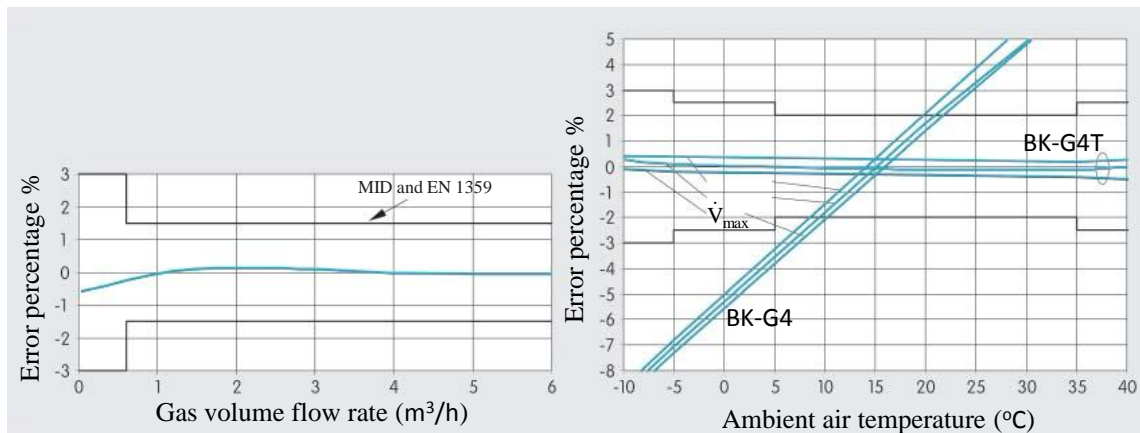


Figure B.1: Calibration of the gas flow meter.

meter. The error percentage ranges from -2% to 5% based on the engine coolant volume flow rate.

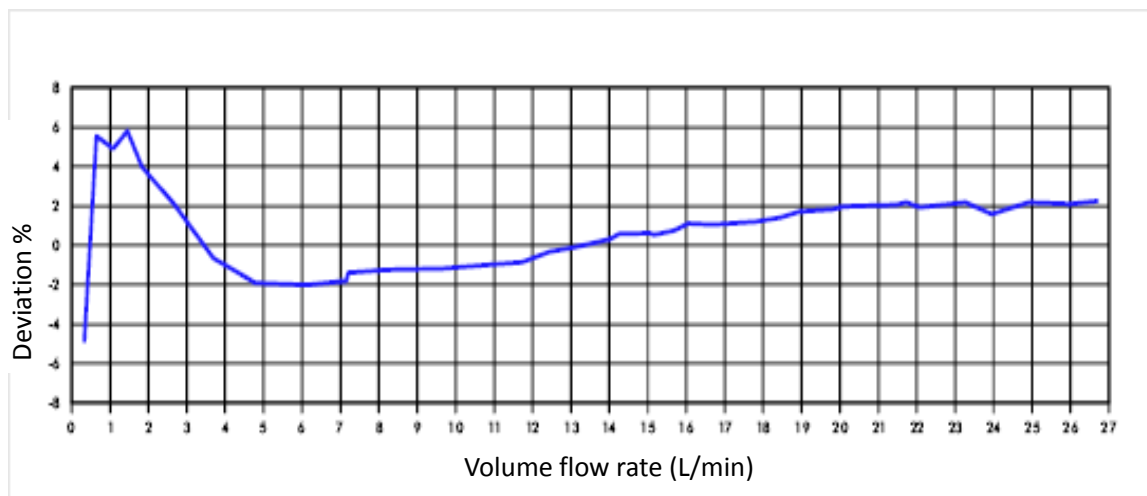


Figure B.2: Calibration of the engine coolant flow meter.

## B.6 Water Flow Meter Calibration

The ultrasonic water flow meter (ultego-II) is calibrated by ista Company. Fig. B.6 illustrates the results of the calibration for the water flow meter. The error percentage ranges from -5% to 3% based on the water volume flow rate. Higher water volume flow rate gives lower resulting error.

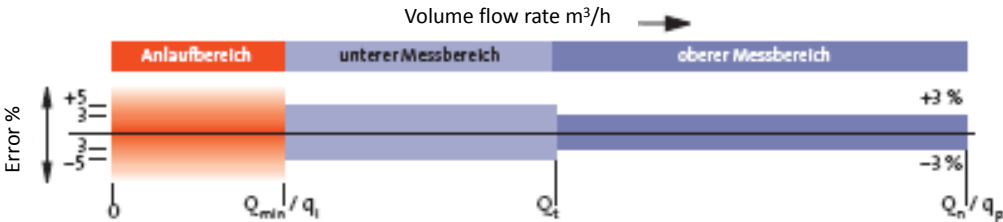


Figure B.3: Calibration of the water flow meter.



# Appendix C

## SPECIFICATIONS OF THE INSTRUMENTATION DEVICES

The specifications of the instrumentation devices that have been used in this work are listed below.

### C.1 Data Acquisition Card

Field Point FP-1000 data acquisition card has been used to receive the signals of the measuring instruments and send it to the recoding program. The main specifications of the data acquisition card are explained in Table C.1.

Table C.1: Specifications of the data acquisition card.

<i>Type FP-1000</i>	1 RS-232 port
<i>Maximum terminal bases per bank</i>	9
<i>Baud rates</i>	300, 1200, 2400, 9600 and 19200
<i>Maximum number of banks</i>	25
<i>Operating temperature</i>	-40°C to +70°C
<i>Operating relative humidity</i>	5 % to 90 % noncondensing

### C.2 Pressure Switch

Digital pressure switches have been used to measure the refrigerant pressure. The main specifications of the pressure switches are shown in Table C.2.

### C.3 Refrigerant Flow Meter

KROHNE Optimass 7000-T10 has been used to measure the refrigerant mass flow rate. The main specifications of the refrigerant flow meter is illustrated in Table C.3.

Table C.2: Specifications of the pressure switches.

<i>Type</i>	Ceraphant-PTC31
<i>Measuring range</i>	0 to 40bar
<i>Process temperature</i>	-40°C to +100°C
<i>Accuracy</i>	deviation < 0.5 %
<i>Non-repeatability</i>	< 0.2 %
<i>Response time</i>	$\leq 20ms$

Table C.3: Specifications of the refrigerant flow meter.

<i>Type</i>	Optimass 7000-T10
<i>Nominal flow rate</i>	2700kg/h
<i>Process temperature</i>	-40°C to +150°C
<i>Accuracy</i>	deviation 0.1 %
<i>Non-repeatability</i>	< 0.05 %

## C.4 Gas Flow Meter

Diaphragm gas meter BK-G4 has been used to measure the gas volume flow rate. The main specifications of the diaphragm gas meter is illustrated in Table C.4.

Table C.4: Specifications of the diaphragm gas meter.

<i>Type</i>	BK-G4
<i>Measuring range</i>	1.4 $ft^3/h$ to 200 $ft^3/h$
<i>Pulse output</i>	1 $ft^3$ /pulse
<i>Working temperature</i>	-20°C to +60°C
<i>Maximum operating pressure</i>	5 psig

## C.5 Engine Coolant Flow Meter

Turbine engine coolant flow meter (FHKU 100 Arnite) has been used to measure the engine coolant volume flow rate. The main specifications of the engine coolant flow meter is illustrated in Table C.5.

## C.6 Water Flow Meter

Ultego II water flow meter has been used to measure the water flow rate through the indoor unit. The main specifications of the water flow meter is illustrated in Table C.6.



Table C.5: Specifications of the diaphragm gas meter.

<i>Type</i>	FHKU 100 Arnite
<i>Measuring range</i>	3 l/min to 30 l/min
<i>Measuring accuracy</i>	$\pm \%2$
<i>Temperature range</i>	-10°C to +65°C
<i>Working pressure</i>	20 bar at 20°C
<i>Repetition</i>	$< \pm \%0.25$

Table C.6: Specifications of the water flow meter.

<i>Type</i>	Ultego II
<i>Nominal water volume flow rate</i>	6m <sup>3</sup> /h
<i>Measuring accuracy</i>	$\pm \%3$
<i>Temperature range</i>	5°C to +65°C
<i>voltage</i>	3.5VDC



# Appendix D

## UNCERTAINTY ANALYSIS

The uncertainty analysis indicates the implication error of the measured parameters on the uncertainty of the results. Detailed analysis of the various experimental parameters is carried out using the differential method described by Moffat [91], Kline and McClintok [92] and Holman [93].

### D.1 Water Temperature

The minimum reading of the water temperature = 6°C

Resolution of the thermometer = 0.1°C

Accuracy of the thermometer = 0.1 %

Thus, the maximum relative error in measuring the water temperature can be obtained as follows;

$$e_{\vartheta_{wat}} = \left| \frac{\delta\vartheta_{wat}}{\vartheta_{wat}} \right| = \frac{0.1}{6} \times 100 + 0.1 = 1.76 \% \quad (\text{D.1})$$

### D.2 Refrigerant Temperature

The minimum reading of the refrigerant temperature = -3°C

Resolution of the thermometer = 0.1°C

Accuracy of the thermometer = 0.1 %

Thus, the maximum relative error in measuring the refrigerant temperature can be calculated as follows;

$$e_{\vartheta_{ref}} = \left| \frac{\delta\vartheta_{ref}}{\vartheta_{ref}} \right| = \frac{0.1}{-3} \times 100 + 0.1 = 3.43 \% \quad (\text{D.2})$$

### D.3 Refrigerant Pressure

The minimum reading of the refrigerant pressure = 0.7 bar

Resolution of the thermometer = 0.01 bar

Accuracy of the thermometer = 0.5 %

Thus, the maximum relative error in measuring the refrigerant pressure can be estimated as follows;

$$e_{p_{ref}} = \left| \frac{\delta p_{ref}}{p_{ref}} \right| = \frac{0.01}{0.7} \times 100 + 0.5 = 1.92 \% \quad (\text{D.3})$$

## D.4 Engine Coolant Temperature

The minimum reading of the engine coolant temperature = 20°C

Resolution of the thermometer = 0.1°C

Accuracy of the thermometer = 0.1%

Thus, the maximum relative error in measuring the engine coolant temperature can be evaluated as follows;

$$e_{\vartheta_{coolant}} = \left| \frac{\delta \vartheta_{coolant}}{\vartheta_{coolant}} \right| = \frac{0.1}{20} \times 100 + 0.1 = 0.6 \% \quad (\text{D.4})$$

## D.5 Refrigerant Specific Enthalpy

Refrigerant specific enthalpy is based on the measured values of both refrigerant temperature and refrigerant pressure. Thus, the uncertainty of the refrigerant specific enthalpy can be obtained as;

$$e_{h_{ref}} = \left| \frac{\delta h_{ref}}{h_{ref}} \right| = \sqrt{\left| \frac{\delta p_{ref}}{p_{ref}} \right|^2 + \left| \frac{\delta \vartheta_{ref}}{\vartheta_{ref}} \right|^2} = 3.93 \% \quad (\text{D.5})$$

## D.6 Water Specific Enthalpy

Water specific enthalpy is based only on the measured water temperature. Thus, the uncertainty of the water specific enthalpy can be computed as;

$$e_{h_{wat}} = \left| \frac{\delta h_{wat}}{h_{wat}} \right| = \sqrt{\left| \frac{\delta \vartheta_{wat}}{\vartheta_{wat}} \right|^2} = 1.76 \% \quad (\text{D.6})$$

## D.7 Refrigerant Mass Flow Rate

The minimum reading of the refrigerant mass flow rate = 0.086 kg/s

Resolution of the flow meter = 0.001 kg/s

Accuracy of the flow meter = 0.1%

Thus, the maximum relative error in measuring the refrigerant mass flow rate can be calculated as follows;

$$e_{\dot{M}_{ref}} = \left| \frac{\delta \dot{M}_{ref}}{\dot{M}_{ref}} \right| = \frac{0.001}{0.086} \times 100 + 0.1 = 1.26 \% \quad (\text{D.7})$$

## D.8 Refrigerant Heat Loads and Compression Power

The refrigerant heat loads and the compression power are calculated from Eqn.5.1 and Eqn.5.13 in which refrigerant mass flow rate is multiplied into enthalpy difference. Thus, the maximum relative error in refrigerant heat loads and compression power can be evaluated as follows;

$$\left| \frac{\delta \dot{P}_{comp}}{\dot{P}_{comp}} \right| = \left| \frac{\delta \dot{Q}_{indoor}}{\dot{Q}_{indoor}} \right| = \sqrt{\left| \frac{\delta p_{ref}}{p_{ref}} \right|^2 + \left| \frac{\delta \vartheta_{ref}}{\vartheta_{ref}} \right|^2} = 4.12 \% \quad (D.8)$$

## D.9 Gas Volume Flow Rate

The minimum reading of gas volume flow rate = 1.188 m<sup>3</sup>/h

Resolution of the gas flow meter = 0.001 m<sup>3</sup>/h

Accuracy of the gas flow meter = 2 %

Thus, the maximum relative error in measuring the gas volume flow rate can be obtained as follows;

$$e_{\dot{v}_{gas}} = \left| \frac{\delta \dot{v}_{gas}}{\dot{v}_{gas}} \right| = \frac{0.001}{1.188} \times 100 + 0.1 = 2.08 \% \quad (D.9)$$

## D.10 Gas Engine Heat Energy

Gas engine heat energy is based only on the measured gas volume flow rate. Thus, the uncertainty of the gas engine heat energy can be computed as;

$$e_{\dot{Q}_{gas}} = \left| \frac{\delta \dot{Q}_{gas}}{\dot{Q}_{gas}} \right| = \sqrt{\left| \frac{\delta \dot{v}_{gas}}{\dot{v}_{gas}} \right|^2} = 2.08 \% \quad (D.10)$$

## D.11 Water Volume Flow Rate

The minimum reading of the water volume flow rate = 1.82 m<sup>3</sup>/h

Resolution of the water flow meter = 0.001 m<sup>3</sup>/h

Accuracy of the water flow meter = 3 %

Thus, the maximum relative error in measuring the water volume flow rate can be estimated as follows;

$$e_{\dot{v}_{wat}} = \left| \frac{\delta \dot{v}_{wat}}{\dot{v}_{wat}} \right| = \frac{0.001}{1.82} \times 100 + 0.1 = 3.05 \% \quad (D.11)$$

## D.12 Water Heat Load

The water heat load is calculated from Eqn.5.2 in which water mass flow rate is multiplied into enthalpy difference. Thus, the maximum relative error in water heat load can be evaluated as follows;

$$\left| \frac{\delta \dot{Q}_{wat}}{\dot{Q}_{wat}} \right| = \sqrt{\left| \frac{\delta \dot{v}_{wat}}{\dot{v}_{wat}} \right|^2 + \left| \frac{\delta \vartheta_{wat}}{\vartheta_{wat}} \right|^2} = 3.52\% \quad (\text{D.12})$$

### D.13 Engine Coolant Volume Flow Rate

The minimum reading of the engine coolant volume flow rate =  $0.40 \text{ m}^3/\text{h}$

Resolution of the engine coolant flow meter =  $0.001 \text{ m}^3/\text{h}$

Accuracy of the engine coolant flow meter = 2%

Thus, the maximum relative error in measuring the engine coolant volume flow rate can be calculated as follows;

$$e_{\dot{v}_{wat}} = \left| \frac{\delta \dot{v}_{wat}}{\dot{v}_{wat}} \right| = \frac{0.001}{0.4} \times 100 + 0.1 = 2.25\% \quad (\text{D.13})$$

### D.14 Engine Coolant Heat Loads

The engine coolant heat loads are calculated from Eqn.5.8 and Eqn.5.9 in which engine coolant mass flow rate is multiplied into enthalpy difference. Thus, the maximum relative error in engine coolant heat loads can be estimated as follows;

$$\left| \frac{\delta \dot{Q}_{rad}}{\dot{Q}_{rad}} \right| = \left| \frac{\delta \dot{Q}_{HR}}{\dot{Q}_{HR}} \right| = \sqrt{\left| \frac{\delta \dot{v}_{coolant}}{\dot{v}_{coolant}} \right|^2 + \left| \frac{\delta \vartheta_{coolant}}{\vartheta_{coolant}} \right|^2} = 2.32\% \quad (\text{D.14})$$

### D.15 Primary Energy Ratio

The system primary energy ratio is calculated from Eqn.5.16 in which indoor unit capacity is divided by gas engine heat energy. Thus, the maximum relative error in primary energy ratio can be obtained as follows;

$$\left| \frac{\delta PER}{PER} \right| = \sqrt{\left| \frac{\delta \dot{Q}_{indoor}}{\dot{Q}_{indoor}} \right|^2 + \left| \frac{\delta \dot{Q}_{gas}}{\dot{Q}_{gas}} \right|^2} = 3.52\% \quad (\text{D.15})$$

## Appendix E

# FLOW CHART OF THE SIMULATION PROGRAM

The simulation program is developed to analysis the GEHP performance for different operating conditions. The input data for the program are water inlet temperature, water flow rate, ambient air temperature and engine speed while the output main results are the system cooling capacity, gas engine energy consumption and primary energy ratio. The program is established using EES software. The program sequence consists of two parts scroll compressor modelling and system performance calculation. The output results of the scroll compressor modelling such as refrigerant mass flow rate and compressor power are obtained after iteration process till minimum error between measured and simulated data are obtained. Then, the refrigerant mass flow rate is used to calculate the cooling capacity using the available heat transfer correlations until a minimum resulting error is obtained between the measured and the calculated cooling capacity. On the other hand, the compressor power is used to calculate the gas engine energy consumption using the given gas engine correlation. The system primary energy ratio is calculated as final result for the simulation program. Fig. E.1 illustrates flow chart of the simulation program.

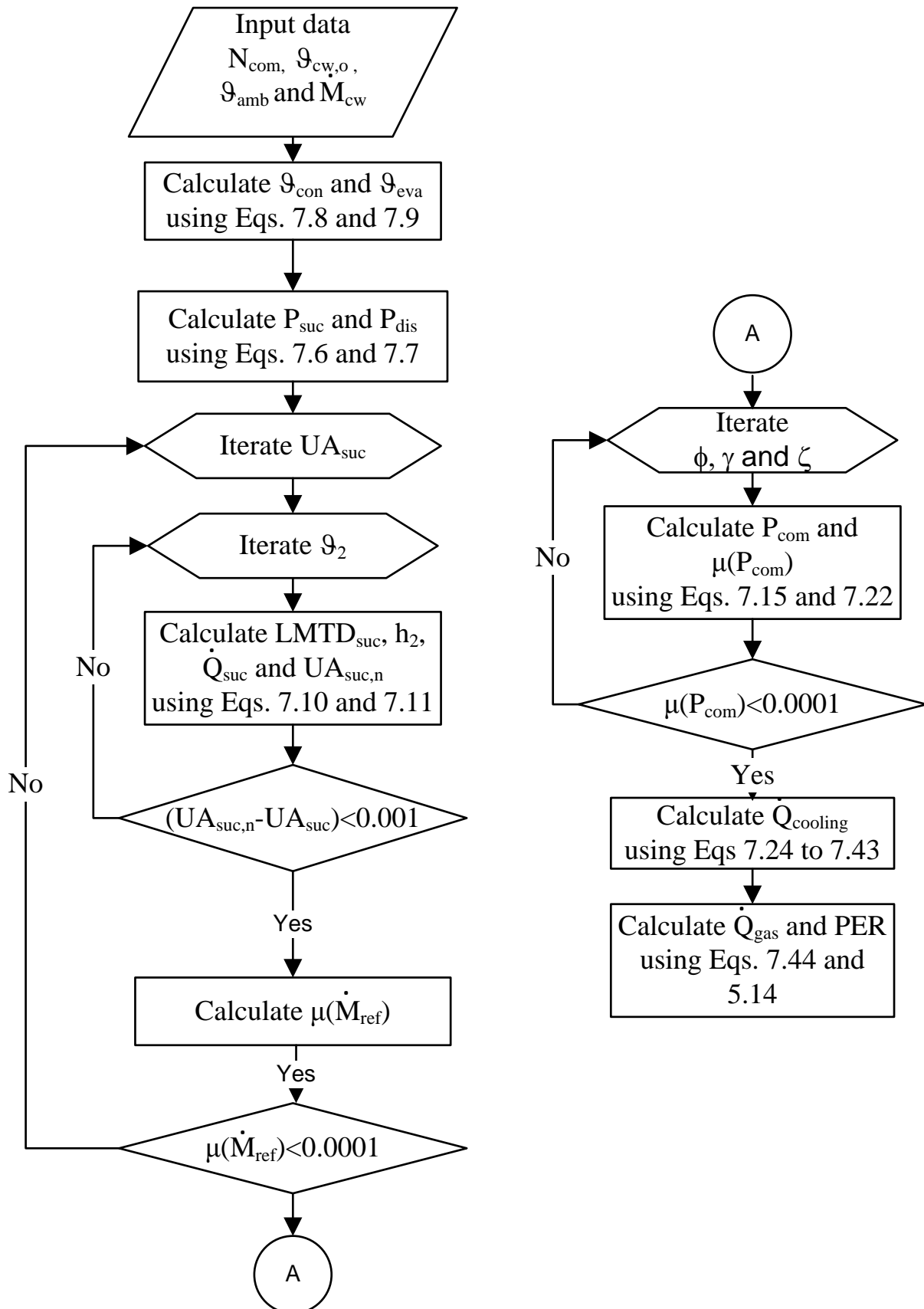


Figure E.1: Flow chart of the simulation program.



# Bibliography

- [1] H. J. Laue, *9 Heat pumps*. Heinloth, K. (ed.). SpringerMaterials - The Landolt-Börnstein Database (<http://www.springermaterials.com>), 2006.
- [2] K. Watanabe, “Thermodynamic property studies in progress for alternative refrigerant mixtures: An overview,” in *International Ondol Conference*, Seoul, Korea, 1996.
- [3] M. E. Jonsson and E. Granryd, “Multipurpose heat pump for domestic applications,” in *IIF-IIR- Commission E2 and B2- Linz*, Austria, 1997.
- [4] J. P. Meyer and G. P. Greyvenstein, “Hot water for homes in South Africa with heat pumps,” *Energy*, vol. 16, pp. 1039–1044, 1991.
- [5] G. P. Greyvenstein and J. P. Meyer, “The viability of heat pumps for the heating of swimming pools in South Africa,” *Energy*, vol. 16, pp. 1031–1037, 1991.
- [6] S. Garimella, “Innovations in energy efficient and environmentally friendly space-conditioning systems,” *Energy*, vol. 28, pp. 1593–1614, 2003.
- [7] A. N. Ajah, A. Mesbah, J. Grievink, P. M. Herder, P. W. Falcao, and S. Wennekes, “On the robustness, effectiveness and reliability of chemical and mechanical heat pumps for low-temperature heat source district heating: a comparative simulation-based analysis and evaluation,” *Energy*, vol. 33, pp. 908–929, 2008.
- [8] A. Hepbasli and L. Ozgener, “Development of geothermal energy utilization in turkey: a review,” *Renewable and Sustainable Energy Reviews*, vol. 8, pp. 433–460, 2004.
- [9] O. Ozgener and A. Hepbasli, “A review on the energy and exergy analysis of solar assisted heat pump systems,” *Renewable and Sustainable Energy Reviews*, vol. 11, pp. 482–496, 2007.
- [10] Z. Yang, S. G. Zhang, B. Liu, and Y. T. Ma, “Evaluation of gas-engine heat pumps and other heating and cooling systems about the energy efficiency and economic benefit,” *Acta Energiæ Solaris Sinica*, vol. 22, pp. 171–175, 2001.
- [11] M. X. Li, Y. T. Ma, J. G. Wang, and F. Kang, “Study of the multiple objective comprehensive evaluation for heating and air-conditioning systems,” *Journal of Tianjin University Science and Technology*, vol. 36, pp. 311–315, 2003.

- [12] Z. Yang, Z. Haibo, and Z. Wu, "Technical and economic analysis of gas engine driven heat pump in China," *International Journal of Global Energy*, vol. 20, pp. 223–232, 2003.
- [13] G. A. Nowakowski and R. L. Busby, "Advances in natural gas cooling," *ASHRAE Journal*, vol. 43, pp. 47–52, 2001.
- [14] M. D. D'accadia, M. Sasso, and S. Sibilio, "Field test of a small-size gas engine driven heat pump in an office application: first results," *International Journal of Ambient Energy*, vol. 16, pp. 183–191, 1995.
- [15] F. Ulrich, "Gas reciprocating engine heat pump," *HLH Heizung Luftung/Klima Haustechnik*, vol. 27, pp. 449–452, 1976.
- [16] E. Rebhan, *Energie hand buch*. Springer, 2002.
- [17] S. Li, W. Zhang, R. Zhang, D. Lv, and Z. Huang, "Cascade fuzzy control for gas engine driven heat pump," *Energy Conversion and Management*, vol. 46, pp. 1757–1766, 2005.
- [18] F. A. Holland, F. A. Watson, and S. Devotta, "Thermodynamic design data for heat pump systems," in *Pergamon Press*, Oxford, 1982.
- [19] G. A. Nowakowski, M. Inada, and M. P. Dearing, "Development and field testing of a high-efficiency engine-driven gas heat pump for light commercial applications," *ASHRAE Transactions*, vol. pt. 1, pp. 994–1000, 1992.
- [20] A. G. Nowakowski, "An introduction and status update on unitary engine-driven heat pumps," *ASHRAE Journal*, vol. 38, pp. 42–47, 1996.
- [21] Z. Lian, S. Park, W. Huang, Y. Baik, and Y. Yao, "Conception of combination of gas-engine-driven heat pump and water-loop heat pump system," *International Journal of Refrigeration*, vol. 28, pp. 810–819, 2005.
- [22] R. Lazzarin and M. Noro, "District heating and gas engine heat pump: economic analysis based on a case study," *Applied Thermal Engineering*, vol. 26, pp. 193–199, 2006.
- [23] A. Ficarella and D. Laforgia, "Energy conservation in alcohol distillery with the application of pinch technology," *Energy Conversion and Management*, vol. 40, pp. 1495–1514, 1999.
- [24] Y. Xie, L. Lun, Z. Yu, and X. Zhang, "Performance of cogeneration system incorporating gas engine driven heat pump," *Challenges of Power Engineering and Environment*, Springer, vol. 2, pp. 61–63, 2007.
- [25] W. Bussmann, "Heating of the dortmundwellinghofen open air swimming pool with a gas heat pump (two years of operational experience)," in *Collection of technical papers AIAA/ASME/ASCE/AHS structures, structural dynamics and materials conference*, pp. 26–34, 1978.

- [26] E. Flurschetz, "Use of heat pump in an integrated municipal energy supply system," *Elektrowaerme Int Ed A*, vol. 36, pp. 164–167, 1978.
- [27] W. Struck, E. Willeitner, and G. Kok, "Generation of heat with diesel and gas-motor-heat-pumps," *Klim Kaelte Ing*, vol. 6, pp. 279–284, 1978.
- [28] O. Heiburg and W. Lohstaeter, "Energy conservation in the heating and hot water supply of multi-family houses with the help of a gas-enginedriven heat pump which can operate in a monovalent way up to -12 degree C outside temperature," *Heizen mit Sonne*, pp. 266–274, 1980.
- [29] H. J. Menkveld, "Laboratory test results and practical implications of the use of a gas engine driven compression heat pump," in *Congre' s, Pompes a' chaleur et circulation dair dans les locaux clematises. Institut international du froid. Commissions B1, B2, E1, E2. Reunions*, pp.355-365, 1981.
- [30] H. Morokoshi, S. Inoue, K. Fujio, I. Okuda, S. Suzuki, H. Yamada, and F. Nakajima, "Gas-engine-driven cooling/heating hot-water supply system," *National Technical Report*, vol. 30, pp. 35–42, 1984.
- [31] V. A. H. Eustace, "Testing and applications of a high temperature gas engine driven heat pump," *Journal of Heat Recovery Systems*, vol. 4, pp. 257–263, 1984.
- [32] M. Ogura, T. Kawasaki, M. Motokawa, and F. Terada, "The first commercialized direct-expansion type gas engine heat pump," *Government Inst Inc Publishing*, 1987.
- [33] G. Nowakowski, G. Metren, and J. Brogan, "Field performance of a 3-ton natural gas engine-driven heating and cooling system," *ASHRAE Transactions*, vol. pt. 2, pp. 1382–1388, 1995.
- [34] V. J. Wolfe and R. P. Getman, "Gas engine heat pump performance in a southern climate," *ASHRAE Transactions*, vol. pt. 2, pp. 1389–1395, 1995.
- [35] T. L. Cornell, R. L. Hedrick, and W. W. Bassett, "Performance characterization of an engine-driven gas heat pump in a single-family residence," *ASHRAE Transactions*, vol. Pt.1, pp. 1430–1435, 1993.
- [36] G. H. Van-Dijk and T. M. Lemmens, "Natural-gas-driven heat pumps in the netherlands-on field experiences and future perspective," in *International Gaz research conference proceedings*, 2001.
- [37] H. Boye, G. Geike, J. Schmidt, R. Praetor, and F. Scheffel, "Energieeffiziente kopplung einer gaswaermepumpe mit einem klimazentralgeraet," *KI Luft- und Kaeltetchnik*, vol. 43, pp. 24–33, 2007.
- [38] C. W. Sohn, F. H. Holcomb, D. J. Sondeno, and J. M. Stephens, "Field-tested cooling performance of gas-engine-driven heat pumps," *ASHRAE Transactions*, vol. pt. 2, pp. 232–239, 2008.

- [39] T. Kaneko, M. Obitani, and T. Imura, "Performance of a four-ton gas-engine-driven heat pump," *ASHRAE Transactions*, vol. Pt. 1, pp. 989–993, 1992.
- [40] Y. L. Li, X. S. Zhang, Y. G. Yin, Z. Guan, and Y. Jiang, "Experimental research on variable speed operation of cold-hot water unit driven by gas engine," *Journal of Southeast University (natural science Ed)*, vol. 35, pp. 298–301, 2005.
- [41] R. R. Zhang, X. S. Lu, S. Z. Li, and A. Z. Gu, "Analysis of energy consumption and running cost of gas engine-driven heat pump," *Journal of Harbin Institute of Technology*, vol. 38, pp. 1243–1246, 2006.
- [42] S. Sanaye, M. A. Meybodi, and M. Chahartaghi, "Modeling and economic analysis of gas engine heat pumps for residential and commercial buildings in various climate regions of iran," *Energy and Buildings*, vol. 42, pp. 1129–1138, 2010.
- [43] J. Brenn, P. Soltic, and C. Bach, "Comparison of natural gas driven heat pumps and electrically driven heat pumps with conventional systems for building heating purposes," *Energy and Buildings*, vol. 42, pp. 904–908, 2010.
- [44] Z. Xu and Z. Yang, "Saving energy in the heat-pump air conditioning system driven by gas engine," *Energy and Buildings*, vol. 41, pp. 206–211, 2009.
- [45] M. Maddox, "Savings at leisure," *HAC*, vol. 56, pp. 40–42, 1986.
- [46] L. A. Howe, R. Radermacher, and K. E. Herold, "Combined cycles for engine driven heat pumps," *International Journal of Refrigeration*, vol. 12, pp. 21–28, 1989.
- [47] S. B. Riffat, A. P. Warren, and R. A. Webb, "Rotary heat pump driven by natural gas," *Heat Recovery Systems and CHP*, vol. 15, pp. 545–554, 1995.
- [48] Y. Zhao, Z. Shigang, and Z. Haibe, "Optimization study of combined refrigeration cycles driven by an engine," *Applied Energy*, vol. 76, no. 4, pp. 379–389, 2003.
- [49] S. Göktun, "Performance analysis of a heat engine driven combined vapor compression-absorption-ejector refrigerator," *Energy Conversion and Management*, vol. 41, pp. 1889–1895, 2000.
- [50] Q. Lin and Y. Min, "Research on primary energy ratio of the gas engine-driven heat pump under different run mode," in *Asia-Pacific Power and Energy Engineering Conference, APPEEC 2010, Chengdu*, 2010.
- [51] L. Ying-Lin, Z. Xiao-Song, and C. Liang, "A novel parallel-type hybridpower gas engine-driven heat pump system," *International Journal of Refrigeration*, vol. 30, pp. 1134–1142, 2007.
- [52] Y. Li, X. Zhang, and W. Wu, "Isolated energy-supply system based on hybrid power gas engine-driven heat pump," *Journal of Southeast University (Natural Science Edition)*, vol. 38, pp. 1011–1016, 2008.

- [53] S. Yagyu, I. Fujishima, J. Corey, and I. Satoh, "Design, simulation and test results of a heat-assisted three-cylinder stirling heat pump (C-3)," in *Proceeding of 32nd IECEC*, pp.1033-1038, 1997.
- [54] S. Yagyu, I. Fujishima, Y. Fukuyama, T. Morikawa, N. Obata, J. Corey, and et al, "Performance characteristics of a gas engine driven stirling heat pump," in *Am Inst Aeronau Astronaut*, pp.85-91, 2000.
- [55] Z. Yang, B. Liu, S. Zhang, and D. Xie, "Controlling study of the unitary airto-air gas-engine driven heating and cooling system," *Acta Energiæ Solaris Sinica*, vol. 24, pp. 493–496, 2003.
- [56] Y. Zhao, Z. Haibo, and F. Zheng, "Modeling and dynamic control simulation of unitary gas engine heat pump," *Energy Conversion and Management*, vol. 48, no. 12, pp. 3146–3153, 2007.
- [57] R. D. Ott, A. Zaltash, and J. W. Klett, "Utilization of a graphite foam radiator on a natural gas engine-driven heat pump," in *ASME international mechanical engineering congress and exposition*, 2002.
- [58] F. C. Chen, V. C. Mei, and R. E. Domitrovic, "Test of an improved gas engine-driven heat pump," in *Proceedings of the 1998 ASHRAE Winter Meeting. Part1, San Francisco, USA*, 1998.
- [59] Y. Li and X. Zhang, "Defrosting process and theory analysis of the multi-split gas engine-driven heat pump by waste heat," *Acta Energiæ Solaris Sinica*, vol. 29, pp. 18–23, 2008.
- [60] Z. J. Xu and Z. Yang, "Energy consumption in gas engine driven-heat pump with the humidity control function," *Journal of Jilin University (Engineering and Technology Edition)*, vol. 38, pp. 34–38, 2008.
- [61] J. W. MacArthur and E. W. Grald, "Unsteady compressible two-phase flow model for predicting cyclic heat pump performance and a comparison with experimental data," *International Journal of Refrigeration*, vol. 12, pp. 29–41, 1989.
- [62] M. D. D'accadia, M. Sasso, and S. Sibilio, "Optimum performance of heat engine driven heat pumps: A finite-time approach," *Energy Conversion and Management*, vol. 38, pp. 401–413, 1996.
- [63] Z. Yang, S. Zhang, and H. Zhao, "Dynamic study of the exhaust heat recovery system for a gas engine-driven heat pump," *Acta Energiæ Solaris Sinica*, vol. 25, pp. 712–716, 2004.
- [64] R. R. Zhang, X. S. Lu, S. Z. Li, W. S. Lin, and A. Z. Gu, "Analysis on the heating performance of a gas engine driven air to water heat pump based on a steady-state model," *Energy Conversion and Management*, vol. 46, pp. 1714–1730, 2005.

- [65] Y. Shin, H. Yang, C. S. Tae, and S. Cho, "Dynamics modeling of a gas engine-driven heat pump in cooling mode," *Journal of Mechanical Science and Technology*, vol. 20, pp. 278–285, 2006.
- [66] S. Sanaye and M. Chahartaghi, "Thermal modelling and operating tests for the gas engine-driven heat pump systems," *Energy*, vol. 35, pp. 351–363, 2010.
- [67] J. Deng, W. Li, and Z. Zhang, "Performance analysis of a household gas engine driven heat pump at varied environment temperature," *Journal of Xi'an Jiaotong University*, vol. 41, pp. 28–31, 2007.
- [68] D. Achim and J. Manfred, "Technical and economic investigation of the possible use of gas engine heat pumps for room heating," *Energietechnik Leipzig*, vol. 31, pp. 447–451, 1981.
- [69] B. Joerg, "Gas engine heat pump for one- and two-family houses," *GWF, Gas - Erdgas*, vol. 124, pp. 191–197, 1983.
- [70] G. J. Newbert, "Energy efficient drying, evaporation and similar processes," *Journal of Heat Recovery Systems*, vol. 5, pp. 551–559, 1985.
- [71] S. A. Tassou, "Heat recovery from sewage effluent using heat pumps," *Heat Recovery Systems and CHP*, vol. 8, pp. 141–148, 1988.
- [72] G. G. Maidment, X. Zhao, and S. B. Riffat, "Combined cooling and heating using a gas engine in a supermarket," *Applied Energy*, vol. 68, pp. 321–335, 2001.
- [73] R. Lazzarin and M. Noro, "Local or district heating by natural gas: which is better from energetic, environmental and economic point of views?" *Applied Thermal Engineering*, vol. 26, pp. 244–250, 2006.
- [74] Z. G. Sun, R. Z. Wang, and W. Z. Sun, "Energetic efficiency of a gas engine driven cooling and heating system," *Applied Thermal Engineering*, vol. 24, pp. 941–947, 2004.
- [75] Z. G. Sun, "A combined heat and cold system driven by a gas industrial engine," *Energy Conversion and Management*, vol. 48, pp. 366–369, 2007.
- [76] Z. Sun, "Experimental investigation of integrated refrigeration system (IRS) with gas engine, compression chiller and absorption chiller," *Energy*, vol. 32, pp. 431–436, 2008.
- [77] I. Y. Mahderekal, R. G. Gaylord, T. Young, K. Hinderliter, and E. Vineyard, "Design and development of a gas-engine-driven heat pump," in *2nd International Conference on Energy Sustainability*, 2008.
- [78] A. Hepbasli, Z. Erbay, F. Icier, N. Colak, and E. Hancioglu, "A review of gas engine driven heat pumps (GEHPs) for residential and industrial applications," *Renewable and Sustainable Energy Reviews*, vol. 13, pp. 85–99, 2009.

- [79] S. K. Creamer and H. J. Saunders, "Evaluation of a catalytic converter for a 3.73kw natural gas engine," *Society of Automotive Engineers of China*, pp. 9–20, 1993.
- [80] A. R. Ganji, "Environmental and energy efficiency evaluation of residential gas and heat pump heating," *Journal of Energy Resources Technology, Transactions of the ASME*, vol. 115, pp. 264–271, 1993.
- [81] R. Radermacher and D. Jung, "Theoretical analysis for replacement refrigerants for R-22 for residential uses," *ASHRAE Transactions*, vol. 99, pp. 333–343, 1993.
- [82] S. Devotta, A. V. Waghmare, N. N. Sawant, and B. M. Domkundwar, "Alternatives to HCFC-22 for air conditioners," *Applied Thermal Engineering*, vol. 21, pp. 703–715, 2001.
- [83] S. N. Kondepudi, "Drop-in testing of R-32 blends as R-22 alternatives in a split-system air conditioner," *ASHRAE Transactions*, vol. 99, pp. 406–413, 1993.
- [84] P. A. Domanski and D. A. Didion, "Thermodynamic evaluation of R22 alternative refrigerants and refrigerant mixtures," *ASHRAE Transactions*, vol. 99, pp. 627–635, 1993.
- [85] D. B. Bivens, M. B. Shiflett, W. D. Wells, G. S. Shealy, A. Yokozeki, D. M. Kolliopoulos, K. A. Allgood, and T. E. C. Chisolm, "HFC-22 alternatives for air conditioners and heat pumps," *ASHRAE Transactions*, vol. 101, pp. 1065–1071, 1995.
- [86] ASHRAE, "American society of heating refrigerating and air-conditioning engineers," *HVAC Systems and Equipment Handbook, ASHRAE, Atlanta, Georgia, USA*, 2000.
- [87] S. A. Klein, "EES-Engineering Equation Solver, Professional Version," *Middleton, WI: F-Chart Software*, 2010.
- [88] ASHRAE, "American society of heating refrigerating and air-conditioning engineers," *Refrigeration Handbook, ASHRAE, Atlanta, Georgia, USA*, 2006.
- [89] DIAdem, "Dynamic integrated assignment and demand modelling," *Base Edition 10.2, USA*, 2006.
- [90] K. Taira, "Development of a 2.5-rt multiple-indoor-unit gas engine heat pump," *ASHRAE Transactions*, vol. 24, pp. 982–988, 1998.
- [91] R. Moffat, "Describing the uncertainties in experimental results," *Experimental Thermal and Fluid Science*, vol. 1, pp. 3–17, 1988.
- [92] S. J. Kline and F. A. McClintok, "Describing the uncertainties in experimental results," *Mechanical engineering*, 1953.
- [93] J. P. Holman, *Experimental Methods for Engineers*. McGraw-Hill, Seventh Edition, 2001.

- [94] F. Stiemle, "Development in air-conditioning," in *Proceeding of IIF-IIR conference (Commissions B1, B2, E1 and E2)*, Bucharest, Romania, 1996.
- [95] E. Elgendy and J. Schmidt, "Experimental investigation of gas engine driven heat pump used in water cooling," *online Journal on Power and Energy Engineering*, vol. 1, pp. 90–94, 2010.
- [96] ASHRAE, "American society of heating refrigerating and air-conditioning engineers," *Application Handbook*, ASHRAE, Atlanta, Georgia, USA, 2007.
- [97] E. Elgendy, J. Schmidt, A. Khalil, and M. Fatouh, "Experimental performance of a combined heating and cooling system driven by gas engine," *Tenth International Congress of Fluid Dynamics ASME-ICFD10, December 16-19, 2010, Cairo, Egypt*.
- [98] H. Boye, F. Scheffel, E. Elgendy, and J. Schmidt, "Energieeffizienter betrieb von gasmotorwärmepumpen," *Deutsche Klte-Klima-Tagung 17-19 November, Magdeburg, Germany, 2010*.
- [99] E. Elgendy, J. Schmidt, A. Khalil, and M. Fatouh, "Performance of a gas engine driven heat pump for hot water supply systems," *Energy*, vol. 36, pp. 2883–2889, 2011.
- [100] E. Elgendy, G. Boye, J. Schmidt, A. Khalil, and M. Fatouh, "Experimental investigation of heat recovery options for gas engine driven heat pump system," *World Renewable Energy Congress 2011- Sweden linkping 8-13 may 2011*.
- [101] E. Elgendy, J. Schmidt, A. Khalil, and M. Fatouh, "Performance of a gas engine heat pump using R410A for heating and cooling applications," *Energy*, vol. 35, pp. 4841–4847, 2010.
- [102] E. Elgendy and J. Schmidt, "Experimental study of gas engine driven air to water heat pump in cooling mode," *Energy*, vol. 35, pp. 2461–2467, 2010.
- [103] C. Cuevas and J. Lebrun, "Testing and modelling of a variable speed scroll compressor," *Applied Thermal Engineering*, vol. 29, pp. 469–479, 2009.
- [104] E. Winandy, S. O. Claudio, and L. Jean, "Experimental analysis and simplified modelling of a hermetic scroll refrigeration compressor," *Applied Thermal Engineering*, vol. 22, pp. 107–120, 2002.
- [105] M. Duprez, D. Eric, and F. Marc, "Modelling of reciprocating and scroll compressors," *International Journal of Refrigeration*, vol. 30, pp. 873–886, 2007.
- [106] E. Winandy and L. Jean, "Scroll compressors using gas and liquid injection: experimental analysis and modelling," *International Journal of Refrigeration*, vol. 25, pp. 1143–1156, 2002.
- [107] <http://www.bitzer.de>.



- [108] E. Elgendy, J. Schmidt, A. Khalil, and M. Fatouh, "Modelling and validation of scroll refrigeration compressor," *Tenth International Congress of Fluid Dynamics ASME-ICFD10, December 16-19, 2010, Cairo, Egypt*.
- [109] D. H. Han, K. J., and L. Y. H. Kim, "Experiments on characteristics of evaporation of R410A in brazed plate heat exchangers with different geometric configurations," *Applied Thermal Engineering*, vol. 23, pp. 1209–1225, 2003.
- [110] <http://www.gea-phe.com/germany/startseite/>.
- [111] R. A. Troupe, J. C. Morgan, and J. Priffiti, "The plate heater versatile chemical engineering tool," *Chemical Engineering Progress*, vol. 56, pp. 124–128, 1960.
- [112] G. A. Longo and A. Gasparella, "Refrigerant R134a vaporisation heat transfer and pressure drop inside a small brazed plate heat exchanger," *International Journal of Refrigeration*, vol. 30, pp. 821–830, 2007.
- [113] C. Marvillet, "Welded plate heat exchangers as refrigerants dry-ex evaporator," *Design and Operation of Heat Exchangers, Springer-Verlag*, pp. 255–268, 1992.
- [114] D. Sterner and B. Sunden, "Performance of plate heat exchangers for evaporation of ammonia," *Heat Transfer Engineering*, vol. 27, pp. 45–55, 2006.
- [115] C. C. Thonon, R. Vidil, and C. Marvillet, "Recent research and developments in plate heat exchangers," *Journal of Enhanced Heat Transfer*, vol. 2, pp. 149–155, 1995.
- [116] Z. H. Ayub, "Plate heat exchanger literature survey and new heat transfer and pressure drop correlations for refrigerant evaporators," *Heat Transfer Engineering*, vol. 24, pp. 3–16, 2003.
- [117] Y. Y. Yan and T. F. Lin, "Evaporation heat transfer and pressure drop of refrigerant R134A in a plate heat exchanger," *ASME Journal of Heat Transfer*, vol. 121, pp. 118–127, 1999.
- [118] E. Djordjevic and S. Kabelac, "Flow boiling of R134a and ammonia in a plate heat exchanger," *International Journal of Heat and Mass Transfer*, vol. 51, pp. 6235–6242, 2008.
- [119] G. A. Longo and A. Gasparella, "Heat transfer and pressure drop during hfc refrigerant vaporisation inside a brazed plate heat exchanger," *International Journal of Heat and Mass Transfer*, vol. 50, pp. 5194–5203, 2007.
- [120] G. A. Longo, A. Gasparella, and R. Sartori, "Experimental heat transfer coefficients during refrigerant vaporisation and condensation inside herringbone-type plate heat exchangers with enhanced surfaces," *International Journal of Heat and Mass Transfer*, vol. 47, pp. 4125–4136, 2004.

- [121] F. Tboas, M. Valls, M. Bourouis, and A. Coronas, "Flow boiling heat transfer of ammonia/water mixture in a plate heat exchanger," *International Journal of Refrigeration*, vol. 33, pp. 695–705, 2010.
- [122] Y. Y. Hsieh, T. F. L. Winandy, and S. O. C. L. Jean, "Saturated flow boiling heat transfer and pressure drop of refrigerant R410A in a vertical plate heat exchanger," *International Journal of heat and mass transfer*, vol. 45, pp. 1033–1044, 2002.
- [123] H. Kumar, "The plate heat exchanger: Construction and design," *Institute of Chemical Engineering Symposium Series 86*, pp. 1275–1288, 1984.
- [124] R. L. Heavner, H. Kumar, and A. S. Wanniarachchi, "Performance of an industrial heat exchanger: Effect of chevron angle," *AIChE Symposium Series*, vol. 89, pp. 262–267, 1993.
- [125] A. S. Wanniarachchi, U. Ratnam, B. E. Tilton, and K. Dutta-Roy, "Approximate correlations for chevron-type plate heat exchangers," *30th National Heat Transfer Conference, ASME HTD*, vol. 314, pp. 145–151, 1995.
- [126] P. Haberschill, L. Gay, P. Aubouin, and M. Lallemand, "Performance prediction of a refrigerating machine using R407C: the effect of the circulating composition on system performance," *International Journal of Energy Research*, vol. 26, pp. 1295–1311, 2002.
- [127] Y. S. Kim, "An experimental study on evaporation heat transfer characteristics and pressure drop in plate heat exchanger," Ph.D. dissertation, Yonsei University, 1999.
- [128] J. Marriott, "Where and how to use plate heat exchangers," *Process Heat Exchange, Chemical Engineering Magazine (V. Cavaseno, ed.)*, McGraw-Hill, New York, 1979.
- [129] G. Schnabel and J. W. Palen, "Wärmeübergang an senkrechten berieselten flächen," *VDI Wärmeatlas, 8th ed. Berlin, Springer-Verlag*, 1997.
- [130] A. C. Talik, L. W. Swanson, L. S. Fletcher, and N. K. Anand, "Heat transfer and pressure drop characteristics of a plate heat exchanger," *ASME/JSME Thermal Engineering Conference*, vol. 4, pp. 321–329, 1995.
- [131] R. A. Buonopane and R. A. Troupe, "A study of the effects of internal rib and channel geometry in rectangular channels," *AIChE Journal*, vol. 15, pp. 585–596, 1969.
- [132] E. Elgandy, J. Schmidt, A. Khalil, and M. Fatouh, "Modelling and validation of a gas engine heat pump working with R410A for cooling applications," *Applied Energy*, p. In Press, 2011.
- [133] C. D. Rakopoulos and G. C. Mavropoulos, "Experimental instantaneous heat fluxes in the cylinder head and exhaust manifold of an air-cooled diesel engine," *Experimental Thermal and Fluid Science*, vol. 12, pp. 1265–1281, 2000.

### ***Persönliche Daten***

*Name:* Essam Elgendy  
*Adresse:* Jerichower Str. 54, 39114 Magdeburg  
*Telefon:* 017650624763  
*E-mail:* essam.elgendy@st.ovgu.de  
*Familienstand:* verheiratet, 2 Kinder  
*Staatsangehörigkeit:* Ägypten  
*Geburtsdatum:* 10.11.1973 in Kairo - Ägypten

### ***Schulbildung***

*September 1979 - Juni 1991* Grundschule, Mittelstufe, Oberstufe in Kairo Abitur

### ***Studium***

*Oktober 1991 - September 1996* B.Sc. Helwan Universität, Fakultät für Maschinenbau, Abteilung Mechanische Leistung, Kairo, Ägypten Note: Sehr Gut (83.67%)

*Februar 1998 - Oktober 2001* M.Sc - Helwan Universität, Fakultät für Maschinenbau, Abteilung Mechanische Leistung, Kairo, Ägypten erste Studienjahr - Sehr Gut (84%) zweiten Studienjahr - ausgezeichnet (92%)

*Oktober 2003 - Oktober 2005* Ph. D - Helwan Universität-Fakultät für Maschinenbau - Abteilung Mechanische Leistung. Ph. D erste Studienjahr - ausgezeichnet (90%) Ph.D zweiten Studienjahr - Sehr Gut (85%)

*Sommer semester 2008/2009* Otto-von-Guericke -Universität Magdeburg Fakultät für Verfahrens- und Systemtechnik Institut für Strömungstechnik und Thermodynamik - CFD Note: 1.3

*Sommer semester 2009/2010* - Wärme-und Stofftransport Note: 1.3 - Ansys Note: 1.3

## **Veröffentlichungen Journals**

*Fatouh M., Nabil, M. and Elgendy, E., "Performance of a vapor compression heat pump using R134a for cooling and heating applications", Engineering Research Journal, Helwan University, Faculty of Eng., Mattarria, Cairo, Egypt, August 2002.*

*Khalil, A., Fatouh, M. and Elgendy, E., "Ejector design and simulation of a vapor jet refrigeration system working with R134a", Engineering Research Journal, Helwan University, Faculty of Eng., Mattarria, Cairo, Egypt, 2007.*

*Elgendy E., Schmidt J., "Experimental study of gas engine driven air to water heat pump in cooling mode", Energy 2010;35(6);2461-2467.*

*Elgendy E., Schmidt J., "Experimental Investigation of Gas Engine Driven Heat Pump Used in Water Cooling", online Journal on Power and Energy Engineering, OJPEE 2010, 1(3); 90-94.*

*Elgendy E., Schmidt J., Khalil A., Fatouh M., "Performance of a Gas Engine Heat Pump using R410A for Heating and Cooling Applications", Energy 2010; 35(12);4941-4948.*

*Elgendy E., Schmidt J., Khalil A., Fatouh M., "Performance of a Gas Engine Driven Heat Pump for Hot Water Supply Systems", Energy 2011, 36(5); 2883-2889.*

*Fatouh M., Elgendy E. "Experimental investigation of a vapor compression heat pump used for cooling and heating applications", Energy 2011, 36(5); 2788-2795.*

*Khalil A., Fatouh M., Elgendy E. "Ejector design and simulation of a vapor jet refrigeration system working with R134a", International Journal of Refrigeration; In press.*

*Elgendy E., Schmidt J., Khalil A., Fatouh M., "Modelling and Validation of a Gas Engine Heat Pump Working with R410A for Cooling Applications", Applied Energy 2011, In press.*

## **Veröffentlichungen Conferences**

*Fatouh M., Nabil, M. and Elgendy, E., "Exergy analysis of a vapor compression heat pump working with R12 alternatives", 8th International conference on Aerospace Science and Aviation Technology, Military Technical College, 4-6 May, 1999, Cairo, Egypt, Vol. 1, pp. 457-471.*

*Elgendy E., Schmidt J., "Experimental investigation of gas engine heat pump in cooling mode", The 2009 World Congress on Power and Energy Engineering WCPEE.09, 5-8 October, 2009, Cairo, Egypt.*

*Boye H., Scheffel F., Elgendy E. and Schmidt J., "Energieeffizienter Betrieb von Gasmotorwärmepumpen ", Deutsche Klte-Klima-Tagung 2010 Magdeburg, 17-19 November, 2010, Magdeburg, Germany.*

*Elgendy E., Schmidt J., Khalil A., Fatouh M., "Experimental Performance of a Combined Heating and Cooling System Driven by Gas Engine", Tenth International Congress of Fluid Dynamics ASME-ICFD10, December 16-19, 2010, Cairo, Egypt.*

*Elgendy E., Schmidt J., Khalil A., Fatouh M., "Modelling and Validation of Scroll Refrigeration Compressor", Tenth International Congress of Fluid Dynamics ASME-ICFD10, December 16-19, 2010, Cairo, Egypt.*

*Elgendy E., Boye G., Schmidt J., Khalil A., Fatouh M., "Experimental Evaluation of a Gas Engine Driven Heat Pump Incorporated with Heat Recovery Subsystems for Water Heating Applications", World Renewable Energy Congress 8-13 May 2011, Sweden.*